

# Dielectric Characterisation of Soil

Max A. Hilhorst



## Proefschrift

ter verkrijging van de graad van doctor  
op gezag van de rector magnificus  
van de Landbouwniversiteit Wageningen,  
dr. C.M. Karssen,  
in het openbaar te verdedigen  
op dinsdag 3 februari 1998  
des namiddags te vier uur in de Aula

1998

ISBN 90-5485-810-9

This thesis is also available as a publication nr. 98-01, ISBN 90-5406-162-6 of the DLO Institute of Agricultural and Environmental Engineering (IMAG-DLO), P.O. Box 43, NL-6700 AA Wageningen, The Netherlands.

This research was made possible by:



**Wageningen  
Agricultural  
University**



**i m a g - d l o**



**European Commission  
FAIR1 PL95 0681**

## ABSTRACT

Hilhorst, M.A., 1997. Dielectric characterisation of soil. Doctoral Thesis, Wageningen Agricultural University, Wageningen, The Netherlands, 141p., 44 figures, 11 tables, 136 equations, 111 references, English and Dutch summaries.

The potential of dielectric measuring techniques for soil characterisation has not been fully explored. This is attributed to the complex and incomplete theory on dielectrics, as well as to the lack of sensors suited for practical applications.

The theory on dielectric properties of soils is described, evaluated, and expanded. Colloidal polarisation of soil particles appears to be negligible. The polarisability of air bubbles in the soil matrix is made plausible. The Maxwell-Wagner effect is expressed in the form of a Debye function. A soil texture parameter is introduced that can be derived from dielectric measurements at three frequencies. Newly derived are a relationship between the soil water matric pressure and the dielectric relaxation frequency, a dielectric mixture equation with depolarisation factors that account for electromagnetic field refractions at the boundary between two soil materials, and a model to predict permittivity versus frequency from soil porosity, water content, and matric pressure.

A model of sensors for Frequency Domain (FD) measurements as well as for Time Domain Reflectometry (TDR) is described. An integrated circuit (ASIC) has been developed that is based on synchronous detection and is intended for practical low-cost dielectric sensors. Algorithms correct for phase errors, parasitic impedances of the ASIC and electrical length of electrodes and wiring. These elements are incorporated in a new FD sensor, operated at 20 MHz.

The new theory is tested in different ways using the new FD sensor and TDR. Calibration curves of water content versus electrical permittivity of different soil types compare reasonably well with predicted curves. The Maxwell-Wagner effect increases with increasing water content and specific surface area. The electrical conductivity of the extracted soil solution can be determined by simultaneous measurements of the electrical permittivity and bulk conductivity. This method proved accurate for glass beads and for most tested soils. Soil layers polluted with chlorinated solvents or oil are detected by measuring the same parameters as function of depth. The frequency dependence of the bulk electrical conductivity, attributed to the Maxwell-Wagner effect, is analysed by measurements at three frequencies.

Hydrating concrete is shown to simulate the dielectric behaviour of soils of different textures. Its dielectric spectrum from 10 MHz to 1 GHz illustrates the effect of water binding (> 100 MHz) and the Maxwell-Wagner effect (< 100 MHz). Around 100 MHz concrete exhibits only small changes of the dielectric properties; this is known to occur also for soils of different textures. The compressive strength of concrete appears to be predictable from the electrical permittivity at 20 MHz, due to the Maxwell-Wagner effect.

Due to the simplification to apply a single sine wave rather than a pulse or step function, existing theory is inadequate to correct TDR measurements of water content for the effect of electrical conductivity. TDR electrical conductivity measurements are found to be low-frequency (< 3 MHz) measurements.

*Additional keywords:* soil suction, pressure head, moisture content, impedance spectroscopy, transmission lines, porous materials, capacitive, refractive index, soil physics

## VOORWOORD, *PREFACE*

Water speelt een belangrijke rol in vrijwel alle aspecten van de bodemkunde of plantenteelt. Het geeft aan de bodem bijzondere elektrische (diëlektrische) eigenschappen. Daardoor kan het watergehalte van de bodem elektrisch worden gemeten. Dankzij de aanwezigheid van water in de bodem, worden de diëlektrische eigenschappen ook beïnvloed door bijvoorbeeld het kleigehalte, de hoeveelheid meststoffen of door de mate waarin het water aan bodemdeeltjes hecht. Deze bodemparameters kunnen daarom ook elektrisch worden bepaald. In dit proefschrift beschrijf ik de mogelijkheden van het diëlektrische karakteriseren van de bodem.

Van alle personen die direct of indirect aan dit proefschrift hebben meegewerkt wil ik als eerste Piet Ploegaert memoreren die in 1982 is overleden. Hij heeft aan de toenmalige Technisch en Fysische Dienst voor de Landbouw (TFDL) het pionierswerk op het gebied van diëlektrische watergehalte-sensoren verricht. Vanaf 1983 heb ik zijn werk mogen voortzetten.

In de jaren tachtig bleek het diëlektrisch meetprincipe voor het bepalen van het watergehalte van de bodem, zoals Piet Ploegaert en ik dat hadden uitgewerkt, goed te voldoen. De productie en het onderhoud van deze sensoren bleken echter te arbeidsintensief en daardoor te duur. Het werd ons duidelijk dat alleen met een "chip" deze problemen konden worden opgelost. Een chip kan op een kleiner oppervlak zowel meer als degelijkere elektronica bevatten en kan in grote aantallen tegelijk geproduceerd worden voor de laagst mogelijke productie kosten.

Dankzij Frans Kampers kwamen er middelen beschikbaar van de Dienst Landbouwkundig Onderzoek (DLO) en de TFDL om een chip te ontwikkelen. *It was our intention to contract out the chip development. This turned out to be too expensive due to the risks involved. Still the discussion with specialists in the design of integrated circuits was fruitful and had an important impact on the design. We got some useful ideas from Ernst Nordholt (CATENA-microelectronics b.v., Delft) and from Will Barnes (LSI-Logic Limited, Sidcup, Kent, England).* Overtuigd van de mogelijkheden, hebben Jos Balendonck (IMAG-DLO) en ik de chip-ontwikkeling zelf ter hand genomen. Jos heeft het digitale deel ontwikkeld en ik het analoge hoogfrequente deel. Het digitale deel bestuurt de chip en maakt de koppeling met een computer mogelijk. Het analoge deel meet de diëlektrische eigenschappen van de bodem. Hoewel Mans Jansen (IMAG-DLO) niet actief betrokken was bij de chipontwikkeling, was hij een goed klankbord voor discussies op het gebied van analoge en hoogfrequente elektronica.

*The chips are produced at SGS-Thomson in France. The assistance of Henry Revet (ANACA, SGS-Thomson, Grenoble) in the lay-out phase, was indispensable for an optimal high frequency result. The complex program for the automatic test equipment for testing the chips was developed in close collaboration with Edwige Fremy (ANACA, SGS-Thomson, Grenoble).* Met zorg voor het gevoelige hoogfrequente meetgedeelte, heeft Henk van Roest (IMAG-DLO) de eerste sensor, en daarna vele prototypes, met de chip gerealiseerd en getest. De test- en meetsoftware voor zowel de personal computer als een handmeter zijn ontwikkeld door Peter Nijenhuis (IMAG-DLO). Verder hebben van IMAG-DLO aan deze ontwikkeling

meegewerkt: Gijs deVries, Max Wattimena, Wim Haalboom en de instrumentmakers: Ries van Ginkel, Rinus Hoogstede en Goos van Eck.

Nadat de eerste diëlektrische bodemvochtgehaltesensor functioneerde, bleken al snel meer toepassingen mogelijk. Om die applicaties uit te werken was het noodzakelijk eerst de diëlektrische eigenschappen van de bodem beter te begrijpen. De huidige theorie was daartoe niet toereikend en moest worden uitgediept of aangevuld. Dit onderzoek werd gedeeltelijk gefinancierd als Strategische Expertise Ontwikkeling (SEO) door DLO en IMAG en gedeeltelijk door het EU-IVth Framework project Waterman. Het leidde tot nieuwe inzichten en mogelijkheden voor het diëlektrisch karakteriseren van de bodem. *Clarifying and stimulating were discussions with Prof. Grand (author of "Dielectric behaviour of biological molecules in solution", 1978) and Paul de Loor (FEL-TNO, Den Haag). Clark Topp (Centre for land and Biological Resources Research, Ottawa, Canada) is acknowledged for discussions on dielectric measurements in general, and in particular for some supplementary details of his research concerning the calibration of TDR as published in 1980. I thank Richard Whalley (Silsoe Research Institute, England) for discussions on dielectric measuring technology, as also for reviewing the manuscript of this thesis.* Professoren P. Wollants (Universiteit Leuven, België) en G.H. Bolt (LUW-Wageningen) alsmede Jozua Laven (TU-Eindhoven) worden bedankt voor kritische kanttekeningen op het gebied van de thermodynamica.

Het hoofdstuk over de detectie van vervuilde bodemlagen moest noodzakelijkerwijs kort blijven door het vertrouwelijke karakter van de experimenten. Toch zijn hiervoor zeer veel veldgegevens verzameld door Dick Pluimgraaff en Ruud Mosterd (GeoMil Equipment b.v., Alphen a/d Rijn). De soepele wijze van samenwerken vond ik erg plezierig.

Wim Stenfert Kroese (OFFIS, Rotterdam) gaf ons opdracht te onderzoeken of het mogelijk is diëlektrisch de sterkte van beton te bepalen. Er volgde een boeiend onderzoek, dat leidde tot een gezamenlijk patent. Achteraf bleek de opgebouwde kennis over de diëlektrische eigenschappen van beton ook leerzaam voor die van de bodem. Nuttig waren de gesprekken met René Braam (IMAG-DLO) en Klaas Breugel (TU, Delft). Voorts bedank ik de heer Stekelenburg (Edese Beton Centrale, Wageningen) voor zijn medewerking aan de eerste praktijkproeven. Ton van Beek (TU-Delft), die de toepassing van de diëlektrische-betonsterktesensor in detail onderzoekt, wil ik bedanken voor onmisbare opmerkingen en aanvullingen.

Op deze plaats wil ik ook hen bedanken die meer in het algemeen belangrijk waren bij de totstandkoming van dit proefschrift. Hoewel Kees Schurer (IMAG-DLO) niet actief deelnam in het promotieteam, heeft hij wel vele uren kritisch naar mijn ideeën geluisterd. Met Gert Visscher (IMAG-DLO) heb ik leerzame gesprekken gevoerd over relatieve luchtvochtigheid. Ook Rob Buré, Theo Gieling en mijn kamergenote Marjolijn Kuypers vormden een goed klankbord. De extra aandacht die ik aan het proefschrift kon wijden werd mogelijk gemaakt door het waarnemen van veel van mijn normale dagelijkse taken door Jos Balendonck (IMAG-DLO) en Frans Kampers (IMAG-DLO). Als dat nodig was, wist Roxanne van Haastert (IMAG-DLO) altijd "klantvriendelijk" maar effectief vele telefoontjes af te vangen of mijn geheugen op te frissen. Mijn haat-liefde verhouding met de computer moest nog al eens in goede banen worden geleid door Wojtek Sablik (IMAG-DLO, I&M) en zijn afdeling. Bij het uitvoeren van een onderzoek als dit, zijn veel mensen van IMAG-DLO

actief op de achtergrond. Hun bijdragen zijn niet altijd zichtbaar, maar daarom niet minder waardevol. Hiermee wil ik hen allen bedanken.

Het proefschrift is totstandgekomen onder begeleiding van mijn promotor professor Reinder Feddes (Waterhuishouding, Landbouw Universiteit Wageningen). Hij heeft kritisch en zeer gedetailleerd het manuscript doorgenomen en het op energieke wijze met mij besproken. De inbreng van mijn copromotoren Chris Dirksen (Waterhuishouding, Landbouw Universiteit Wageningen) en Frans Kampers (ná 1996 cDLO, Wageningen) waren van dezelfde aard en aanvullend. Frans was er altijd op gespist dat ook niet-ingewijden het proefschrift moeten kunnen lezen. Chris heeft mij waardevolle experimentele data ter beschikking gesteld en samen hebben we een aantal zinnige experimenten uitgevoerd. Ik wil hen bedanken voor hun inzet en begeleiding.







Tijdens het schrijven van dit voorwoord keek ik even om en zag daar Ria, Wouter en Suzan. Het was een heel weerzien! Zij kenden alleen mijn rug nog. Ik heb hen dan ook op gepaste wijze bedankt voor alle geduld en stimulans, maar ook voor het medeleven als ik een hoofdstuk weer opnieuw schreef.

Max A. Hilhorst

*The desire to experiment, to know, often compels me to take a step which interrupts the continuity of my work – this of course because experiment fascinates me more than experience. Just as I prefer acquiring knowledge to knowledge itself.*

*Eduardo Chillida, Spanish sculptor.*

# CONTENTS

	<b>1. INTRODUCTION .....</b>	<b>1</b>
	1.1 GENERAL .....	1
	1.2 MEASUREMENT AND INTERPRETATION OF DIELECTRIC SOIL PROPERTIES .....	2
	1.3 AIMS AND OUTLINE OF THIS THESIS .....	5
	<b>2. THEORY ON DIELECTRIC PROPERTIES OF POROUS MATERIALS.....</b>	<b>7</b>
	2.1 INTRODUCTION TO DIELECTRIC POLARISATION AND RELAXATION .....	7
	2.2 RELATIONSHIP BETWEEN DIPOLAR RELAXATION AND SOIL MATRIC PRESSURE .....	11
	2.3 COUNTERION DIFFUSION POLARISATION.....	18
	2.4 MAXWELL-WAGNER EFFECT .....	21
	2.5 DEVELOPMENT OF A NEW DIELECTRIC MIXTURE EQUATION.....	27
	2.6 PERMITTIVITY OF SOIL.....	33
	<b>3. A NEW SENSOR FOR DIELECTRIC SOIL CHARACTERISATION.....</b>	<b>45</b>
	3.1 A GENERAL MODEL FOR DIELECTRIC SENSORS.....	46
	3.2 DESIGN OF AN INTEGRATED CIRCUIT FOR DIELECTRIC SENSORS.....	49
	3.3 GENERAL CONSIDERATIONS ON ELECTRODE DESIGN FOR DIELECTRIC SENSORS .....	63
	3.4 A NEW DIELECTRIC SENSOR.....	69
	<b>4. APPLICATIONS.....</b>	<b>73</b>
	4.1 DIELECTRIC SOIL WATER CONTENT MEASUREMENTS .....	73
	4.2 ELECTRICAL CONDUCTIVITY MEASUREMENTS OF THE SOIL SOLUTION.....	83
	4.3 FREQUENCY DEPENDENCY OF ELECTRICAL CONDUCTIVITY OF BULK SOIL .....	93
	4.4 DIELECTRIC CONTAMINATED SITE INVESTIGATION.....	95
	4.5 DIELECTRIC PROPERTIES OF SOIL ILLUSTRATED BY HARDENING CONCRETE .....	97
	<b>SUMMARY AND CONCLUSIONS .....</b>	<b>109</b>
	<b>SAMENVATTING EN CONCLUSIES.....</b>	<b>117</b>
	<b>REFERENCES.....</b>	<b>127</b>
	<b>LIST OF MAIN SYMBOLS.....</b>	<b>135</b>
	<b>CURRICULUM VITAE .....</b>	<b>141</b>





# 1. INTRODUCTION

## 1.1 GENERAL

The water molecule is one of the smallest, but also one of the most interesting molecules. Water plays an important role in nearly all aspects of soil and agricultural science. An optimum application of water and nutrients to the crop is essential for a healthy and cost-effective growth. Excessive use of water and over-fertilisation result in serious environmental problems, while sustainable cropping systems are characterised by a controlled use of resources. There is an increasing demand, therefore, for real-time techniques to measure soil water content and nutrients concentration in growing media. Special detection systems are required to investigate or monitor soil pollution in situ.

One promising measuring technique is based on the relationship between the dielectric properties of soil and its water and ion contents. These dielectric properties can be seen as the response of electrical soil properties to the application of an electric field. They can be determined by measuring the capacitance and conductance between two or more electrodes embedded in the soil. Such an electrically based measuring technique is ideally suited for automation.

The capacitance is a function of the dielectric constant. Compared with dry soil, the dielectric constant of water is high and dominates that of soil, enabling soil water content determinations by measuring the capacitance. The bulk electrical conductivity of a soil is a function of both its water content and the total dissolved solids. Knowing the water content and the bulk electrical conductivity of a soil its nutrient content can be derived.

Dielectric soil properties are frequency-dependent. This dependence is due to the soil texture and the various stages of water binding by the soil matrix. Consequently, it should be possible to derive information on the soil texture or the water-binding properties from the dielectric spectrum of soil.

The most important drawback for using the dielectric properties of soil is the complexity of the dielectric theory that describes the interaction between the soil water and the textural and compositional soil properties. This interaction involves a number of physical processes that are not well understood. Until now, no complete model is available that can describe the dielectric properties of soil. Calibration is another point of concern. The dielectric measuring technique is an indirect method. The output signals of a dielectric sensor must be related, i.e. calibrated, to soil parameters under well-defined conditions.

Finally, despite the growing availability of dielectric sensors for soil water content, there is still a need for low-cost, reliable and easy-to-use dielectric sensors for practical field applications. Apart from soil water content sensors, there are no dielectric sensors available for in-situ measuring the ionic conductivity of the soil solution, the soil matric pressure, or the soil texture. Full exploration of the dielectric measuring technique requires in-depth research.



## 1.2 MEASUREMENT AND INTERPRETATION OF DIELECTRIC SOIL PROPERTIES

Smith-Rose [1933] already showed the relationship between the dielectric properties of a soil and its water content. It was not possible to fully explore the possibilities of dielectric sensors mainly because of the lack of reliable and easy-to-use instrumentation. It took many years before this relationship became a basis for routine measurements of soil water content. During the last two decades, however, both the knowledge of dielectric soil properties and the availability of dielectric sensors have increased considerably.

To understand the impact of water and its ionic conductivity on the dielectric properties of soil, it is important to understand the interaction of electromagnetic (EM) waves with soil. Asymmetrically charged molecules, such as water, have permanent dipoles that line up in an external EM field. Atomic and electronic processes add to the polarisation of the material. The dielectric constant of a material is a measure of its polarisability and is a function of the applied frequency of the EM field. Because of the permanent dipole of the water molecule, the dielectric constant of water is very high (80). Dry soil is only polarisable by atomic and electronic polarisation, leading to a low dielectric constant ( $< 5$ ). This difference makes it possible to measure the amount of water in soil.

Most users do not understand the principles of dielectric sensors only this far. Many processes arising from dielectric absorption and ionic conduction at the surface of the soil particles, however, determine the dielectric properties of a soil as well. In fact, the dielectric constant of soil is not a constant, but varies with frequency, and depends on physical parameters such as soil texture, soil water content and type and concentration of ions in the soil solution. It is better to consider the dielectric constant as part of the complex permittivity which for bulk soil includes dielectric polarisation, dielectric absorption and ionic conduction phenomena. The permittivity can be derived from the impedance between two electrodes inserted into the soil. A common model for this impedance is that of a parallel connection of a capacitor and a conductor. The real part of the permittivity can be found from the capacitance, being a measure of dielectric polarisation. The imaginary part of the permittivity, which can be found from the conductance, is related to the electrical conductivity of the soil solution, which in turn is a measure of the sum of ionic conductivity and dielectric absorption.

Before using a dielectric sensor, the measured dielectric data should be related (calibrated) to the water content or the electrical conductivity of the soil involved. Such a calibration curve depends on the measuring frequency, soil type and soil density, and is only valid for one measuring frequency. When applying a calibration curve in the field, one should be aware that spatial variability of the soil composition and density cause a spread in the measurements.

Two basic measuring methods are in use for dielectric soil characterisation. Time Domain Reflectometry (TDR) which became popular in the eighties and Frequency Domain (FD) sensors which increased in popularity more recently.

TDR involves the measurement of the propagation velocity and attenuation of an electric step or pulse function applied to two or more electrodes placed in the soil. Such a signal contains a wide range of frequencies. Normally, the dominating frequencies are between 100 MHz and 1 GHz. The propagation velocity is a function of the capacitance between the electrodes. This velocity corresponds with the time needed for a signal to propagate along the electrodes and to reflect at the end of the line. This reflection time correlates with the dielectric soil properties and consequently with the soil water content. The speed



of the reflected wave is not only a function of the capacitance but also of the conductance between the electrodes. Thus, measurement errors may be expected if the electrical conductivity of the soil is unknown. However, this conductance corresponds with the attenuation and can be calculated from the amplitude of the signal applied and that of the reflected signal.

TDR is in fact a special form of Time Domain Spectroscopy (TDS). According to a historical review on TDS by Grant *et al.* [1978], this technique was already used in 1951 by Davidson, Auty and Cole. The objective of a TDS system is to observe the shape and size of the input and output pulses in the time domain, from which, the frequency response by means of a Fourier transformation can be calculated. In the middle of the sixties, Hewlett Packard developed equipment with a frequency response up to 12 GHz. At first, mainly electronics engineers used this equipment. It took until 1969 before Fellner-Feldegg [1969] introduced TDS into the field of liquid dielectrics. In the early seventies, it was already possible to deal with conductive solutions. In my opinion, this early work might have been valuable in speeding up the introduction of TDR in soil science, but I have not been able to find extensive references to this early work in recent work.

Davis [1975] proposed the use of TDR for measuring soil water content. Only after Topp *et al.* [1980] had published their calibration data, however, the potential of TDR for soil science was recognised and adopted by many scientists. The availability of cable testers made by Tektronix and other manufacturers facilitated the introduction of TDR. Later instrumentation became available tailored to water content measurements from Soilmoisture Equipment Corporation, which still needed graphical interpretation of the reflected waveforms. The automated interpretation of the waveforms made TDR more user-friendly [Heimovaara, 1993]. Sensors designed by IMKO [1991] use the propagation time of an impulse. This technique allowed for simpler and pure electronic detection of the reflected impulses.

With the help of a Fourier transform, it is possible to perform TDR measurements with network analysers. For this purpose precise and high-level analysers are commercially available, e.g. Hewlett Packard and Rohde & Schwarz. The other way around is the use of TDR for analysis in the frequency domain as described by Heimovaara [1993] and references reviewed by Grant *et al.* [1978].

In general, TDR instrumentation can be accurate but is expensive, requires skilled operators and is not well suited for use in agricultural practice. Still, TDR is widely used as a research tool for soil water content measurements, is well evaluated, whereas much literature is available on its principle, calibration and practical use [e.g. Topp *et al.*, 1982 or Whalley, 1993]. The work on TDR improved the knowledge of the dielectric behaviour of soil. The main disadvantages are the complexity of the data analyses and the price in mass production, which are serious obstacles for the application of dielectric sensor technology for e.g. automatic irrigation of a greenhouse or a grassland.

FD techniques are characterised by the application of a single sine wave. The capacitance and conductance can be calculated from the impedance measured between the two electrodes. Also, this impedance can be determined from the signal reflected at the soil surface. Most FD techniques are invasive. Remote Sensing (RS) by means of satellites, aeroplanes or radar installations, however, is a non-invasive FD technique. RS uses the interaction of EM waves with the earth surface and requires no contact with the soil. This interaction was firstly recognised by pioneers in radio science at the beginning of this century. Later, RS attracted the attention of soil scientists to the dielectric behaviour of soil. With RS, the reflection and absorption of EM waves between 1 GHz and 10 GHz are a measure of the dielectric



properties of the earth surface. The most important frequency range for RS is between 1 GHz and 10 GHz. Since EM waves are absorbed into the soil, examination of only a relatively thin upper layer of the soil is possible. In-depth knowledge of the dielectric properties of soils is indispensable for the interpretation of the data [De Loor, 1990]. Instrumentation is needed to verify in situ the dielectric soil properties found..

Probably, the oldest invasive FD instrument is the impedance bridge. The complex impedance (capacitance and conductance) is measured between two or more electrodes placed in the soil. The bridge must be balanced with reference impedances for the frequency involved. The frequency range used was normally less than 100 MHz. Ferguson [1953] reviewed a number of impedance bridges. Until now, a reliable impedance measurement at a high electrical conductivity was only possible with the help of vector voltmeters or advanced and expensive network analysers [Grant *et al.*, 1978; Nyfors & Vainikainen, 1989; Jenkins *et al.*, 1990]. Network analysers are used in the laboratory. They are not well suited for field work and require a skilled operator.

In other fields of dielectric material research, important improvements were made in the late eighties. High-quality dielectric spectrum analysers became commercially available, including measuring cells (special electrode configurations). These FD instruments, available from e.g. Hewlett Packard and Solartron, are applicable at frequencies from less than 1 Hz to over 10 GHz and helped to improve our general knowledge on dielectrics considerably.

Simple sensors intended for agricultural practice, use the shift in the resonance frequency of an oscillator [Babb, 1951; Turski & Malicki, 1974; Wobschall, 1978; Heathman, 1993]. A common problem with most of these commercially available FD sensors is their sensitivity to the electrical conductivity of the soil, mainly because of the lack of electric length compensation. The length of the electrodes and wiring cause measurement errors depending on the electrical conductivity. Phase errors introduced by the limited frequency bandwidth of the active part of the input circuitry (usually an LC oscillator) are generally underestimated, as well. The sensor developed by Hilhorst [1984] had special conductivity and electrical length compensation circuitry. A large number of prototypes operating between 10 MHz and 20 MHz found their way into the Dutch agricultural research community. They showed promising results [Halbertsma *et al.*, 1987; Van Dam *et al.*, 1990; Hilhorst *et al.*, 1992]. This sensor was not suited for mass production, and never emerged from the prototype phase. After 1995, field instrumentation became available based on standing wave or reflection coefficient measuring techniques. These methods are less sensitive to electromagnetic interference than resonance frequency techniques. An example is the "Theta probe", a sensor made by Delta-T [1995] measuring only water content. Vitel [1995] made a sensor for measuring the water content as well as the electrical conductivity of bulk soil. Both are suitable for relative low-conductive soils ( $< 0.1 \text{ S m}^{-1}$ ). They both have an analogue output. This might be seen as a drawback. However, in spite of the modern digital control and data storage equipment, most data loggers for horticultural applications still have analogue inputs. A supplied calibration plot converts the output voltage to soil water content.

The above mentioned FD and TDR instrumentation is either not accurate or intended for laboratory use only. They are not well suited for mass production and require skilled operators. This is a serious obstacle to a broader use of the dielectric measuring technique.



### 1.3 AIMS AND OUTLINE OF THIS THESIS

In agricultural practice, the measurement of soil water content is the main application of dielectric sensing techniques. This in spite of the possibility to measure also the electrical conductivity of the soil solution, the soil water potential and the soil texture. The aim of this study is threefold:

- to increase the theoretical knowledge of the dielectric behaviour of soil (Chapter 2);
- to develop a low-cost and simple to use dielectric sensor (Chapter 3); and
- to demonstrate the potential of dielectric soil characterisation (Chapter 4).

One of the objectives is to provide the reader with sufficient background and new instrumentation for a more effective exploration of the potentials of dielectric characterisation of soil.

Chapter 2 covers the most important aspects of the theory on dielectrics for soil science. A review of the impact of water on the dielectric properties of soil is given. Some parts of the general theory on dielectrics are applied to soil and supplemented by the author with missing parts. The frequency dependence of soil dielectric properties is analysed. The impact of soil texture on the Maxwell-Wagner effect is described. Also the impact of the matric potential on the frequency dependence of the dielectric properties of soil is analysed and compared with data found in the literature. A new mixing equation will be developed and compared with some of the existing equations. *The result is a theoretical model that can predict the dielectric properties of soil as a function of frequency, water content, matric pressure and porosity.*

Chapter 3 concerns the development of a new FD sensor that facilitates dielectric measurements in the field. *The core of this sensor is an Application Specific Integrated Circuit (ASIC) containing most of the electronics.* Problems associated with the design of the ASIC are highlighted. The principles chosen for the design are described. A version of the final sensor is developed for a measuring frequency of 20 MHz. A functional model is described for simulating this new FD sensor starting from the impedance at the input, up to the data processing in the software. This chapter also deals briefly with the problems associated with electrode contact, length and measuring volume. Some validation results using known dielectrics are given.

Chapter 4 illustrates the applicability of the theory using the new FD sensor as well as TDR. Calibration curves found for TDR, for the FD sensor and for those predicted using the theoretical model developed in Chapter 2 will be compared. *Next, the relationship between both the electrical permittivity and conductivity of the bulk soil and the electrical conductivity of the soil solution is derived and tested.* The frequency dependence of the electrical conductivity of the bulk soil is described by the Maxwell-Wagner effect. Furthermore, changes in the chemical composition in case of soil pollution will be detected using simultaneous measurements of the real and imaginary parts of the permittivity. The dielectric properties of hydrating concrete will be related to the development of compressive strength. Finally, some aspects of the dielectric behaviour of soil will be illustrated by a comparison with the hydration process of concrete.







## 2. THEORY ON DIELECTRIC PROPERTIES OF POROUS MATERIALS

### 2.1 INTRODUCTION TO DIELECTRIC POLARISATION AND RELAXATION

Polar molecules, such as water, are asymmetrically charged and possess a permanent dipole moment. A water molecule may be modelled roughly as a positive and negative point charge separated by a certain distance. On a microscopic scale, each charge imposes its own electric field resulting in forces on its neighbours. Positive charges will attract negative charges, while charges of equal sign will repel. In an electric field, polar molecules tend to line up in the direction of the field and become further polarised. The resultant electric field is the vector sum of all individual electric fields. In equilibrium and without any external electric field, the total electric field strength on a macroscopic scale is zero. This is only true if the dipoles are randomly oriented. Application of an external electric field will disturb this random orientation. The dipoles tend to line up and the material becomes polarised. Charge will move a little from one point to another causing an electric current to flow. This current can be measured externally and is a measure of the ability to polarise the material. After some time the material will find a new equilibrium. Energy is stored. Polar molecules are fluctuating continuously due to thermal energy. This random process tends to neutralise the external electric field. After removing the applied electric field, the stored energy dissipates within a certain time. This process is called dielectric relaxation.

The process of dielectric polarisation and relaxation will be treated briefly in this chapter. For a more comprehensive treatment of dielectric polarisation, the reader is referred to textbooks such as Hasted [1973], Grand [1978] and references therein. For more details on the theory on electromagnetic (EM) fields and waves, one is referred to Lorrain [1988].

Magnetic properties of a material will also affect its dielectric properties. Soils in general are non-magnetic. Although some rare soils exhibit magnetic properties, the impact on the dielectric behaviour of soil will not be discussed in this section.

#### **Polarisation and permittivity**

Consider a capacitor formed by two metal plates. The application of an electric potential will charge the plates. The electric field in a point of space between the plates is a situation evoked by the presence of the charges on the plates. Bring a charge,  $Q$ , in between the two plates. The electric field ( $E$ -field) between the plates will result in a force acting on that charge. The  $E$ -field and the resulting force acting on the charge are vector quantities. The force vector,  $\underline{F}$ , is related to the  $E$ -field vector,  $\underline{E}$ , by

$$\underline{F} = Q\underline{E} \quad (2.1)$$



The force between two point charges,  $Q_1$  and  $Q_2$ , in a homogeneous medium which extends to distances much greater than the distance between the two point charges,  $d$ , is given by Coulomb's law:

$$F = \frac{Q_1 Q_2}{4\pi\epsilon_0\epsilon_r d^2} \underline{r}_{1,2} \quad (2.2)$$

where  $\epsilon_0 = 8.854 \cdot 10^{-12} \text{ F m}^{-1}$  is the permittivity of free space,  $\epsilon_r$  the dimensionless relative permittivity of a material with respect to that of free space and the unit vector  $\underline{r}_{1,2}$  points from  $Q_1$  to  $Q_2$ .  $F$  is repulsive if the two charges have the same sign, and attractive if they have different signs. The charges are measured in coulombs, the force in Newtons and the distance in meters. The product  $\epsilon_0\epsilon_r$  is termed the absolute permittivity of a medium.

As explained, when we bring soil in between the two plates of a capacitor, forces will act on the charged molecules (dipoles) and particles. They orient themselves in the  $E$ -field, and the soil becomes polarised. However, spontaneous fluctuations of the molecules tend to randomise this alignment. The process of random fluctuations of the molecules, due to thermal energy, is known as the Brownian motion. Eventually, a dynamic equilibrium is established among the molecules as a result of the two effects.  $\epsilon_r$  is a measure of the competition between these two effects; i.e. a measure of polarisability.

The polarisation of permanent dipoles with and without the application of an external  $E$ -field is illustrated in Figure 2.1.

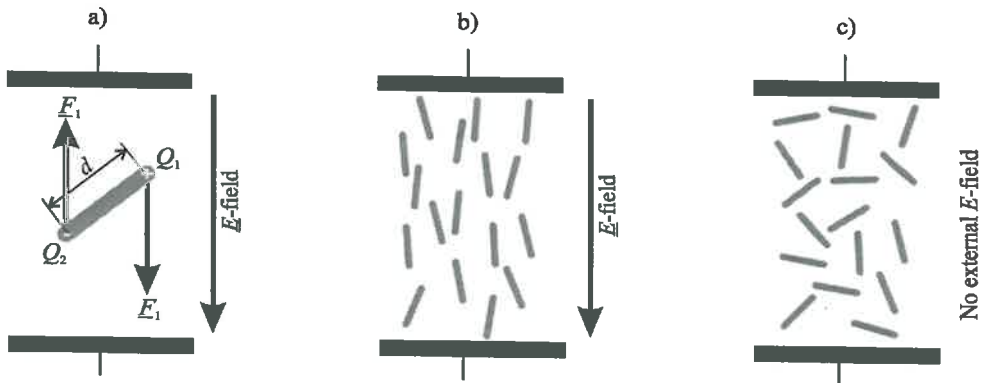


Figure 2.1. a) Polarisation of a dipole in an EM field between two plates of a capacitor. The forces  $F_1$  and  $F_2$ , acting on the two charge centres  $Q_1$  and  $Q_2$  with distance  $d$ , are the result of the application of an electric field  $E$  on the dipole.  
 b) An ensemble of aligned dipoles.  
 c) The ensemble of dipoles after it has experienced Brownian motion.

### Frequency dependence of permittivity

The  $E$ -field can be either static or alternating with frequency  $f$ . For non-polar materials dielectric polarisation is only due to displacement of electron clouds or a change of the distance between charged atoms (ions), accompanied by resonant phenomena occurring at frequencies in the far infrared region, at about 3 THz - 100 THz and above. This type of





polarisation on an atomic level is also called distortion polarisation. At  $f < 10$  GHz, these polarisation mechanisms are almost without losses, independent of frequency and temperature. For polar materials, the dipolar polarisation adds to the distortion polarisation.

After removing an  $E$ -field, the induced energy will be dissipated within a certain time. By applying an alternating field, energy will be stored and/or absorbed depending on the frequency applied. This frequency dependence of the polarisation process can be described by a complex representation of the relative permittivity  $\epsilon_r$ . *In this thesis the complex relative permittivity will be referred to as permittivity, denoted with  $\epsilon$ , only.* The permittivity is defined as

$$\epsilon = \epsilon' - j\epsilon'' \quad (2.3)$$

where the real part of the permittivity,  $\epsilon'$ , is a measure of the total polarisability, including non-polar and dipolar polarisation of the material constituents. For a static  $E$ -field is  $\epsilon'$  usually referred to as dielectric constant. The dielectric constant of materials is always higher than that of free space.

The imaginary part of the permittivity,  $\epsilon''$ , represents the total energy absorption or energy loss. The energy losses include dielectric loss,  $\epsilon''_d$ , and loss by ionic conduction [e.g. Hasted, 1973]:

$$\epsilon'' = \epsilon''_d + \frac{\sigma}{2\pi\epsilon_0 f} \quad (2.4)$$

where  $\sigma$  is the ionic conductivity of the water in the soil pores and  $f$  the frequency of the  $E$ -field applied. In soil science it is not customary to use  $\epsilon''$  as given in (2.4). More practical is the specific electrical conductivity of the pore water,  $\sigma_w$ , which can be defined as

$$\sigma_w = 2\pi f \epsilon''_w \epsilon_0 \quad (2.5)$$

where  $\epsilon''_w$  is the imaginary part of the permittivity of water. (Often in soil science this electrical conductivity is referred to as  $EC$ ).  $\sigma_w$  includes dielectric losses. If dielectric losses are negligible  $\sigma_w$  approximates the specific ionic conductivity,  $\sigma$ , i.e.  $\sigma_w \approx \sigma$ . The specific electrical conductivity of the bulk soil,  $\sigma_b$ , is approximately proportional to  $\sigma_w$  and to a function of the soil water content,  $g(\theta)$ , i.e.  $\sigma_b = \sigma_w g(\theta) \approx \sigma g(\theta)$ . The dimensionless soil water content is denoted by  $\theta$ , and defined as the volume fraction of water in the soil also called volumetric water content.

The reorientation of polar molecules in an alternating  $E$ -field is not instantaneous. This phenomenon will be treated in more detail for water in Section 2.2. At very low frequencies the permittivity of water,  $\epsilon_w$ , approaches the dielectric constant of water,  $\epsilon_{wf \rightarrow 0}$ , in a static  $E$ -field. With increasing frequency the water molecules become too slow to follow the fast alternating electric field. The polarisability will decrease and the energy applied will be absorbed. For  $f \rightarrow \infty$  the permittivity of water will decrease to  $\epsilon_{wf \rightarrow \infty}$ , a value for the polarisation at atomic level. For the dry solid material in soil, polarisation consists only of distortion polarisation. The permittivity of dry soil is less than 5. Dipole polarisation and polarisation at atomic level are additive. At room temperature and low frequencies,  $\epsilon_w \approx 80$ . Thus,  $\epsilon$  of soil is dominated by the soil water content, allowing its measurement using soil dielectric properties. In Figure 2.2 a qualitative illustration is given of the interaction of EM waves with water. The impact of EM waves on  $\epsilon'$  and  $\epsilon''$  as a function of frequency is shown.

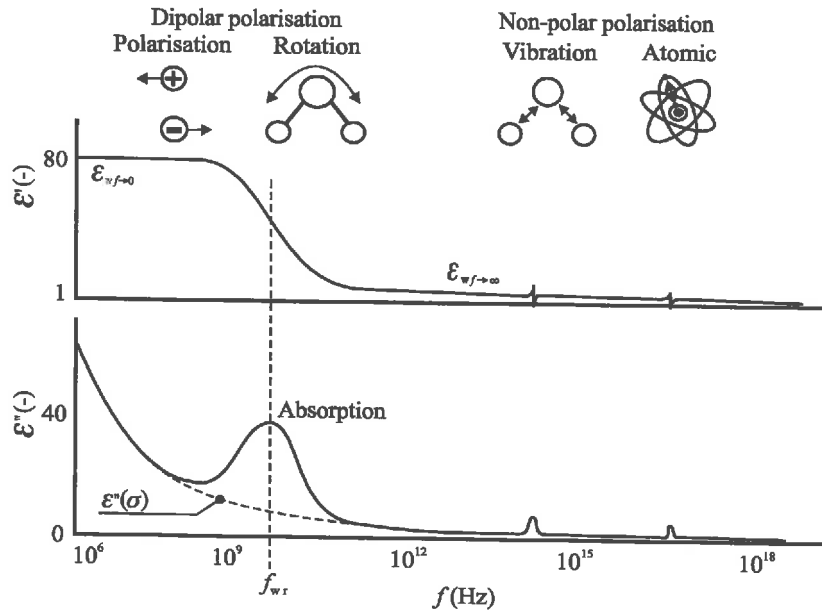


Figure 2.2. A qualitative representation of EM wave interactions with water, showing the real and imaginary part of the permittivity,  $\epsilon'$  and  $\epsilon''$ , as a function of frequency  $f$ . At the low-frequency end, dipolar polarisation is dominant, at the high-frequency end, distortion polarisation is dominating. The dielectric absorption peak of water is added to the dashed absorption line due to ionic conduction with a maximum at the relaxation frequency of water,  $f_{wr}$ .

### Debye relaxation function

The electrical complex permittivity,  $\epsilon$ , of a polar substance as expressed by (2.3), is frequency-dependent. The frequency dependence for a single relaxation process, according to experimental results of Kaatz & Uhlendorf [1996], is best described by the Debye [1929] relaxation function

$$\epsilon = \epsilon' - j\epsilon'' = \frac{\Delta\epsilon}{1 + jf/f_r} + \epsilon_{f \rightarrow \infty} \quad (2.6)$$

where  $f_r$  is called the relaxation frequency of the material and  $\Delta\epsilon = (\epsilon_{f \rightarrow 0} - \epsilon_{f \rightarrow \infty})$  the dielectric increment or difference between polarisation in a static  $E$ -field,  $\epsilon_{f \rightarrow 0}$ , and distortion polarisation,  $\epsilon_{f \rightarrow \infty}$ . From (2.4) and (2.6) it can be shown that the real and imaginary parts of (2.3) are

$$\epsilon' = \frac{\Delta\epsilon}{1 + (f/f_r)^2} + \epsilon_{f \rightarrow \infty} \quad (2.7)$$

and

$$\epsilon'' = \frac{\Delta\epsilon(f/f_r)}{1 + (f/f_r)^2} + \frac{\sigma}{2\pi\epsilon_0 f} \quad (2.8)$$



At the relaxation frequency, the real part of the permittivity,  $\epsilon'$ , is decreased to half its dielectric increment; i.e.  $\epsilon' = \epsilon_{f \rightarrow \infty} + (\Delta\epsilon / 2)$ . The imaginary part of the permittivity,  $\epsilon''$ , reaches its maximum for the relaxation frequency; i.e. with  $\sigma = 0$  the dielectric loss is  $\epsilon''_d = \Delta\epsilon / 2$ .

In Figure 2.3,  $\epsilon'$  and  $\epsilon''$  are plotted according to (2.7) and (2.8) for pure water. According to Kaatze [1996], the Debye parameters at 0 °C for ice are  $\epsilon_{ice f \rightarrow 0} = 92$ ,  $\epsilon_{ice f \rightarrow \infty} = 3.17$ ,  $f_{ice r} = 9$  kHz and for water at the same temperature  $\epsilon_{w f \rightarrow 0} = 88$ ,  $\epsilon_{w f \rightarrow \infty} = 5.2$ , and  $f_{w r} = 9$  GHz. For water  $\epsilon''_w$  is given for  $\sigma = 0.1 \text{ S m}^{-1}$  and  $\sigma = 0 \text{ S m}^{-1}$ . For more details on the dielectric properties of water, see Kaatze [1996] and references therein.

Basic aspects of dielectric polarisation of materials have been presented. The theory is applied to water (i.e. free water). In soil, however, the energy status of the water bound to the solid phase differs from that of free water. In the next sections the impact of bound water on the dielectric properties of soil and several other aspects of dielectric polarisation of soil will be explained.

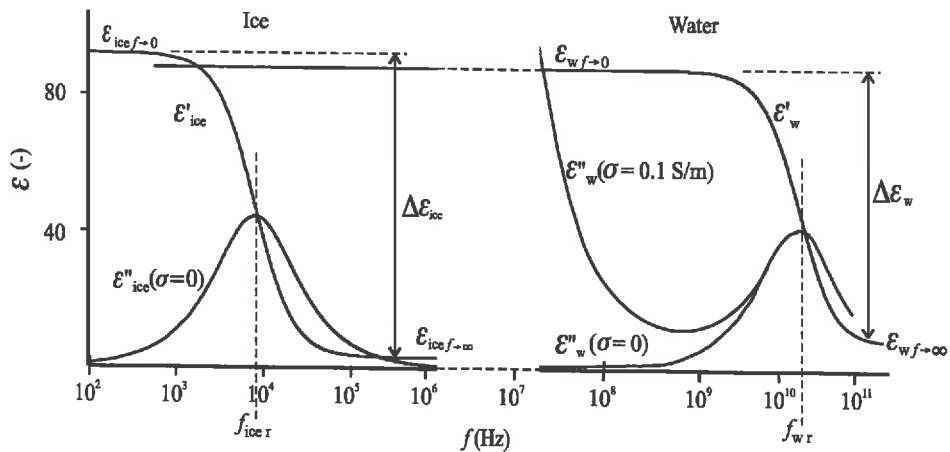


Figure 2.3. The real and imaginary parts of the permittivity for ice,  $\epsilon'_{ice}$  and  $\epsilon''_{ice}$ , and for water,  $\epsilon'_w$  and  $\epsilon''_w$ , at radio frequencies and 0 °C according to the Debye relaxation function. The absorption term  $\epsilon''_w$  is shown for an ionic conductivity  $\sigma = 0.1 \text{ S m}^{-1}$  and  $\sigma = 0 \text{ S m}^{-1}$  [Kaatze, 1996]. The relaxation frequency for ice,  $f_{ice r}$ , and water,  $f_{w r}$ , are 9 kHz and 9 GHz respectively.  $f \rightarrow 0$  denotes permittivity values for  $f \ll f_r$ ,  $f \rightarrow \infty$  those for  $f \gg f_r$ . The dielectric increment is denoted by  $\Delta\epsilon$ .

## 2.2 RELATIONSHIP BETWEEN DIPOLAR RELAXATION AND SOIL MATRIC PRESSURE

Two important factors that determine the frequency dependence of the dielectric permittivity of soil are the intermolecular bonds between water molecules and the bonds between water molecules and soil particles. In this section I will derive a relationship will between water-binding properties of soil and its dielectric properties.



Soil is a three-phase system consisting of solid particles, water and air. The solid phase forming the pore system is called the soil matrix. Water can be bound to the soil matrix. The degree of binding varies from unbound or free water at a great distance from the surface, to heavily bound or adsorbed water. According to Koorevaar *et al.* [1983] water is bound to the soil matrix by a combination of:

- adhesive forces: binding between the solid phase and water molecules,
- cohesive forces: binding between water molecules, and
- osmotic forces: binding due to gradients in chemical potentials in electric double layers [Bolt & Miller, 1958; Raythatha & Sen, 1986].

Water-binding properties of a soil matrix can be described using its thermodynamic properties [Slatyer, 1967]. If water becomes bound to the soil matrix, it is not capable of doing as much work as free water, hence it has lost energy. Similarly, a mix of water and cement or gypsum will generate heat during the process of hydration. This is an extreme example of the loss of energy for bound water analogous to the binding of water in soil.

### Potential of soil water

The energy status of soil water is given by the difference in Gibbs' free energy between its ground or reference state (free water) and its actual state (bound water). It is simply called the total water potential  $\psi_t$ . Under thermodynamic equilibrium conditions,  $\psi_t$  represents the amount of energy per unit mass ( $\text{J kg}^{-1}$ ) that is needed to transport, reversibly and isothermally, an infinitesimal quantity of water, from a pool of pure water, at atmospheric pressure  $p_0 = 0.1 \text{ MPa}$ , at a temperature of  $20^\circ\text{C}$  and at specified elevation, to the soil water at the point under consideration. Total potential  $\psi_t$  is the summation of pneumatic, gravitational, matric and osmotic potential [Koorevaar *et al.*, 1983; ISO/TC, 1996].

For a small soil sample under equilibrium conditions, the pneumatic and gravitational potentials can be neglected. The osmotic potential of the equilibrium soil solution is considered the same everywhere and thus will not cause water binding to the soil matrix. However, gradients in osmotic potential in an electric double layer (for instance around clay platelets) results in osmotic forces causing water to adhere to the soil matrix. This kind of water binding is included in the matric potential,  $\psi_m$ . The matric potential represents thus all forces that retain water to the soil matrix. If the density of water,  $\rho_w$ , is constant the soil matric potential can be expressed as a pressure. This pressure equivalent of the soil matric potential,  $p_m$ , is defined as the amount of energy per unit volume ( $\text{J m}^{-3}$  or Pa); it is related to  $\psi_m$  as  $p_m = \rho_w \psi_m$ .

If soil is exposed to air, it will dry or wet, until a thermodynamic equilibrium is reached, depending on the potentials on both sides of the liquid-vapour interface.  $p_m$  is related to the relative humidity of air,  $e/e_s$ , by [e.g. Slatyer, 1967]

$$p_m = \frac{RT}{V} \ln(e/e_s) \quad (2.9)$$

where  $T$  is the absolute temperature,  $R$  the universal gas constant and  $V$  the partial molar volume of water. The relative humidity of air is the ratio between the vapour pressure,  $e$ , and the saturation vapour pressure,  $e_s$ , of water at temperature  $T$ .

Dirksen & Dasberg [1993] showed for a broad range of soil types only a small difference between the water content calculated for the first layer of water molecules on the particle surface, and the water content measured for air-dry soil samples. In the experiment



of Dirksen & Dasberg  $e/e_s \approx 0.50$ , corresponding with  $p_m = -100$  MPa. This hygroscopic water content,  $\theta_h$ , is a function of the specific surface area,  $S_A$ , of the soil matrix.  $S_A$  and consequently  $\theta_h$  increase with increasing silt or clay content. For the experiment of Dirksen & Dasberg,  $\theta_h$  varied between 0.02 for sandy soils with low  $S_A$ , and 0.12 for a Vertisol and a Bentonite with high  $S_A$ . For this thesis,  $\theta_h$  will be defined as the water content adsorbed to soil at ambient conditions with  $e/e_s = 0.50$ .

The two limits for  $p_m$  between which a monomolecular layer of water can exist depends to a large extent on the mineral composition of the soil particles [De Boer, 1953]. The lower limit is where the first layer of adsorbed water will escape from the particle surface. A soil is assumed to be completely dry if this layer of water molecules is removed using the oven-dry method at 105 °C. The upper limit for  $p_m$  for which the number of water layers starts to increase, depends on the particle material and according to the foregoing may be assumed  $p_m > -100$  MPa.

The highest value of  $p_m$ ,  $p_m = 0$  MPa, applies to a soil saturated with water. No energy is needed to add or remove water at great distance from a soil particle surface. Note that in soil physics the atmospheric pressure,  $p_0$ , is taken as reference for the matric pressure. Thus,  $p_m = 0$  MPa corresponds with the matric pressure at  $p_0 = 0.1$  MPa.

### The relationship between soil matric pressure and dielectric relaxation

To derive a relationship between the dielectric properties of soil and the soil matric pressure,  $p_m$ , some assumptions have to be made. According to data of Hasted [1973], the permittivity of water and ice at the same temperature are approximately equal at the two extremes of the frequency spectrum:  $\epsilon_{wf \rightarrow 0} \approx \epsilon_{ice f \rightarrow 0}$  and  $\epsilon_{wf \rightarrow \infty} \approx \epsilon_{ice f \rightarrow \infty}$ . Therefore, both  $\epsilon_{wf \rightarrow 0}$  and  $\epsilon_{wf \rightarrow \infty}$  will be treated as constants independent of the binding state or dielectric relaxation of the water.

Comparison of the thermodynamic properties of water with those of other liquids, suggests that hydrogen bonds greatly affect the properties of water [Eisenberg & Kauzmann, 1969]. The cohesive forces between water molecules are extraordinarily strong. The most likely cause is the hydrogen bonding between molecules in the liquid. In soil a water molecule is also bound to the particle surfaces by one or more hydrogen bonds. Hydrogen bonds prevent molecules from reorienting in a fast changing electromagnetic field. As can be deduced from the kinetic rate theory [Glasstone *et al.*, 1941], the relaxation frequency,  $f_r$ , is related to the probability of making or breaking hydrogen bonds during the time  $\tau = 1/(2\pi f_r)$  of one period. According to this theory, the dielectric relaxation frequency for water is given by

$$f_r = \frac{kT}{2\pi h} e^{-\frac{\Delta G^*}{RT}} \quad (2.10)$$

where  $\Delta G^*$  is the change in molar Gibbs' free energy required to break an OH...O bond,  $h$  is Planck's constant,  $k$  is Boltzmann's constant,  $T$  is the absolute temperature and  $R$  the universal gas constant. When a molecular bond is broken, it is almost immediately followed by the creation of a new bond.

The Gibbs' function is defined as  $G = H - TS$ , where  $H$  is the enthalpy,  $S$  the entropy and  $T$  the absolute temperature. Thus,  $\Delta G^* = \Delta H^* - T\Delta S^*$  where  $\Delta H^*$  is the molar activation enthalpy and  $\Delta S^*$  the molar activation entropy. According to Kaatze & Uhlendorf [1981] and



Grant [1978], the weak temperature dependency of  $\Delta H^*$  and  $\Delta S^*$  is negligible between  $-5^\circ\text{C}$  and  $60^\circ\text{C}$ . For liquid water,  $\Delta S^*$  is approximately independent of the binding forces. Thus,  $\Delta H^*$  corresponds approximately with the energy required to make or break a hydrogen bond. Expression (2.10) may be rewritten in terms of activation enthalpy

$$f_r \approx \frac{kT}{2\pi h} e^{-\frac{\Delta H^*}{RT}} \quad (2.11)$$

In the following, the subscript 0 denotes values for free water at a reference atmospheric pressure  $p_0 = 0.1\text{ MPa}$  and  $20^\circ\text{C}$ , while values without this subscript refer to molecules experiencing a certain level of binding force at the same temperature.

Any binding force acting on a water molecule will add to  $\Delta G^*$ , i.e.  $\Delta G^* > \Delta G^*_0$ . From (2.10) or its approximation of (2.11) the ratio between  $f_r$  and  $f_{r0}$  becomes

$$\frac{f_r}{f_{r0}} = e^{\frac{\Delta G^*_0 - \Delta G^*}{RT}} \approx e^{\frac{\Delta H^*_0 - \Delta H^*}{RT}} \quad (2.12)$$

The difference  $(\Delta G^*_0 - \Delta G^*)$  can be related to the soil matric pressure,  $p_m$ . Consider a water molecule located exactly at the vapour-liquid interface anywhere in the matrix.  $p_m$  is related to the difference between the chemical potential or partial molar free enthalpy of the water molecule in the reference state,  $\mu_0$ , and its actual potential  $\mu$ , by [Slatyer, 1967],

$$p_m V = \mu_0 - \mu \quad (2.13)$$

where  $V$  is the partial molar volume of water. It is shown in textbooks on thermodynamics [e.g. Harrison, 1963 or Roos & Wollants, 1995] that the chemical potential,  $\mu$ , of a pure substance is equivalent to  $\Delta G^*$ ; i.e.

$$p_m V = \Delta G^*_0 - \Delta G^* \quad (2.14)$$

I assume the water at the location under consideration to be pure. Then  $p_m V$  may be substituted in (2.12) and the relationship between  $f_r$  and  $p_m$  becomes

$$f_r = f_{r0} e^{\frac{p_m V}{RT}} \quad (2.15)$$

As  $p_m$  is defined at the liquid surface, (2.15) applies only to molecules at the vapour-liquid interface.

Consider a water molecule located at the vapour-liquid interface somewhere in the soil matrix. The impact of  $p_m$ , and thus of  $\Delta G^*$  on  $f_r$  for the molecule at this location can be found from (2.15). If this interface is displaced, by adding water to the soil matrix,  $p_m$  and  $(\Delta G^*_0 - \Delta G^*)$  will increase (they become less negative). For a molecule at the new location  $\Delta G^*$  and  $f_r$  are closer to values for free water. However,  $\Delta G^*$  and therefore  $f_r$  for the molecule at the first location is not changed since the force fields acting on this molecule are still the same. This suggests that a relationship exists between the Debye relaxation function as given by (2.6) and the soil water retention characteristic. With (2.15) substituted in (2.6) the permittivity,  $\epsilon$ , as a function of frequency,  $f$ , can be calculated for each stage of water binding individually. The advantage of (2.15) is that it relates dielectric properties to the energy status of soil water in terms very common in soil physics. In Sections 2.4 and 2.5 it





will be shown how (2.15) can be used to calculate a dielectric spectrum from a soil water retention characteristic, and vice versa.

### Relaxation frequency for a monomolecular water layer at a soil particle surface

For a monolayer of water molecules, there will not be much spread in relaxation frequency,  $f_r$ . With  $e/e_s = 0.5$  and using (2.9) and (2.15),  $f_r \approx 8$  GHz for the hygroscopic water in the experiments of Dirksen & Dasberg [1993]. The measurements of Dirksen & Dasberg [1993] are carried out by means of TDR, for which the dominant measuring frequency is around 150 MHz. They found a reasonable match for most soils between the expected effect on the permittivity due to the hygroscopic water content,  $\theta_h$ , and the measurements. From this it may be concluded that for hygroscopic water  $f_r < 150$  MHz is more realistic. Hoekstra & Delaney [1974] showed that for a low-conductive Goodrich clay there was almost no decrease in permittivity for frequencies between 10 MHz and 100 MHz and a continuously declining permittivity for 100 MHz and higher. From this it is even more likely that  $f_r < 10$  MHz.

### Comparison with data found in literature

Data found in the literature and interpreted by me, can be compared with the relationship between relaxation frequency and soil matric pressure as derived in this section. Table 2.1 gives an overview of the data found for the activation enthalpy,  $\Delta H^*$ , the relaxation frequency,  $f_r$ , and the soil matric pressure,  $p_m$ . A number of points are found that correspond with (2.9), (2.11) or (2.15). The curves for  $f_r$  and  $p_m$  are shown as a function of  $\Delta H^*$  in Figure 2.4. The following observation can be made:

1. Kaatz & Uhlendorf [1978] found  $\Delta H^*_0 = 20.5$  kJ mol<sup>-1</sup> and  $f_{r0} = 17$  GHz for free water at 20 °C and atmospheric pressure. Free water corresponds with the very last fraction of water for which  $p_m \approx 0$ , needed to saturate the soil. Dirksen & Dasberg [1993] showed that for soil a monomolecular layer of water exists at  $e/e_s \approx 0.50$ . According to (2.9)  $e/e_s = 0.50$  corresponds to  $p_m = -100$  MPa for which  $f_r = 8$  GHz according to (2.15).
2. Hoekstra & Doyle [1971] found for water adsorbed to Na-montmorillonite and  $\gamma$ -alumina a dielectric dispersion at a frequency of about 1 GHz.  $\Delta H^*$  was 25 kJ mol<sup>-1</sup> at a temperature in the range of -15 °C to -50 °C. According to (2.11)  $f_r = 1$  GHz for  $\Delta H^* = 25$  kJ mol<sup>-1</sup> at 0 °C, which is close to their result.
3. Rolland & Bernard [1951] found  $\Delta H^* \approx 52.5$  kJ mol<sup>-1</sup> for water adsorbed to silica gel (approximately one layer). It is known that for silicagel a temperature of over 120 °C is needed to dry it completely. This corresponds to  $f_r \approx 10$  kHz and  $p_m \approx -2 \cdot 10^3$  MPa at 20 °C according to (2.9) and (2.15), respectively.
4. Hasted [1973] found  $\Delta H^* = 55$  kJ mol<sup>-1</sup> with  $f_r = 9$  kHz for ordinary ice at 0 °C. A soil is assumed to be completely dry if the first, ice-like layer of water molecules is removed from the particle surface, using the oven-dry method at 105 °C. It may be assumed that this water layer has  $\Delta H^* \approx 55$  kJ mol<sup>-1</sup>, corresponding to  $f_r \approx 10$  kHz and  $p_m \approx -2 \cdot 10^3$  MPa at 20 °C according to (2.9) and (2.15), respectively.
5. For water adsorbed to settled concrete, most of the literature [Breugel, 1991] shows values between 40 kJ mol<sup>-1</sup> and 60 kJ mol<sup>-1</sup>. A temperature of >1000 °C is needed to remove water from concrete.



6. Iwata [1995] reported for water bound to the surface of clay  $\Delta H^* > 55 \text{ kJ mol}^{-1}$  and consequently from (2.9)  $f_r < 10 \text{ kHz}$ . For some clays a temperature of more than  $400 \text{ }^\circ\text{C}$  is needed to remove all the water. One may expect that not all the water is removed from soil using the oven-dry method at  $105 \text{ }^\circ\text{C}$ . The remaining water fraction is usually assumed to be part of the soil matrix.

Table 2.1. Data found in literature and interpreted by the present author. These data make the relationship between soil matric pressure and dielectric relaxation plausible. All data are given for a temperature of  $20 \text{ }^\circ\text{C}$  and presented in order of increasing  $\Delta H^*$ .

Reference	Type of water binding	Activation enthalpy $\Delta H^*$ ( $\text{kJ mol}^{-1}$ )	Dielectric relaxation frequency $f_r$ (MHz)	Soil matric pressure $p_m$ (MPa)	Remarks
Kaatze & Uhlendorf [1981]	Free	20.5	$17 \cdot 10^3$	-0.1	Water at great distance from a particle or pore surface
Dirksen & Dasberg [1993]	Hygroscopic	22.3 **	$8 \cdot 10^3$ **	-100 *	Monomolecular water layer in soil for $e_{le,s} = 0.50$
Hoekstra & Doyle [1971]	To Na-montmorillonite and $\gamma$ -alumina	25.1	$1 \cdot 10^3$	-250 ***	-15 $^\circ\text{C}$ to -52 $^\circ\text{C}$
Rolland & Bernard [1951]	To silica gel	52,5	$10 \cdot 10^3$ **	$\approx -2 \cdot 10^3$ ***	Water evaporated at temperature $> 120 \text{ }^\circ\text{C}$
Hasted [1973]	Ice	55	$9 \cdot 10^3$	$\approx -2 \cdot 10^3$ ***	Ordinary ice at $0 \text{ }^\circ\text{C}$
---	Hygroscopic	55 **	$10 \cdot 10^3$ **	$\approx -2 \cdot 10^3$ ***	Lower boundary of hygroscopic water content; an "ice-like" monomolecular water layer and water evaporated at $105 \text{ }^\circ\text{C}$
Breugel [1991]	To settled concrete	40 - 60	---	$\approx -2 \cdot 10^3$ ***	Water evaporated at temperature $> 1000 \text{ }^\circ\text{C}$
Iwata [1995]	To clay	$> 55$	$< 10 \cdot 10^3$ **	$< -2 \cdot 10^3$ ***	Water evaporated at temperature $> 400 \text{ }^\circ\text{C}$

\* Calculated from the relative humidity using (2.9).

\*\* Calculated from the soil water pressure using (2.15).

\*\*\* Calculated from the activation enthalpy using (2.11).



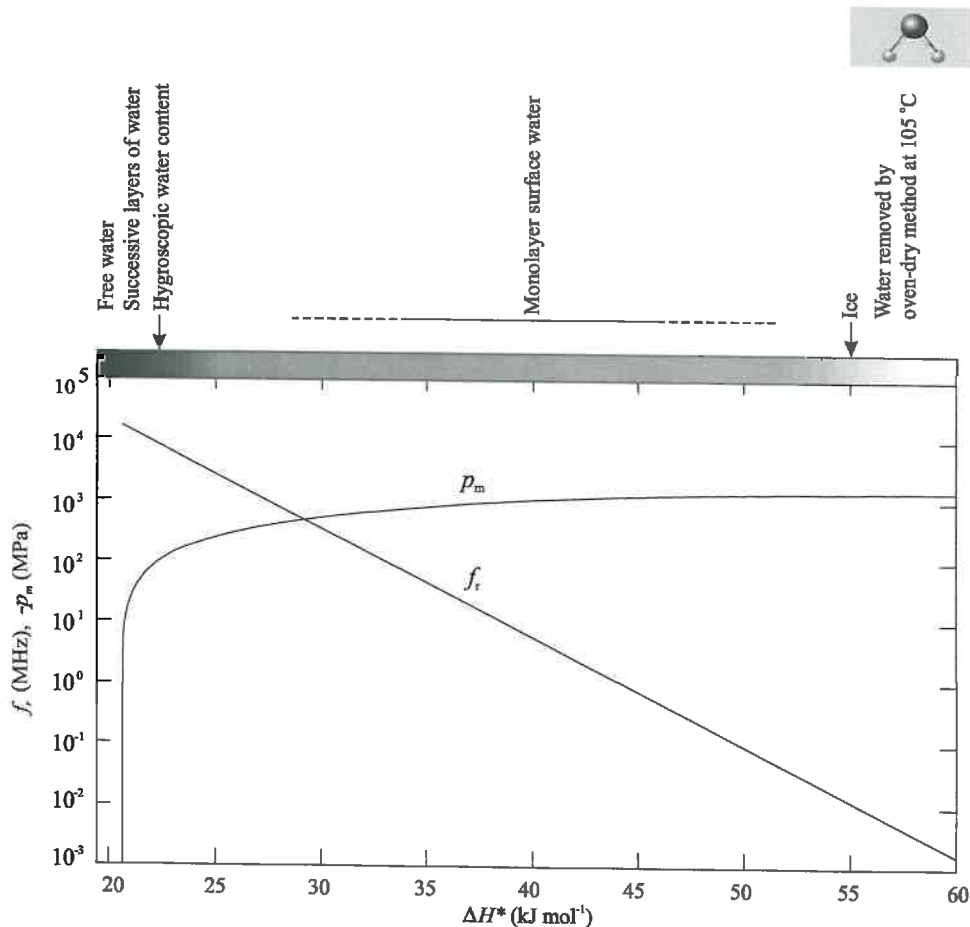


Figure 2.4. An overview of the relationship between the different energy states of bound water in soil. The relaxation frequency,  $f_r$ , and the soil matric pressure,  $p_m$ , are plotted as a function of activation enthalpy,  $\Delta H^*$ . The bar on top of the graph is an indication of the number of water layers bound to the matrix surface. Note the relatively sharp transition from "free" to hygroscopic water at  $p_m \approx -100$  MPa.

## Conclusions

The relationship (2.15) was found between the dielectric relaxation frequency,  $f_r$ , of bound water in soil and its energy status expressed in terms of soil matric pressure,  $p_m$ . The impact of bound water on  $f_r$  can be calculated from  $p_m$ . This conclusion was illustrated using the dielectric and water retention properties of porous materials as found in the literature. These examples suggest that a temperature  $> 105^\circ$  is needed to remove all water from the soil material. For practical use, however, the water fraction left is small and often regarded as part of the soil matrix.

For soil, a monolayer of surface water can exist between  $-100$  MPa  $> p_m > -2 \cdot 10^3$  MPa corresponding to  $8$  GHz  $> f_r > 10$  kHz, but it has been argued that  $10$  MHz  $> f_r > 10$  kHz is a more realistic expectation.



*A relationship between the matric pressure and the dielectric properties of soil implies that the hysteresis (i.e. the difference between adsorption and desorption) observed for the soil water retention characteristic, also applies to the dielectric spectrum.*

*The permittivity of soil to a substantial part results from a mixture of different layers of water, each with its own dielectric properties resulting from the water-binding energy status.*

## 2.3 COUNTERION DIFFUSION POLARISATION

The presence of ions in the pore water of the soil matrix will give rise to a number of polarisation and relaxation phenomena affecting the low-frequency end of the dielectric spectrum. One of these effects is counterion diffusion polarisation [Chew, 1982]. This effect is a function of the ion concentration and thus of the specific ionic conductivity,  $\sigma$ . An increase in  $\sigma$  causes the measured permittivity,  $\epsilon$ , to increase especially at lower frequencies and may obscure soil water content measurements.

Counterion diffusion polarisation is a surface phenomenon. It is dominant at frequencies  $< 100$  kHz, but can still contribute to  $\epsilon$  measured at frequencies  $> 1$  MHz. Because this thesis focuses on the dielectric behaviour of soil in the frequency range between 1 MHz and 1 GHz, counterion polarisation will be treated only briefly.

Soil is a mixture of water, solids and air. For a near-saturated soil, air is distributed in the form of air bubbles. With respect to ion concentration effects, it is my opinion that air bubbles should be treated like colloidal particles.

### Counterion diffusion polarisation

For the treatment of counterion diffusion polarisation, also referred to as colloidal dielectric dispersion [O'Brien, 1986], the handbook of Polk & Postow [1986] will be followed closely. In an EM field ionic diffusion in the electric double layer on the surface of a soil particle will lead to polarisation of this layer. The magnitude of counterion diffusion polarisation is proportional to the surface charge density of the particle. Counterion diffusion polarisation is illustrated in Figure 2.5.

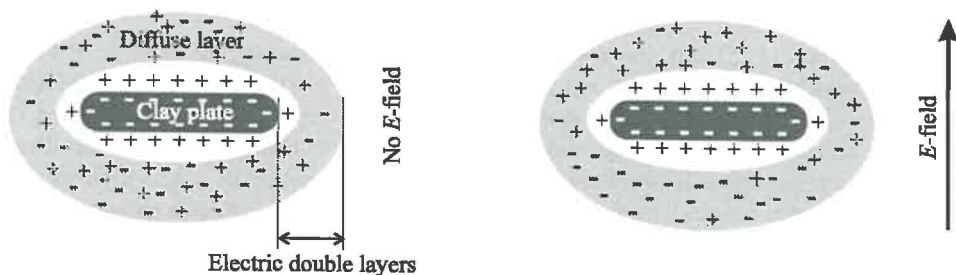


Figure 2.5. An illustration of counterion diffusion polarisation due to separation of cations and anions in an electric double layer around a clay plate.



Schwarz [1962] considered the case of a macroscopic sphere of radius  $r$  with counterion surface charge density  $\delta_0$  in which the thickness of the electric double layer is much smaller than the particle diameter. For the permittivity of a *particle* exhibiting counterion polarisation Schwarz [1962] found

$$\varepsilon_c = \frac{\Delta\varepsilon_c}{1 + j\frac{f}{f_{c\tau}}} + \varepsilon_{c\ f \rightarrow \infty} \quad (2.16)$$

where the subscript c indicates counterion polarisation,  $f_{c\tau}$  is the relaxation frequency,  $\varepsilon_{c\ f \rightarrow \infty}$  is the permittivity for  $f \gg f_{c\tau}$  and  $\Delta\varepsilon_c$  is the dielectric increment.  $f_{c\tau}$  is given by

$$f_{c\tau} = \frac{2ukT}{\varepsilon_0 r^2} \quad (2.17)$$

where  $u$  is the surface mobility of the counterions in  $\text{m}^2 \text{V}^{-1} \text{s}^{-1}$ . Note that  $f_{c\tau}$  is inversely proportional to the square of the particle radius,  $r$ .  $\Delta\varepsilon_c$  is given by

$$\Delta\varepsilon_c = \frac{q_c^2 \delta_0}{\varepsilon_0 kT} \quad (2.18)$$

where  $q_c$  is the charge of a counterion. The particle size distribution of soil may extend over several orders of magnitude, from  $< 1 \text{ nm}$  to  $> 1 \text{ mm}$ . It can be expected that the spread in  $f_{c\tau}$  for each particle will be accordingly wide and consequently the value for  $\varepsilon_c$  will be low. Table 2.2 illustrates the large magnitude of such effects and the "low" relaxation frequencies involved. The data for polystyrene spheres between  $0.044 \mu\text{m}$  and  $0.59 \mu\text{m}$  are adapted by Polk & Postow from Schwarz [1962]. I estimated the data for polystyrene spheres of  $1.17 \mu\text{m}$  and  $0.188 \mu\text{m}$  from Schwan [1957].

Table 2.2. Electric properties of polystyrene spheres in a suspension with a volume fraction close to 0.30. From: Schwarz [1962]. The \* data are from Schwan [1957].

Particle radius $r$ ( $\mu\text{m}$ )	Permittivity of particle $\varepsilon$ (-)	Relaxation frequency $f_{c\tau}$ (kHz)
1.17*	$\approx 8.000$	$\approx 2$
0.59	10.000	0.6
0.28	3.000	1.8
0.188*	$\approx 2.000$	$\approx 50$
0.094	2.450	15
0.044	540	80

Counterion polarisation of particles takes place in the first layers of water molecules and its contribution to  $\varepsilon$  of the soil is therefore most pronounced at lower water contents. As an example we consider a clay particle of  $5 \text{ nm}$  with sodium counterions. For  $u \approx 0.05 \text{ m}^2 \text{V}^{-1} \text{s}^{-1}$  a relaxation frequency  $f_{c\tau} \approx 10 \text{ MHz}$  can be found from (2.17). As mentioned before, this relaxation frequency will be smeared out over a broad frequency band. Because of that the



magnitude of  $\varepsilon_c$  is expected to be small. For some clays, e.g. Bentonite, the thickness of the electric double layer is not smaller than the particle diameter, making the prediction of counterion polarisation more complicated. In this thesis the effect of counterion polarisation will be assumed to be negligible.

### Polarisation of air bubbles

The orientation of molecules at the air-water interface differs from that of bulk water. Their orientation is not random, the air-water interface will be charged and an electric double layer will be formed. Not only colloidal soil particles, but also an air bubble in the pore water will be surrounded by an electric double layer and exhibit counterion diffusion polarisation. It will affect the dielectric response of a soil. I expect that polarisation of air bubbles will be most pronounced in the water content range between full and half saturation (Figure 2.6). This effect reaches a maximum when air inclusions can form spheres. For a fixed measuring frequency, the real part of the permittivity,  $\varepsilon'$ , will increase with decreasing air bubble size and go to zero near saturation where the air bubbles vanish. In the water content range between roughly half and full saturation, the increase in  $\varepsilon'$  is expected to lead to an "S"-shaped calibration curve  $\varepsilon'(\theta)$ . The accompanying relaxation frequencies will be spread over a broad frequency range, since the air bubbles will have dimensions varying between the size of the pores and infinitesimally small. Because of the small dimensions involved, the spectrum is expected to extend over 100 MHz. No literature on my hypothesis of polarisable air inclusions could be found. However, some evidence for its existence can be found by carefully observing published calibration data  $\varepsilon'(\theta)$ .

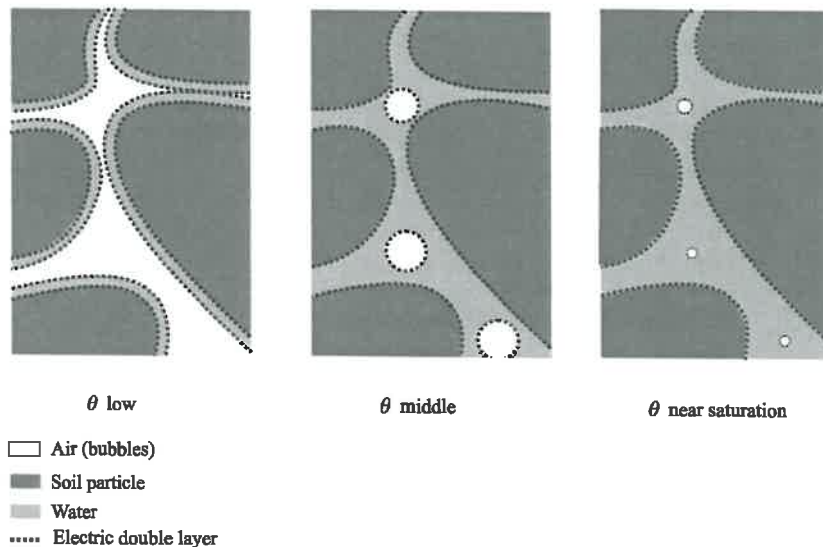


Figure 2.6. The electric double layer around an air bubble will exhibit counterion polarisation. Air bubbles will appear at middle range water contents and disappear towards saturation.



Apart from polarisation, air inclusions will affect the permittivity due to their shape and size which changes as a function of  $\theta$  [Endres & Knight, 1992]. The shape of an air inclusion will be oblate for adsorption while for desorption the shape tends to be prolate. Thus, hysteresis in the relationship between  $\varepsilon$  and  $\theta$  is expected. Under equilibrium conditions air bubbles tend to form spheres. This is due to the fact that water molecules at the water surface will arrange towards a minimum energy configuration. The hysteresis due to the shape of the bubbles is only expected during water flow.

## Conclusions

*Counterion polarisation of soil particles is of minor importance for dielectric measurements at frequencies > 1 MHz. It is a complicated mechanism that can be ignored for soil in most cases. It is recommended, however, always to be aware of possible errors due to this simplification. It is argued that air bubbles should be treated like particles, with respect to counterion polarisation effects.*

## 2.4 MAXWELL-WAGNER EFFECT

The Maxwell-Wagner effect [Maxwell, 1873; Wagner, 1914] is the most important phenomenon that affects the low-frequency end of the dielectric spectrum. It has been reviewed in detail by Hanai [1968] and Dukhin & Shilov [1974]. The Maxwell-Wagner effect is often referred to as interfacial polarisation, but I believe that the term interfacial polarisation in this context is misleading. It is not really a polarisation phenomenon but rather the result of the distribution of conducting and non-conducting areas, as can be seen from electric network theory. It is a macroscopic phenomenon that depends on the differences in bulk dielectric properties of the soil constituents. This effect is dominant in a frequency range between roughly 0.1 MHz and 500 MHz, the most popular frequency range for  $\theta$  measurements.

### Equivalent circuit for the Maxwell-Wagner dispersion

Let us consider a soil, saturated with water, between two plates of a capacitor. Going from one plate to the other, one passes regions of non-conducting solids and regions of conductive pore water. The Maxwell-Wagner effect can best be illustrated by considering the pore water and the solids as a capacitor consisting of a series connection of two dielectric slabs, as shown in Figure 2.7b. Both slabs are represented by capacitors. The capacitance,  $C$ , of a capacitor formed by two parallel plates and a dielectric in between is given by

$$C = \varepsilon \varepsilon_0 \frac{A}{d} \quad (2.19)$$

where  $A$  is the area of the plates,  $\varepsilon$  the permittivity of the dielectric with thickness  $d$ . In the following, the subscript  $w$  denotes values for the first capacitor formed by the average water layer, and the subscript  $s$  denotes values for the second capacitor formed by an average solid layer. The capacitance, permittivity and relaxation frequency as measured between the electrodes, from which the Maxwell-Wagner relaxation can be calculated, are denoted by subscript MW.

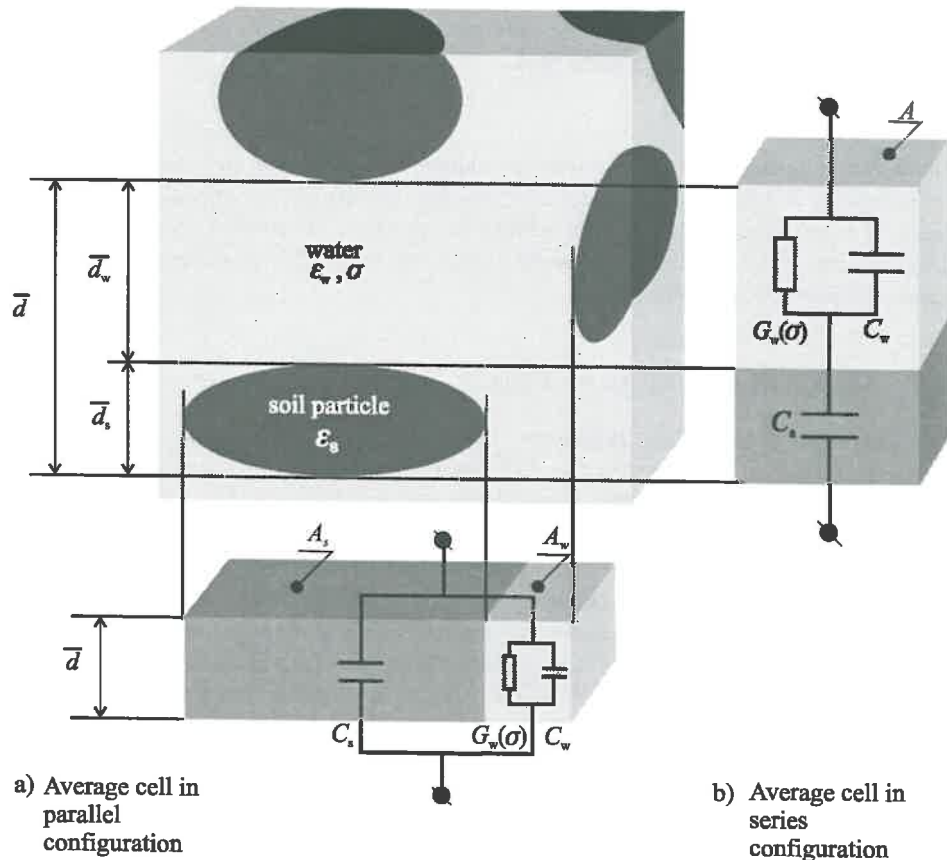


Figure 2.7. Equivalent circuit for the Maxwell-Wagner dispersion [Maxwell, 1873; Wagner, 1914] due to differences in bulk dielectric properties of soil constituents. Two models are shown in the form of an average cell of the soil.

Model a) is a parallel connection of the foregoing but with equal layer thickness and different areas for water,  $A_w$ , and solids,  $A_s$ . The water is conductive with conductivity,  $\sigma$ , and permittivity  $\epsilon_w$ , and the solids are non-conductive with permittivity  $\epsilon_s$ .

Model b) consists of a series connection of two capacitors; one is formed by the water,  $C_w$ , with a parallel conductor,  $G(\sigma)$ , due to ionic conduction of the water, and the other is formed by the solids,  $C_s$ . The average thickness of the water layers is  $\bar{d}_w$ , and that of the solids is  $\bar{d}_s$ .



The subscript  $i$  refers to a series connection. The total capacitance of the series connection of the circuit of Figure 2.7b is given by

$$C_{MWi} = \frac{1}{1/C_w + 1/C_s} \quad (2.20)$$

The first slab represents the permittivity,  $\epsilon_w$ , and ionic conductivity,  $\sigma$ , of the pore water layer with average thickness  $d_w$ . It is assumed that dielectric losses are negligible. Hence

$$\epsilon_{MWw} = \epsilon'_{MWw} - j \frac{\sigma}{2\pi f \epsilon_0} \quad (2.21)$$

The second slab is non-conductive, representing the permittivity of a solid layer with average thickness  $\bar{d}_s$ . The average thickness of the two capacitors together is  $\bar{d} = (\bar{d}_w + \bar{d}_s)$ .

The two slabs of Figure 2.7b represent an average cell for which the average thickness of the layers  $\bar{d}_w$  and  $\bar{d}_s$  can be linked to parameters of a real soil, such as the water content,  $\theta$ , the porosity,  $\phi$ , and the specific surface area,  $S_A$ . Let  $K$  be such a linking function; i.e.  $K(\theta, \phi, S_A)$ . For real soils  $K$  is unknown, but it can be calculated or found experimentally. For the simple example of the average cell of Figure 2.7b,  $K$  can be defined as

$$K = \bar{d} / \bar{d}_s \quad (2.22)$$

and

$$\frac{K}{K-1} = \bar{d} / \bar{d}_w \quad (2.23)$$

The texture parameter  $K$  is a dimensionless normalised parameter independent of the distance between the two plates. Note that it is not the dimension of the particle but rather the shape that determines  $K$ . Two soils with only spherical particles of different dimensions but equally packed, will have the same  $K$ . From (2.19), (2.20) and (2.21), after rearranging the terms and substituting  $K$ , the resulting  $\epsilon_{MWi}$ , as measured across the two slabs, can be described by

$$\epsilon_{MWi} = \frac{K}{\frac{K-1}{\epsilon'_{MWw} - j \frac{\sigma}{2\pi f \epsilon_0}} + \frac{1}{\epsilon_{MWs}}} \quad (2.24)$$

which can be split into a real and an imaginary part. It can be shown, by straightforward algebraic manipulation, that the real part of  $\epsilon_{MWi}$  is not only a function of  $\epsilon'_{MWw}$  but also of  $\sigma$  and  $f$ .

It is possible to put the Maxwell-Wagner effect as described by (2.24) into the form of the Debye relaxation of (2.6). The limit for infinitely high frequencies,  $\epsilon_{MWi, f \rightarrow \infty}$ , and that for the static case,  $\epsilon_{MWi, f \rightarrow 0}$ , of the apparent permittivity due to the Maxwell-Wagner effect are, respectively,

$$\epsilon_{MWi, f \rightarrow 0} = K \epsilon_{MWs} \quad (2.25)$$

and

$$\epsilon_{MWi, f \rightarrow \infty} = \frac{K}{\frac{K-1}{\epsilon'_{MWw}} + \frac{1}{\epsilon_{MWs}}} \quad (2.26)$$





The "relaxation" frequency of the Maxwell-Wagner effect,  $f_{MW\tau}$ , is the frequency for which the real part of  $\epsilon_{MWi}$  in (2.24) is equal to its imaginary part:

$$f_{MW\tau} = \frac{\sigma}{2\pi \epsilon_0 [\epsilon'_{MWw} + (K-1)\epsilon_{MWs}]} \quad (2.27)$$

Note that, if  $K$  is close to 1,  $f_{MW\tau}$  depends only on  $\sigma$  of the pore water.  $\epsilon'_{MWw}$  and  $\epsilon_{MWs}$  are constants. Using (2.26), (2.25) and (2.27) it is possible to write (2.24) into the form of a Debye relaxation

$$\epsilon_{MWi} = \frac{\Delta\epsilon_{MWi}}{1 + j \frac{f}{f_{MW\tau}}} + \epsilon_{MWi, f \rightarrow \infty} \quad (2.28)$$

where the dielectric increment of the Maxwell-Wagner effect is  $\Delta\epsilon_{MWi} = (\epsilon_{MWi, f \rightarrow 0} - \epsilon_{MWi, f \rightarrow \infty})$ . Note that  $\epsilon_{MWi, f \rightarrow \infty}$  is the permittivity of the material without the Maxwell-Wagner effect. It can be useful to write (2.28) in a slightly different form:

$$\epsilon_{MWi} = \left[ \frac{\frac{\epsilon_{MWs}(K-1)}{\epsilon'_{MWw}}}{1 + j \frac{f}{f_{MW\tau}}} + 1 \right] \epsilon_{MWi, f \rightarrow \infty} \quad (2.29)$$

where the term within brackets is the normalised Debye function. This term depends only on the permittivities of the water, the solids and  $K$ .  $\epsilon_{MWi, f \rightarrow \infty}$  is the permittivity of a material at frequencies that are high compared with  $f_{MW\tau}$ .

Only if the factor  $(K-1)$  becomes sufficiently high, there will be a small spread in relaxation due to a spread in  $K$ , as can be seen from (2.27). Thus, an arbitrary system has approximately a single relaxation frequency. It can be modelled with (2.26), (2.25), (2.27) and (2.28) or (2.29). In the rest of this thesis the subscript  $MW_i$  will be replaced by  $MW$ .

The value for  $\epsilon_{MW, f \rightarrow \infty}$  corresponds to the permittivity only due to polarisation phenomena,  $\epsilon_p$ , in the case that bound water effects (see Section 2.6) are negligible.

The impact of a spread in the layer thickness on  $f_{MW\tau}$  is small, as can be seen from (2.27).  $f_{MW\tau}$  is mainly a function of  $\sigma$ . Note that for a soil drying as a result of evaporation, the concentration of ions in the pore water will increase, and so do  $\sigma$  and  $f_{MW\tau}$ .

As an example, consider two hypothetical clay types, saturated with water, having plates of 5 nm and 10 nm thickness, respectively. I represent the clays by the parallel cell. The water film covering the clay plates is on average 20 nm thick,  $\epsilon'_{MWw} = 80$ ,  $\epsilon_{MWs} = 5$  and  $\sigma = 0.1 \text{ S m}^{-1}$ . The normalised real part of the permittivity,  $\epsilon'_{MWi}/\epsilon_{MWi, f \rightarrow \infty}$ , resulting from the Maxwell-Wagner effect for these two clays, is calculated using (2.29) and plotted as a function of frequency in Figure 2.8.

In the foregoing, only a series connection of the water layer and the solid layer was discussed. In practice the orientation of the clay plates is unknown. The series connection is one of the two extreme orientations as shown by Figure 2.7a and Figure 2.7b. Let us now consider the parallel configuration, denoted with  $//$ . The total capacitance of the parallel connection for two capacitors is

$$C_{MW//} = C_w + C_s \quad (2.30)$$





Using (2.19) and (2.21) this can be written as

$$\varepsilon_{MW//} = \frac{1}{d} \left( \varepsilon_{MWs} \bar{A}_s + \varepsilon'_{MWw} \bar{A}_w - j \frac{\sigma}{2\pi f \varepsilon_0} \bar{A}_w \right) \quad (2.31)$$

where  $\bar{A}_s$  and  $\bar{A}_w$  are the average areas of the solids and the water, respectively. It can be seen from (2.31) that, for the parallel case, the real part of  $\varepsilon_{MW//}$  is independent of  $f$  and  $\sigma$ . The phase shift of the current through  $C_s$  and the through  $C_w$  will not change for varying  $G_w$ . Comparing (2.31) with (2.20) makes clear that the parallel configuration does not lead to an additional relaxation. Hence, no Maxwell-Wagner relaxation will take place.

For soil, the measured dielectric increment,  $\Delta\varepsilon_{MW}$ , is smaller than  $\Delta\varepsilon_{MWi}$  as calculated using the simplified expression (2.29), depending on the real configuration of parallel and series elements. Note that  $\Delta\varepsilon_{MW}$  is independent of  $\sigma$ .

The natural orientation of clay plates can vary from randomly oriented to sandwich-oriented. From a dielectric point of view, the sandwich structure can be represented by the two extremes; the series and the parallel model. Only the series model gives rise to a Maxwell-Wagner relaxation with a relaxation frequency determined by the permittivity and conductivity of the water. *The measurement of  $\varepsilon_{MW}$  will be orientation-sensitive for plate-condensated clays.* However, it was not possible to find evidence from the literature for the existence of orientation sensitivity.

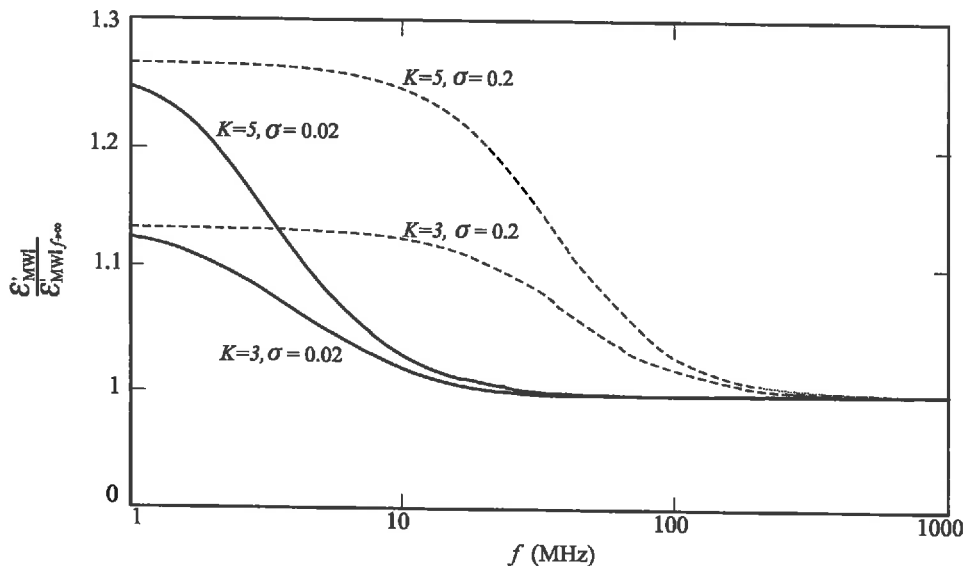


Figure 2.8. A representation of the appearance of the Maxwell-Wagner relaxation in a dielectric spectrum for saturated clay. The clay plates are assumed to have average thicknesses of 5 nm and 10 nm and an average water film of 20 nm, i.e. texture parameter  $K = 5$  and  $K = 3$ , respectively. The ionic conductivity is  $\sigma = 0.2 \text{ S m}^{-1}$  for the dashed lines and  $\sigma = 0.02 \text{ S m}^{-1}$  for the solid lines. The normalised real part of the permittivity,  $\varepsilon'_{MW}/\varepsilon'_{MW, f \rightarrow \infty}$ , is calculated according to (2.29).



### Maxwell-Wagner effect characterised using a three-frequency measuring method

It is difficult to know all parameters necessary to predict  $\epsilon_{MW}$  as described by (2.28) or (2.29). However, these equations can still serve as a practical tool to analyse the dielectric properties of an unknown soil in order to find information on its textural properties.

As shown before, the real part of the permittivity for the Maxwell-Wagner effect at low frequencies,  $\epsilon_{MW f \rightarrow 0}$ , is a function of the soil texture parameters expressed by  $K(\theta, \phi, S_A)$ , where  $\theta$  is the water content,  $\phi$  the porosity and  $S_A$  the specific surface area. To determine  $K(\theta, \phi, S_A)$ , I propose to use the series cell approximation as discussed before. For this cell,  $K(\theta, \phi, S_A)$  is a measure of the ratio between the average solid and average water layer thicknesses. I will refer to  $K(\theta, \phi, S_A)$  with only  $K$ .

The real part of the permittivity for the Maxwell-Wagner effect at infinite high frequencies,  $\epsilon_{MW f \rightarrow \infty}$ , is equal to the permittivity of the bulk soil if it is not affected by the Maxwell-Wagner effect. In Section 2.2 it is explained that the impact of bound water is small for frequencies roughly below 150 MHz (monomolecular layer of water with a single relaxation frequency). Therefore, the dielectric spectrum will be almost flat without the Maxwell-Wagner effect and only the Maxwell-Wagner effect determines the low frequency end of the spectrum. It is possible to calculate the three Debye parameters of the Maxwell-Wagner effect,  $\epsilon_{MW f \rightarrow 0}$ ,  $\epsilon_{MW f \rightarrow \infty}$  and  $f_{MW \tau}$  from permittivity measurements at three different frequencies. From  $\epsilon_{MW f \rightarrow \infty}$  the permittivity of the water and the solids,  $\epsilon'_{MW w}$  and  $\epsilon'_{MW s}$ , can be estimated and subsequently the texture parameter  $K$  can be derived from (2.29). Since  $\epsilon_{MW f \rightarrow \infty}$  is not affected by the Maxwell-Wagner relaxation and to a minor extend by the bound water content, I expect this is a good measure of the water content.

Let the three frequencies be in the ratio  $f_1 : f_2 : f_3 = 1 : 2 : 3$ . They should be chosen well within the expected Maxwell-Wagner relaxation region. To avoid bound water to influence the measurement, a good choice for the three measuring frequencies might be below 150 MHz. For these frequencies one will measure  $\epsilon'_1$ ,  $\epsilon'_2$  and  $\epsilon'_3$ , respectively. Using straightforward algebraic manipulations on (2.28) it can be shown that

$$f_{MW \tau} = f_1 \sqrt{\frac{5\epsilon'_1 - 32\epsilon'_2 + 27\epsilon'_3}{5\epsilon'_1 - 8\epsilon'_2 + 3\epsilon'_3}} \quad (2.32)$$

$$\epsilon_{MW f \rightarrow \infty} = \frac{8\epsilon'_1 \epsilon'_3 - 3\epsilon'_1 \epsilon'_2 - 5\epsilon'_2 \epsilon'_3}{5\epsilon'_1 - 8\epsilon'_2 + 3\epsilon'_3} \quad (2.33)$$

$$\Delta\epsilon_{MW} = (\epsilon_1 - \epsilon_{MW f \rightarrow \infty}) \left( 1 + \frac{f_1^2}{f_{MW \tau}^2} \right) \quad (2.34)$$

Note that (2.32), (2.33) and (2.34) are valid for all frequencies if they are in the ratio 1 : 2 : 3 e.g. 10 MHz, 20 MHz and 30 MHz.

### Conclusions

*The Maxwell-Wagner effect can be described in the form of a single relaxation process according to the Debye function and is the main reason for increases in permittivity at  $f < 150$  MHz. This is well below frequencies where the impact of bound water relaxations*



(Section 2.2) plays a dominant role. It has been shown that the limit of  $\varepsilon_{MW}$  for  $f \rightarrow \infty$ , i.e.  $\varepsilon_{MW f \rightarrow \infty}$ , equals the permittivity of the soil not affected by the Maxwell-Wagner effect. The amplitude of the Maxwell-Wagner effect,  $\varepsilon_{MW}$ , put in the form of a normalised Debye function, comes on top of  $\varepsilon_{MW f \rightarrow \infty}$ . Because of this and the single relaxation process, it is possible to calculate the three parameters of the Debye function from measurements at three-frequencies. It is convenient to choose these frequencies in a ratio of 1 : 2 : 3 somewhere around the expected relaxation frequency, for which (2.32), (2.33) and (2.34) can be used.

*It is possible to divide the dielectric spectrum into two parts at roughly around 150 MHz, the higher frequencies dominated by bound water relaxations and the lower frequencies dominated by the Maxwell-Wagner effect. Both parts can be described by means of a Debye function, providing an elegant and practical tool for the dielectric characterisation of soil using three frequencies.  $\varepsilon_{MW f \rightarrow 0}$  is shown to be related to the texture.  $\varepsilon_{MW f \rightarrow \infty}$  is related only to the water content.*

## 2.5 DEVELOPMENT OF A NEW DIELECTRIC MIXTURE EQUATION

Until now, different polarisation mechanisms and the Maxwell-Wagner effect have been treated separately. The total permittivity of soil, as measured between the plates of a capacitor, is the result of all these mechanisms. Soil is a heterogeneous material. It is a mixture of differently shaped granules, water films, air inclusions and organic matter. For dielectric measurements a thoroughly mixed soil, large in comparison with the dimensions of its constituents, can be treated as a homogeneous mass. Its dielectric properties, as measured on a macroscopic scale, are determined by the corresponding properties of the individual constituents and the different polarisation phenomena. The relationship between the permittivity as measured on both a macroscopic scale and a microscopic scale can be described using mixture equations, often referred to as mixing formulas or mixing rules. The impact of microstructural and compositional soil properties on  $\varepsilon$  is complex and not well understood. Therefore, currently it is only possible to describe and predict  $\varepsilon$  using empirical mixture equations. In this section I will derive a new dielectric mixture equation.

### Current mixture equations

The distribution of electric field strength,  $\underline{E}$ , being a vector in the  $x, y, z$  space, for the individual constituents of a slab of soil is complex. The mean field strength,  $\overline{E}$ , in the mixture can be determined from the theories given by Böttcher [1952], De Loor [1956], Bordewijk [1973], Böttcher & Bordewijk [1978], Sihvola [1988] and references therein. From this,  $\varepsilon$  can be calculated. It is, however, a rather difficult and not very practical exercise to determine  $\overline{E}$  mathematically from the contributions of the local  $\underline{E}$ 's of the soil constituents. It can partly be done for ellipsoids, but for particles and pores of arbitrary shapes it is virtually impossible.

Many mixture equations have been published, but none of them is universally applicable. Some use one or more empirical parameters which are not linked to any soil parameter. Other equations are only valid for static problems or for frequencies  $> 1$  GHz. For an in-depth discussion on mixture equations the reader is referred to Cole-Cole [1941], Davidson-Cole [1951], Tinga *et al.* [1973], Wang & Schmugge [1980], Dobson *et al.* [1985],



Priou [1992], Kobayashi [1996] and references therein.

Percolation phenomena, e.g. hysteresis and non-stable transitions, may arise as the continuous phase changes from air to water and vice versa. *Percolate* means to flow through. Percolation is a non-linear phenomenon; a very abrupt change in the behaviour of certain parameters of a percolating material. The geometry of the matter where percolation takes place is very special; if there are even small changes in the fractions of the components forming the material, the structure behaves totally differently. Due to the large difference in the magnitudes of the permittivities of water and dry soil the permittivity of soil is subject to uncertainties in the vicinity of the volume fractions that correspond to percolating points. For some remarks on percolation phenomena in connection with dielectric mixtures, the reader is referred to Han & Choi [1996] and Sihvola [1996].

In the following I will derive a new dielectric mixture equation using the principle of superposition of  $E$ -fields. This equation also contains parameters that have to be determined experimentally. It will be shown later, however, that these parameters can be linked to physical soil parameters. For a more detailed treatment of EM wave theory, see also Lorrain *et al.* [1988] or other textbooks.

### New mixture equation

To measure the permittivity,  $\epsilon$ , of soil, an electric field  $\underline{E}$  shall be applied between two metal plates with the soil in between: the soil becomes polarised. For linear and isotropic dielectrics such as soils, the polarisation vector  $\underline{P}$  is proportional to  $\underline{E}$  and points in the same direction. The proportionality factor is the electrical susceptibility ( $\epsilon-1$ ) of the material. If  $\underline{E}$  is a function of time, then  $\underline{P}$  is a function of time as well. This causes a motion of bound charges to and from the plates. The resulting current can be measured and is a function of  $\underline{P}$ . The relationship between  $\underline{E}$ ,  $\underline{P}$  and  $\epsilon$  on a macroscopic scale is given by

$$\underline{P} = \epsilon_0(\epsilon - 1)\underline{E} \quad (2.35)$$

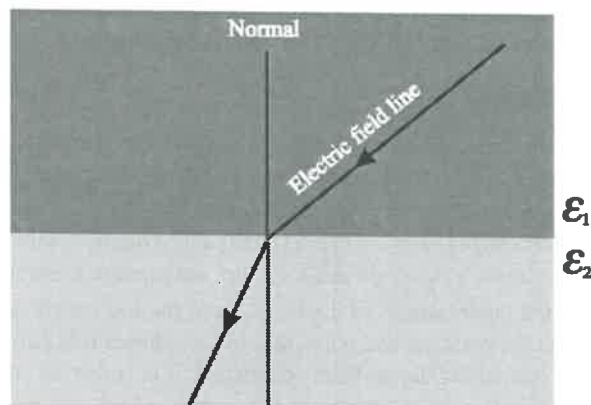


Figure 2.9. Refraction of electric field lines crossing the interface of two dielectrics with  $\epsilon_1 > \epsilon_2$  for the permittivities of the two materials.



If an  $E$ -field is applied to a medium consisting of two dielectrics, the amplitude of  $\underline{E}$  in one of the two dielectrics will differ from that in the other depending on the difference in their permittivities. The direction of  $\underline{E}$  will change according to the refraction of electric field lines crossing the interface of the two dielectrics, as shown in Figure 2.9.

Using the principle of superposition and taking into account the assumptions and comments discussed by e.g. Böttcher [1952] and Reynolds [1955], the total  $\underline{E}$  of all constituents appears to have the same direction and amplitude as the  $\underline{E}$  field applied. I assume that the microscopic structure of normal soils is sufficiently anisotropic to justify this statement. In the following I also assume that the individual inclusions of the  $i^{\text{th}}$  constituent are large in number and randomly as well as uniformly distributed and have dimensions much smaller than the measured volume. Then, this constituent may be treated as a macroscopic body with permittivity  $\epsilon_i$ , a mean electric field strength  $\underline{E}_i$ , and a mean polarisation  $\underline{P}_i$  both pointing in the same direction as the applied field. Since  $\epsilon$  is not a vector, it can be seen from (2.35) that the principle of superposition applies to  $\underline{P}$  as well. Thus, on a macroscopic scale the soil may be thought of as being homogeneous with permittivity  $\epsilon$ , polarisation  $\underline{P}$  and electric field  $\underline{E}$ . The polarisation of the soil between the plates is defined by (2.35), from which  $\epsilon$  can be found. The relationship between macroscopic and microscopic polarisation is illustrated in Figure 2.10.

Consider the  $i^{\text{th}}$  constituent that occupies a volume fraction  $v_i$  of a soil with volume  $V$  where  $v_i$  is a dimensionless quantity. The microscopic mean polarisation for this constituent is  $\underline{P}_i$ . If only this constituent is placed in the volume  $V$ , then the mean polarisation  $\underline{P}$  for this volume is

$$\underline{P} = \underline{P}_i v_i \quad (2.36)$$

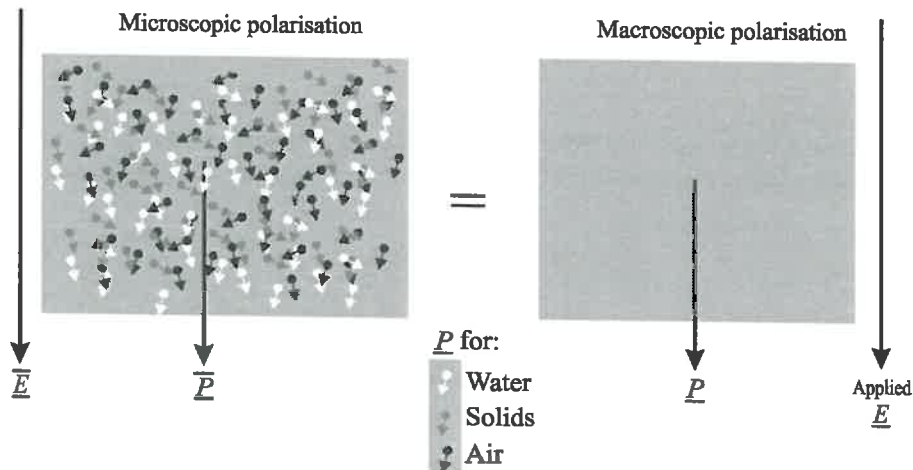


Figure 2.10 Illustration of polarisation distribution for a mixture of particles with permittivity  $\epsilon_s$ , water with permittivity  $\epsilon_w$ , and air with permittivity  $\epsilon_a$ . The macroscopic polarisation,  $\underline{P}$ , and electric field,  $\underline{E}$ , are equal and point in the same direction as the averaged microscopic polarisation,  $\underline{P}$ , and averaged electric field,  $\underline{E}$ .



Soil contains  $n$  constituents, each with volume fraction  $v_i$  and a microscopic mean polarisation. The macroscopic mean polarisation of a soil can be written as

$$\bar{P} = \sum_{i=1}^n \bar{P}_i v_i \quad (2.37)$$

where the summation of all volume fractions  $\sum_{i=1}^n v_i = 1$ . With (2.35) substituted for each constituent in (2.37)  $\bar{P}$  can be written as

$$\bar{P} = \sum_{i=1}^n \varepsilon_0 (\varepsilon_i - 1) \bar{E}_i v_i \quad (2.38)$$

The polarisation on a macroscopic scale,  $\underline{P}$ , is equal to the sum of all mean polarisations on a microscopic scale,  $\bar{P}$ . From (2.35) and (2.38) it follows that

$$(\varepsilon - 1) \underline{E} = \sum_{i=1}^n (\varepsilon_i - 1) \bar{E}_i v_i \quad (2.39)$$

The coordinate system between the plates can be chosen such that the  $y$  direction is perpendicular to the plates. Then, the  $x$  and  $z$  directions are parallel to the plates. As explained before,  $\underline{E}$  and  $\bar{E}_i$  are assumed to point both in the same direction i.e.  $y$  direction. The  $x$  and  $z$  components are zero. Now the field vectors may be treated as scalars, i.e.  $E$  and  $\bar{E}_i$ , respectively. This allows the introduction of the function  $S_i$ , defined by

$$S_i = \frac{\bar{E}_i}{E} \quad (2.40)$$

The effect of  $S_i$  is analogous to depolarisation, therefore,  $S_i$  will be referred to as the dielectric depolarisation factor.  $S_i$  substituted in (2.39) will finally yield *the new mixture equation*

$$(\varepsilon - 1) = \sum_{i=1}^n (\varepsilon_i - 1) S_i v_i \quad (2.41)$$

for which  $S_i$  remains to be determined either theoretically or experimentally.  $S_i$  and  $v_i$  have values between 1 and 0, and so does  $\left(1 - \sum_{i=1}^n S_i v_i\right)$ . The error made by neglecting

$\left(1 - \sum_{i=1}^n S_i v_i\right)$  in (2.41) will be  $< 1$  which is small compared to  $\varepsilon > 25$ , a value for soils close to saturation. The depolarisation factors for dry soil will be close to 1 due to the small differences in permittivities of the constituents. The error made for dry soil with the latter assumption will be  $\ll 1$ .





For this thesis an error  $< 1$  is regarded as acceptable, allowing to approximate (2.41) by

$$\varepsilon \approx \sum_{i=1}^n \varepsilon_i S_i v_i. \quad (2.42)$$

### Comparison with other mixture equations

In the following the mixture equation (2.41) or its approximation (2.42) will be compared with some equivalent mixture equations found by other authors. Differences and similarities will be discussed.

For  $S_i = 1$ , the new mixture equation (2.41) is strikingly identical to the one derived by Silberstein [1895] using thermodynamics for a mixture of fluids. He considered the mixture on one side of a semi-permeable membrane stretched across the field in a parallel plate capacitor. On the other side of the membrane was a pure sample of one of the components in the mixture. He assumed the thermodynamic and electric energy to be independent. By considering the thermodynamic equilibrium of the system, for an infinitely small volume of pure substance passing through the membrane to dilute the mixture, he found the same equation as (2.41) if  $S_i$  is set to 1. That  $S_i = 1$  for fluids follows from the fact that each molecule of the different constituents in the fluid experiences the same electric field applied. There is no refraction of  $E$ -fields on this scale. The polarisation of each molecule is the direct result of the electric field applied. In soil, however, one molecule within a group of molecules, such as in a particle, experiences a refracted  $E$ -field.

A different group of published mixture equations is based on Birchak's [Birchak *et al.*, 1974] "exponential model":

$$(\varepsilon)^\alpha = \sum_{i=1}^n (\varepsilon_i)^\alpha v_i \quad (2.43)$$

where the exponent  $\alpha$  is an empirical constant to correct for average shape and field refraction, equivalent to the depolarisation factor  $S_i$ . With  $S_i = 1$  mixture equation (2.42) is analogous to (2.43) for  $\alpha = 1$ . For  $\alpha = 1$  mixture equation (2.43) reduces to the sum of the volume fractions of the permittivities of each component. In this case the material can be modelled as a parallel connection of capacitors. For  $\alpha = -1$  this model is a series connection of capacitors. The  $\alpha$ -values of 1 and -1 are considered the extremes and are illustrated in Figure 2.11. All other constituent orientations should fall in between. For  $\alpha = 0.5$  mixture equation (2.43) suggests similarity with the "refractive index mixing" model. This value of  $\alpha$  was proposed by Heimovaara [1993], Whalley [1993], White *et al.* [1994] and others. Whalley expected a physical basis for  $\alpha = 0.5$ . The main outcome of these authors was that, based on the refractive index model,  $\sqrt{\varepsilon}$  can be considered to be a linear function of the water content  $\theta$ , described by two parameters. However, the refractive index mixture model for polar substances is only approximately true. The discrepancy between (2.43) and (2.41) implies that  $\alpha$  has no physical meaning for microstructural and compositional analyses of the dielectric behaviour of a soil mixture.

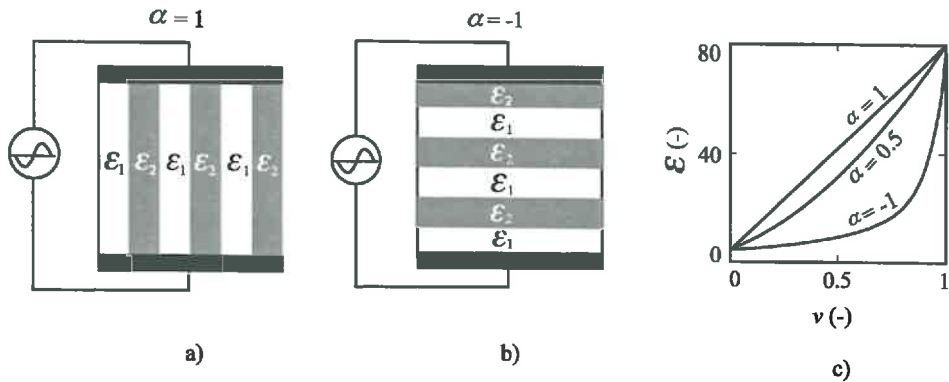


Figure 2.11. The two extremes for Birchak's model (2.43) [Birchak *et al.* 1974] with  $\alpha = 1$  and  $\alpha = -1$ . The electric equivalent for  $\alpha = 1$  is given in a) and for  $\alpha = -1$  in b). The graphs in c) illustrate the corresponding relations between  $\epsilon$  and volume fraction  $v$ . Also shown is a curve for  $\alpha = 0.5$ , which is often referred to as the refractive index model.

Philip [1897] derived the refractive index model for fluids. He used Maxwell's [1873] relationship  $n^2 = \epsilon$ , where  $n$  is the refractive index of light. Philip assumed that the material is non-magnetic and found for a mixture of two materials, denoted with the subscripts 1 and 2, the mixture equation

$$(\sqrt{\epsilon} - 1) = (\sqrt{\epsilon_1} - 1)v_1 + (\sqrt{\epsilon_2} - 1)v_2 \quad (2.44)$$

or in terms of refractive index

$$(n - 1) = (n_1 - 1)v_1 + (n_2 - 1)v_2. \quad (2.45)$$

Philip showed for fluids that the use of this model can lead to erroneous results when calculating the permittivity of the constituents from the measured permittivity. For small values of  $\epsilon_1$  and  $\epsilon_2$  (2.44) is approximately equivalent to the new mixture equation (2.41) with  $S_i = 1$ , because of the approximation

$$(\epsilon - 1) = (\sqrt{\epsilon} + 1)(\sqrt{\epsilon} - 1) \approx 2(\sqrt{\epsilon} - 1). \quad (2.46)$$

For  $\epsilon \leq 1.4$  the approximation error of (2.46) is less than 10 % and for  $\epsilon \leq 2.3$  less than 20 %. Thus the refractive index model for light applies only approximately to dielectric mixtures, where  $\epsilon$  is less than about 2. For soils  $\epsilon \gg 2$ . Thus the use of the refractive index mixture model leads to erroneous results, and substitution of  $n^2$  for  $\epsilon$  is confusing. There is no rigid theoretical foundation for  $\alpha = 0.5$  and thus it is not appropriate to use the refractive index instead of  $\sqrt{\epsilon}$  for analysing dielectric mixtures.

De Loor [1990] proposed, instead of  $\epsilon$ , to relate  $n$  to  $\theta$ . His proposal was more solidly based on the propagation and refraction of EM waves as measured using Remote Sensing (RS) or TDR. The term refractive index should be reserved for this purpose only. Of course apart from the accuracy, there is no objection against using  $n$  or  $\sqrt{\epsilon}$  in plotting calibration data.





The reasonable fit of Birchak's model with experiments as reported in literature for  $\alpha = 0.65$  [Dobson & Ulaby, 1985],  $\alpha = 0.5$  and  $\alpha = 0.33$  [Landau & Lifshitz, 1960; Looyenga, 1965], is accidental and can be explained by the choice of the measuring frequency. The lower the frequency the higher  $\alpha$ , due to the effect of bound water as described in Section 2.2. Most data were obtained from TDR ( $> 150$  MHz) and RS ( $> 1$  GHz). With  $\theta \approx 0.33$ ,  $\epsilon_w = 80$ , and  $\epsilon_s \approx 5$  for glass beads, the permittivity calculated from (2.43) becomes  $\epsilon \approx 30$  with  $\alpha = 1$ ,  $\epsilon \approx 20$  with  $\alpha = 0.5$ , and  $\epsilon \approx 15$  with  $\alpha = 0.33$ . I found  $\epsilon = 28$  at 20 MHz for glass beads with a diameter of 0.2 mm (0.16 mm - 0.26 mm) saturated with water and at a temperature of 20 °C. For glass beads with a diameter of 0.03 mm (0.01 mm - 0.06 mm) I found  $\epsilon = 26$ .

### Conclusions

*The introduction of the depolarisation factor  $S_i$  in mixture equation (2.41) for each constituent of a soil, is in my view the most accurate and effective way to relate the dielectric properties of a slab of soil measured on a macroscopic scale to those on a microscopic scale.*

*The use of the refractive index mixture model for analysing soil, leads to erroneous results, and substitution of  $n^2$  for  $\epsilon$  is confusing.*

In contrast with the empirical factor in Birchak's model [Birchak *et al.*, 1974],  $S_i$  is directly related to the  $E$ -field refraction in the soil which in turn depends upon its microstructural and compositional properties. The approximation of (2.41) by (2.42) is sufficiently accurate for soils and will be used in this thesis.

## 2.6 PERMITTIVITY OF SOIL

In the preceding sections it was explained how dielectric properties are related to some compositional and textural properties of soil. It is also shown how the permittivity measured on a macroscopic scale is related to dielectric properties on a microscopic scale. The theory covers a frequency range from roughly 1 MHz up to 20 GHz. However, the different parts of the theory in the previous sections are still not linked. In this section I construct a model that includes all aspects of the theory that I have described. This model is to be incorporated in the relationship between the dielectric properties of soil and some parameters common in soil science.

### A model for the dielectric behaviour of soil

In Section 2.4 a mixture equation was derived that relates the measured permittivity,  $\epsilon$ , to a weighted sum of the permittivities of the individual soil constituents. The weighting factor or depolarisation factor,  $S_i$ , depends on the changing shape of the water film as a function of water content,  $\theta$ ; i.e.  $S_i(\theta)$ . There is a depolarisation factor for each  $i^{\text{th}}$  constituent, i.e. for air, for solids, and for each successive layer of water at the surface of the soil particles. Hence (2.42) can be written as

$$\epsilon \approx \sum_{i=1}^n \epsilon_i S_i(\theta) v_i \quad (2.47)$$



Counterion polarisation, as described in Section 2.3, is neglected in this thesis but may be added to (2.47) like the other polarising components. The Maxwell-Wagner effect is not really a polarisation phenomenon and shall not be included as a sum term in the summation of (2.47). Firstly, the measured permittivity due to polarisation phenomena,  $\epsilon_p$ , will be worked out in more detail. Next, the apparent permittivity due to the Maxwell-Wagner effect,  $\epsilon_{MW}$ , will be included.

Soil is a mixture of solids, water and air. With (2.47),  $\epsilon_p$  of soil can be written as the sum of the permittivities of the fractions of its constituents by

$$\epsilon_p = S_w(\theta)\epsilon_w + S_s(\theta)(1-\phi)\epsilon_s + S_a(\theta)(\phi-\theta)\epsilon_a \quad (2.48)$$

where the porosity of the soil is given by  $\phi$ ,  $\epsilon_w$  is the permittivity of water,  $\epsilon_s$  that of solids and  $\epsilon_a$  that of air.  $S_w(\theta)$ ,  $S_s(\theta)$  and  $S_a(\theta)$  are the depolarisation factors for water, solids and air, respectively. The symbol  $\theta$  refers to the entire water content regardless of its energy states. Mixture equation (2.48) is valid if  $\epsilon_w$  is constant, which is true at frequencies either very high or very low with respect to the relaxation frequency of the soil water. Then  $S_w(\theta)$  is equal for each layer of water.

As explained in Section 2.2, the energy states of a water molecule is a function of its distance to a soil particle. The matrix pressure,  $p_m$ , and the dielectric relaxation frequency,  $f_{wr}$ , can both be related to the Gibbs' free energy of the water molecules. On this basis it is possible to find  $f_{wr}(p_m)$  as given by (2.15). The relationship between  $\theta$  and  $p_m$  is called the soil water retention characteristic. It is a measure of the water-binding properties of the soil matrix. Consider an infinitesimal thin layer of water with soil matrix pressure  $p_m$ . The differential water capacity [Koorevaar *et al.*, 1983] for this layer is defined as  $g(p_m) = \frac{d\theta}{dp_m}$ ; i.e. the first derivative of the soil water retention characteristic. The volume fraction of water is  $d\theta = g(p_m)dp_m$ . The permittivity of a soil water layer is a function of frequency,  $f$ . To find this function,  $f_{wr}(p_m)$  has to be substituted in the Debye relaxation function (2.6). The contribution of the permittivity of one water layer to the macroscopic permittivity of soil also depends on  $d\theta$  and  $S_w(\theta)$  according to (2.47). Thus, with  $f_{wr}(p_m)$  in (2.6) and considering (2.47) the macroscopic permittivity,  $\epsilon_w$ , resulting from the water layer with matric pressure  $p_m$ , can be written as

$$\epsilon_w(p_m) = \left[ S_w(\theta) \frac{\Delta\epsilon}{1 + jf/f_{wr}(p_m)} + S_{wf \rightarrow \infty}(\theta) \epsilon_{wf \rightarrow \infty} \right] g(p_m) dp_m \quad (2.49)$$

where  $S_{wf \rightarrow \infty}(\theta)$  accounts for the effect of electric field discontinuities due to  $\epsilon_{wf \rightarrow \infty}$ . To find the contributions of all water layers from  $p_m(\theta=0)$  to  $p_m(\theta)$ , the individual contributions have to be totalled according to (2.47). For infinitesimal thin layers of water this summation can be replaced by an integration, yielding

$$\epsilon_w = \int_{p_m(\theta=0)}^{p_m(\theta)} \left[ S_w(\theta) \frac{\Delta\epsilon}{1 + jf/f_{wr}(p_m)} + S_{wf \rightarrow \infty}(\theta) \epsilon_{wf \rightarrow \infty} \right] g(p_m) dp_m \quad (2.50)$$



Considering that  $S_w(\theta)$ ,  $S_{wf \rightarrow \infty}(\theta)$  and  $\varepsilon_{wf \rightarrow \infty}$  are not functions of  $p_m$ , this can be worked out to yield

$$\varepsilon_w = S_w(\theta) \int_{p_m(\theta=0)}^{p_m(\theta)} \frac{\Delta\varepsilon}{1 + jf/f_{wr}(p_m)} g(p_m) dp_m + S_{wf \rightarrow \infty}(\theta) \varepsilon_{wf \rightarrow \infty} \quad (2.51)$$

After substituting (2.51) in (2.48), a general expression for  $\varepsilon_p$  can be found:

$$\varepsilon_p = S_w(\theta) \int_{p_m(\theta=0)}^{p_m(\theta)} \frac{\Delta\varepsilon}{1 + jf/f_{wr}(p_m)} g(p_m) dp_m + S_{wf \rightarrow \infty}(\theta) \varepsilon_{wf \rightarrow \infty} + S_s(\theta)(1-\phi) \varepsilon_s + S_a(\theta)(\phi-\theta) \varepsilon_a \quad (2.52)$$

With (2.52) the dielectric spectra can be calculated from a soil water retention characteristic, and vice versa.

The relationship between  $\varepsilon'_p$  and the soil water retention characteristic, as explained in Section 2.2, is illustrated in Figure 2.12. Note that the soil water retention characteristic is usually presented as  $p_m(\theta)$ . The permittivity as a function of frequency is given for three curves at water contents  $\theta_1$ ,  $\theta_2$  and  $\theta = \phi$ . Two calibration curves,  $\varepsilon'(\theta)_{f_1}$  and  $\varepsilon'(\theta)_{f_2}$ , are also given for water content measurements at two measuring frequencies, for example  $f_1$  for FD (at 20 MHz) and  $f_2$  for TDR ( $\approx 150$  MHz).

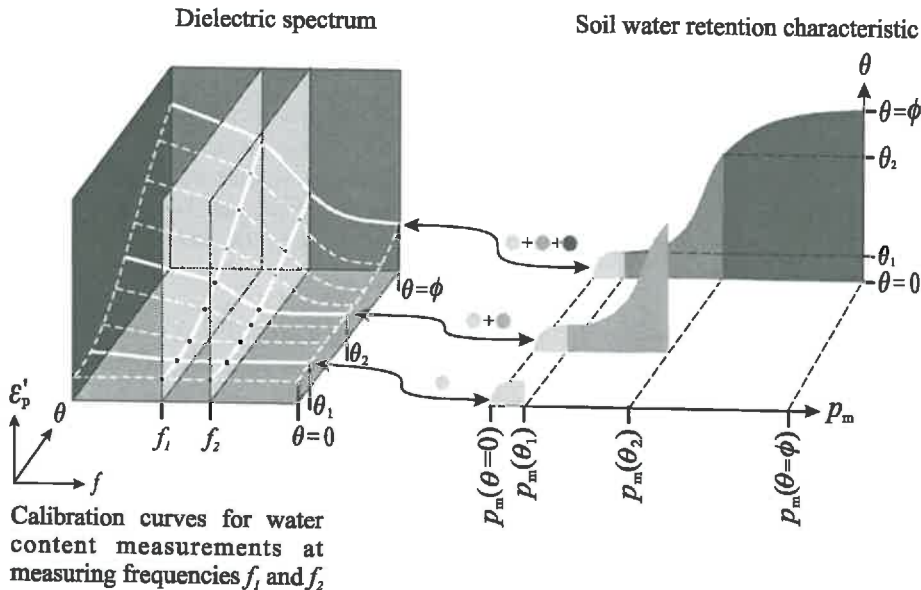


Figure 2.12. An illustration of the relationship between the soil water retention characteristic,  $p_m(\theta)$ , and the dielectric spectrum,  $\varepsilon_p(f, \theta)$ . From the dielectric spectrum it is possible to find a calibration curve,  $\varepsilon'_p(\theta)$ , for a discrete measuring frequency  $f_1$  or  $f_2$ .



### Estimation of depolarisation factors

To calculate  $\varepsilon'_p(\theta)_{f=\text{constant}}$  or  $\varepsilon_p(f)_{\theta=\text{constant}}$  from (2.52), the  $S_i(\theta)$ -values need to be known. They can be determined empirically. Let us consider glass beads with a diameter  $> 0.2$  mm. The Maxwell-Wagner effect for glass beads of this dimension is negligible. The dielectric properties at 20 °C for glass beads, air and water are  $\varepsilon_s \approx 5$ ,  $\varepsilon_a = 1$ ,  $\varepsilon_{wf \rightarrow 0} = 80.2$  and  $\varepsilon_{wf \rightarrow \infty} = 5.6$ , respectively. The depolarisation factors  $S_i(\theta)$  can be found from some extreme cases of (2.52), i.e. saturation, for infinitely low and infinitely high frequencies and for dry soil only:

$S_a(\theta)$ : For dry soils,  $S_a$  is determined only by the difference between  $\varepsilon_a$  and  $\varepsilon_s$ . Since air is the continuous phase and  $\varepsilon_a < \varepsilon_s$ ,  $S_a(\theta = 0) \approx 1$ . For wet soil,  $S_a$  is determined only by the difference between  $\varepsilon_a$  and  $\varepsilon_{wf \rightarrow 0}$  of the air-water interface. Also in this case,  $\varepsilon_a < \varepsilon_{wf \rightarrow 0}$ ; therefore the error made by assuming  $S_a(\theta) \approx 1$  is small. For  $\theta \rightarrow \phi$  the air in the pores disappears and the error becomes zero. The error made by assuming  $S_a(\theta) = 1$  for an arbitrary water content can, therefore, be regarded as acceptably small.

$S_s(\theta)$  and  $S_{wf \rightarrow \infty}(\theta)$ : For a dry soil with  $\theta = 0$ , (2.52) reduces to

$$\varepsilon_p = S_s(0)(1 - \phi)\varepsilon_s + \phi\varepsilon_a \quad (2.53)$$

For dry glass beads,  $\varepsilon_p = 3.7$  was measured. This supports that  $S_s(0) \approx S_s(\phi) \approx 1$  is a reasonable approximation. Next, consider a saturated soil ( $\theta = \phi$ ) and  $f \gg f_{wr}$  for any bound water relaxation. Assume for practical situations,  $\varepsilon_{wf \rightarrow \infty} \approx \varepsilon_s$ . Then it follows  $\varepsilon_p \approx \varepsilon_{wf \rightarrow \infty}$ . There are no electric field discontinuities in this case. Hence, it follows that  $S_s(\phi) = S_{wf \rightarrow \infty}(\phi) = 1$ .

$S_w(\theta)$ : For  $\theta = \phi$ , refraction takes place only at water-solid interfaces. For  $\phi > \theta > 0$  the refractive properties at the water-solid interfaces will stay unaffected until the last layer of water molecules evaporates, resulting in a constant depolarisation factor,  $S$ . The shape and thickness of the water film covering the particles will change with the water content resulting in a varying depolarisation factor,  $S(\theta)$ . From this a model can be deduced for the depolarisation factor  $S_w(\theta)$ . Split  $S_w(\theta)$  in a  $\theta$ -depending part  $S(\theta)$ , and the constant  $S$ :

$$S_w(\theta) = S(\theta)S \quad (2.54)$$

From measurements on glass beads for  $\theta = \phi$  it was found that  $\phi = 0.331$  and  $\varepsilon' = 28.5$ , from which  $S_w(\phi) \approx 1$  can be calculated by means of (2.48). I expect that  $S = (1/3)$ ; this in analogy with the shape factor for randomly oriented spheroids as described by Reynolds [1955] and De Loor [1956].  $S(\theta)$  is difficult to determine due to the unknown shape of the water films around the soil particles. However, the postulated form

$$S(\theta) = \frac{1}{2\phi - \theta} \quad (2.55)$$

showed a good fit with the  $\varepsilon'_p(\theta)$  curve measured for glass beads. The substitution of  $S$  and  $S(\theta)$  in (2.54) will yield

$$S_w(\theta) = \frac{1}{3(2\phi - \theta)} \quad (2.56)$$



At frequencies  $f \ll f_{wr}$  and after substituting the depolarisation factors, (2.52) reduces to

$$\epsilon_p = \frac{1}{3(2\phi - \theta)} \theta \Delta \epsilon_w + \theta \epsilon_{wf \rightarrow \infty} + (1 - \phi) \epsilon_s + (\phi - \theta) \epsilon_a \quad (2.57)$$

In Table 2.3 a comparison is made for the permittivity measured for glass beads at 20 MHz and the permittivity calculated according to (2.57).

Table 2.3. The permittivity as function of the water content of glass beads measured at 20 MHz and calculated according to (2.57).

Volumetric water content $\theta$ (-)	Permittivity	
	$\epsilon'_p$ measured (-)	$\epsilon'_p$ calculated (-)
0.0	3.71	3.68
0.11	9.57	9.34
0.19	14.92	14.69
0.23	17.65	18.32
0.27	23.00	21.80
0.33	28.54	30.22

### Comparison of (2.52) with data from literature

The validity of this empirical and hypothetical approach to determining the  $S_i$  factors can be made acceptable by comparing data from the literature with data calculated according to (2.52). The calculations are done for  $\epsilon_s = 4$ ,  $\epsilon_a = 1$ ,  $\epsilon_{wf \rightarrow 0} = 80.2$  and  $\epsilon_{wf \rightarrow \infty} = 5.6$ , respectively.

Two cases are selected from data published by Topp *et al.* [1980]. The first case is the generally accepted calibration equation for TDR by Topp, which is accurate for sand in general, but represents an average for a number of sandy loam and clay loam soils. I will refer to this equation as for an average soil:

$$\epsilon_{\text{average soil}} = 3.03 + 9.3 \theta + 146 \theta^2 - 76 \theta^3 \quad (2.58)$$

The second case holds only for vermiculite:

$$\epsilon_{\text{vermiculite}} = 2.45 + 1.8 \theta + 83.1 \theta^2 - 22.2 \theta^3 \quad (2.59)$$

The porosity of "average soils" was  $\phi \approx 0.46$  and of vermiculite  $\phi = 0.56$ , both estimated from the water content ranges given. The wave form for Topp's TDR equipment was not available. From private communication with Topp a rise time of  $\tau = 1$  ns was found to be a fair estimate. Thus the equivalent measuring frequency for which (2.58) and (2.59) are valid, is  $f = 1/(2\pi\tau) = 150$  MHz. The water retention data according to Table 2.4 were not given by Topp, but estimated on the basis of a textbook [e.g. Koorevaar *et al.*, 1983]. A plot of the soil water retention characteristics of Table 2.4 is given in Figure 2.13.

Equation (2.52) will be put in the form of the summation of the contributions of  $k$  water layers, since the data of Table 2.4 do not allow the use of the integration. Each layer has an



average soil matric pressure  $\frac{p_{mi} + p_{m(i-1)}}{2}$  and a water content  $\theta_i - \theta_{i-1}$ . Substituting  $S_w$ ,  $S_s$  and  $S_a$ , this will yield an expression for the water content  $\theta_k$  at measuring frequency  $f$ :

$$\varepsilon_p(\theta_k) = \frac{1}{3(2\phi - \theta_k)} \sum_{i=1}^k \frac{(\varepsilon_w f \rightarrow 0 - \varepsilon_w f \rightarrow \infty)}{1 + j \frac{f}{f_{wr0} e^{\frac{(p_{mi} + p_{m(i-1)}) V}{2 RT}}}} (\theta_i - \theta_{i-1}) + \theta_k \varepsilon_w f \rightarrow \infty + (1 - \phi) \varepsilon_s + (\phi - \theta_k) \varepsilon_a \quad (2.60)$$

where  $k$  refers to a particular  $\theta$ - $p_m$  pair in Table 2.4 and  $i$  to successive  $\theta$ - $p_m$  pairs from  $i = 1$  to  $i = k$ . The results for  $\varepsilon'_p(\theta)$ , calculated with (2.60), are given in Figure 2.14 together with Topp's data. For this calculation  $f$  was held constant and  $\theta$  variable. The reasonable fit between the calculated and measured curves validate the values found for  $S_i$ . It also proves that the  $S_i$ 's are valid for a broad range of soil types.

The dielectric spectra for both soils found from (2.60), with  $\theta$  being constant and  $f$  being variable between 1 MHz and 100 GHz, are shown in Figure 2.15. Since the retention characteristics are estimations, Figure 2.14 and Figure 2.15 serves only as qualitative illustrations.

Table 2.4. Soil matric pressure versus water content, estimated for two of the soils used by Topp *et al.* [1980].

Number of data set k	Soil matric pressure $p_m$ (MPa)	Volumetric water content	
		$\theta_{\text{average soil}}$ (-)	$\theta_{\text{vermiculite}}$ (-)
1	-1,000	0	0
2	-100	0.02	0.08
3	-10	0.04	0.21
4	-1	0.06	0.35
5	-0.1	0.11	0.44
6	-0.01	0.30	0.48
7	-0.001	0.45	0.51
8	-0.0001	0.46	0.54

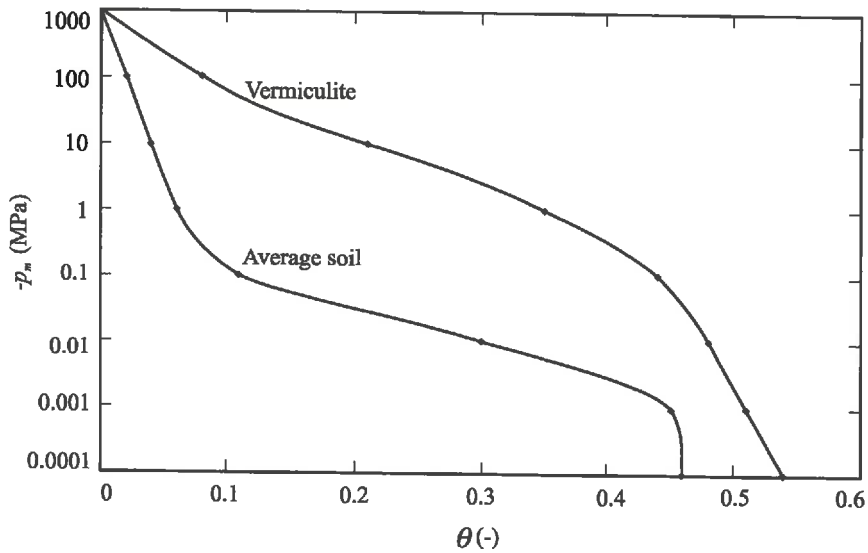


Figure 2.13. A plot of the soil water retention curves,  $p_m(\theta)$ , according to Table 2.4, estimated for the soils used by Topp *et al.* [1980].

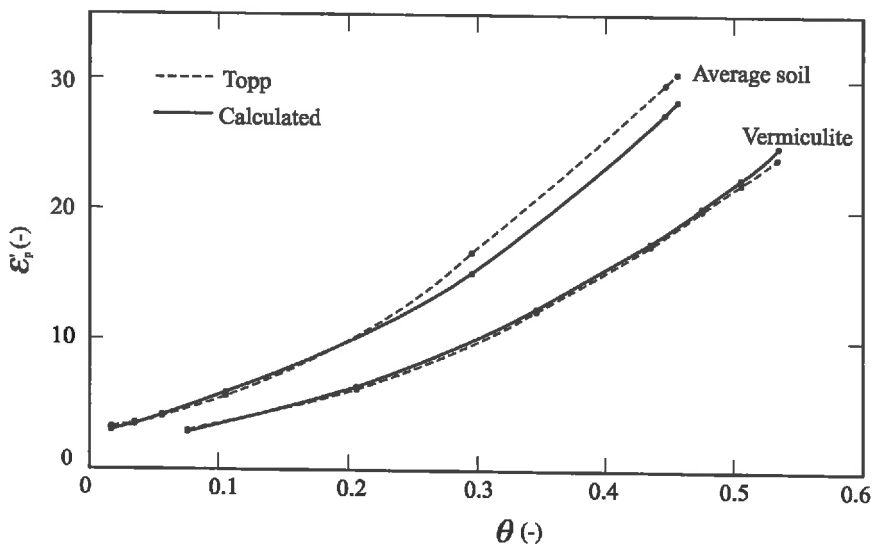


Figure 2.14. A comparison between two calibration curves,  $\epsilon'_p(\theta)$ , calculated according to (2.60) with data from Table 2.4 and measured according to Topp *et al.* [1980].



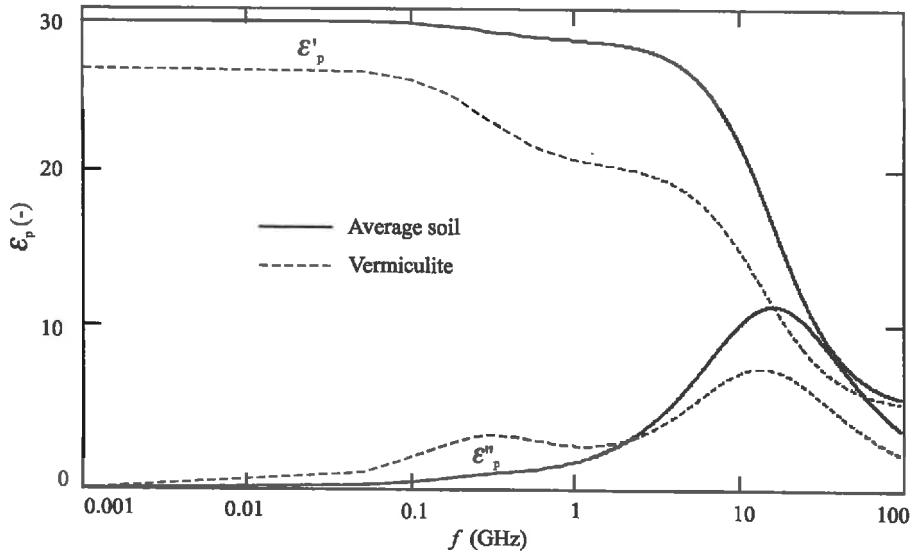


Figure 2.15. Dielectric spectra,  $\epsilon_p(f)$ , for an average soil and for vermiculite, calculated according to (2.60) with data from Table 2.4. Shown is the real,  $\epsilon'_p$ , and imaginary,  $\epsilon''_p$ , part of the permittivity due to polarisation phenomena as a function of frequency,  $f$ , and at saturation.

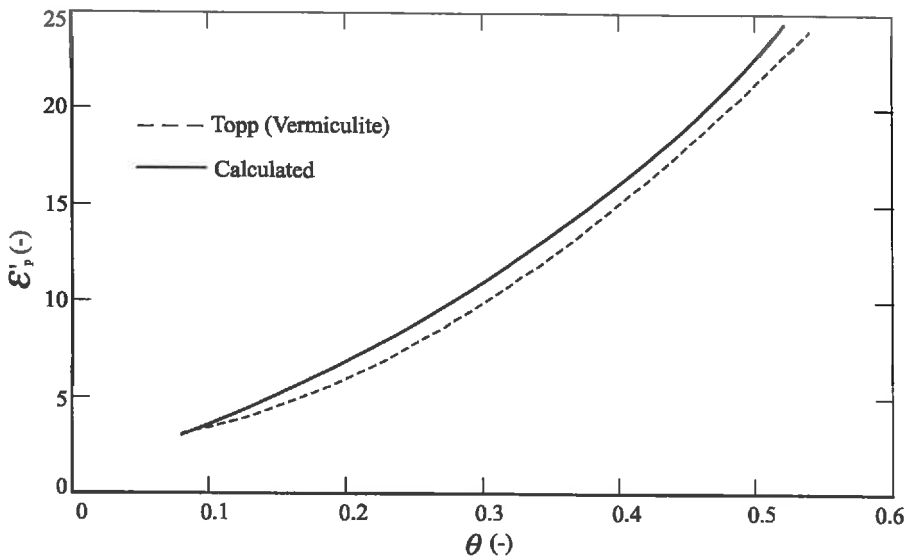


Figure 2.16. The real part of the permittivity due to polarisation phenomena,  $\epsilon'_p$ , versus water content,  $\theta$ , for a hygroscopic water content  $\theta_h = 0.08$  for vermiculite. The solid line is calculated using (2.61). The calibration curve of (2.59) according to Topp *et al.* [1980] for vermiculite is plotted as a reference.



### Simplification

Up to this point, a gradual change in relaxation frequency,  $f_r$ , is supposed. In view of the relatively sharp transition in  $f_r(p_m)$  occurring at  $p_m \approx -100$  MPa or  $f_r = 8$  GHz (see Figure 2.4), a simplification of (2.60) may be considered. Split the water content into "free" and "hygroscopic" water. Free water will be denoted with the subscript f and hygroscopic water with the subscript h. Assume for hygroscopic water  $f_{hr} \ll f$  and for free water  $f_{fr} \gg f$ . The contribution of the hygroscopic water content,  $\theta_h$ , to  $\varepsilon_p$  is only due to  $\varepsilon_{hf \rightarrow \infty} = \varepsilon_{wf \rightarrow \infty}$  and is already included in the term  $\theta_i \varepsilon_{wf \rightarrow \infty}$ . The contribution of the free water content,  $\theta - \theta_h$ , to  $\varepsilon_p$  is only due to  $\varepsilon_{if \rightarrow 0} = \varepsilon_{wf \rightarrow 0}$ . With these approximations the real part of (2.60) becomes

$$\varepsilon'_p = \frac{(\theta - \theta_h)}{3(2\phi - \theta)} (\varepsilon_{wf \rightarrow 0} - \varepsilon_{wf \rightarrow \infty}) + \theta \varepsilon_{wf \rightarrow \infty} + (1 - \phi) \varepsilon_s + (\phi - \theta) \varepsilon_a \quad (2.61)$$

with the restriction  $\theta > \theta_h$ . A plot for vermiculite with  $\theta_h = 0.08$  calculated according to (2.61) is presented in Figure 2.16, together with Topp's curve. *In Chapter 4 equation (2.61) will be applied to a number of practical measuring problems.*

### Maxwell-Wagner effect

So far, only the effect of bound water on a water content calibration curve and on the dielectric spectrum has been treated. The comparison with data measured by Topp is reasonably accurate since for TDR the impact of the Maxwell-Wagner effect is small. Now the Maxwell-Wagner effect will be included. Using the series model for the Maxwell-Wagner effect (Section 2.4), the high frequency limit for the permittivity  $\varepsilon_{MW f \rightarrow \infty}$  is determined by the series connection of dielectrics discarding conductivity. The low-frequency limit is determined by polarisation due to the air and solid fractions. A term  $K$  accounts for the texture of the soil and the ionic conduction of the pore water.  $K$  is the ratio between the thickness of the average water layer including the solids and that of the solids only.

For  $\varepsilon_{MW s}$  the contribution of air has to be included, and for  $\varepsilon_{MW w}$  the depolarisation factors shall be taken into account. Note that the thickness of the water layer, and consequently the water content,  $\theta$ , is included in  $K$ . The air fraction  $\phi - \theta$  is not included in  $K$ . It shall be included in  $\varepsilon_{MW s}$ .

Let us assume that the total capacitance,  $C_{MW}$ , as dealt with in Section 2.4, averaged over a volume of soil, is the same as can be calculated with the permittivity of a heterogeneous material as shown in Section 2.5. Then, the high-frequency limit of the Maxwell-Wagner effect is

$$\varepsilon_{MW f \rightarrow \infty} = \varepsilon'_p \quad (2.62)$$

where  $\varepsilon'_p$  is described by (2.61). In (2.29)  $\varepsilon_{MW s}$  is equal to the solid and air terms of  $\varepsilon'_p$ . Using the simplified expression for  $\varepsilon'_p$  as described by (2.61),  $\varepsilon_{MW s}$  can be derived from

$$\varepsilon_{MW s} = (1 - \phi) \varepsilon_s + (\phi - \theta) \varepsilon_a \quad (2.63)$$

Furthermore, in (2.29)  $\varepsilon_{MW w}$  is equal to the water terms of  $\varepsilon'_p$  of (2.61). Therefore,  $\varepsilon'_{MW w}$  follows from

$$\varepsilon'_{MW w} = \frac{1}{3(2\phi - \theta)} (\varepsilon_{wf \rightarrow 0} - \varepsilon_{wf \rightarrow \infty}) + \varepsilon_{wf \rightarrow \infty} \quad (2.64)$$



Finally, with (2.63) and (2.64) substituted in (2.29), the permittivity of soil can be described by

$$\varepsilon = \left[ \frac{\varepsilon_{MWs}(K-1)}{\varepsilon'_{MWw} + 1} + 1 \right] \varepsilon'_p \quad (2.65)$$

where  $\varepsilon'_p$  is described by (2.61).

To use (2.65) to predict soil water contents first  $K$  must be known. The relationship between  $K$  and the soil texture is not well defined yet. Therefore, (2.65) will not be applied to the dielectric characterisation of soils in this thesis. Still (2.65) and the underlying theory gives insight in the dielectric behaviour of soil. This will be demonstrated in Section 4.5 using the dielectric properties of concrete. The dielectric behaviour of concrete is very similar to that of soil, but with all aspects in extreme.

### Discussion and conclusions

In this section a new model (2.61) for the dielectric properties of soil was described. This model links parameters very common in soil science to the dielectric behaviour of soil. In this way it is possible to characterise the soil from its dielectric behaviour. For instance, from dielectric measurements we can derive the water content,  $\theta$ , the soil matric pressure,  $p_m$ , the porosity,  $\phi$ , and textural information. It is shown that the permittivity is a function of porosity. The  $\phi$ -value for an arbitrary soil is normally unknown. Without knowing this parameter it is not possible to predict a calibration curve  $\varepsilon'(\theta)$ . The same applies to  $K$  and the hygroscopic water content. Calibration curves found by Topp *et al.* [1980] indicate a clear spread depending on soil type. For instance, if  $\varepsilon' = 15$  is measured, the corresponding  $\theta$  may range between  $\theta = 0.2$  for glass beads to  $\theta = 0.4$  for vermiculite. At a number of occasions Topp [1996] has pointed out that the so-called "Topp" curve is not universal. Also Dirksen & Dasberg [1993] and Dirksen & Hilhorst [1994] showed for sensors working in either the time domain or in the frequency domain that the "Topp" curve is not universally applicable. Therefore, *calibration of  $\varepsilon'(\theta)$  for a soil of interest is unavoidable if an accuracy of better than  $\pm 0.1$  is required.*







### 3. A NEW SENSOR FOR DIELECTRIC SOIL CHARACTERISATION

The relationship between compositional and textural properties of soil and its dielectric behaviour, expressed in terms of electrical permittivity, was treated in Chapter 2. The permittivity,  $\epsilon$ , is a complex quantity expressing the ability to polarise a material. The real part,  $\epsilon'$ , is a measure of the polarisation or energy storage and the imaginary part,  $\epsilon''$ , a measure of the energy absorption or dielectric loss. It has been shown, theoretically, that  $\epsilon$  can be used as a measure of porosity, water content, matric potential, texture and ion concentration. A well-known model for a dielectric, like soil, between two conductive electrodes is a lossy capacitor. The equivalent circuit for such a capacitor is a loss-free capacitor,  $C$ , with a conductor  $G$  in parallel.  $C$  represents the energy storage capability of a dielectric and is related to  $\epsilon'$ .  $G$  represents the energy loss due to the ionic conduction,  $\sigma$ , as well as the dielectric loss,  $\epsilon''$ .  $C$  and  $G$  are the quadrature components of the complex impedance,  $Z$ , between the electrodes.

Dielectric measurements can be performed using techniques common in electronic engineering. A successful group of instrumentation for  $\epsilon$  measurements in soil is based on Time Domain Reflectometry (TDR) Davis [1975]. A transmission line is formed by two parallel rods placed in the soil. An electrical pulse or step function, containing frequencies in a broad band width, propagates between two parallel rods and reflects at the end of the line. The travel time and attenuation with respect to the applied signal is a measure of  $\epsilon'$  and  $\epsilon''$  of the soil. Popular TDR instrumentation are the cable tester made by Tektronix and the instrumentation intended especially for measurements of the soil water content, made by Soil moisture Equipment Company, which make use of a step function for the propagation time measurements. Sensors designed by IMKO [1991] measure the propagation time of an impulse which allows for a pure electronic detection of the reflected pulse as well as for simpler electronics. With the help of Fourier analysis it is possible to perform TDR measurements using network analysers. Precise and high-level analysers for this purpose are commercially available, e.g. Hewlett Packard and Rohde & Schwarz. In general, TDR instrumentation can be accurate but is expensive, requires skilled operators and is not well suited for agricultural practice. Hence, serious obstacles for the application of dielectric sensor technology for routine use in the field. However, TDR is still widely used for  $\theta$  measurements [Topp *et al.*, 1982; Heimovaara, 1993; Whalley, 1993] due to the high demand for water content sensors.

Until recently, a reliable  $\epsilon$  measurement especially at radio frequencies (RF) and high  $\sigma$ , was only possible with the help of advanced and expensive laboratory equipment. The oldest instrument to measure  $Z$  is the impedance bridge. A number of impedance bridges were reviewed by Ferguson [1953]. The bridge had to be balanced with a reference impedance at the frequency of interest. More recently, we have the availability of vector voltmeters and



advanced network analysers for use in the laboratory. This type of instrumentation works in the Frequency-Domain (FD) at one or more discrete frequencies. It measures the amplitude and phase shift of the signal resulting from the application of a (sine wave) test signal to the rods, from which  $C$  and  $G$  can be calculated. More user-friendly FD instrumentation, intended for field use, is based on the use of a shift of the resonance frequency of an oscillator [Babb, 1951; Tursky & Malicki, 1974; Wobschall, 1978; Hilhorst, 1984; Hilhorst *et al.*, 1992; Heathman, 1993]. Recently, other field instrumentation has become available using standing wave-form or reflection coefficient measuring techniques [Delta-T, 1995]. These methods are less sensitive to electromagnetic interference (EMI).

Both TDR and FD sensors have demonstrated their potential in  $\theta$  and  $\sigma$  measurements. Up to now most dielectric sensors have been used for research purposes due to their high cost and the difficulty of use. In general farmers who want to use such sensors for irrigation scheduling purposes are not sufficiently skilled to operate them. In addition, due to the heterogeneous nature of the water distribution in soils, various sensors per field are needed for averaging, making the price per sensor an important issue. *In the following a new sensor will be described for dielectric soil characterisation. The permittivity measurement is based on synchronous detection at a discrete frequency. All the necessary analogue and digital electronics are integrated on a single application-specific integrated circuit (ASIC), being a single-chip four-channel vector voltmeter. The use of an ASIC guarantees the lowest price in high-volume production.*

In Section 3.1 a general model of a dielectric sensor is described. In Section 3.2 the development of an ASIC for water content measurements is treated on a system level. Next, some aspects concerning the electrodes are treated. Finally, a complete sensor will be described in Section 3.4 with some validation results.

### 3.1 A GENERAL MODEL FOR DIELECTRIC SENSORS

In this section a number of electronic engineering topics will be introduced briefly. For more comprehensive treatments, see textbooks on electronic engineering [e.g. Lorrain *et al.*, 1988; Balanis, 1989].

The application of an electric potential,  $U$ , across the electrodes of capacitor,  $C$ , will displace a charge,  $Q$ , causing an alternating current to flow from one electrode to the other. The relationship between  $Q$ ,  $U$  and  $C$  is given by

$$Q = UC \quad (3.1)$$

The displaced charge is related to the current through the capacitor,  $i_C$ , as a function of time,  $t$ , by

$$Q = \int i_C(t) dt \quad (3.2)$$

A potential across the electrodes that alternates as a function of time,  $u(t)$ , will displace an alternating charge,  $q(t)$ , causing an alternating electric current  $i_C(t)$ .





The relationship between  $q(t)$  and  $i_C(t)$  in the interval  $t_1$  to  $t_2$  is

$$q(t) = \int_{t_1}^{t_2} i_C(t) dt \quad (3.3)$$

The voltage,  $u(t)$ , that develops across the capacitor due to  $i_C(t)$ , is given by

$$u(t) = \frac{1}{C} \int_{t_1}^{t_2} i_C(t) dt \quad (3.4)$$

If the current through the capacitor is a sine wave with radian frequency  $\omega$ , i.e.  $i_C(t) = |i_C| \cos(\omega t)$ , it can be seen from (3.4) that  $u(t) = |u| \sin(\omega t)$ . The phase of the amplitude of  $i_C(t)$  is  $90^\circ$  ahead with respect to  $u(t)$ .  $i_C(t)$  is an imaginary quantity and may be represented by  $j i_C(t)$ , where  $j^2 = -1$ . In contrast, the voltage  $u(t) = |u| \sin(\omega t)$  across a conductor is in-phase with the current through it i.e.  $i_G(t) = |i_G| \sin(\omega t)$ , where  $i_G(t)$  is a real quantity. Note that only the in-phase component will cause power dissipation or energy loss. The  $90^\circ$  out-of-phase component will store energy or charge the capacitor. The total current through a parallel combination of a conductor and a capacitor can be written in complex notation as  $i = i_G + j i_C$ .

The complex impedance of the circuit,  $Z$ , is defined by  $Z = u/i$ . In the context of this section it is often more convenient to use the admittance defined by  $Y = 1/Z = i/u$ . In the following, either  $Z$  or  $Y$  will be used depending on the readability of the equations. The in-phase component or conductance is defined as  $G = i_G/u$  and the  $90^\circ$  out-of-phase component or susceptance as  $\omega C = i_C/u$ . With these expressions  $Y$  can conveniently be written as

$$Y = \frac{i_G}{u} + j \frac{i_C}{u} = G + j\omega C \quad (3.5)$$

$Y$  can be represented graphically in a complex impedance plane by a rotation vector with length  $|Y| = \sqrt{G^2 + \omega C^2}$  and phase  $\alpha = \arctan(\omega C/G)$  with respect to  $G$ .

From electronic circuit theory it is known that the relationship between the complex permittivity according to (2.3),  $\epsilon$ , and  $C$  is

$$C = \epsilon \epsilon_0 \kappa \quad (3.6)$$

where  $\kappa$  is a geometry factor which is determined by the distance between the electrodes and their areas. With this, the admittance,  $Y$ , of a lossy capacitor can be described by

$$Y = j\omega \epsilon \epsilon_0 \kappa = \omega \epsilon'' \epsilon_0 \kappa + j\omega \epsilon' \epsilon_0 \kappa \quad (3.7)$$

where  $\epsilon$  is the complex permittivity according to (2.3) and  $\omega$  the angular frequency. The real component can be represented by a conductor. The imaginary term can be represented by the susceptance of a capacitor; hence (3.5) and (3.7) are identical. Consequently,  $Y$  may be represented graphically in a complex permittivity plane by a rotation vector with length  $|Y| = \omega \epsilon_0 \kappa \sqrt{\epsilon''^2 + \epsilon'^2}$  and phase  $\alpha = \arctan(\epsilon'/\epsilon'')$  with respect to  $\epsilon''$ . The electrodes may have arbitrary shapes such as plates, rods or discs. Soil water content sensors are normally equipped with two or more parallel rods as electrodes.



As an example,  $\kappa$  for two parallel rods [Fink & Christiansen, 1982] is expressed as

$$\kappa = \frac{\pi l}{\ln(d/r)} \quad (3.8)$$

where  $l$  represents the length,  $r$  the radius and  $d$  the distance between the rods.

Let us apply a current,  $i$ , to the rods. A complex voltage,  $u = iY$  will then develop across the capacitor. This complex voltage with amplitude,  $|u|$ , and phase,  $\alpha$ , relative to the applied current can be expressed by  $u = |u|e^{j\alpha}$ . The amplitude and phase of  $i$  and  $u$  can be measured using a vector voltmeter of which the admittance

$$Y = \frac{i}{|u|e^{j\alpha}} \quad (3.9)$$

can be determined. An electric model for such a dielectric measurement is given in Figure 3.1. Knowing the applied current and the measured voltage with its phase, the unknown admittance can be calculated, and consequently  $G$  and  $C$  from (3.5). From (3.5) and (3.7) the real and imaginary parts of the permittivity,  $\epsilon'$  and  $\epsilon''$ , can be found:

$$\epsilon' = \frac{C}{\epsilon_0 \kappa} \quad (3.10)$$

$$\epsilon'' = \frac{G}{\omega \epsilon_0 \kappa} \quad (3.11)$$

It is more practical to work with electrical conductivity of the bulk soil,  $\sigma_b$ , (Chapter 2.1) which can be found from (3.11) and (2.5):

$$\sigma_b = \frac{G}{\kappa} \quad (3.12)$$

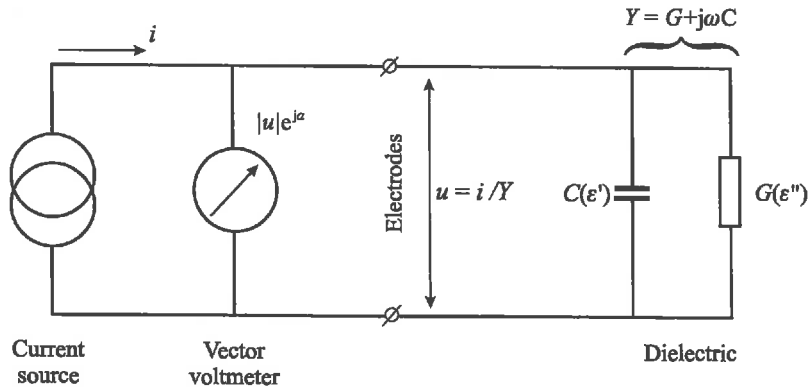


Figure 3.1. Electric model for measuring the dielectric properties of materials. The current,  $i$ , will develop a voltage,  $u$ , across the admittance,  $Y$ , with amplitude,  $|u|$ , and phase shift,  $\alpha$ , with respect to  $i$ . The quadrature components of the permittivity,  $\epsilon'$  and  $\epsilon''$ , can be calculated from  $Y$ .



## 3.2 DESIGN OF AN INTEGRATED CIRCUIT FOR DIELECTRIC SENSORS

From experience [Hilhorst *et al.*, 1992] it is known to be essential to process the sensitive input signals as close to the electrodes as possible in order to reduce errors due to length variations of the wiring and the bending of cables. electromagnetic interference (EMI) can also be minimised by using short cables. Phase response of electronic circuitry causes errors proportional to conductivity [Hilhorst, 1984]. Phase response errors of an electronic circuit are small for short wiring and small parasitic capacitors, as is the case on a monolithic integrated circuit (IC). From a reliability point of view, an IC makes a sensor solid and dependable. It has a lower mean-time-between-failures than a comparable circuit built with discrete components on a printed-circuit board [Fink & Christiansen, 1982]. Finally, an IC guarantees the lowest possible cost in mass production. Therefore, an application specific integrated circuit (ASIC) for the measurement of a complex impedance was designed .

*In this section the ASIC as designed by Hilhorst et al. [1993] will be described.* Although, the digital part of the ASIC as designed by J. Balendonck at IMAG-DLO (see Hilhorst *et al.* [1993]) is beyond the scope of this thesis, some aspects will be highlighted. The analogue part of the ASIC performs both the current source and the vector voltmeter functions. First the requirements will be discussed. Then the measuring principle and its realisation will be treated on the system level. Attention will be paid to critical circuit details such as the impedance input circuitry.

### Accuracy, dynamic range and maximum phase error requirements

The global requirements for the impedance measuring system, based on experiences with a dielectric water content and ionic conductivity sensor as described by Hilhorst [1984], are:

- complex impedance measurements at frequencies between 10 MHz and 30 MHz,
- capacitance measurements up to 100 pF with an accuracy of 1 pF and a resolution of 0.1 pF at 20 MHz,
- conductance measurements up to 100 mS with an accuracy of 1 mS and a resolution of 0.1 mS at 20 MHz,
- on-board analogue to digital conversion with RS232 output,
- low power consumption and single 5 V supply,
- no manual adjustment points.

For soil moisture measurements, the maximum susceptance at 20 MHz of the capacitor,  $C_{\max}$ , between the rods is  $\omega C_{\max} = 12.6 \text{ mS}$ , where  $\omega = 2\pi f$  is the radial frequency and  $f$  the measuring frequency. This is much smaller than the maximum conductance  $G_{\max} = 100 \text{ mS}$  in parallel with it. For the desired accuracy of the system, therefore, it is sufficient to concentrate on the accuracy of the capacitance measurement in parallel with  $G_{\max}$ . This requires an accuracy of  $\Delta C = 1 \text{ pF}$  on a scale of 100 pF. The admittance,  $Y$ , of the parallel combination of  $C$  and  $G_{\max}$  is

$$Y = G_{\max} + j\omega C \quad (3.13)$$



from which the phase angle,  $\alpha$ , can be derived:

$$\alpha = \arcsin \frac{\omega C}{G_{\max}} \quad (3.14)$$

The error of the capacitance measurement,  $\Delta C$ , and consequently the phase error,  $\Delta\alpha$ , may be found from substituting them in (3.14);

$$\alpha + \Delta\alpha = \arcsin \frac{\omega(C + \Delta C)}{G_{\max}} \quad (3.15)$$

The angles  $\alpha$  and  $\Delta\alpha$  are small for  $G_{\max} \gg \omega C_{\max}$ . Using straightforward goniometric manipulations and with the approximations  $\cos(\Delta\alpha) \approx 1$ ,  $\cos(\alpha) \approx 1$  and  $\sin(\Delta\alpha) \approx \Delta\alpha$ , (3.15) can be written as

$$\Delta\alpha = \arcsin \frac{\omega \Delta C}{G_{\max}} \quad (3.16)$$

The phase accuracy should be better than  $\Delta\alpha = \arcsin(0.125 \text{ mS} / 100 \text{ mS}) = 0.07^\circ$  for the required capacitance accuracy. The dynamic range  $G_{\max} / \omega \Delta C = 100 \text{ mS} / 0.125 \text{ mS} = 800$ . Therefore, the requirements for the electronics at 20 MHz are:

- phase errors  $< 0.07^\circ$ , and
- dynamic range  $> 800$ .

#### The impedance measuring system at a glance

The following is intended to provide a general introduction to the impedance measuring system on board of the ASIC as described in this section. The system errors associated with the measurement of a complex impedance will be introduced using a vector diagram. Then, a simplified block diagram of the impedance measuring system on the ASIC will be described briefly.

As explained earlier the complex impedance,  $Z$ , may conveniently be represented by its admittance,  $Y$ , as given by (3.5).  $Y$  can be found from measuring the voltage developed across  $Y$  on the application of a known current. A voltage measurement is always subjected to dc offset errors. If the ac component of the voltage across  $Y$  is shifted by  $180^\circ$ , the measurement will return a negative value for  $Y$ , but the sign of the dc offset will be unchanged. The  $180^\circ$  phase shift can accurately be realised using a switch. To measure the two quadrature components of  $Y$ ,  $G$  and  $jB = j\omega C$ , the measuring instrument should be able to measure exactly at  $0^\circ$  and  $90^\circ$ . This cannot be achieved without phase error. These phase errors will be represented by  $\phi_0$  and  $\phi_{90}$ .

In Figure 3.2 the vectors  $Y$  and  $-Y$  and their quadrature components are plotted. The measured vectors, denoted by  $M$ , are plotted with grey lines in the same plane as the real admittance showing how they are related to  $Y$ . Subtraction of the vectors  $G_{M0^\circ}$  and  $G_{M180^\circ}$  measured for a phase shift of  $0^\circ$  and  $180^\circ$  yield the vector  $G_M$  which is corrected for offset errors. Likewise, the vector  $B_M$  can be found. Using reference components with known  $G$  and  $B$ , the angle's  $\phi_0$  and  $\phi_{90}$  with respect to  $G_M$  and  $B_M$  can be calculated.  $G_M$  and  $B_M$  are plotted with dashed lines. Next, an arbitrary admittance can be measured with this procedure. A simplified block diagram of the impedance measuring principle is shown in Figure 3.3.

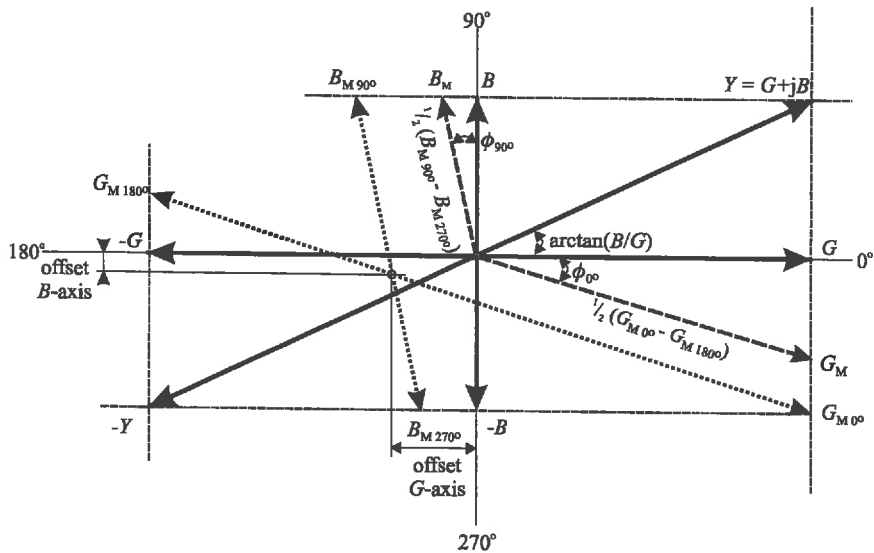


Figure 3.2. Vector diagram showing how the measured values, denoted by M, with phase errors,  $\phi_0$  and  $\phi_{90}$ , and the offsets on the B and G axis, are related to the real values in the complex admittance plane  $Y = G + jB$ , where G represents the conductance and B the susceptance. The measured values are drawn as dotted lines. The dashed lines are the vectors corrected for offset and calculated from the measured values.

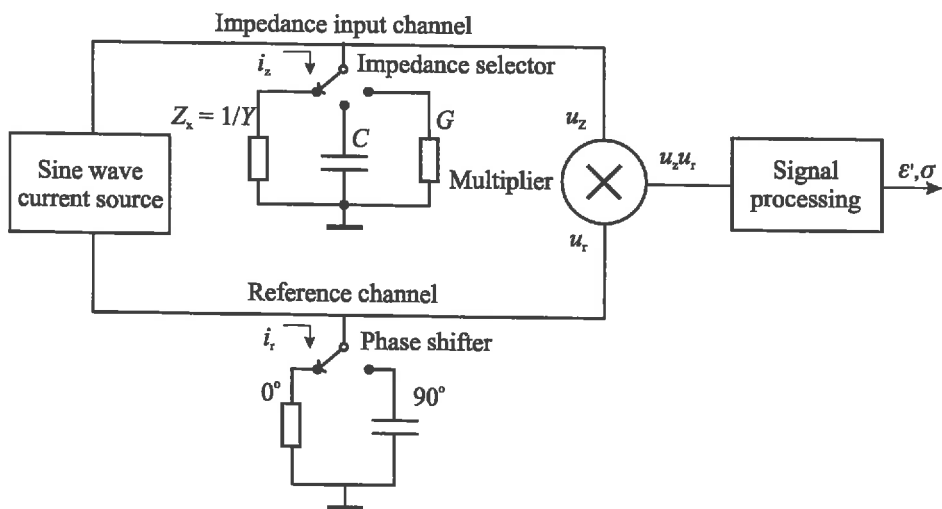


Figure 3.3. Simplified block diagram of the impedance measuring principle.



The principle is known as synchronous detection, i.e. detection of a signal of the same frequency as a reference signal. The detector is frequency-selective as well as phase-sensitive. Here, the two signals are sine waves generated by a current source. One of these currents is fed to the impedance input channel,  $i_z$ , the other with equal phase is used as the reference current,  $i_r$ . The unknown impedance of the soil between the electrodes,  $Z_x$ , can be connected to the impedance input channel using the impedance selector. A voltage,  $u_z$ , will develop across  $Z_x$ . Since  $Z_x$  is a parallel combination of a conductor and a capacitor, it is a complex quantity and the phase of  $u_z$  is shifted by an angle  $\alpha$  with respect to  $i_r$ .

The reference current is fed to either a resistor or a capacitor via the phase shifter switch. The reference voltage,  $u_r$ , developed will accordingly be shifted by  $0^\circ$  or  $90^\circ$  with respect to  $u_z$ . For the sake of simplicity the phase shifts are assumed to be exact. Both voltages are fed to a multiplier. The result of multiplying the two sine waves,  $u_z u_r$ , is a signal composed of a constant and a sine wave of the double frequency, as can be seen from the goniometric equality

$$\sin \alpha \sin \beta = \frac{1}{2} \cos(\alpha - \beta) - \frac{1}{2} \cos(\alpha + \beta) \quad (3.17)$$

With the reference,  $u_r$ , shifted by  $\beta$ , the multiplication results in

$$u_z \sin(\omega t + \alpha) u_r \sin(\omega t + \beta) = \frac{u_z u_r}{2} \cos(\alpha - \beta) - \frac{u_z u_r}{2} \cos(2\omega t + \alpha + \beta) \quad (3.18)$$

The double-frequency component can be filtered out leaving the proportionality

$$u_z \sin(\omega t + \alpha) u_r \sin(\omega t + \beta) \propto \frac{u_z u_r}{2} \cos(\alpha - \beta) \quad (3.19)$$

which is a function of both  $\alpha$  and the amplitude of  $u_z$  if  $u_r$  is constant. The angles  $\alpha$  and  $u_z$  can be determined from two measurements with  $\beta = 0^\circ$  and  $\beta = 90^\circ$ . This enables the separation of the two quadrature components of  $Z_x$ . In case  $Z_x$  is a resistor, for which  $\alpha = 0^\circ$ , the left hand side of (3.19) is  $(u_z u_r)/2$  for  $\beta = 0^\circ$  and zero for  $\beta = 90^\circ$ . In case  $Z_x$  is a capacitor, for which  $\alpha = 90^\circ$ , the left hand side of (3.19) is zero for  $\beta = 0^\circ$  and  $(u_z u_r)/2$  for  $\beta = 90^\circ$ . The absolute value of  $Z_x$  can be found from a calibration measurement using both the capacitor,  $C$ , and the conductor,  $G$ , selected by the impedance selector. The latter also enables us to eliminate a number of uncertainties arising from imperfections of the current source, temperature sensitivity, etc. The signal processor, consisting of both hardware and software, contains a filter to remove the double-frequency component. The geometry factor of the electrodes can be determined automatically, guided by the PC software using known dielectrics such as water. For an unknown dielectric such as soil, finally, the permittivity,  $\epsilon$ , and ionic conductivity,  $\sigma$ , can be calculated from  $C$  and  $G$  by the software.

### The impedance measuring system

A more detailed block diagram of the impedance measuring principle is shown in Figure 3.4. The measuring principle is based on synchronous detection. As described earlier, synchronous detection involves the multiplication of a reference sine wave with a sine wave of which the amplitude and phase are modulated by the impedance of interest. To decompose the unknown signal in the two quadrature components, the reference sine wave is applied in phase and  $90^\circ$  out of phase.

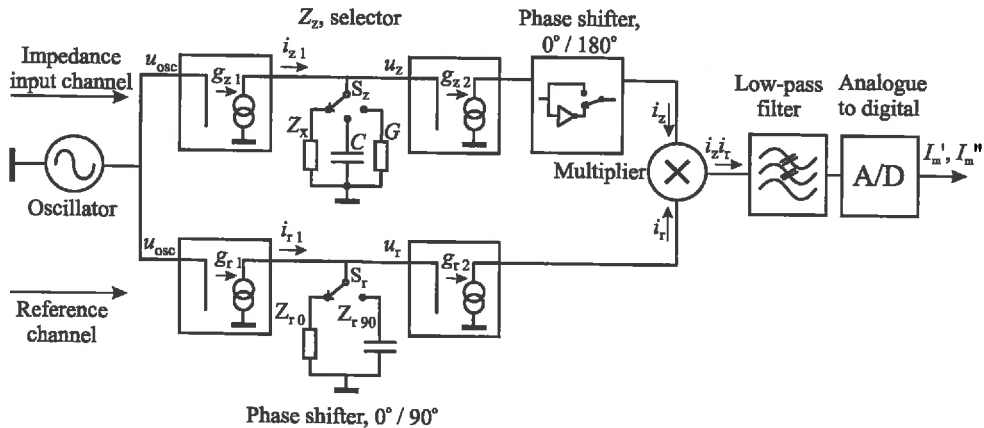


Figure 3.4. Block diagram of the impedance measuring principle as designed by Hilhorst *et al.* [1993].

An HF oscillator produces a differential sine wave voltage  $u_{osc} = |u_{osc}| \sin(\omega t)$ , where  $t$  is time and  $|u_{osc}|$  the amplitude of  $u_{osc}$ . This signal, as shown in Figure 3.4, is fed to the impedance input channel, via a transconductance amplifier with gain  $g_{z1}$ . A transconductance amplifier generates an output current on the application of an input voltage. Ideally, it requires no input current and the output impedance is infinitely high. The voltage developed at the output is proportional to the impedance connected to it. The output current of  $g_{z1}$ ,  $i_{z1} = u_{osc} g_{z1}$ , flows through the complex impedance  $Z_z = 1/(G + j\omega C_z)$ .  $Z_z$  is the impedance connected to the impedance channel by the switch  $S_z$ , which is switched in a predefined sequence, by the control logic.  $Z_z$  can be the unknown  $Z_x$ , the reference conductance  $G$  or the reference capacitance  $C$ . Both references have maximum scale values and include parasitics. The voltage,  $u_z$ , developed across  $Z_z$  is  $u_z = i_{z1} Z_z$ . The second transconductance amplifier with gain  $g_{z2}$  transforms  $u_z$  into  $i_z = u_z g_{z2}$ . Finally the output current of the measuring channel can be written as:

$$i_z = p |Z_z| \sin(\omega t + \alpha_z + \phi_z) \quad (3.20)$$

where  $p = g_{z1} g_{z2} |u_{osc}|$ ,  $\alpha_z$  is the phase shift caused by  $Z_z$ , and  $\phi_z$  is the total phase error of the impedance channel. This error is caused by imperfections of  $g_{z1}$ ,  $g_{z2}$ , the switches and the wiring.

Decomposition of  $i_z$  into its quadrature components is possible with synchronous detection. After rectification of  $i_z$ , a dc output current,  $I_m$ , will be obtained which is a function of  $Z_z$ . Synchronous detection involves multiplication of  $i_z$  by a reference current,  $i_r$ . The multiplication of two sine waves results in a sine wave of the doubled frequency and a parameter. The ac signal with the doubled frequency can be filtered out. The parameter is a dc current,  $I_m$ , and is related to the amplitude and phase difference between the input currents. The quadrature components of  $i_z$  are obtained by shifting the reference by  $0^\circ$  and  $90^\circ$ , respectively. For analogue monolithic integrated circuits the multiplier function is normally implemented using a Gilbert multiplier [Gilbert, 1974]. The advantage of synchronous detection over other methods is that it contains no resonance circuits that have to





be adjusted. It is ideally suited to be integrated in an integrated circuit. It is insensitive to signals with other frequencies than exactly the one at its reference input, making the circuit almost immune to electromagnetic interference (EMI). Finally, a synchronous detector easily accommodates a dynamic range of more than three decades. This allows to work with low-level signals reducing electromagnetic radiation to a minimum.

The reference current,  $i_r$ , is generated by the reference channel in the same way as  $i_z$ . The reference channel consists of two fixed impedances,  $Z_{r0}$  and  $Z_{r90}$ , again switched in a predefined sequence. Parasitics in parallel with  $Z_{r0}$  and  $Z_{r90}$ , phase errors due to the switch, the wiring and the transconductance amplifiers,  $g_{r1}$  and  $g_{r2}$ , are included in the phase error term of the reference channel,  $\phi_r$ . Therefore,  $Z_{r0}$  and  $Z_{r90}$  can be treated to be ideal, i.e. they cause  $i_r$  to shift by  $\beta = 0^\circ$  or  $\beta = 90^\circ$  depending on the setting of the switch  $S_r$ . Similar to  $i_z$  we can write for the reference current

$$i_r = q \sin(\omega t + \beta + \phi_r) \quad (3.21)$$

where  $q = g_{r1}g_{r2}|Z_r||u_{osc}|$ ,  $|Z_r|$  represents the absolute value of  $Z_{r0}$  or  $Z_{r90}$ , respectively, depending on the setting of switch  $S_r$ . Multiplication of (3.20) with (3.21) yields

$$i_m = i_z i_r = P |Z_z| [\cos(\alpha_z - \beta + \phi) - \cos(2\omega t + \alpha_z + \beta + \phi_z + \phi_r)] \quad (3.22)$$

where  $P = pq/2$  is the overall transfer constant and  $\phi = \phi_z - \phi_r$  the overall phase error. After removing the  $2\omega$  component using a low-pass filter  $I_m$  will remain.

The two quadrature components of  $I_m$ ,  $I'_m$  and  $I''_m$ , can be derived now.  $I_m$ ,  $P = P_{0^\circ}$  and  $\phi = \phi_{0^\circ}$  are obtained with the reference shifted by  $\beta = 0^\circ$ .  $I''_m$ ,  $P = P_{90^\circ}$  and  $\phi = \phi_{90^\circ}$  are obtained with the reference shifted by  $\beta = 90^\circ$ . The result for  $I_m$  is

$$I_m = P_{0^\circ} |Z_z| \cos(\alpha + \phi_{0^\circ}) \quad \text{and} \quad I''_m = P_{90^\circ} |Z_z| \sin(\alpha + \phi_{90^\circ}) \quad (3.23)$$

To block dc currents the different electronic functions of a discrete electronic circuit, intended to operate upon only ac currents, are normally coupled via capacitors. These capacitors are of high values,  $1 \mu\text{F}$  or more and bulky. The design of monolithic integrated circuits do not allow the integration of such large capacitors due to the limited area available on the surface of an IC. The circuit will be dc-coupled, from the oscillator up to the output of the input of the analogue to digital converter and a dc offset current,  $I_{m \text{ offset}}$ , must be taken into account.  $I_{m \text{ offset}}$  is composed of a fixed dc current and a dc current depending on the setting of the switches. The first one can be eliminated by repeating the measurements with an additional  $180^\circ$  phase shift. After converting the analogue output current  $I_m$  to a digital signal, it can be further processed by software. Subtraction of the  $0^\circ$  and  $180^\circ$  shifted results yields only the quadrature components

$$I = \frac{1}{2} \left[ \left( I_{m0^\circ} + I_{m \text{ offset}} \right) - \left( I_{m180^\circ} + I_{m \text{ offset}} \right) \right] \quad \text{and} \\ I'' = \frac{1}{2} \left[ \left( I''_{m0^\circ} + I''_{m \text{ offset}} \right) - \left( I''_{m180^\circ} + I''_{m \text{ offset}} \right) \right] \quad (3.24)$$

where  $I$  and  $I''$  represent the real and imaginary parts, respectively, of a new complex plane  $I = I' + jI''$  for which  $I$  is proportional to  $Z_z$ .



The offset current that depends on the settings of the switches will be eliminated differently. The problem could not be solved mathematically. Special circuitry regulates in a control loop the offset current of the impedance input channels for each measuring state. A detailed description of this circuit is beyond the scope of this thesis.

### Retrieving the measured impedance from the output signals of the ASIC

In the following, a mathematical algorithm will be developed to calculate  $Z_z$  and of this the permittivity from the output signals of the ASIC.

The accuracy of values for gain, resistors and capacitors on an integrated circuit are not better than + or - 20 % and the temperature stability is usually poor. To reach a measuring accuracy of 1 pF it is necessary to perform reference measurements before or after measuring  $Z_x$ . Thus, the measurements at  $0^\circ$ ,  $90^\circ$ ,  $180^\circ$  and  $270^\circ$  have to be performed for  $Z_x$ ,  $C$  and  $G$ . First  $I'$  and  $I''$  have to be calculated according to (3.24).

For simplicity, let us assume first that both the reference capacitor,  $C$ , and conductor,  $G$ , are ideal and not affected by parasitics. Then, the phase of  $i_z$  is  $\alpha_G = 0^\circ$ ,  $\alpha_C = 90^\circ$  and  $\alpha_x = \arctan(\omega C_x/G_x)$ , respectively. The results of the series of measurements can be written as:

$$I'_G = P_{0^\circ} \left| \frac{1}{G} \right| \cos(0^\circ + \phi_{0^\circ}) \quad (3.25)$$

$$I'_C = P_{0^\circ} \left| \frac{1}{\omega C} \right| \cos(90^\circ + \phi_{0^\circ}) \quad (3.26)$$

$$I'_x = P_{0^\circ} \left| \frac{1}{G_x^2 + \omega^2 C_x^2} \right| \cos(\alpha_x + \phi_{0^\circ}) \quad (3.27)$$

$$I''_G = P_{90^\circ} \left| \frac{1}{G} \right| \sin(0^\circ + \phi_{90^\circ}) \quad (3.28)$$

$$I''_C = P_{90^\circ} \left| \frac{1}{\omega C} \right| \sin(90^\circ + \phi_{90^\circ}) \quad (3.29)$$

$$I''_x = P_{90^\circ} \left| \frac{1}{G_x^2 + \omega^2 C_x^2} \right| \sin(\alpha_x + \phi_{90^\circ}) \quad (3.30)$$

From this set of data it is possible, using straightforward goniometric and algebraic manipulations, to calculate all system parameters and finally the unknown  $Z_x$ .  $P_{0^\circ}$  and  $\phi_{0^\circ}$  can be derived from (3.25) and (3.26),  $P_{90^\circ}$  and  $\phi_{90^\circ}$  are derived from (3.28) and (3.29).

Both references are not ideal, as was assumed. Parallel with the reference capacitor there is a parasitic conduction term,  $G_p$ , and a parasitic capacitance term,  $C_p$ . Let  $\alpha_G \neq 0$ . If  $C_p \ll C$  and  $\omega C_p \ll G$ , then  $C_p$  may be estimated from (3.25). In the same way  $G_p$  may be estimated from (3.29) if  $G_p \ll G$  and  $G_p \ll \omega C$ . From these values the real reference impedance for  $C$  and  $G$  can be recalculated. This procedure can be repeated until the



required accuracy has been reached. In this way, a reasonable start guess for all other circuits built with the ASIC will be found. Only if extreme accuracy is required, this procedure must be repeated

for each measurement cycle. From (3.27) and (3.30) the angle  $\alpha_x$  and consequently the unknowns  $G_x$  and  $C_x$  can be calculated.

One of the advantages of an IC is that all electronics of the impedance input channel and the shift impedance inputs of the reference channel can be built equal, allowing to assume that all impedances have the same parasitics. In the following it is assumed that the parasitics are known and already included. Using the foregoing, an algorithm will be developed to calculate  $Z_x$ .

The parameters  $C$ ,  $G$ , and  $\omega$  are known and I assume  $C_p$  and  $G_p$  to be known too. Including  $C_p$  and  $G_p$  results in a complex  $|Z_C|$  and  $|Z_G|$ , respectively for the impedances at the  $C$  and  $G$  inputs.  $|Z_C|$  and  $\alpha_C$  and  $|Z_G|$  and  $\alpha_G$  can be calculated from

$$|Z_C| = \frac{1}{\sqrt{G_p^2 + (\omega C)^2}} \quad \text{and} \quad \alpha_C = \arctan\left(\frac{\omega C}{G_p}\right) \quad (3.31)$$

$$|Z_G| = \frac{1}{\sqrt{G^2 + (\omega C_p)^2}} \quad \text{and} \quad \alpha_G = \arctan\left(\frac{\omega C_p}{G}\right) \quad (3.32)$$

These values will be considered to be constants.

The measured values are  $I_x$  and  $I''_x$ ,  $I_C$  and  $I''_C$ ,  $I_G$  and  $I''_G$ . The phase shift errors  $\phi_0$  and  $\phi_{90}$  can be calculated from, respectively:

$$\phi_{0^\circ} = \arctan \left[ \frac{\frac{|Z_C| \cos(\alpha_C)}{I_C} - \frac{|Z_G| \cos(\alpha_G)}{I_G}}{\frac{|Z_C| \sin(\alpha_C)}{I_C} - \frac{|Z_G| \sin(\alpha_G)}{I_G}} \right] \quad \text{and}$$

$$\phi_{90^\circ} = \arctan \left[ \frac{\frac{|Z_C| \cos(\alpha_C)}{I''_C} - \frac{|Z_G| \cos(\alpha_G)}{I''_G}}{\frac{|Z_C| \sin(\alpha_C)}{I''_C} - \frac{|Z_G| \sin(\alpha_G)}{I''_G}} \right] + 90^\circ \quad (3.33)$$

Next  $|Z_x|$  and  $\alpha_x$  can be calculated from, respectively:

$$|Z_x| = \frac{|Z_C| \cos(\alpha_C + \phi_{0^\circ})}{\cos(\alpha_x + \phi_{0^\circ})} \cdot \frac{I_x}{I_C} \quad \text{and} \quad \alpha_x = \arctan \left[ \frac{I''_x \cos(\phi_{0^\circ}) - I_x \sin(\phi_{90^\circ})}{I_x \cos(\phi_{90^\circ}) - I''_x \sin(\phi_{0^\circ})} \right] \quad (3.34)$$

The unknown capacitance,  $C_x$ , and the conductance,  $G_x$ , can be calculated from, respectively:

$$C_x = \frac{1}{\omega |Z_x|} \sin(\alpha_x) \quad \text{and} \quad G_x = \frac{1}{|Z_x|} \cos(\alpha_x) \quad (3.35)$$

Finally, the values for  $\epsilon'$  and  $\sigma$  can be derived.



Due to limited space, power etc., a sensor is often equipped with a minimum of signal-processing power. Goniometric functions should be avoided for a simple processor configuration. Goniometric functions can be avoided using the following equalities

$$\sin[\arctan(x)] = \frac{x}{\sqrt{1+x^2}} \text{ and } \cos[\arctan(x)] = \frac{1}{\sqrt{1+x^2}} \quad (3.36)$$

sequentially substituted in (3.31) until (3.35). Because the substitution results in lengthy formulas, the result will not be reproduced here.

### Design aspects of the analogue part of the ASIC

Similar components on two individual ASIC's can differ by as much as 20 %. With the described measuring principle the absolute accuracy is determined mainly by the reference components and not by the electric ASIC parameters. It was even possible to calculate phase errors and parasitics in parallel with the unknown. The main uncertainty of this method is the quality of the switches. The difference in phase errors between the measuring stages may not exceed  $0.07^\circ$ . Fortunately, the matching between electric parameters of components on the same ASIC is better than 1%, and parasitics are relatively low. Parasitic capacitors can be as low as 0.1 pF. However, any connection made through the casing of the ASIC can have a parasitic capacitance as high as 10 pF. To fully benefit from the high matching accuracy, all circuitry and the lay out should be designed as identical and symmetrical as possible with a minimum of connections through the casing.

It has been shown by Steyaert *et al.* [1991] that the phase differences at 900 MHz, between two circuits sharing the same ASIC can be  $< 3^\circ$ . He used transistors with an  $f_T = 9$  GHz and paid special attention to the circuit symmetry and lay out. The transition frequency,  $f_T$ , is a transistor parameter for which frequency its gain is reduced to 1. By scaling down the result of Steyaert *et al.* [1991] to 20 MHz, it can be seen that the phase requirement is achievable. A first-order scaling yields  $3^\circ (900 \text{ MHz} / 20 \text{ MHz}) = 0.067^\circ$ , which is the required value. For this calculation a first-order roll-off for the phase at 900 MHz was assumed. In reality at 900 MHz, even on an ASIC, one must take into account multiple roll-offs. In case of a high-frequency ( $> 1$  GHz) production process for ASIC's one may assume only one roll-off at 20 MHz. Therefore, the situation is expected to be better for this ASIC.

The resistance of metallisation patterns on an ASIC posed additional problems. Normally, the specific resistance of a track is poorly specified. Without special care, the resistance of a 3 to 4 mm long track may be as high as 50  $\Omega$ . This in combination with the parasitic capacitors, can already cause more than  $0.1^\circ$  phase error differences. To get round this problem, critical tracks are made as wide as possible and routed from a star at the pad.

The dominating errors are caused by deviations in gain, band width and phase of the active components. Other sources of error are caused by bad power line couplings and non-linearities. In addition, harmonics will add to the measurement errors. To eliminate errors caused by the power lines, all HF circuitry have to be balanced. This assures the highest power supply rejection ratio and the lowest EMI sensitivity. It requires differential stages for the oscillator up to the synchronous detector. The synchronous detector is used in the linear mode. A limiter would cause large phase shifts [Wagdy, 1986] and a broad spectrum of harmonics for which the system would be sensitive. Because of these strong requirements,



and following Steyaert *et al.* [1991], the circuit design, lay out, and place-and-route had to be done manually on the transistor level.

A simplified circuit diagram of the final analogue part of the ASIC is shown in Figure 3.5. It fully demonstrates the differential structure, with respect to the power lines and ground, of the final circuit for ac signals, as was required. This structure ensures the ac signal flow to stay within the circuit. Closed loop amplifier configurations are avoided, they would certainly give rise to HF instability.

On its way from the oscillator up to the synchronous detector the signal passes five n-p-n transistors. Let us assume that each transistor in its function has a 3 dB band width of at least  $f_{3\text{ dB}} = (1/3) f_T$ . The  $f_{3\text{ dB}}$  band width is the frequency for which the gain is reduced by 1/2. Assuming a single roll-off, due to a first-order integration in the gain function, the phase of each stage at  $f_{3\text{ dB}}$  is  $45^\circ$  going to  $90^\circ$  for  $f \rightarrow \infty$ . The total phase shift is approximately  $225^\circ$ . If the matching between two transistors is better than 1 %, then the uncertainty is  $2.25^\circ$  at  $f_{3\text{ dB}}$ . The minimum  $f_T$ , to meet a phase requirement of  $0.07^\circ$ , for the bipolar transistors can now be estimated. Assume a single roll-off, the phase error at  $f_T$  is roughly  $f_T / f_{\text{osc}}$  times smaller at  $f_{\text{osc}}$ . Therefore, with  $f_{\text{osc}} = 20\text{ MHz}$   $f_T$  should be  $\gg 3 f_{\text{osc}} (2.25^\circ / 0.07^\circ) = 2\text{ GHz}$ .

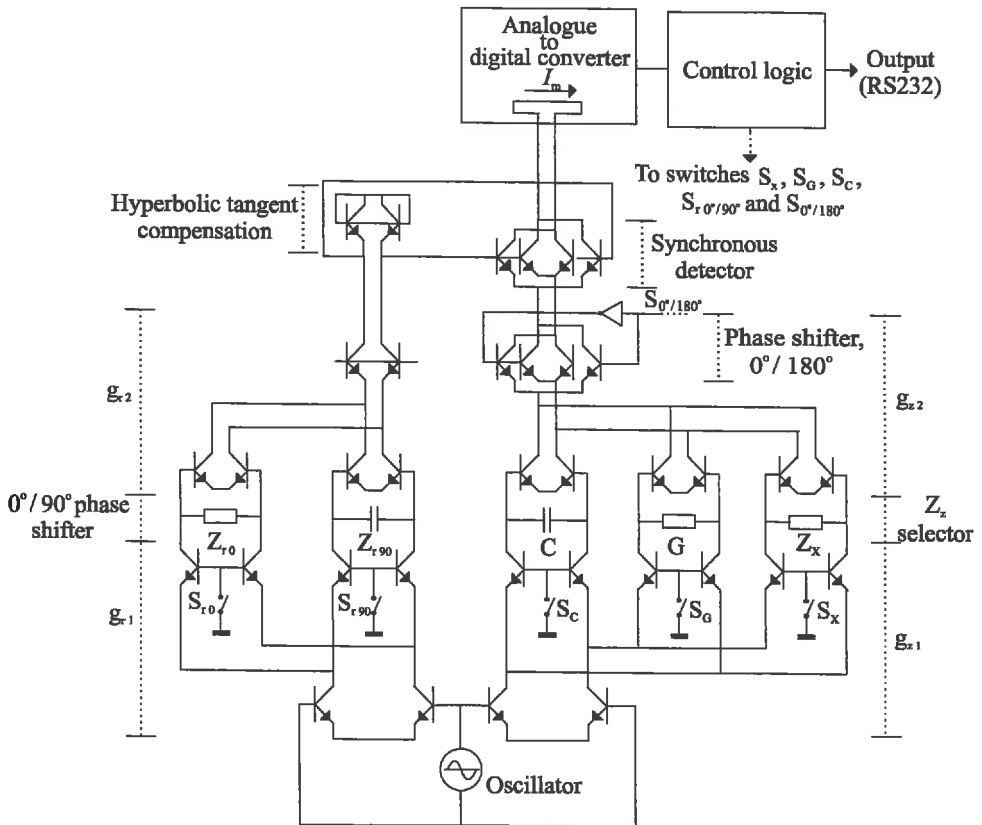


Figure 3.5. Simplified schematic diagram of the analogue part of the ASIC.



The sine wave crystal oscillator generates a differential output voltage. It is a fully balanced bridge-type oscillator, and shows very good frequency stability and extremely high power supply rejection ratio, while no external adjustments are necessary. The even harmonics are < 30 dB and the odd harmonics < 50 dB. This was measured with the control logic running. The oscillator has a shut down and amplitude control pin.

Both the reference channel and the Z channel are fed by the same signal, with equal phase and amplitude. The output voltage of the oscillator is converted to current using a differential transconductance amplifier followed by a common-base stage to eliminate Miller feedback in the first stage and to provide an elegant switching configuration. Miller feedback is an apparently, large capacitance at the input due to the current flowing from the output of a transistor back to its input via the parasitic capacitor between output and input. The result is a poor frequency and phase response. This switchable input circuitry is followed by the distinctive impedances; the unknown, the references and the shift components. The voltage developed across these impedances is differential. Next, this voltage is converted back to current using a differential transconductance amplifier.

The reference channel ends in a common base circuit again to limit Miller feedback. Finally, the reference signal passes an inverse hyperbolic tangent compensation circuit before it is fed to the reference input of the synchronous detector. The impedance input channel also ends in a common base circuit. It protects from Miller feedback and provides the possibility for an excellent  $0^\circ/180^\circ$  balanced phase shifter.

The synchronous detector is used in the linear mode. The output of the detector is directly coupled to the current input of a normal current-to-frequency converter. This converter generates a 100 kHz carrier output signal modulated by the voltages developed across the distinctive impedances, switched in the predefined sequence by the control logic. The frequency measurement is realised with a 5 digit decade counter. The limited band width of the current-controlled oscillator and the integration time of the frequency measurement automatically perform the required low-pass filtering at the output of the mixer.

### **Design aspects of the digital part of the ASIC**

The digital part of the ASIC is designed by J. Balendonck at IMAG-DLO (see Hilhorst *et al.* [1993]).

The system clock of the control logic can be either derived from the analogue HF oscillator via an internal pre-scaler, or provided externally. The logic toggles the switches in the analogue part through the 24 required states. These include states for impedance measurements, states for multiplexing externally applied analogue signals and states for housekeeping. The logic provides means to adapt the predefined sequence for special applications, for instance for phase measurements on externally applied signals.

The output frequency of the current controlled oscillator is measured using a 5 decade counter with an integration time of 0.1 s. One measuring cycle of 24 states then takes 2.4 s. The contents of the counter is transmitted from the ASIC to a read out system using a RS232 connection. The transmitted data contains the measuring state number and corresponding data. The read out system will normally contain a micro controller that can be used for post-processing of the raw sensor data. Therefore, computing circuitry have to be included in the ASIC. The read out system can be e.g. a battery-operated hand-held meter or a personal computer.





Scan-path techniques are used to make the ASIC testable. The testability, including controllability and observability, is analysed using ViewFault. With a set of 2850 test vectors, a fault coverage of more than 93 % could be obtained.

A special circuit senses the supply voltage and generates a reset signal for the control logic as soon as the supply voltage passes predefined limits. This eliminates the need for an external reset signal or power control circuitry.

The control logic is realised in CMOS on the same ASIC using 616 standard cells, which is equivalent to 1345 gates.

### **Realisation of the ASIC**

The ASIC contains four impedance inputs instead of the three mentioned before. The fourth one allows a second unknown impedance to be measured with one ASIC. It makes the circuit suitable for a number of new applications. However, these applications are beyond the scope of this thesis.

The circuit is implemented as a mixed analogue/digital ASIC, realised in the BiCMOS STKM 2000 standard cell process of SGS Thomson [Cailon, 1990]. A standard cell process means that all components used to compose the circuit are defined and characterised by the silicon foundry. Only the necessary components are integrated. This is in contrast with an array where all components are already integrated on the ASIC, only a metalisation pattern is needed to compose the circuit. A standard cell approach instead of an array is advantageous for phase error optimisation of the analogue part and for effectively balancing the HF circuitry for a good power supply rejection ratio.

The full circuitry was designed and simulated using Workview with the SGS Thomson STKM2000 toolkit, ViewFault, and SPICE, implemented on a SUN workstation. At the development no tests on breadboard scale using discrete components for parts of the circuit were performed. SGS-Thomson guaranteed the circuit to perform according to our simulations making breadboard tests unnecessary. Figure 3.6a shows a microphotograph of the ASIC. The lay out of the impedance input cell is shown in more detail in Figure 3.6b. The transition frequency of the NPN transistors is 7 GHz and that of the PNP transistors 2.5 GHz. Although some special handling was needed to meet the HF requirements, the bulk netlists are processed automatically. Because the ASIC size is "pad limited", the free ASIC area was used to create 3 on-board power supply decoupling capacitors of 1.5 nF each. They are located between the digital and analogue circuitries, effectively reducing EMI between the two. Together with the bonding and other wiring inductances, this also provides excellent supply decoupling for HF. An on-board analogue multiplexer with three inputs makes it possible to process analogue signals from other sensors, such as for temperature or pH. The digital circuitry is realised in CMOS on the same ASIC. The ASIC measures 4 mm by 4.5 mm. Total power consumption is about 35 mA at 5 V.

### **Design validation**

Numerous tests and simulations have been carried out to characterise the final ASIC. The most critical design parameters are the phase response and consequently the accuracy of the capacitance measurement. To demonstrate this, some results of a simulation and those of measurements using the final ASIC are selected.





For phase error simulations of the impedance channel the synchronous detector was replaced by a  $100\ \Omega$  resistor, and  $10\ \Omega // 100\ \text{pF}$  connected to the impedance inputs. The phase response was simulated between the oscillator output and this resistor in worst, typical and best case situations according to the SGS Thomson STKM2000 library. This means that the parameters of all components were changed such that they represent the worst and best cases for deviations with respect to the typical situation. With a power supply of 5 V, at  $20\ ^\circ\text{C}$  and at 20 MHz, the phase error was:  $\phi_{Z\ \text{WORST}} = 13.45^\circ$ ,  $\phi_{Z\ \text{TYPICAL}} = 13.49^\circ$  and  $\phi_{Z\ \text{BEST}} = 13.39^\circ$  respectively. The maximum difference between these results is  $0.1^\circ$  which is in close agreement with the required  $0.07^\circ$ .

Many dielectric sensors were made following the first ASIC in 1993. They all used the same ASIC and the algorithm. An example of the output of an ASIC, working at 20 MHz, and the capacitance, the conductance, and the phase errors calculated from it are given in Table 3.1. For demonstration purpose no external impedance was connected to the x input. In this way, the ASIC measures its own parasitics.

Results for capacitance and conductance measurements were reproducible within the requirements. The results for the phase errors are different for each ASIC and sensitive to temperature and changes in the supply voltage, showing the ability of the system to correct it.

Table 3.1. An example of the output of an ASIC, working at 20 MHz. The reference capacitor,  $C$ , and conductor,  $G$ , include the estimated parasitics  $C_p$  and  $G_p$ . The x input was left open to enable the ASIC to measure its own input parasitics. The unknown capacitance,  $C_x$ , and conductance,  $G_x$ , are calculated from the measured data  $I_x$ ,  $I'_x$ ,  $I_C$ ,  $I'_C$ ,  $I_G$  and  $I'_G$ , using the algorithm given in the text.

Input		Output		Results using (3.31) to (3.35)	
$G_x = \text{open}$	$C_x = \text{open}$	$I_x = 18828$	$I'_x = 13744$	$G_x = 1.56\ \text{mS}$	$C_x = 5.98\ \text{pF}$
$G_p = 1.58\ \text{mS}$	$C + C_p = 105.9\ \text{pF}$	$I_C = 501$	$I'_C = 2567$	$\phi_0 = -4.27^\circ$	$\phi_{90} = 17.10^\circ$
$G + G_p = 101.58\ \text{mS}$	$C_p = 5.9\ \text{pF}$	$I_G = 3021$	$I'_G = 1068$		

## Conclusions

*With the described measuring system, it is possible to perform precise complex impedance measurements.* The circuit is realised as an ASIC utilising a standard cell process and using common design techniques. SPICE simulations for worst, typical and best process values for the real circuit confirmed that a maximum phase error of less than  $\pm 0.07^\circ$  is feasible at 20 MHz. Many sensors built using this ASIC confirmed the simulation results. The phase accuracy is mainly determined by the reference components and the mismatch of electric parameters from transistors sharing the same ASIC.

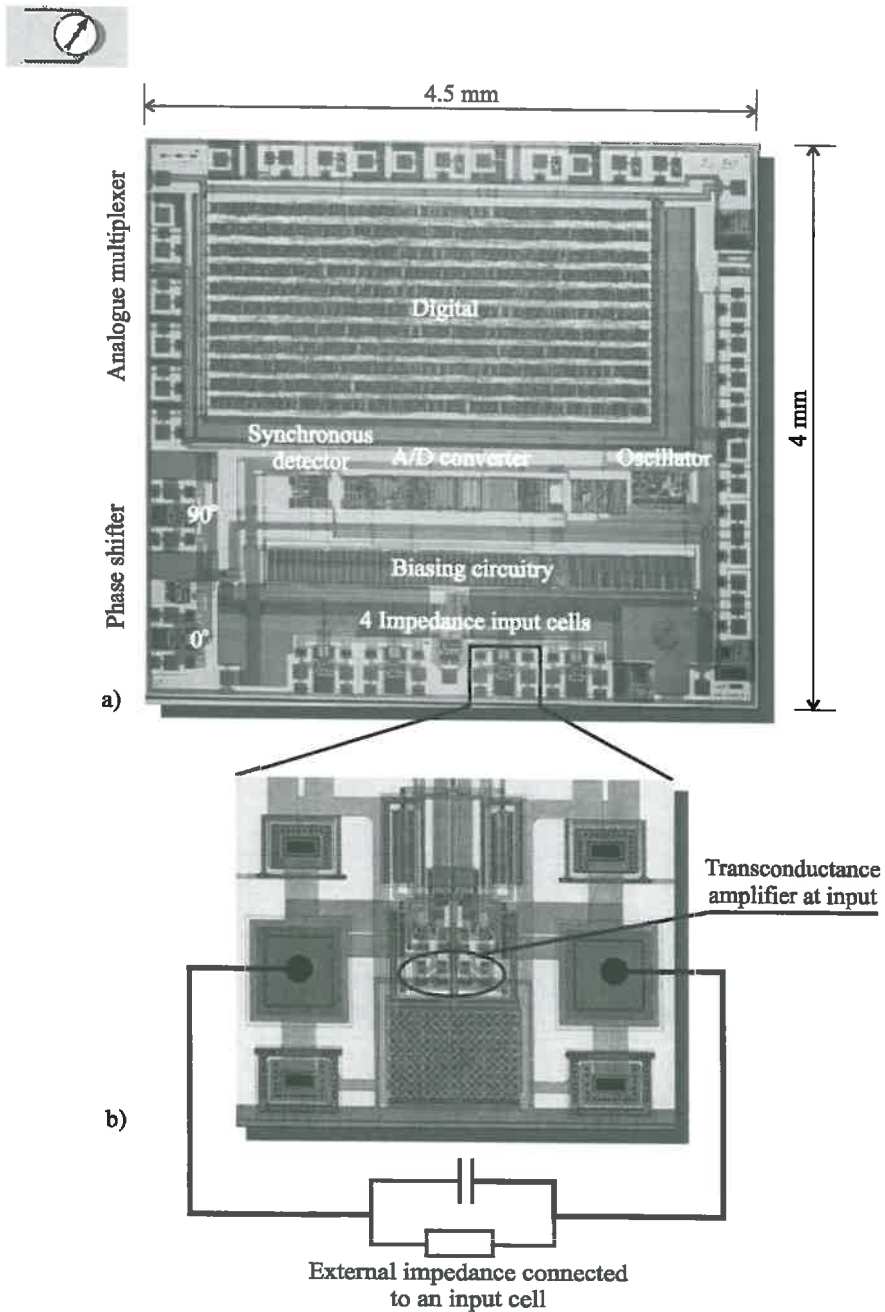


Figure 3.6. a) Photograph of the ASIC-layout. The upper half of the ASIC is occupied by the digital part. The small strip at the left contains a 3-channel analogue multiplexer. The upper quarter of the lower half contains the synchronous detector, the analogue-to-digital converter, the oscillator, and most of the biasing circuitry. The lower quarter is mainly occupied by the four impedance input circuits and some power supply protection circuitry. The  $0^\circ / 90^\circ$  phase shifter is located at the left of the lower half of the ASIC. b) Layout of one of the impedance input cells. Note its symmetrical layout.



### 3.3 GENERAL CONSIDERATIONS ON ELECTRODE DESIGN FOR DIELECTRIC SENSORS

#### Electrical length of electrodes and wiring

In practice permittivity measurements are not as straightforward as Section 3.1 suggests. Electrodes, and the wiring that connect them to the electronics, always have a certain length. Number and configuration of the electrodes can differ according to application. Configurations with three or four rods are common but also other configuration such as two or more rings on a stick are often used. It is not possible to extensively treat all possible configurations in this section. Three or more rods can be modelled as two rods since the outer rods are connected to each other. Also rings on a stick can be modelled as two rods. To study the effect of the electrical length of electrodes and wiring on a permittivity measurement, a generalised two-rod configuration as shown in Figure 3.7 will be used.

A dielectric sensor is shown in Figure 3.7a consisting of a current source, a vector voltmeter and two electrodes. The wiring and coupling capacitors between the electrodes and electronics are also shown. The current source is connected to the electrodes and the voltage developed is measured with the vector voltmeter. In case of frequency domain measurements, the current is a sine wave. The sine wave needs some time to travel along the electrodes and wiring. In addition, part of the current will reflect at the end of the electrodes and travel back to the source. The voltage developed across the electrodes is the result of the summation of the applied and reflected currents.

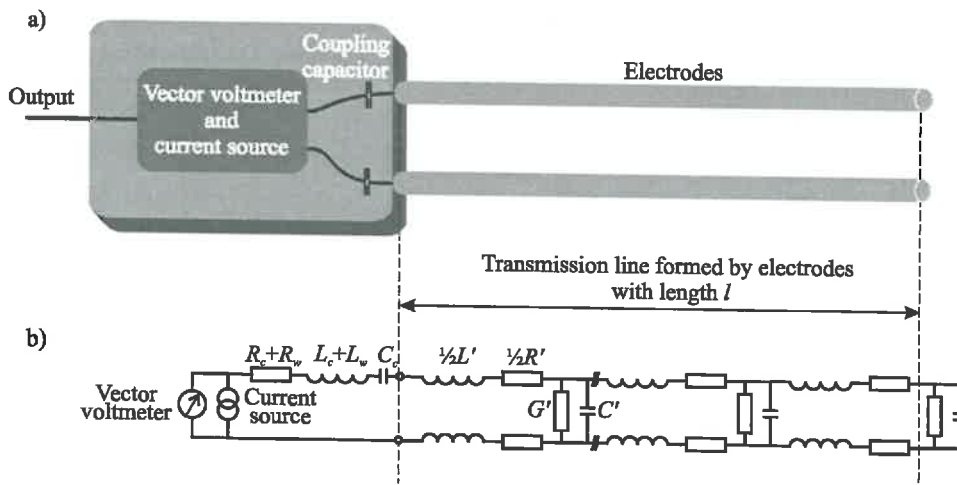


Figure 3.7. a) A dielectric soil water content sensor. The vector voltmeter measures the response to the application of a current at the input of the transmission line with length  $l$ . b) Electric model for this sensor. The distributed parameters of the transmission line are represented by inductor,  $L'$ , resistor,  $R'$ , capacitor,  $C'$ , and conductance  $G'$ . Parasitics due to wiring and coupling capacitors are represented by  $R_w$ ,  $L_w$ ,  $R_c$ ,  $L_c$  and  $C_c$ , respectively.



The electrodes form a transmission line for which the electric model is shown in Figure 3.7b. For an extensive treatment of transmission lines see Wadell [1991]. From the applied current and resulting voltage the capacitance,  $C$ , and conductance,  $G$ , between the electrodes can be calculated.  $C$  and  $G$  are related to real part of the permittivity,  $\epsilon'$ , and the imaginary part of the permittivity,  $\epsilon''$ , respectively.

The transmission line can be thought to be built up from infinitesimal small pieces of the physical transmission line. Each segment consists of a parallel capacitor/conductor combination,  $C'$  and  $G'$ , with in series a resistor  $R'$ , and inductor  $L'$ . The distributed parallel capacitor/conductor combinations of a line segment are defined as the partial derivatives of  $C$  and  $G$  as a function of the electrode length  $l$ ;

$$C' = \partial C / \partial l \quad (3.37)$$

and

$$G' = \partial G / \partial l \quad (3.38)$$

These equations represent the capacitance and conductance per unit length, respectively. The electrodes themselves are represented by a distributed series inductor  $L'$  and series resistor  $R'$ . In practice, to overcome dc problems between the electrodes, there is always a coupling capacitor  $C_C$  with parasitic inductor  $L_C$  and loss resistor  $R_C$  between the electronics and electrodes. The wiring parasitics between electrodes and electronic system are represented by  $L_W$  and  $R_W$ .

Note that the model of Figure 3.7 is applicable to all dielectric measuring instruments working either in the frequency or in the time domain. Time-domain measurements involve the application of currents with frequencies in a broad-frequency band. For TDR the vector voltmeter should be replaced by an oscilloscope screen in order to observe the wave-form developed on the application of a step or pulse function. Due to the high frequencies (> 100 MHz) involved, often a sampling oscilloscope is used for this purpose. With a Fourier transformation the result of a time-domain measurement can be transformed to the frequency domain.

Following the general theory on transmission lines (see for textbooks e.g. Wadell [1991]) the impedance looking from the source into an open-ended transmission line with length  $l$  is

$$Z = Z_0 \coth \gamma l \quad (3.39)$$

where  $Z_0$  is the characteristic impedance and  $\gamma$  the propagation constant of the line.  $Z_0$  and  $\gamma$  are defined as, respectively

$$Z_0 = \sqrt{\frac{R + j\omega L}{G + j\omega C}} \quad (3.40)$$

$$\gamma = \sqrt{(R + j\omega L)(G + j\omega C)} \quad (3.41)$$



Solving (3.39) is only possible using an iterative algorithm which is a time-consuming job for a sensor with limited computation power. However, for values of  $\gamma l \ll 1$  the approximation  $\coth x \approx 1/x$  may be used in order to reduce (3.39) to

$$Z \approx \frac{1}{l(G + j\omega C)} = \frac{1}{G + j\omega C} \quad (3.42)$$

The transmission line behaves like a lossy capacitor. The permittivity may be calculated from (3.42) using (3.10) and (3.11). In the following the use of (3.42) for a real sensor will be demonstrated for water. It will be shown that this approximation is not sufficiently accurate. However, as will be shown, a simple modification of this model can provide a correction.

Let us consider a set of two electrodes with a rod length  $l = 5$  cm of radius  $r = 1.5$  mm being at a distance  $d = 1.5$  cm in water. The measuring frequency for this case is chosen to be 20 MHz, based on good experiences with previous water content sensors as described by Hilhorst [1984] and evaluated by Halbertsma *et al.* [1987] and Hilhorst *et al.* [1992]. The inductance of the transmission line can be calculated from

$$L = \frac{\mu_0 \mu l}{\pi} \ln \frac{d}{r} \quad (3.43)$$

where  $\mu_0 = 4\pi \cdot 10^{-7}$  H m<sup>-1</sup> is the permeability of free space and  $\mu$  is the relative permeability;  $\mu = 1$  for air. From (3.43) it follows that  $L = 46$  nH.  $R$  can be calculated but this is difficult.  $R$  is a function of the surface condition of the electrodes, the quality of the connection with the electrodes, skin effect etc. From experience, it is known that  $R$  has a value between 0.5  $\Omega$  and 2  $\Omega$  for 20 MHz.  $R$  is assumed to be approximately 1  $\Omega$ . The capacitance  $C = 86$  pF is calculated using the geometry factor  $\kappa$  according to (3.8). The calculated values for  $L$  and  $C$  are in line with practical results.

The requirement  $\gamma l \ll 1$  can be fulfilled for values of  $G < 0.01$  S with acceptable errors. In Figure 24 the errors  $C_{\text{error}}$  and  $G_{\text{error}}$  are plotted as the differences between the values for  $C$  and  $G$  applied and those calculated according to (3.39) and (3.42), respectively.

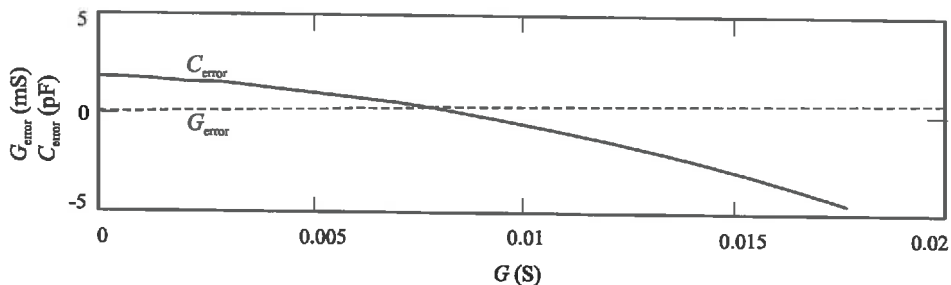


Figure 3.8. Error for capacitance,  $C_{\text{error}}$ , as a function of conductance,  $G$ . The dashed line is the error for conductance,  $G_{\text{error}}$ , as a function of  $G$ . The errors are calculated as the difference between values applied and those calculated according to (3.39) and its approximation (3.42). The frequency used is 20 MHz.

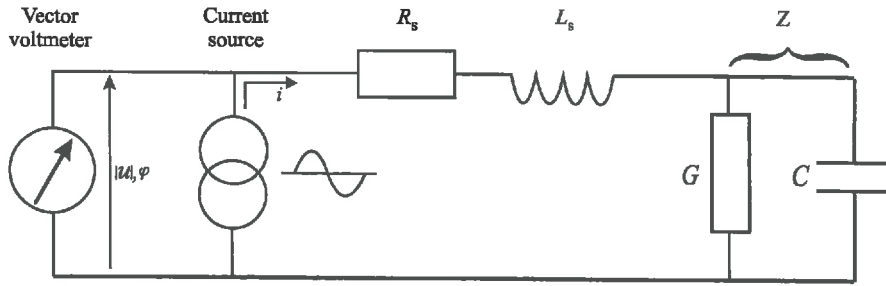


Figure 3.9. Simplified electric model for a dielectric soil water content sensor as given in Figure 3.7, including electrical length of electrodes and wiring. The transmission line is replaced by the parallel combination of  $G$  and  $C$ . The resulting error is corrected using  $R_s$  and  $L_s$ .

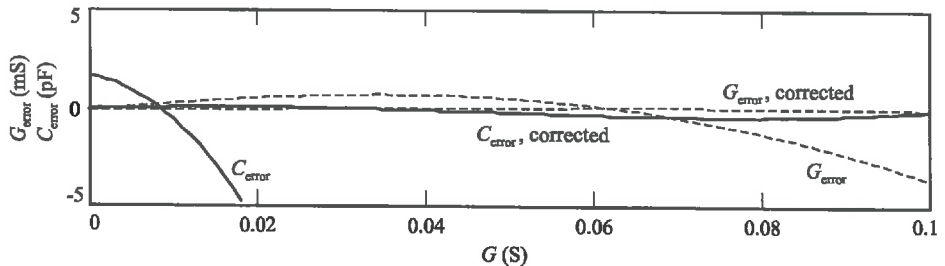


Figure 3.10. Absolute error for the capacitance,  $C_{error}$ , and the conductance,  $G_{error}$ , as a function of conductance,  $G$ . The errors are calculated as the difference between values applied and those calculated according to (3.39) and (3.42) for the uncorrected case and (3.39) and (3.44) for the corrected case. The frequency used is 20 MHz.

When  $C_{error}$  becomes too high for  $G < 0.015$ , (3.42) needs correction. The difference between (3.39) and (3.42) may be approximated by an inductor,  $L_s$ , and a resistor,  $R_s$ , in series with the electrodes as shown in Figure 3.9. For this approximation the impedance  $Z$  can be written as

$$Z = \frac{1}{G + j\omega C} + j\omega L_s + R_s \quad (3.44)$$

The errors  $C_{error}$  and  $G_{error}$  calculated as the differences between the applied values and those calculated according to the use of (3.39) and (3.44), respectively, are plotted as a function of  $G$  in Figure 3.10. The conductance range is extended to  $G = 0.1$  S. The errors calculated as the difference between the applied values and those calculated according to (3.39) and (3.42) are also plotted. The values of the correction components  $L_s = 15.16$  nH and  $R_s = 0.41$   $\Omega$  are chosen in such a way that the errors for  $G = 0$  and  $G = 0.1$  S are minimal.

Apart from the errors mentioned above, there are errors which originate from parasitic series inductors,  $L_w$ , and series resistances,  $R_w$ , due to the wiring between electrodes and





electronics and  $L_C$  and  $R_C$ , due to imperfect coupling of capacitors. These errors are shown in Figure 3.7b. The measured values for  $C$  and  $G$  have to be compensated for these parasitics, too. This may be done conveniently by adding  $L_w$ ,  $R_w$ ,  $R_C$  and  $L_C$  to  $L_s$  and  $R_s$ . Subtracting  $R_s$  and  $j\omega L_s$  from the measured data makes it possible to calculate  $C$  and  $G$  from (3.42).

Concluding for a single-frequency measurement at 20 MHz the generalised model of Figure 3.7 may be simplified to that of Figure 3.9. This model can be used for any frequency as long as  $\omega C < G$  and  $\gamma l \ll 1$ . The values for  $R_s$  and  $L_s$  can be determined from two measurements, one in water of low conductivity and the other in water of high conductivity. The real part of the permittivity of water,  $\epsilon'_w$ , and hence  $C$  is constant for both cases.

The simplified approach as depicted in Figure 3.9 has been used successfully in previous versions of sensors, such as described by Hilhorst [1984] for soil water content measurements in soils with a electrical conductivity of the bulk  $\sigma_b < 0.2 \text{ S m}^{-1}$ . Such values for  $\sigma_b$  are sometimes found for saturated clays in the field but are considered high for normal soils. Also sensors for water content measurements in rockwool substrates as described by Hilhorst *et al.* [1992] where  $\sigma_b$  can be as high as  $1 \text{ S m}^{-1}$ , have been constructed successfully using this method. However, the measurement becomes highly sensitive to  $L_s$  and  $R_s$  at  $1 \text{ S m}^{-1}$  and more. The sensors as described by Hilhorst [1984] and Hilhorst *et al.* [1992] were not equipped with a mathematical correction for  $R_s$  and  $L_s$ . To eliminate  $R_s$  and  $L_s$  the coupling capacitor which is connected in series with the electrodes was tuned in such a way that the circuit was in series resonance. For series resonance the impedance of the circuit is low-resistive and may be neglected.

### Some practical considerations on electrode design of a dielectric sensor

Many users of dielectric sensors for soil water content measurements are not aware of a number of practical design aspects of the electrodes. Some of the more important design aspects will be mentioned and briefly discussed. Normally, electrode design to a large extent is determined by the application and often worked out intuitively.

The electrodes of a dielectric sensor for soil water content measurements should be designed in such a way that they facilitate easy insertion with minimum disturbance of the soil and the largest possible but well defined sampled volume. A dielectric sensor normally has two or more rod-shaped electrodes to be inserted into the soil. The field of influence, that determines the sampled volume, for a two rod sensor is relatively large compared with that of a three or multi-rod sensor. Therefore, the advantage of two rods is that of a maximum sampled volume with minimum disturbance of the soil. The disadvantage of a large sampled volume is the uncertainty for the user as to whether the sensor is located sufficiently far away from disturbing objects or from the soil surface.

The general-purpose sensor described in this section has three rods, with the outer rods connected to each other. A three rod configuration approximates the principle of a coaxial transmission line. As shown by Knight *et al.* [1994] the more outer rods the better the approximation. For a coaxial line the field of influence, is concentrated only between the rods. With three rods the volume of influence is better defined than for two rods. However, the energy density is higher on the surface of the rods making the sensor sensitive to rod/soil contact problems. Using more rods may partly solve this problem but insertion of the sensor becomes more troublesome. The high-energy density close to the rods dominates the volume of influence. The sampled volume can only be increased by increasing the length and/or





diameter of the rods. Increasing the distance between the rods will result in only little increased sampled volume. The soil in the middle of the rods has almost no influence on the measurement. Contact problems with the soil and spatial distribution of the electric field around the rods apply equally to both the new FD sensor as well as TDR.

The rods are in electrical contact with the soil. Interfering currents may flow from the soil through the rods to the electronics. This can cause noisy readings. From an EMI point of view a two-rod sensor can be driven and measured using perfectly balanced electronics, reducing EMI. If one rod is  $+u$ , then the other is  $-u$  leaving the soil exactly at zero potential and the sensor will not transmit to its environment. On the other hand both rods receive interference equally and no current will flow through the input circuitry. Received interference is not "seen" by the input circuitry. For a three-rod system the soil will be at  $1/3$  of the applied voltage if the rods are still driven in a balanced manner. Interference is no longer equally received. Part of the interference signals is seen by the electronics and will cause measurement noise. This can be circumvented by choosing the surface area of the middle rod twice that of an outer rod. This can be explained as follows. The two outer rods are connected to each other. The capacitance between the three rods can be split into two equal capacitors with the middle rod in common. For three rods of equal diameter the charge density on the surface of the middle rod is twice as high as the charge density on the surface of the outer rods. Consequently the current density on this surface is also twice as high. With the surface area of the middle rod being twice that of an outer rod, the current density on the surface of the middle rod will be equal to that through the outer rods. However, the sensors used for this thesis contained three rods with equal dimensions. They were already produced and no EMI problems are expected in our test environment.

The electric double layer at the boundary between the rod surface and soil forms an unpredictable impedance which is in series with the impedance of the soil. This double layer is best defined and stable for platinum electrodes. Stainless steel, fortunately, is second best and a more economical choice. For a demonstration and more details of this effect, see Lawton & Pething [1993] and references therein. The impact of the double layer, often called electrode polarisation, on the measuring accuracy is difficult to quantify and depends e.g. on electrode material, surface conditions and type and concentration of the ions. The higher the ion concentration in the soil water the higher the impact of the double layer on the measurement accuracy. From my experience this effect is strong at  $f < 1$  MHz, but can still be substantial at  $f > 10$  MHz in a soil where  $\sigma_b > 0.1 \text{ S m}^{-1}$ .

## Conclusions

*For dielectric measurements at 20 MHz and  $\sigma_b < 1 \text{ S m}^{-1}$ , a transmission line can be replaced by a parallel combination of a conductor and capacitor with an inductor and resistor connected in series. This configuration, expressed by (3.44), is a convenient way to overcome the problem of how to solve the hyperbolic goniometric function of (3.39).*

*A good choice for the electrode configuration of a general purpose dielectric sensor appears to be three stainless steel rods with the area of the middle rod twice that of one outer rod.*



### 3.4 A NEW DIELECTRIC SENSOR

#### A sensor for measuring soil dielectric properties at 20 MHz

A dielectric sensor can be constructed in many ways depending on the type of application. The sensor described here is intended for general purpose. In Figure 3.11 a sensor is shown consisting of the described ASIC connected to three electrodes in the form of rods ending in sharp points to facilitate insertion of the sensor into the soil. Three rods approximate the principle of a coaxial transmission line as discussed in Section 3.3. The 60 mm long stainless steel rods are 3 mm in diameter and spaced 15 mm apart. The ASIC is embedded in hard polyurethane moulding. The flexible polyurethane output cable contains the RS232 signal wires and the two power supply wires. This cable can be connected to a micro processor or PC which runs the software for further signal processing.

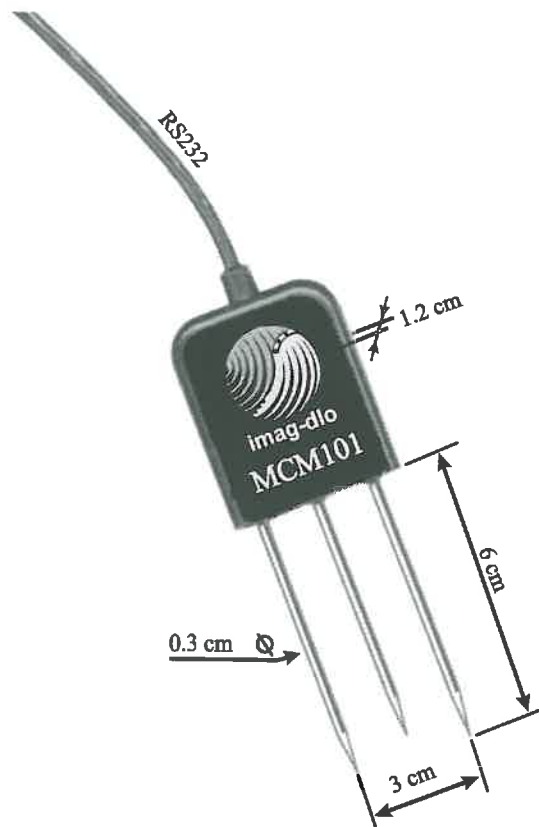


Figure 3.11. The new dielectric sensor for measuring the permittivity and electrical conductivity of the bulk soil at 20 MHz. A temperature sensor is located halfway inside the middle rod.



The real part of the permittivity,  $\epsilon'$ , and the electrical conductivity of bulk soil,  $\sigma_b$ , are temperature-sensitive. It is therefore necessary to measure the temperature. For that purpose a temperature sensor is mounted halfway inside the middle rod. So far, however, little is known about the temperature coefficient of soil. Therefore, temperature corrections are not included in the software. This should be done after the relationship between,  $\epsilon'$ , and the water content,  $\theta$ , as a function of temperature has been investigated for the soil involved.

The data measured by the ASIC are interpreted by special software developed by P.J. Nijenhuis at IMAG-DLO. This software contains the algorithms necessary to calculate the complex impedance from the output data of the ASIC and to facilitate calibration to  $\epsilon'$ ,  $\sigma_b$  and temperature. It also facilitates automatic data sampling and storage.

### Calibration for permittivity and conductivity measurements

To measure  $\epsilon'$  and  $\sigma_b$  accurately a dielectric sensor has to be calibrated. For calibration to other soil parameters, such as water content,  $\theta$ , the relationship between  $\epsilon'$  and these parameters must be established. The calibration procedure is guided by PC-software designed by P.J. Nijenhuis at IMAG-DLO. It determines the  $\epsilon'$  and  $\sigma_b$  scales and the electrical length compensation parameters. The software does the calibration by measuring the complex impedances for water at different  $\sigma_b$  and for air. The calibration points can be freely chosen. The actual calibration values can be typed in, guided by the software.

The sensor is calibrated with reference values of air and water of  $\sigma \approx 0.017 \text{ S m}^{-1}$  (tap-water),  $\sigma = 0.1 \text{ S m}^{-1}$  and  $\sigma = 0.2 \text{ S m}^{-1}$ . The permittivity scale was calibrated between  $\epsilon = 1$  for air and  $\epsilon' = 80.3$  for tap-water at  $20^\circ\text{C}$ . The permittivity scaling data shall be independent of  $\sigma$ . The conductivity scale is determined for  $\sigma = 0$  in air and  $\sigma = 0.2 \text{ S m}^{-1}$  in water. The series inductor for the electrical length compensation is found from the measurements in water at  $\sigma \approx 0.017 \text{ S m}^{-1}$  and  $\sigma = 0.2 \text{ S m}^{-1}$ . Water with a value of  $\sigma = 0.1 \text{ S m}^{-1}$  was used to adjust the series resistor such that the capacitance readings for the three conductivities are equal. The software uses a trial-and-error method for the calibration procedure.

### Validation results for dielectric measurements

A number of the new sensors have been produced for use in soils, where  $\sigma_b < 0.2 \text{ S m}^{-1}$ . After calibration they functioned all within the requirements i.e. within + or - 1% of full scale for both permittivity,  $\epsilon'$ , and conductivity,  $\sigma_b$ , in reference liquids. Figure 3.12 shows, as a typical example, the influence of  $\sigma_b$  on measurements of  $\epsilon'$ . The measurements were done at 20 MHz. The upper curve is for pure water, the middle curve for a mixture of 1/3 water with 2/3 methanol and the lower curves for water-saturated glass beads. The conductivity was varied using increasing amounts of NaCl.

The results of  $\sigma$  measurements are compared with values measured using a customary low-frequency (1 kHz) electrical conductivity meter (Figure 3.13) with four electrodes. The liquid was water at  $20^\circ\text{C}$  with NaCl in various concentrations. Hence, it can be concluded that the new dielectric sensor measures  $\epsilon'$  and  $\sigma_b$  of soil with an accuracy within + or - 1% of full scale for both permittivity and conductivity in reference liquids, which is sufficiently accurate for most soil applications.

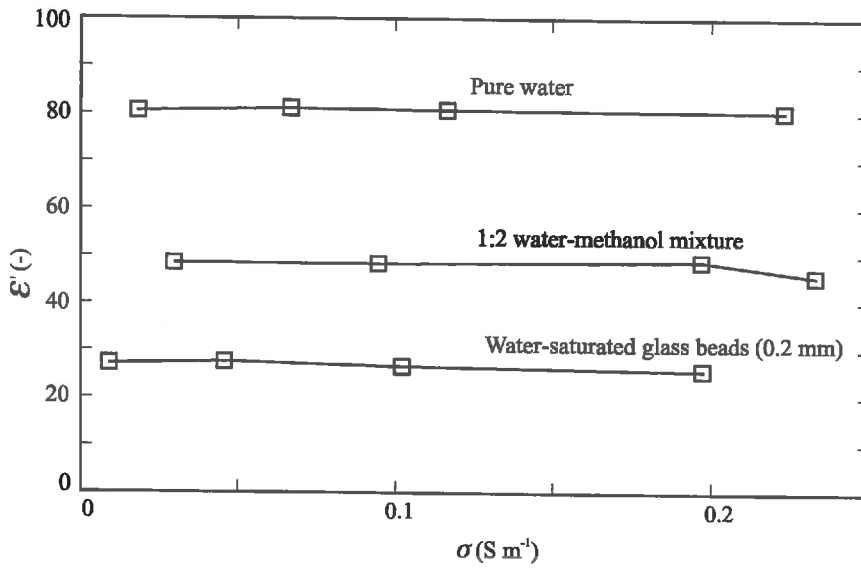


Figure 3.12. The real part of the permittivity,  $\epsilon'$ , versus ionic conductivity,  $\sigma$ , of three mixtures at 20 °C as measured with the new dielectric sensor, as shown in Figure 3.11 working at 20 MHz.

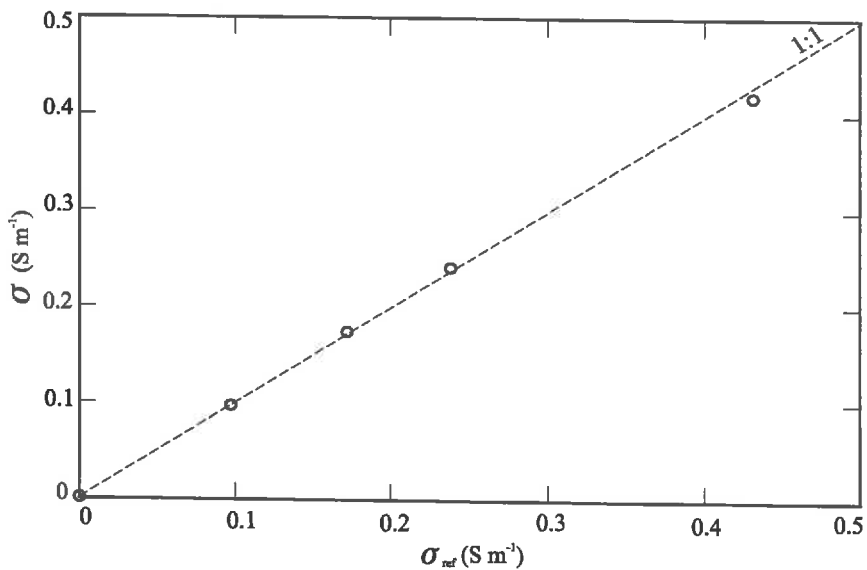


Figure 3.13. Conductivity,  $\sigma$ , at 20 MHz measured with the new dielectric sensor of Figure 3.11 versus  $\sigma_{ref}$  for water-NaCl reference solutions at 20 °C, measured with a laboratory conductivity meter at 1 kHz. The measurements are indicated with o.





## 4. APPLICATIONS

Measurement of the soil water content,  $\theta$ , can be done using the dielectric properties or complex permittivity,  $\epsilon$ , of soil. In Chapter 3 a new sensor for measuring  $\epsilon$  was described. The real part of  $\epsilon$ ,  $\epsilon'$ , can be related to  $\theta$ . These  $\epsilon'(\theta)$  relationships, or calibration curves, are also a function of soil porosity, soil matric pressure, soil texture and measuring frequency. In Chapter 2 I developed a model (2.61) that can predict such calibration curves. Section 4.1 presents calibration curves measured with the new Frequency-Domain (FD) sensor as well as with a Time Domain Reflectometry (TDR) sensor for a variety of soils. These results will be compared with predicted calibration curves.

Also the electrical conductivity of the bulk soil,  $\sigma_b$ , can be measured with these sensors and is affected by a number of soil and equipment variables. Often, the ionic conductivity,  $\sigma$ , or *EC* of the water in the matrix, rather than  $\sigma_b$  is of interest. Malicki *et al.* [1994] described an attractive method to determine  $\sigma$  using simultaneous measurements of  $\sigma_b$  and  $\epsilon'$  by means of TDR. This chapter explores this method for the new FD sensor. The Maxwell-Wagner effect can be characterised by permittivity measurements at three frequencies (Chapter 2). Section 4.3 describes how  $\sigma_b$  is related to  $\epsilon'$  and how the Maxwell-Wagner effect applies to  $\sigma_b$ .

The dielectric properties of soil are affected by all its constituents. Pollutants such as oil and chlorinated solvents change both  $\sigma_b$  and  $\epsilon'$  as well. Section 4.4 shows how simultaneous measurements of  $\sigma_b$  and  $\epsilon'$  can be used to detect polluted soil layers with a modified version of the FD sensor.

Hardening concrete can be used to simulate the dielectric behaviour of soil as a function of soil texture, ion concentration and bound water. During hydration, concrete shows some characteristic events for  $\epsilon'$  as well as for  $\sigma_b$ . These events are related to changes in the microstructural and compositional properties of the material that are characteristic for different soil types. The dielectric properties of concrete will be treated in Section 4.5.

### 4.1 DIELECTRIC SOIL WATER CONTENT MEASUREMENTS

#### Methods and materials

The data of Dirksen & Dasberg [1993] and Dirksen & Hilhorst [1994] were used to compare measured and predicted  $\epsilon'(\theta)$  relationships, which are also called calibration curves. The data were obtained with a Frequency-Domain (FD) sensor and a Time Domain Reflectometry (TDR) sensor.

The TDR measurements were carried out with a TDR cable tester (Tektronix, Model 1502B) with a primary frequency range of 10 MHz to 1 GHz. The 50  $\Omega$  cable between the cable tester and the TDR sensor was 3.2 m long. The waveform obtained on the cable tester



was stored in a personal computer for later retrieval and analysis with programs developed by Heimovaara & Bouten [1990]. The exact point in the TDR wave-forms corresponding with the point of entrance at the electrodes in the soil, was determined from measurements in both air and water [Heimovaara, 1993].

The new FD sensor, as described in Section 3.4, measured  $\epsilon$  in about 2.5 s, without need for further analysis. The imaginary part of the permittivity,  $\epsilon''$ , is the sum of the dielectric losses,  $\epsilon''_d$ , and the loss due to ionic conduction of soil water,  $\sigma$ . The measuring frequency of the FD sensor was 20 MHz. At this frequency  $\epsilon''_d$  is negligible for most soils (see Figure 2.15). Therefore,  $\epsilon''$  was equated to the ionic conductivity of the bulk soil,  $\sigma_b$ , based on a calibration in NaCl solutions and corrected for temperature dependence to a temperature of 20 °C.

The electrode configuration was the same for both sensors, i.e. three rods, 9.6 cm long, 0.2 cm diameter, and 1.0 cm spaced. This allowed as closely as possible a comparison of results obtained with the FD sensor and the TDR sensor. All measurements were made in the laboratory at room temperature.

After the FD or TDR measurements the soil was removed from the cylinders and samples were taken for gravimetric water content determinations, from which the  $\theta$ -values were calculated based on the average bulk density of the packed cylinders. These steps were repeated 8 to 12 times for each soil, resulting in  $\theta$  increments of 0.02 to 0.03.

Eleven of the soils mentioned in the studies of Dirksen & Dasberg [1993] and Dirksen & Hilhorst [1994] are used in this section for which the parameters are summarised in Table 4.1.

Table 4.1. Composition of soils used in this study. The porosity and bulk density are averaged for packed columns. The hygroscopic water content is predicted by  $\theta_h = \delta \rho_b S_A$  where the thickness of one molecular water layer  $\delta = 3 \cdot 10^{-10}$  m, and measured for air dry soil. Source Dirksen & Dasberg [1993] and Dirksen & Hilhorst [1994].

Soil	Clay	Silt	Sand	Organic matter	Porosity, (average)	Bulk density, (average)	Specific surface,	Hygroscopic water content, (predicted)	Hygroscopic water content, (measured)
	(%)	(%)	(%)	(%)	$\phi$ (-)	$\rho_b$ (g cm <sup>-3</sup> )	$S_A$ (m <sup>2</sup> g <sup>-1</sup> )	$\theta_h$ (-)	$\theta_h$ (-)
Fine sand	0	0	100	0	0.48	1.41	≈ 0.1	0	0
Groesbeek	10	70	20	0.95	0.43	1.49	25	0.011	0.017
Wichmond	14	31	55	4.3	0.47	1.36	41	0.017	0.022
Ferrasol-A	63	26	11	0	0.56	1.14	61	0.021	0.025
Munnikenland	40	56	3	5	0.57	1.13	79	0.027	0.035
Mediterranean	40	34	27	0.4	0.47	1.38	93	0.039	0.043
Y-Polder	45	42	13	4.6	0.59	1.08	107	0.035	0.040
Illite	100	0	0	0	0.51	1.30	147	0.057	0.050
Attapulgit	100	0	0	0	0.80	0.55	270	0.045	0.039
Vertisol	86	10	4	1.4	0.63	0.92	428	0.118	0.118
Bentonite	100	0	0	0	0.64	0.94	665	0.187	0.114





The major types of clay minerals mentioned for these soils were determined by X-ray diffraction. This group consisted of five Dutch soils: Fine sand, Groesbeek loess (Typic Hapludalf), Wichmond valley bottom sandy loam (Typic Haplaquept; smectite and vermiculite), Munnikenland fluvial silty clay loam (Typic Haplaquept; illite and koalinite), and Y-Polder marine silty clay (Typic Haplaquept; illite and koalinite); Brazilian Humic Ferralsol (Typic Acrortox; gibbsite and koalinite), a French Mediterranean red soil (Typic Rhodoxeralf; illite and koalinite), a Kenyan pellic Vertisol (Typic Pellustert; smectite), and the three pure clay minerals: Bentonite (smectite, from Osage, WY), Illite (Grundite Co.), and Attapulgitite, also called palygorskite. Attapulgitite is a clay mineral with high water-absorbing capacity with a fibrous morphology, rarely occurring in soils. Mediterranean and Y-Polder soils were used first with TDR. Due to a lack of sufficient soil material they could not be used with FD.

All determinations were made in duplicate. Air-dry soil material (where appropriate, first sieved to < 2.0 mm) was brought stepwise to the desired water content using an atomised water spray assembly (Dirksen & Matula, 1992). After the soil and water were thoroughly mixed at each water content, two acrylic cylinders of 5 cm diameter and 12.5 cm long were packed to a bulk density as uniform as possible.

After the FD and/or TDR measurements, the soil columns were sampled to determine the average wet mass,  $m$ , oven-dried mass,  $m_o$ , and volume,  $V$ . The dry bulk density of the soil,  $\rho_b$ , was then calculated as:

$$\rho_b = \frac{m_o}{V} \quad (4.1)$$

and  $\theta$  as:

$$\theta = \frac{m - m_o}{\rho_w} \frac{1}{V} \quad (4.2)$$

where  $\rho_w$  is the density of water ( $1.0 \text{ g cm}^{-3}$ ).

At first, it was attempted to pack all the columns of the same soil material to the same  $\rho_b$ . Since it is very difficult, if not impossible, to do this at different wetnesses, soil columns were later packed at two to three different  $\rho_b$ 's at each wetness, resulting in an increasing  $\theta$  with increasing  $\rho_b$ . This gave more information about the influence of  $\rho_b$  on the dielectric properties and allowed interpolation. The sensors were pushed into the packed soil columns through tightly fitting holes in a 2 cm thick polyvinyl chloride cylindrical guide to minimise bending of the rather thin, flexible rods, and to center the sensors in the narrow soil columns. The guide was split through the plane of the holes so that it could be removed and the sensors then pushed in all the way.

The specific surface area,  $S_A$ , was measured with ethylene glycol monoethyl ether, which is adsorbed on clay mineral surfaces in a similar way as water [Carter *et al.*, 1986]. The measured hygroscopic water content,  $\theta_h$ , (air dry) was found approximately equal to:

$$\theta_h = \delta \rho_b S_A \quad (4.3)$$

where  $\delta = 3 \cdot 10^{-10} \text{ m}$  is the thickness of a molecular water layer (see also Table 4.1).



### Sensitivity of the permittivity as measured by TDR for the electrical conductivity

With TDR the velocity of a step function propagating along a transmission line is measured. The transmission line is formed by parallel rods placed in the soil. This propagation velocity depends on both the real part of the permittivity,  $\epsilon'$ , and the electrical conductivity of the bulk soil,  $\sigma_b$ , resulting in an apparent permittivity for TDR,  $\epsilon_{TDR}$ . Topp *et al.* [1980] proposed to equate  $\epsilon'$  to  $\epsilon_{TDR}$ , thereby assuming that the effect of  $\sigma_b$  on  $\epsilon_{TDR}$  is negligible. For accurate measurements, however,  $\epsilon_{TDR}$  should be corrected for  $\sigma_b$  to obtain  $\epsilon'$ . According to measurements by Wyseure *et al.* [1997], correction is needed for  $\sigma_b > 0.2 \text{ S m}^{-1}$ .

The application of a step function involves a broad frequency spectrum. Part of the spectrum is attenuated after the signal has been reflected at the end of the transmission line and has returned at the source. The line acts like an electronic low-pass filter. An equivalent circuit for a transmission line is described in Section 3.3. The highest frequency component within the passed frequency band has the highest current component through the capacitors. The current through the capacitor is proportional to  $\epsilon'$ . Therefore, the highest frequency within the passed frequency band dominates the measurement. This frequency is equal to the band width. From electronic filter theory [e.g., Bird, 1980] it is known that the band width of a low-pass filter can be found from the rise time,  $\tau$ , of the output signal on the application of a step function.  $\tau$  is defined as the time needed to reach 0.66 of the amplitude of the reflected step.

The band width of a TDR system,  $f_{TDR}$ , can be calculate from  $\tau$ . When comparing TDR with FD the equivalent measuring frequency for TDR can be approximated by  $f_{TDR}$  which is the frequency of the sine wave current component with the highest amplitude that passed the transmission line.  $f_{TDR}$  is related to  $\tau$  by

$$f_{TDR} = \frac{1}{2\pi\tau} \quad (4.4)$$

$f_{TDR}$  depends on both the  $\epsilon'$  and  $\sigma_b$  of the soil. This frequency dependence was tested using glass beads of 0.2 mm saturated with NaCl-water solutions and for the specified cable length. The results are presented in Table 4.2.

Table 4.2. Equivalent measuring frequency for TDR for different pairs of the real part of the permittivity,  $\epsilon'$ , and the electrical conductivity of the bulk soil,  $\sigma_b$ .

Real part of permittivity $\epsilon'$ (-)	Electrical conductivity of bulk soil $\sigma_b$ ( $\text{S m}^{-1}$ )	Equivalent measuring frequency $f_{TDR}$ (MHz)
80.3	0.01	159
28.0	0.03	187
80.3	0.20	209
28.0	0.16	289



According to White *et al.* [1994]  $\varepsilon_{\text{TDR}}$  is a function of  $\sigma_b$  and can be described as:

$$\varepsilon_{\text{TDR}} = \frac{\varepsilon'}{2} \left[ 1 + \sqrt{1 + \left( \frac{\varepsilon''_d + \frac{\sigma_b}{2\pi f_{\text{TDR}} \varepsilon_0}}{\varepsilon'} \right)^2} \right] \quad (4.5)$$

On first sight (4.5) might be used to calculate the correct  $\varepsilon'$  from  $\varepsilon_{\text{TDR}}$ ,  $\sigma_b$  and  $f_{\text{TDR}}$ , but in my opinion (4.5) leads to confusion and misinterpretation. The equation was derived from the propagation constant,  $\gamma$ , of an EM sine wave in a transmission line as given by (3.41). In turn,  $\gamma$  was derived from the elementary Telegrapher's equations [Wadell, 1991] for the propagation of a sinusoidal wave. With TDR a step function is applied to the line. For a correct interpretation of the reflected signal with respect to  $\varepsilon_{\text{TDR}}$  the Telegrapher's equations should be worked out in the time domain for a step function.

As shown in Table 4.2,  $f_{\text{TDR}}$  is a function of both  $\varepsilon'$  and  $\sigma_b$ . Thus (4.5) cannot be used to adequately correct  $\varepsilon_{\text{TDR}}$  for  $\sigma_b$ . Therefore, although not accurate,  $\varepsilon_{\text{TDR}}$  has not been corrected in this chapter.

#### A comparison between measured and predicted permittivity versus water content relationships

The apparent permittivity obtained from TDR measurements,  $\varepsilon_{\text{TDR}}$ , is compared with the real part of the permittivity predicted according to (2.61),  $\varepsilon'_p$ , for the soils of Table 4.1. Note that no determinations were made near the point of saturation. The differences between the measured and predicted values,  $\Delta\varepsilon = (\varepsilon_{\text{TDR}} - \varepsilon'_p)$ , are plotted in Figure 4.1 as a function of  $\theta$  in order of increasing specific surface,  $S_A$ . For Vertisol and Bentonite the values for  $\Delta\varepsilon$  at  $\theta > 0.3$  are too large to be plotted on this scale. Apart from Groesbeek, Wichmond and the Mediterranean, all soils show a clear increase for  $\Delta\varepsilon$ . This is more pronounced for  $\theta > 0.25$  and for the higher values of  $S_A$ . This increase may be explained by the Maxwell-Wagner effect which is not taken into account in the prediction of  $\varepsilon'_p$  using (2.61). Better results may be expected from predictions using (2.65). To use (2.65) as a predictor the relationship between the parameter  $K$  and soil texture should be analysed first.  $K$  is expected to increase with increasing  $S_A$ . Without taking into account the Maxwell-Wagner effect,  $\Delta\varepsilon$  should increase with increasing  $S_A$ . The result plotted in Figure 4.1 supports this expectation.

The Groesbeek, Wichmond and Mediterranean soils showed a small decrease in  $\Delta\varepsilon$ . These are the soils with the highest bulk densities,  $\rho_b$ . Illite also has a high  $\rho_b$ , but its calibration curve is less clear on this point. There might also be a decrease in  $\Delta\varepsilon$  for Illite, but if so, it is masked by other effects. The decrease for  $\Delta\varepsilon$  may possibly be explained by the depolarisation factor,  $S$ , due to the water-solid interface.  $S$  may be a function of  $\rho_b$ , but the following explanation is more likely. In Section 2.6 it was estimated for glass beads that  $S = 0.33$ . Glass beads are spheres with a smooth surface in contrast with soil particles. For soil,  $S$  may be approximated by that of spheres but should be corrected to account for differing shape and surface roughness. To demonstrate the effect of  $S$  on  $\varepsilon'_p$  the data for the Groesbeek, Wichmond and Mediterranean soils are plotted for both  $S = 0.33$  and  $S = 0.27$  in Figure 4.2. The value  $S = 0.27$  is an estimate chosen in such a way that the curves end around zero.

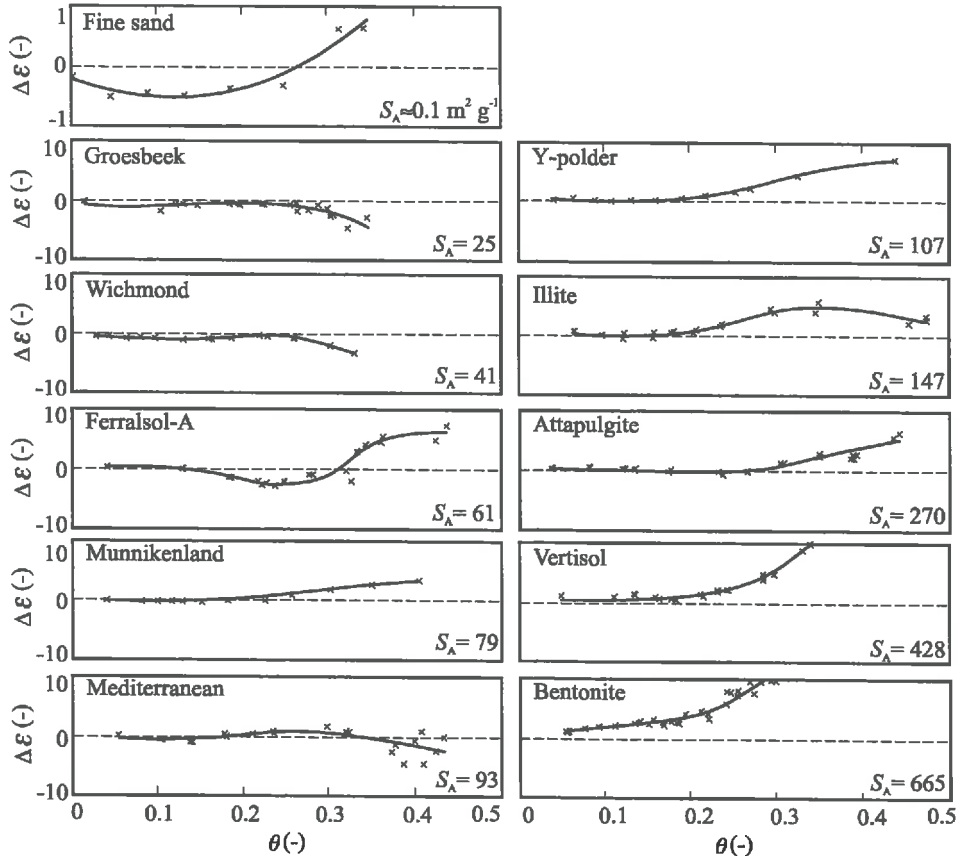


Figure 4.1. Difference  $\Delta\epsilon$  between the apparent permittivity measured with TDR,  $\epsilon_{TDR}$ , and the real part of the permittivity predicted according to (2.61),  $\epsilon'_p$ .  $\Delta\epsilon$  is plotted as a function of water content,  $\theta$ , for the soils of Table 4.1 in the order of increasing specific surface area  $S_A$ .

A third-order polynomial was fitted through the data. The order in which the angles of the S-shaped curves increase corresponds with increasing  $S_A$  for these three soils. This is consistent with the behaviour of the other soils as can be seen from Figure 4.1. *Concluding,  $S = 0.33$  as determined for glass beads seems not to be universally applicable. To obtain high accuracy,  $S$  should be determined for the soil under investigation.*

The effect of air bubbles was not taken into account in the prediction of  $\epsilon'_p$  using (2.61). According to my hypothesis as explained in Section 2.3, air bubbles will lead to an increase in  $\epsilon_{TDR}$  and consequently to an increase in  $\Delta\epsilon$  with increasing  $\theta$ . After  $\epsilon_{TDR}$  has reached a maximum,  $\Delta\epsilon$  will decrease again to approach zero for  $\theta = \phi$ , the pore volume fraction. In Figure 4.1 the effect of air bubbles is most visible for Illite. The S-shaped curves of Figure 4.2 make the hypotheses for air bubble effects acceptable.

$\epsilon_{TDR}$  is sensitive to  $\sigma_b$ , but cannot be corrected using the existing theory on TDR. The resulting measurement error will add to the Maxwell-Wagner effect and will lead to an increase in  $\Delta\epsilon$  especially at high  $\theta$  and high  $\sigma_b$ . It is not possible to distinguish between these two effects on the measurements.

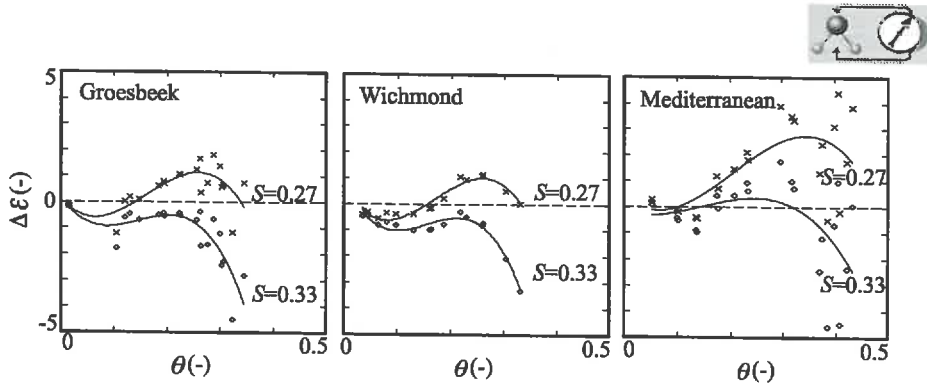


Figure 4.2. The difference  $\Delta\epsilon$  between the apparent permittivity,  $\epsilon_{TDR}$ , measured with TDR and the real part of the permittivity,  $\epsilon'_p$ , predicted according to (2.61). The effect of a smaller depolarisation factor,  $S$ , due to surface roughness and shape of the particles, is shown for  $S=0.33$  and  $S=0.27$  denoted by  $\diamond$  and  $\times$ , respectively. The solid lines are third-order polynomials fitted through the data.  $\Delta\epsilon$  is plotted as a function of water content,  $\theta$ , in order of increasing specific surface,  $S_A$ .

#### Calibration curves for the new FD sensor compared with those for Fine sand measured using TDR and predicted according to (2.61)

It appears useful to compare calibration curves published in the literature with the well-known "Topp curve" [Topp *et al.*, 1980] as a reference. Topp's calibration curve is a generally accepted calibration equation for TDR water content measurements which is accurate for sand in general, but represents an average for a number of sandy-loam and clay-loam soils. Reference will be made here to this equation as being valid for an average soil:

$$\epsilon_{\text{average soil}} = 3.03 + 9.3\theta + 146\theta^2 - 76\theta^3 \quad (4.6)$$

Data measured for 100 % Fine sand of Table 4.1 using the new FD sensor together with data measured with TDR are shown in Figure 4.3. The curve predicted according to (2.61) is also drawn in the same graph. The relationships are nearly identical and located slightly below the Topp calibration curve. The dielectric parameters are the same as for all the other calculations with (2.61), only  $\epsilon_s = 3.5$  instead of 4.0. This is reasonable since both the TDR sensor and the FD sensor measured  $\epsilon' = 2.4$  for  $\theta = 0.0021$  and  $\phi = 0.438$ .  $\phi$  was measured for each point in the graph and used for the prediction of  $\epsilon'_p$  while the Topp curve is not taking  $\phi$  into account. Note that Topp used  $\epsilon_w = 81.5$  at 20 °C as a reference instead of  $\epsilon_w = 80.3$  as used in this thesis.

The measuring frequency for the FD sensor was 20 MHz while the equivalent measuring frequency of the TDR sensor was more than 150 MHz. From this it may be concluded that for pure sand  $\epsilon'$  is about constant between 20 MHz and 150 MHz. This result justifies the use of the calibration curve predicted by (2.61) for Fine sand as a reference. The advantage of (2.61) over Topp's curve is that (2.61) is more fundamental and can allow for differences in porosity,  $\phi$ , and bound water,  $\theta_h$ . Fine sand with  $\phi = 0.48$ ,  $\theta_h \approx 0$  is used as a reference for this section, (2.61). The curve was extrapolated to  $\theta = 0.5$ .

Eight of the soils of Table 4.1 were compared with the predicted curve for Fine sand. The Mediterranean and the Y-Polder soils are not included in this experiment. The FD data, shown in Figure 4.4, generally agree with other experimental data for various soils at 20 MHz [e.g. Smith-Rose, 1933; Campbell, 1990; Wensink, 1993].

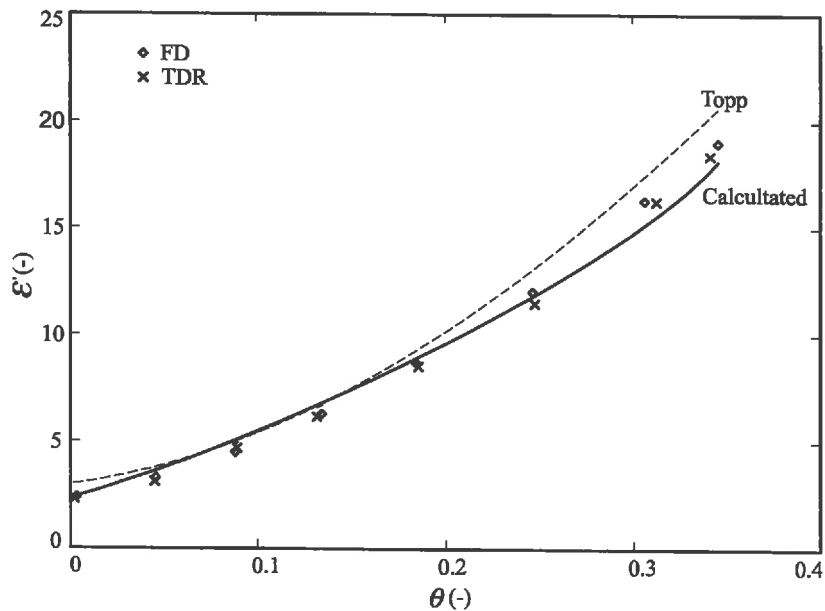


Figure 4.3. The real part of the permittivity,  $\epsilon'$ , as a function of the water content,  $\theta$ , for Fine sand of Table 4.1 measured with the new FD sensor at 20 MHz and a TDR sensor. For comparison, the Topp calibration equation [Topp *et al.*, 1980] and the calibration curve calculated according to (2.61) are also given.

The differences found between the calibration curve for Fine sand (see also Figure 4.3) and the FD data may be attributed to the dielectric behaviour of soils as a function of frequency due to the Maxwell-Wagner effect, counterion polarisation and the impact of air bubbles as explained in Chapter 2. The steeper calibration curves obtained with the FD sensor indicate that it is more sensitive to changes in  $\theta$  than TDR, especially at lower  $\theta$ -values. The solid lines are drawn by hand through the data. Most deviations of the measurements with respect to the lines are due to variations in density. This is most pronounced for Bentonite.

Note the marked discontinuity in the calibration data for Ferralsol around  $\theta = 0.25$ . This behaviour, with the same values for  $\epsilon'$ , was also found by Dirksen & Dasberg [1993] for TDR. This means that the dielectric spectrum between 20 MHz and 150 MHz is flat despite the high clay and silt content of Ferralsol. Ferralsol seems to be an exception to the general theory developed in Chapter 2. There are three possible explanations for the irregular behaviour of Ferralsol. Firstly, it may be attributed to the microporosity of about 25 % within the elementary, clay-sized soil particles, which make up more than 60 % of the texture. According to personal communication between Dirksen and Nitzsche [1994] the unusual form of the calibration curve is likely due to this dual porosity. In my view, following the foregoing, clay-sized soil particles should already lead to a measurable Maxwell-Wagner relaxation. The thin solid walls of the micropores of these particles should magnify the Maxwell-Wagner effect even more. The dielectric behaviour of Ferralsol, however, is in conflict with this interpretation.

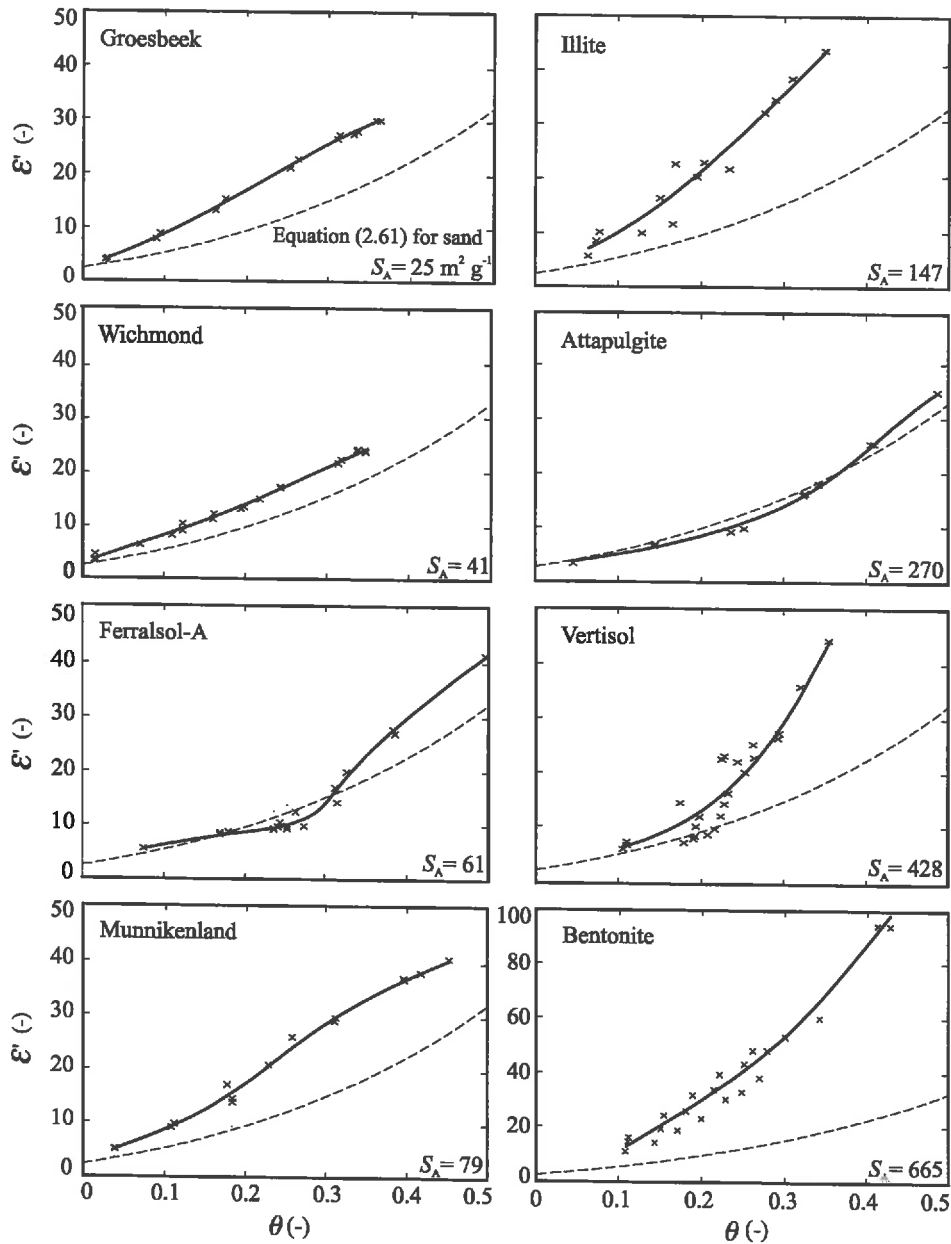


Figure 4.4. The real part of the complex permittivity,  $\epsilon'$ , as a function of the volumetric water content,  $\theta$ , for eight soils of Table 4.1 as measured (x) using the FD sensor [Dirksen & Hilhorst, 1994]. The graphs are presented in order of increasing specific surface,  $S_A$ . For comparison, the dashed lines represent the calibration curve for Fine sand according to (2.61). The solid lines are drawn by hand.





The second possible explanation is the contribution of the magnetic permeability of Ferralsol which consists largely of metal oxides. The third and most likely explanation is that the depolarisation factor  $S$  for the water-solid interface caused this behaviour. In Chapter 2,  $S$  was estimated for glass beads, being solid spheres in a water and/or air continuum. In the case of water in micropores we face the situation of water and air in a solid continuum. According to e.g. De Loor (1956) and Nyfors & Vainikainen [1989], the permittivity for a mixture of water in a low-permittivity environment, as for a solid continuum, should be lower than for a mixture of solids in water. Thus, for Ferralsol it may be expected that  $S < 0.33$  for low values of  $\theta$ . As soon as the micropores are filled,  $S$  will rapidly increase to  $S \approx 0.33$ . It was observed by Dirksen that the physical properties (consistency of the moist soil) changed abruptly around  $\theta = 0.25$ . I think this supports the hypothesis.

Dirksen & Dasberg [1993] showed the need for calibration of a TDR sensor. From Figure 4.4 it is clear that also the FD sensor should be calibrated to measure  $\theta$  accurately. In fact, the need for calibration of the FD sensor at 20 MHz is higher than for TDR. Based on the theory treated in Section 2.4 it is hypothesised that the need for calibration could be reduced as compared to TDR by using a higher measuring frequency for the FD sensor.

## Conclusions

The measurement of the real part of the permittivity of soil with TDR is affected by the electrical conductivity of the soil. Equation (4.5) describing the relationship between the measured reflection time and the permittivity is based on a simplified model derived for a single frequency. These equations are only valid if the conductivity is negligible. *With the existing theory, it is not possible to adequately correct for the effect of conduction on the measured permittivity of soil.* To account for conduction the theory should be based on the application of a step function in the time domain.

The measurement of the complex permittivity of soil with the new FD sensor is not affected by the conductivity of the soil, allowing measurements at conductivity values as high as  $1 \text{ S m}^{-1}$ . Compared with TDR the new FD sensor is more sensitive to the Maxwell-Wagner effect due to the lower measuring frequency. In contrast with TDR, a low and discrete measuring frequency as used with FD, can be used to characterise the Maxwell-Wagner effect for texture analyses or to eliminate it.

*For both, FD and TDR, it is necessary to calibrate the sensors for the relationship between the real part of the permittivity and the water content.* The need for calibration of an FD sensor at 20 MHz is higher than for TDR. The need for calibration can be reduced by using a higher measuring frequency. Values measured using TDR agree well with those predicted according to the theory of Chapter 2 for low and medium water contents ( $< 0.25$ ). At higher water contents and especially for clays the predicted and measured values deviate due to the Maxwell-Wagner effect.

The depolarisation factor,  $S$ , as proposed in Section 2.6 seems to depend on the soil type. The surface roughness and shape of soil particles may be one cause for a decrease in permittivity. More pronounced is the effect of microporosity. For soils containing solids that exhibit microporosity, such as Ferralsol,  $S$  becomes water content-dependent. Although the predicted value of  $S = 0.33$  resulted in reasonable correlations, *for accurate analyses one should consider determining the depolarisation factor as a function of water content for each soil individually.*



For Fine sand the calibration curve predicted by (2.61), and those measured with TDR and the new FD sensor are nearly identical and located slightly below Topp's calibration curve. *The advantage of equation (2.61) over Topp's curve is that (2.61) is more fundamental and can allow for differences in soil porosity and bound water content.*

## 4.2 ELECTRICAL CONDUCTIVITY MEASUREMENTS OF THE SOIL SOLUTION

In semi-arid regions, soil salinity is a great problem. Often, the specific electrical conductivity of the water in the soil matrix,  $\sigma_w$ , (also called electrical conductivity or *EC*) is used as a measure for soil salinity. With "specific" the conductance per meter length of a piece of the material (water or soil) with a cross section of  $1 \text{ m}^2$  is meant. Electrical conduction in the soil solution is attributed to the movement of ions and to dielectric absorptions. It is the intention here to find a measure for the conduction only due to the ions. *To be able to distinguish between the two conduction phenomena the term "ionic conductivity" will be used for the specific ionic conductivity of the water extracted from the soil matrix,  $\sigma$ , given in  $\text{S m}^{-1}$ .* Dielectric absorptions play a role in extracted (free-) water at a frequency above 1 GHz. Most salinity or conductivity meters operate at frequencies less than 1MHz. Therefore, dielectric absorptions be can generally neglected i.e.  $\sigma \approx \sigma_w$ . Since  $\sigma$  is defined as the conductivity of the water extracted from the soil, it is consequently not affected by the soil matrix or the soil water content,  $\theta$ . The electrical conductivity of the bulk soil,  $\sigma_b$ , is a function of  $\theta$  and  $\sigma_w$  and includes the dielectric absorption term of  $\sigma_w$ . Water bound to the soil matrix has a lower relaxation frequency than free water (see Section 2.2). This may not always be neglected, but I will do so for clarity.

One method of measuring  $\sigma$  is by extracting a sample of water from the soil matrix. This is a labour-intensive task and not well suited for automation. Additionally, it is not sure whether all ions are collected in the extracted sample. *It is, however, easier to measure  $\sigma_b$  which is related to  $\sigma$ .* The measurement of  $\sigma_b$  can easily be performed using the FD sensor as described in Section 3.4.  $\sigma$  is related to  $\sigma_b$  by a function which in turn is related to  $\theta$ . Mualem & Friedman [1991] described a frequently used empirical model of the relationship between  $\sigma$  and  $\sigma_b$ . This model requires the determination of  $\theta$ , the porosity,  $\phi$ , and two additional empirical parameters.

Malicki *et al.* [1994] found a high degree of linear correlation between  $\sigma_b$  and the real part of the permittivity  $\epsilon'$  values measured using TDR, for a broad range of soil types. They found an attractive method to calculate  $\sigma$  from simultaneous measurements of  $\sigma_b$  and  $\epsilon'$ . In my opinion, their empirical relationships can be improved. *I will approach the problem from a slightly different angle to derive a more fundamental relationship that is based on both parameters.* The new model will be tested on wet glass beads. Next the model will be applied to simultaneously measured values of  $\sigma_b$  and  $\epsilon'$  taken from Dirksen & Hilhorst [1994]. These data were measured with the 20 MHz-FD sensor described in Section 4.1.

The Maxwell-Wagner effect is expected to apply to  $\sigma_b$  measurements. The resulting frequency dependence is analysed with data obtained with the FD sensor operating at 10 MHz, 20 MHz and 30 MHz for three soils left from the Dirksen & Hilhorst [1994] measurements.



## Relationship between bulk electrical conductivity and ionic conductivity of soil solution

### Theory

The relationships  $\sigma_b$  versus  $\theta$  and  $\varepsilon'$  versus  $\theta$  are similar. This statement can be proven by considering the current density at each point in the soil matrix, starting with Maxwell's four basic equations on electromagnetism [Lorrain *et al.* 1988]. I will make the statement plausible in a way that can be followed easier by readers with no or almost no electronics engineering background, by referring directly to the parallel combination of a capacitor and conductor as equivalent circuit between the electrodes of a dielectric sensor.

First, consider the situation of only water between the electrodes. Then the complex admittance,  $Y_w$ , between the electrodes, is determined by the amplitude of the voltage,  $u$ , across the electrodes and its phase shift,  $\alpha$ , with respect to the sinusoidal current,  $i$ , through the water. The impedance can be calculated from  $Y_w = i/u$ . The problem is illustrated by the vector diagram in Figure 4.5. The current  $i$  can be split into a real component through the conductor,  $i_G$ , and an imaginary component through the capacitor,  $i_B$ . The voltage  $u$  is in phase with  $i_B$ . The current,  $i$ , is ahead with respect to  $u$  by the angle  $\alpha$ . In the same figure the admittance diagram is drawn for  $Y_w$  which is in phase with  $i$ . The conductance,  $G_w$ , is in phase with  $i_G$ . Conductor  $G_w$  represents the conductance due to the ions in the water. The current,  $i_B$ , through the capacitor,  $C_w$ , is  $90^\circ$  ahead with respect to  $u$ . This capacitor  $C_w$  represents the polarisability of the water. For clarity not  $C_w$  but the susceptance  $B_w = \omega C_w$  is drawn in phase with  $i_B$ , where  $\omega$  is the angular frequency.

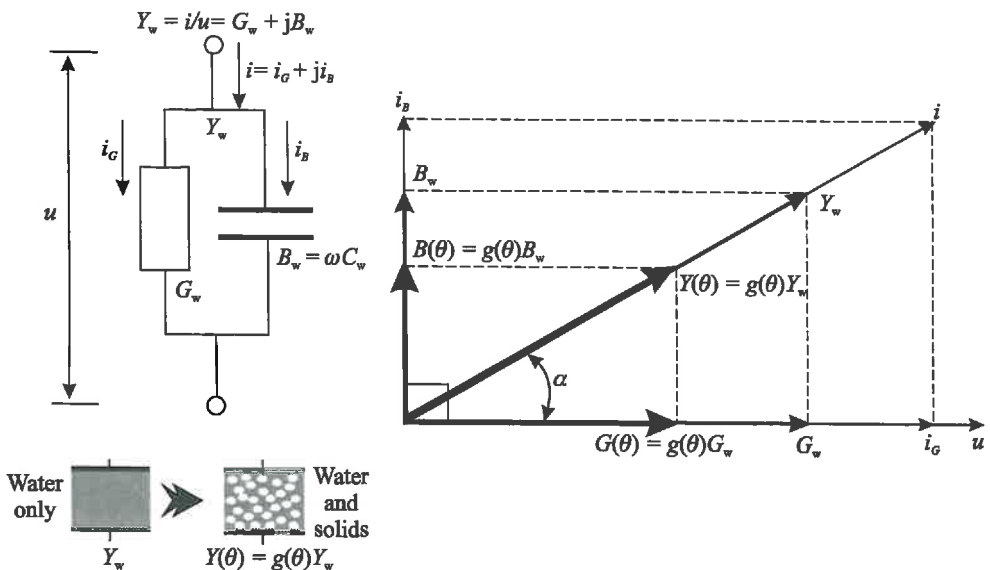


Figure 4.5. The effect of the replacement of water by the solids of soil on the measured admittance  $Y(\theta)$  between the electrodes of a dielectric sensor.



Now, consider the situation that part of the water between the electrodes is replaced by soil. This will have impact on the voltage  $u$  developed across the electrodes. A smaller amount of polarisable material with a high dielectric constant (see also Section 2.5) between the electrodes will lead to smaller susceptance and increased  $u$ . Note that the polarisability of the soil is neglected, this will be included later. Also, the lower amount of material that can conduct current (the ions in the water) is decreased. This too leads to an increase of  $u$ . An increased  $u$  results in a decrease of  $Y_w = i/u$ . Let  $Y$  be related to  $Y_w$  by the function  $g(\theta)$ , then the reduction of  $Y$  can be described by

$$Y(\theta) = Y_w g(\theta) \quad (4.7)$$

and the quadrature components of  $Y(\theta)$ ,  $B(\theta)$  and  $G(\theta)$ , can be described by

$$B(\theta) = B_w g(\theta) \quad (4.8)$$

and

$$G(\theta) = G_w g(\theta) \quad (4.9)$$

Both  $\sigma_b$  and  $\varepsilon'$  can be calculated from the quadrature components of  $Y(\theta)$ ; they are equally affected by the same electric mechanism in the soil.

The next step is including the impact of the Maxwell-Wagner effect in (4.7), (4.8) and (4.9). See for this the illustration of Figure 4.6.

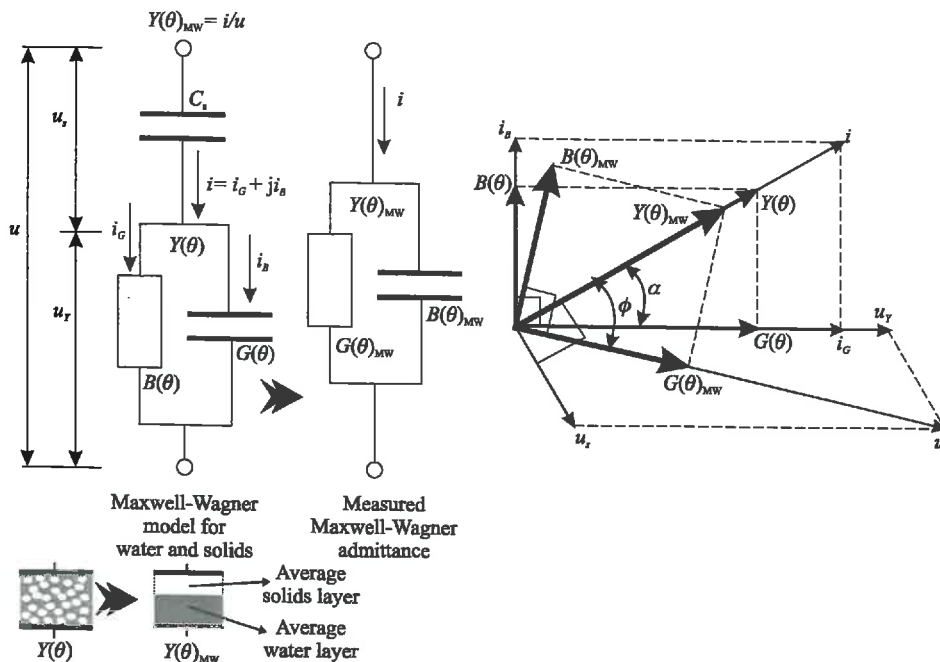


Figure 4.6. The measured admittance between the electrodes,  $Y(\theta)_{MW}$ , due to the Maxwell-Wagner effect, is replaced by a series connection of a capacitor,  $C_s$ , due to the solid and air layers and an admittance due to the admittance,  $Y(\theta)$ , of the water in the soil.



As explained in Section 2.4, the Maxwell-Wagner effect can be modelled as a series connection of a capacitor due to the solids,  $C_s$ , and the admittance,  $Y(\theta)$ , due to the water between the solids. The voltage across the electrodes  $u$ , in Figure 4.6, is the vector sum the voltage  $u_Y$  across the water and the voltage  $u_s$  across the solids. It is visualised how  $Y(\theta)$  appears between the electrodes as  $Y(\theta)_{MW}$ . A measuring devise (e.g. the sensor and software) will not be able to distinguish between  $Y(\theta)$  and  $Y(\theta)_{MW}$ . It will interpret  $Y(\theta)_{MW}$  as a parallel combination of a capacitor with susceptance,  $B(\theta)_{MW}$ , and conductor  $G(\theta)_{MW}$ . However, one expects to measure  $B(\theta)$  and  $G(\theta)$ . The current through  $G$  will be interpreted in phase with  $u$  and the current through the  $B$  as  $90^\circ$  ahead with respect to  $u$ . Due to  $C_s$  being in series with  $Y(\theta)$ :  $Y(\theta)_{MW} < Y(\theta)$ ,  $B(\theta)_{MW} > B(\theta)$  and  $G(\theta)_{MW} < G(\theta)$ .  $Y(\theta)_{MW}$  can be described by

$$Y(\theta)_{MW} = \alpha_Y Y_w g(\theta) \quad (4.10)$$

with quadrature components  $Y(\theta)_{MW}$ ,  $B(\theta)_{MW}$  and  $G(\theta)_{MW}$ , which can be described by

$$B(\theta)_{MW} = \alpha_B B_w g(\theta) \quad (4.11)$$

and

$$G(\theta)_{MW} = \alpha_G G_w g(\theta) \quad (4.12)$$

where  $\alpha_Y$ ,  $\alpha_B$ , and  $\alpha_G$  account for the Maxwell-Wagner effect on  $Y_w$ ,  $B_w$ , and  $G_w$ , respectively.

The electrical conductivity  $\sigma_b$  can be calculated from  $G(\theta)$ , the permittivity  $\epsilon'$  from  $B(\theta)$ . Both  $\sigma_b$  and  $\epsilon'$  are equally affected by the same electrical mechanism in the soil. However, for constant  $\theta$  and frequency the Maxwell-Wagner effect will cause  $G(\theta)_{MW}$  and consequently the measured value of  $\sigma_b$  to decrease, and  $B(\theta)_{MW}$  and consequently the measured value of  $\epsilon'_w$  to increase. The Maxwell-Wagner effect decreases with increasing frequency.

Up to here, only the part of  $Y$  that is affected by  $\theta$  is considered. For dry soil materials,  $\sigma_b = 0$ , but the dry soil material is still polarisable, hence  $\epsilon_{ob=0} \neq 0$ .  $\epsilon_{ob=0}$  appears as an offset to  $\epsilon'_w$ . Now, I postulate the following forms

$$\sigma_b = \alpha_G \sigma g(\theta) p(\theta) \quad (4.13)$$

and

$$\epsilon' = \alpha_B (\epsilon'_w g(\theta) + \epsilon_{s,a}) = \alpha_B \epsilon'_w g(\theta) + \epsilon_{ob=0} \quad (4.14)$$

where  $p(\theta)$  accounts for the freedom of movement of the ions in the soil matrix and  $\epsilon_{s,a}$  is the permittivity of only solids and air (see (2.63)). Note the similarity of (4.14) if (2.61) is substituted in (2.65). The term  $\epsilon_{ob=0} = \alpha_B \epsilon_{s,a}$  is independent of the water content and can serve to find  $\alpha_B$  if  $\epsilon_{s,a}$  is known. In (4.14)  $\alpha_B$  is equivalent to the Maxwell-Wagner contribution to  $\epsilon'_p$  in (2.65). Knowing  $\alpha_B$  the measured  $\epsilon'$  data can be corrected to find the  $\epsilon'_p$  data that can be predicted with (2.61). This implies a possibility of a standard  $\epsilon'(\theta)$  curve to all soils which is mainly affected by  $\phi$ ,  $\epsilon_s$  and  $\theta_h$ . This possibility, however, will not be worked out in detail here.

For ions moving through the lattice of ionic crystals in a dry or almost dry soil,  $p(\theta)$  is mainly determined by a Arrhenius function [see e.g. Lidiard, 1957; Roos & Wollants, 1995]

$$p(\theta) = f \left( A e^{-\frac{\Delta H^*}{RT}} \right) \quad (4.15)$$



where  $\Delta H^*$  is the activation energy required to liberate the ions from the soil matrix and parameter  $A$  is a function of the number of ions available for conduction and their mobility.  $p(\theta)$  accounts for processes influencing  $\sigma_b$  at low water content, such as conduction at the surface of the particles. For high water contents, ions are free to move making the impact of  $p(\theta)$  small, i.e.  $p(\theta) \approx 1$ . Therefore,  $p(\theta)$  will not be worked out in more detail, it was introduced only for completeness.

From (4.13) and (4.14), the ionic conductivity of the soil solution can be written as:

$$\sigma = \frac{\varepsilon'_w \sigma_b}{(\varepsilon' - \varepsilon'_{\sigma_b=0}) p(\theta) \alpha} \quad (4.16)$$

where  $\alpha = \alpha_B \alpha_G$ . The model of (4.16) describes the relationship between  $\varepsilon'_w$  and  $\sigma$  of the water extracted from the soil and their values  $\varepsilon'$  and  $\sigma_b$  as measured in the bulk soil using a dielectric sensor. From two pairs of  $\varepsilon' - \sigma_b$  values the offset  $\varepsilon'_{\sigma_b=0}$  can be determined. The product  $\alpha p(\theta)$  can only be determined if  $\sigma$  is known.  $\sigma$  in turn can be most easily determined from a saturated soil extract. Model (4.16) differs that much from the empirical results of Malicki *et al.* [1994] that a comparison makes no sense.

Concluding, *the ionic conductivity of the soil solution can be calculated from the simultaneously measured real part of the permittivity and the electrical conductivity of the bulk soil.*

#### *Experimental validation of (4.16) with glass beads*

To check whether the  $\sigma$  values calculated according to (4.16) are independent of  $\theta$ , four samples of wet glass beads of 0.2 mm at arbitrary  $\theta$  were prepared by slowly extracting solution from an initially saturated sample. Since  $\sigma$  is not allowed to change with  $\theta$ , drying by evaporation was avoided. The  $\sigma_b - \varepsilon'$  values were measured using the FD sensor at 20 MHz. The experiment started with clean glass beads and  $\sigma$  was measured using before the solution was applied to the sample. The measured  $\sigma_b - \varepsilon'$  values and the  $\sigma$  values calculated according to (4.16) for each water content are given in Table 4.2. The regression line between the  $\varepsilon' - \sigma_b$  columns is

$$\varepsilon' = 189\sigma_b + 7.72 \quad \text{with } R^2 = 0.986 \quad (4.17)$$

from which  $\varepsilon'_{\sigma_b=0} = 7.7$  can be derived.

Since the Maxwell-Wagner effect is expected to be negligible for glass beads and no surface effects are expected at high water contents it is assumed that  $\alpha p(\theta) = 1$ . Values for  $\sigma$  calculated according to (4.16) with the above mentioned values are also given in Table 4.2. From the agreement between the measured and calculated  $\sigma$  values it can be concluded that the assumption  $\alpha p(\theta) \approx 1$  is allowed for glass beads.

Next the validity of (4.16) was tested for different  $\sigma$  values at constant  $\theta$ . Samples of thoroughly mixed water-saturated glass beads with different water-NaCl concentrations were prepared. There was sufficient water left on top of the glass beads to allow both the measurement of the  $\sigma_b - \varepsilon'$  values and the  $\sigma - \varepsilon'_w$  values using the same FD sensor at 20 MHz. The resulting  $\sigma$  values calculated according to (4.16) for  $\alpha p(\theta) = 1$  and  $\varepsilon'_{\sigma_b=0} = 7.7$  are given in Table 4.3.





Table 4.2.  $\epsilon'$ ,  $\sigma_b$  and  $\sigma$  measured in 0.2-mm glass beads with the FD sensor at 20 MHz. The last column lists the  $\sigma$  values calculated according to (4.16) for  $\alpha p(\theta) = 1$  and  $\epsilon'_{\sigma_b=0} = 7.7$ .

Soil water content	Real part of permittivity	Electrical conductivity of the bulk	Ionic conductivity of solution, measured	Ionic conductivity of solution, according to (4.16)
$\theta$ (-)	$\epsilon'$ (-)	$\sigma_b$ (S m <sup>-1</sup> )	$\sigma$ (S m <sup>-1</sup> )	$\sigma$ (S m <sup>-1</sup> )
$\theta = \phi$	26.9	0.10	0.4	0.41
?	21.0	0.07	0.4	0.41
?	18.3	0.06	0.4	0.44
?	15.8	0.04	0.4	0.39

Table 4.3.  $\epsilon'$ ,  $\sigma_b$  and  $\sigma$  values measured in water-saturated 0.2-mm glass beads at 20 MHz with the FD sensor. The last column lists the  $\sigma$  values calculated according to (4.16) for  $\alpha p(\theta) = 1$  and  $\epsilon'_{\sigma_b=0} = 7.7$ .

Real part of permittivity	Electrical conductivity of the bulk	Ionic conductivity of solution, measured	Ionic conductivity of solution, according to (4.16)
$\epsilon'$ (-)	$\sigma_b$ (S m <sup>-1</sup> )	$\sigma$ (S m <sup>-1</sup> )	$\sigma$ (S m <sup>-1</sup> )
27.9	0.062	0.240	0.250
27.0	0.021	0.083	0.085
26.9	0.010	0.040	0.041

Both  $\epsilon'$  and  $\sigma_b$  were measured with an FD sensor equipped with electrodes of a certain cell-constant  $\kappa$ . If the electrodes are in poor contact with the soil, or if they are not completely inserted, or if the field lines are affected by the boundaries of the sample, this will not affect the calculation of  $\sigma$  since both  $\sigma_b$  and  $\epsilon'$  are affected in the same way. Note also that the calculation of  $\sigma$  is independent of the density of the material.

*It can be concluded that with  $\alpha p(\theta) = 1$  and  $\epsilon'_{\sigma_b=0} = 7.7$  the model (4.16) can be used for calculating the ionic conductivity of water in glass beads without calibration.*

#### *Experimental validation of (4.16) with soil*

In this Section the model of (4.16) is applied to experimental values of  $\sigma_b$  and  $\epsilon'$  taken from Dirksen & Hilhorst [1994].

In the derivation of (4.16) it was assumed that the relationships between  $\sigma_b$  and  $\theta$ , and between  $\epsilon'$  and  $\theta$ , are similar. This statement is illustrated using three soils that show very different shapes for their  $\epsilon'$  versus  $\theta$  plots; Groesbeek, Ferralsol-A and Munnikenland. Their compositions are given in Table 4.1. In Figure 4.7,  $\epsilon'$  and  $\sigma_b$  are plotted as function of  $\theta$ . The scale for each soil was chosen such that the very similar shapes of the curves are as visible as possible. Figure 4.7 indicates that an interesting result can be found if  $\sigma_b$  is plotted versus  $\epsilon'$  as has been done in Figure 4.8. All soils, show a high degree of linear correlation between  $\sigma_b$  and  $\epsilon'$ . This result is similar to the results of Malicki *et al.* [1994] for TDR. These





experimental data indicate that the intercepts with the  $\epsilon'$ -axis,  $\epsilon'_{\sigma_b=0}$ , are soil type dependent. In contrast Malicki *et al.* [1994] found  $\epsilon'_{\sigma_b=0} = 6$  as a general figure independent of soil type. The average permittivity of dry soil  $\epsilon' \approx 3.5$  and rarely  $\epsilon' > 5$ , but most of the regression lines in Figure 4.8 show  $\epsilon'_{\sigma_b=0} > 5$ . Although not visible on the graphs, the lines should bend to  $\epsilon' < 5$  at very low  $\theta$ 's. Thus, the values found for  $\epsilon'_{\sigma_b=0}$  are valid only if used with the linear model. The functions  $\epsilon'_{\sigma_b=0} = \alpha_B \epsilon'_{s,a}$  and  $p(\theta)$  given in (4.14) and (4.15) were account for this effect. Since the bending of the linear part of the  $\sigma_b$  versus  $\epsilon'$  lines towards  $\epsilon' \approx 3.5$  is not visible on any graph,  $p(\theta)$  is expected to be only active for the very low water content regions allowing to assume that  $p(\theta) = 1$ .

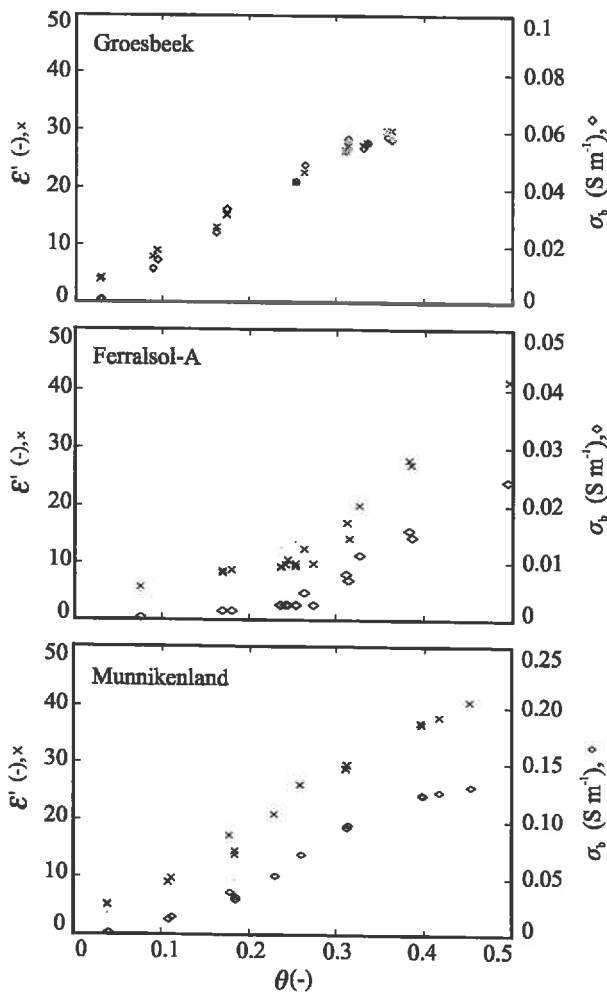


Figure 4.7. The relationship between the real part of the permittivity,  $\epsilon'$ , and the electrical conductivity of the bulk soil,  $\sigma_b$ , as a function of the water content  $\theta$  for three different soil types of Table 4.1

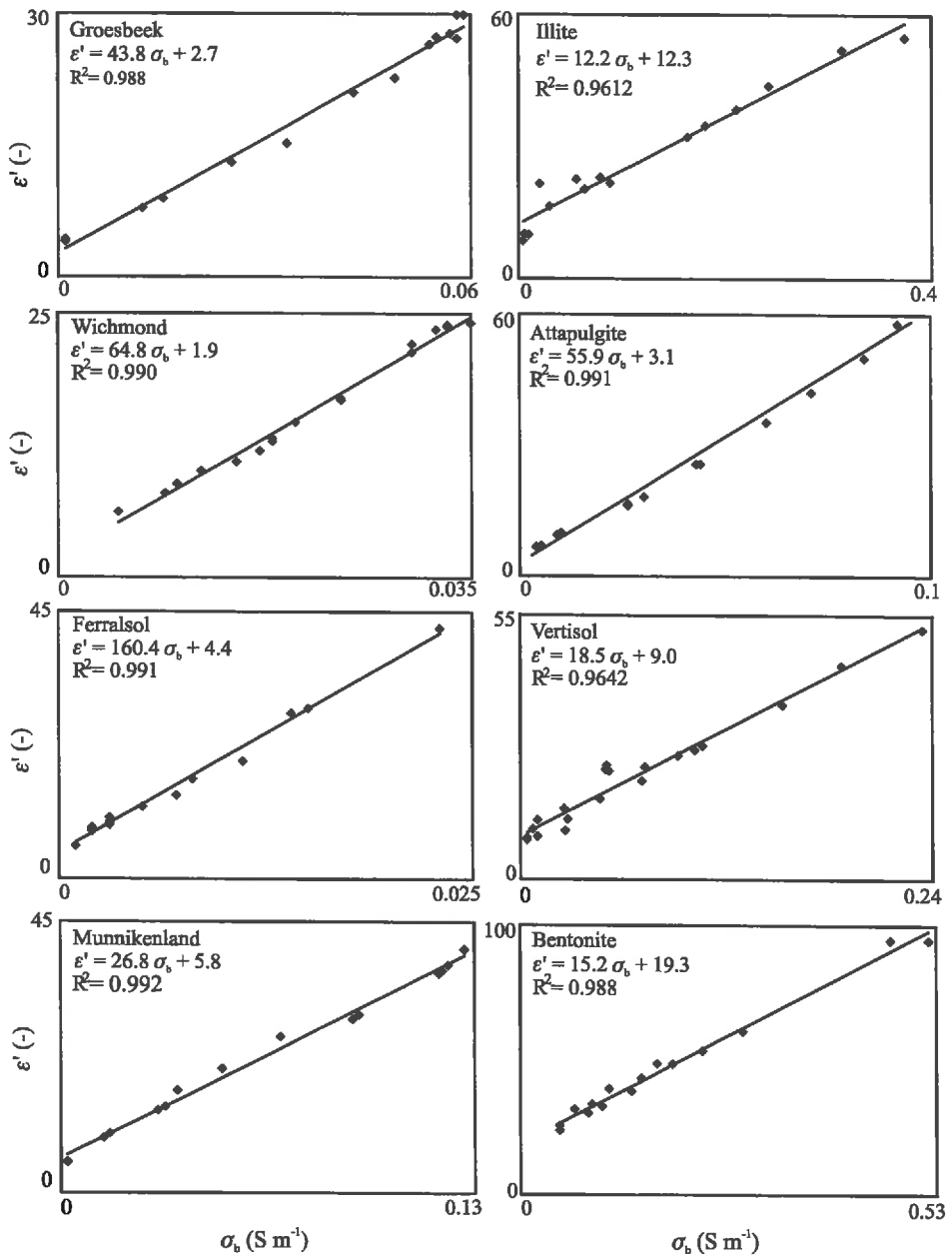


Figure 4.8. Relationships between the real part of the permittivity,  $\epsilon'$ , and the electrical conductivity of the bulk soil,  $\sigma_b$ , for eight different soil types as measured with the FD sensor at 20 MHz. The solid lines are linear regression lines through the measured data.



To demonstrate the validity of the new method of calculating  $\sigma$  from simultaneously measured  $\sigma_b$  and  $\epsilon'$ , values only the data of Dirksen & Hilhorst [1994] are available. Soil material left from this 1994 study were mixed thoroughly with three pore volumes of demineralised water and  $\sigma$  was measured in the water above the soil using a 1-kHz, four-point conductivity meter. Illite, Vertisol and Bentonite could not be mixed sufficiently to use this procedure. To correct for the dilution, the measured  $\sigma$  values were multiplied by 3 to estimate the conductivity of the pore water at saturation. These corrected measured  $\sigma$  values are plotted as a reference, in Figure 4.9. Water bound to the soil matrix may have a lower  $\epsilon'_w$  value than free water, but I will assume  $\epsilon'_w = 80$  at room temperature. I also neglect the Maxwell-Wagner effect, although this may lead to deviations for higher clay contents, since the impact of  $p(\theta)$  is small for high water contents, I assume  $p(\theta) = 1$  for all soils. After substituting all these assumptions for  $\alpha$ ,  $p(\theta)$  and  $\epsilon'_w$ , (4.16) becomes independent of  $\theta$  and yields

$$\sigma \approx \frac{80 \sigma_b}{\epsilon' - \epsilon_{\sigma b=0}} \quad (4.18)$$

With (4.18)  $\sigma$  can be calculated with simultaneous measured values of  $\sigma_b$  and  $\epsilon'$ . Figure 4.9 shows such  $\sigma$  values calculated with measured data of Dirksen & Hilhorst [1994] as function of  $\theta$ .

The measured reference values obtained after correction for the dilution, are indicated by the  $\blacklozenge$  marks, and the solid lines indicate the average of values plotted from high water contents down to the water contents indicated by the dashed lines. The difference between the reference and average values may be due to the unknown value of  $\alpha p(\theta)$ .

The independence of  $\sigma$  on  $\theta$  is clearly illustrated by Figure 4.9. Although there was not sufficient data available to show the decrease for  $\sigma_b$  at low water contents, one can observe a tendency towards zero for  $\sigma$ .

*The presented data indicate that the determination of  $\sigma$  with the simplified equation (4.18) is generally valid for  $\theta > 0.2$ , and in soils with  $S_A < 80$  already for  $\theta > 0.1$ . To improve the accuracy at lower water contents ( $\theta < 0.1$ ), the function  $p(\theta)$  must first be analysed.*

## Conclusions

*The relationship between simultaneously measured values of the real part of the permittivity,  $\epsilon'$ , and the electrical conductivity of the bulk soil,  $\sigma_b$ , is linear with a high regression coefficient. Although not measured, the linear relationship becomes non-linear at low water contents. For an average soil the straight line should bend to end at  $\epsilon' \approx 3.5$ . This phenomenon depends on the type of ions, the mobility at the particle surfaces, and the activation energy.*

Due to the linear relationship between  $\epsilon'$  and  $\sigma_b$ , *the ionic conductivity of the soil solution  $\sigma$  can be found from a simultaneous measurement of  $\epsilon'$  and  $\sigma_b$  independent of  $\theta$ . The relationships of  $\sigma$  with  $\epsilon'$  and  $\sigma_b$  basically depends on the texture of the soil. Reasonably accurate results were found when neglecting this dependence.*

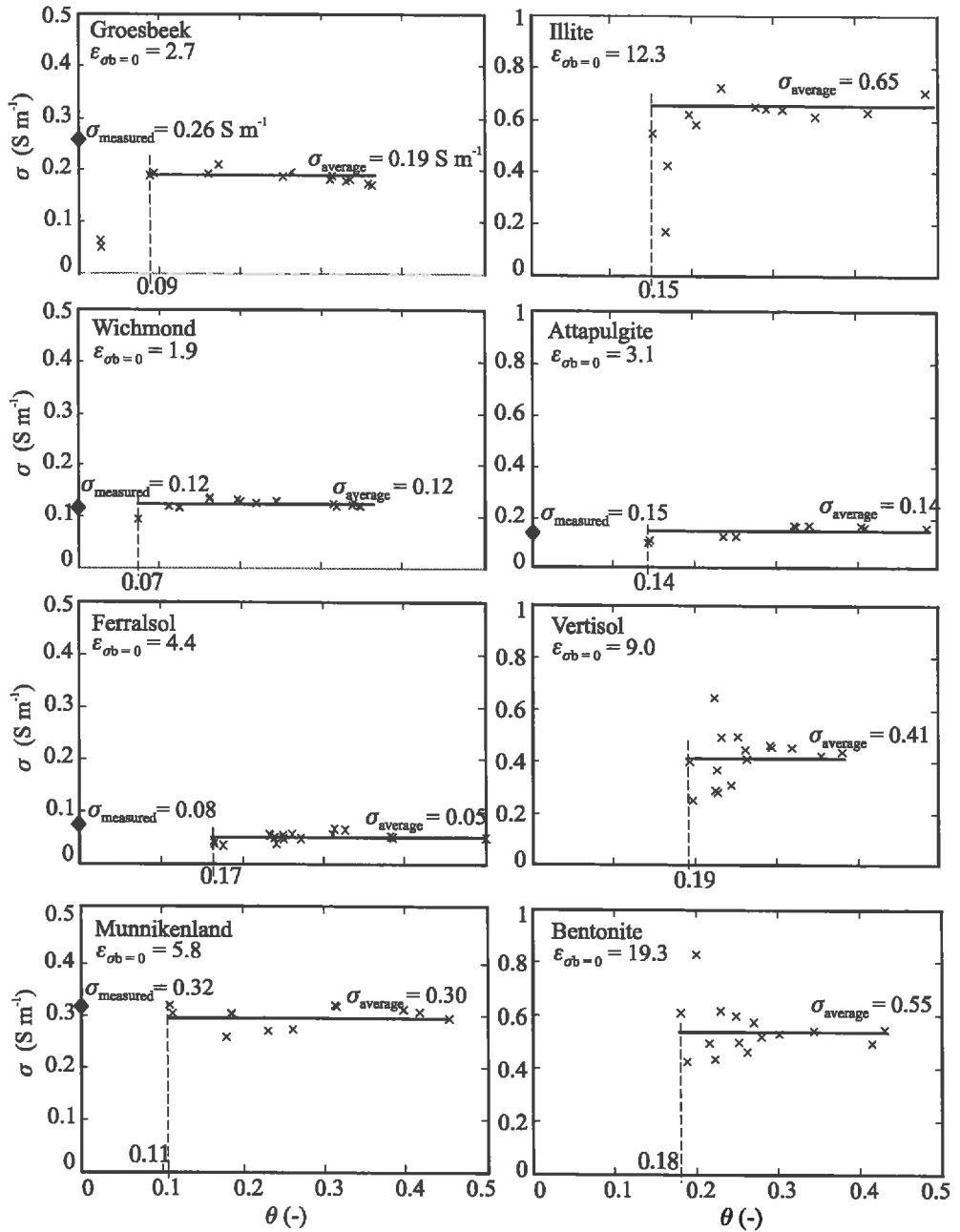


Figure 4.9. Ionic conductivity of the soil solution,  $\sigma$ , versus soil water content,  $\theta$ , for eight different soil types. The solid lines indicate the average of all values from high water contents down to the water contents indicated by the dashed lines. The reference  $\sigma$  values are indicated with  $\blacklozenge$ .



### 4.3 FREQUENCY DEPENDENCY OF ELECTRICAL CONDUCTIVITY OF BULK SOIL

#### TDR conductivity measurements: low frequency measurements

Topp *et al.* [1988] and Heimovaara *et al.* [1995] concluded that the bulk soil electrical conductivity,  $\sigma_b$ , can be derived from the final voltage amplitude in a transmission line after all multiple reflections of a step voltage have died out. This occurs between fifty and a few hundred nano seconds after the step pulse is generated. Assume all reflections are integrated after 50 ns. This integration time corresponds to a frequency of  $1/(2\pi \cdot 50 \cdot 10^{-9}) = 3$  MHz or less. It follows that the  $\sigma_b$  values found for TDR are "low" frequency values.

The following deduction also explains how a conductivity measurement can be performed using TDR. After a few hundred nanoseconds, the length of the transmission line ( $\approx 10$  cm) is infinitely short with respect to the wave length. This means that also the voltage drop over the series inductances and the currents through the capacitors (see the electrical model of a transmission line given in Chapter 3) are negligible. This reduces the problem to a series connection of two resistors, switched on and off to a simple battery. One resistor being the low frequency output resistance of the step function generator ( $50 \Omega$ ) and the other resistor the conductance of the soil between the electrodes. If the open circuit output voltage of the generator is known, the conductance between the electrodes can be determined from the output voltage measured with the electrodes connected. It follows that a TDR conductivity measurement is equivalent to a simple, low-frequency conductivity measurement.

#### Materials and methods

The Maxwell-Wagner effect is expected to apply also to the electrical conductivity of the bulk soil (Section 4.2). To examine this,  $\sigma_b$  was measured with the FD sensor and TDR for different water contents and frequencies on the Groesbeek, Wichmond, and Attapulgate soils (see Table 4.1) left from the Dirksen & Hilhorst [1994] experiments. The TDR measurements were done by Dirksen in 1997 according to the method and apparatus described by Heimovaara *et al.* [1995]. The FD measurements were carried out at 10 MHz, 20 MHz, and 30 MHz. The electrical conductivity of the bulk soil for infinitely high frequencies,  $\sigma_{MW f \rightarrow \infty}$ , and that for infinite low frequencies,  $\sigma_{MW f \rightarrow 0}$ , were calculated according to equivalents of (2.32), (2.33) and (2.34). For this purpose,  $\Delta\epsilon_{MW}$ ,  $\epsilon_{MW f \rightarrow \infty}$ ,  $\epsilon'_1$  ( $\epsilon'$  at 10 MHz),  $\epsilon'_2$  ( $\epsilon'$  at 20 MHz), and  $\epsilon'_3$  ( $\epsilon'$  at 30 MHz) are replaced by  $\Delta\sigma_{MW}$ ,  $\sigma_{MW f \rightarrow \infty}$ ,  $\sigma_1$ ,  $\sigma_2$ , and  $\sigma_3$ , respectively, yielding

$$\sigma_{MW f \rightarrow \infty} = \frac{8\sigma_1\sigma_3 - 3\sigma_1\sigma_2 - 5\sigma_2\sigma_3}{5\sigma_1 - 8\sigma_2 + 3\sigma_3} \quad (4.19)$$

$$\Delta\sigma_{MW} = \left( \sigma_1 - \sigma_{MW f \rightarrow \infty} \right) \left( 1 + \frac{f_1^2}{f_{MW r}^2} \right) \quad (4.20)$$



The low frequency values are calculated from

$$\sigma_{MWf \rightarrow 0} = \sigma_{MWf \rightarrow \infty} + \Delta\sigma_{MW} \quad (4.21)$$

where  $\Delta\sigma_{MW}$  has a negative sign due to the decrease of  $\sigma_b$  towards lower frequencies.

### Experimental characterisation of the Maxwell-Wagner effect for electrical conductivity

The experimental results given in Table 4.5 show a high correlation between the low frequency values of the TDR measurements and the values calculated for  $\sigma_{MWf \rightarrow 0}$ . This table strongly supports the hypothesis that  $\sigma$  can be related to  $\sigma_b$ , as  $\epsilon'_w$  was related to  $\epsilon'$ , including the Maxwell-Wagner effect. It also proves that  $\sigma_b$  as measured with TDR is a low-frequency value as can be calculated for  $\sigma_{MWf \rightarrow 0}$  from the Maxwell-Wagner effect. The texture parameter  $K$ , which determines  $\Delta\sigma_{MW}$ , is related to the specific surface area,  $S_A$ . The data in Table 4.5 are sorted in order of increasing  $S_A$ ; this is also the order of increasing  $\Delta\sigma_{MW}$  and  $K$ . As an illustration, the frequency dependence of the bulk electrical conductivity is calculated for Attapulgitte at  $\theta = 0.52$  and plotted in Figure 4.10.

Table 4.5. The variables,  $\sigma_b$ ,  $\sigma_{MWf \rightarrow 0}$ ,  $\sigma_{MWf \rightarrow \infty}$  and  $\Delta\sigma_{MW}$  calculated from the Maxwell-Wagner effect according to (4.19), (4.20) and (4.21). The  $\sigma_b$  values measured with the FD sensor and with TDR are given for comparison. The soils are listed in order of increasing specific surface area.

Soil type	Water content $\theta$ (-)	Specific surface area $S_A$ ( $m^2 g^{-1}$ )	Electrical conductivity of bulk soil, $\sigma_b$ ( $mS m^{-1}$ )							
			TDR < 3 MHz	measured				calculated		
				FD sensor				$\sigma_{MWf \rightarrow \infty}$	$\Delta\sigma_{MW}$	$\sigma_{MWf \rightarrow 0}$
				10 MHz	20 MHz	30 MHz	30 MHz			
Grosbeek	0.15		10	12	14	15	16		10	
	0.29	25	23	25	27	28	29	-6	23	
	0.36		28	29	31	32	33		27	
Wichmond	0.23		26	24	26	28	34		23	
	0.34	41	29	31	34	36	39	-11	29	
	0.37		35	35	37	39	45		34	
Attapulgitte	0.52		39	48	54	56	58		38	
	0.71	270	69	74	81	84	87	-20	66	

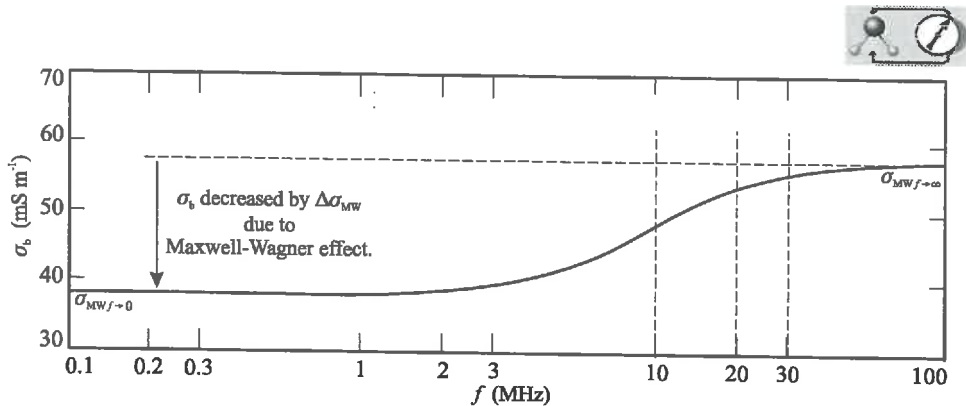


Figure 4.10. The frequency dependence of  $\sigma_b$  due to the Maxwell-Wagner effect of Attapulgitte with  $\theta = 0.52$ . The low- and high-frequency values of  $\sigma_b$  are indicated by  $\sigma_{MW f \rightarrow 0}$  and  $\sigma_{MW f \rightarrow \infty}$ . The conductivity decrement,  $\Delta\sigma_{MW}$ , is equivalent to the dielectric increment  $\Delta\epsilon$ .

### Conclusions

From the linear relationship between  $\sigma_b$  and  $\epsilon'$  it is concluded that a similar relationship as found for  $\epsilon'$  versus  $\theta$  can be derived for  $\sigma_b$  versus  $\theta$ , using the same procedure as described for  $\epsilon'$  in Chapter 2. Therefore, the Maxwell-Wagner effect also applies to  $\sigma_b$ , causing an increase of  $\epsilon'$  for decreasing frequencies. The Maxwell-Wagner effect can be described by a Debye function and thus  $\epsilon'$  and  $\epsilon''$  are inversely related. The Maxwell-Wagner effect decreases  $\sigma_b$  at frequencies low compared to the Maxwell-Wagner relaxation frequency. According to Section 2.4, these frequencies are  $< 150$  MHz. The measuring frequency of most conductivity meters is less than 10 kHz. Therefore,  *$\sigma_b$  measurements with low frequency conductivity meters are subject to the Maxwell-Wagner effect.* The Maxwell-Wagner effect can be characterised by means of conductivity measurements. The advantage is that  $\sigma_b$  can be measured more accurately than  $\epsilon$ .

Finally, it was shown that  *$\sigma_b$  measurements with TDR generate values for frequencies  $< 3$  MHz.*

## 4.4 DIELECTRIC CONTAMINATED SITE INVESTIGATION

In the preceding sections, of this Chapter the ionic conductivity of the pore water,  $\sigma$ , was obtained by simultaneous measurements of  $\sigma_b$  and  $\epsilon'$  with the FD sensor described in Section 3.4. Although less accurate, the  $\sigma_b / \epsilon'$  ratio is often used as a measure of the free ion concentration. It is well-known that anomalous values of this ratio can indicate the presence of pollutants. For this purpose it is sufficient to monitor only  $\sigma_b / \epsilon'$ . A far more interesting result can be obtained by assuming that this ratio is dominated by the natural composition of a saturated soil and that this composition does not vary much over a small vertical distance in undisturbed soils. That pollutants which are more dense than water form small droplets or thin layers on top of impermeable soil layers. This affects the dielectric properties [Redman & Annan, 1992] causing small unnatural changes in the ratio  $\sigma_b / \epsilon'$  as a function of soil depth,  $z$ . Thus, it is expected that the ratio between the derivatives  $d\sigma_b / dz$  and  $d\epsilon' / dz$  are indicative of the presence of certain pollutants. Since we intended only to indicate and not to quantify





possible polluted soil layers, only the absolute values were used to define the following pollution indicator

$$p = \frac{|d\sigma_b/dz| + a}{|d\epsilon'/dz| + b} \quad (4.22)$$

The sensitivity of  $p$  ( $S F^{-1}$ ) can be adjusted with the constants  $a$  ( $S m^{-2}$ ) and  $b$  ( $F m^{-2}$ ). Empirically, an optimal result was found for  $a = 0.01 S m^{-2}$  and  $b = 0.01 F m^{-2}$ .

The pollution indicator was tested with a new dielectric probe for the investigation of chemically contaminated sites. The probe was developed in close cooperation with GeoMil Equipment b.v. in The Netherlands. It contains the ASIC described in Chapter 3, placed in a cylindrical cone and connected to two ring-shaped electrodes with a diameter of 3.5 cm, 0.5 cm width, at 5 cm distance. While the probe was mechanically pushed into the soil with a speed of 0.5 cm/s,  $\epsilon'$  and  $\sigma_b$  were measured simultaneously, as a function  $z$  at 1-cm intervals. Figure 4.11a shows the results for a non-polluted site and Figure 4.11b for a site polluted with chlorinated solvents and oil.

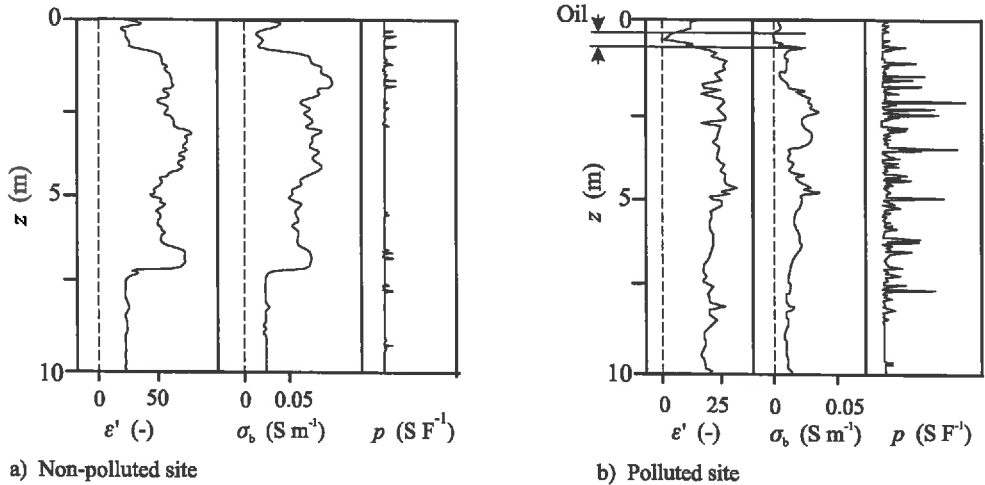


Figure 4.11. Profiles of  $\epsilon'$ ,  $\sigma_b$ , and the pollution indicator,  $p$ , for a) a non-polluted site and b) a site polluted with chlorinated solvents and oil. The needles for  $p$  indicate a soil layer polluted with chlorinated solvents. The oil layer can be found from characteristic changes in permittivity and conductivity.

This method was tested on 4 polluted and 3 non-polluted sites yielding results similarly to those of Figure 4.11. I can not give the data for the other sites since they are confidential, but Figure 4.11 adequately illustrates the general results.

Pollutants such as oil are less dense than water and gather on top of the ground water table. The pollution indicator was not able to locate these oil layers, but it was still possible to recognise them from their typical dielectric behaviour. They exhibit a decrease in  $\epsilon'$  to less than 5 together with a decrease in  $\sigma_b$  to approximately zero and followed by a rapid increase to the "natural" values for water-saturated soils. As indicated in Figure 4.11b, a waste-oil layer was detected at a depth of about 0.5 m and smeared out to a depth of about 0.75 m.



## Conclusion

The ability to measure  $\varepsilon'$  and  $\sigma_b$  simultaneously is attractive for contaminated site investigation. *The ratio between the derivatives of  $\varepsilon'$  and  $\sigma_b$  with depth yields a pollution indicator. The addition of offsets to the derivatives increases its sensitivity.*

## 4.5 DIELECTRIC PROPERTIES OF SOIL ILLUSTRATED BY HARDENING CONCRETE

Chapter 2 deals with the development of a model that describes the dielectric behaviour of soil. For frequencies  $> 100$  MHz, the permittivity due to polarisation phenomena can be described by (2.52) or by the more practical approximation (2.61). For lower frequencies, the model was expanded for the Maxwell-Wagner effect, yielding (2.65). The underlying theory is also applicable to other porous materials, such as concrete. The dielectric behaviour of concrete has been described by e.g. Tobio [1957], De Loor [1961, 1996] and Al-Qadi *et al.* [1995]. Concrete is a mixture of cement, water and additives such as sand and gravel. From a dielectric point of view, young hardening concrete exhibits a similar behaviour as soil, but in extremes. Only the cement-water mixture, i.e. the cement-paste, is subjected to the hydration process. During hydration molecular water will be incorporated into a complex molecule with the minerals in the concrete. Sand and gravel are filling substances that need not be considered in the treatment of the hydration process.

After mixing, the cement paste can be compared with a sandy or loamy soil saturated with water of high ion content. During the hydration process the texture of cement paste, and consequently its dielectric properties are continuously changing. After some time it will exhibit a clay-like texture and finally it will develop a skeleton comparable with porous rock. The situation of particles dispersed in water is transformed into a porous structure with water dispersed in the pores. The hydration process continues in the pores. During the whole hydration process, the mixture is saturated with water. Therefore, a number of effects associated with unsaturated soil do not occur in concrete.

First, the hydration process of cement paste will be described briefly. Next, it will be shown that changes in the degree of hydration, and consequently in the compressive strength, are reflected in changes in the dielectric properties. After a short description of the materials and used instrumentation, an overview of the dielectric behaviour of concrete as a function of frequency and time and its comparison with soils of different texture is described. Finally, an overview will be given of a number of phenomena characteristic of certain changes in the microstructural properties of concrete.

### The hardening process of young concrete

The hardening process of cement paste can be divided into an early, middle and late period. The following description of the chemical and structural development of early-age concrete is compiled from Breugel [1991].

**The early period (0 to 3-6 hours):** After applying the water, part of the cement grains dissolve in the first minutes. After mixing,  $\text{Ca}^{2+}$  ions will saturate the pore water. Meanwhile, other ions are formed as well, e.g.  $\text{OH}^-$ ,  $\text{SO}_4^{2-}$ ,  $\text{K}^+$  and  $\text{Na}^+$ . The dissolution of the water-soluble



parts of the cement is an exothermic process. Consequently, the temperature rises noticeably. Thereafter, the cement will be more or less inactive for more than 3 hours.

Not all the cement dissolves directly. Once a part of the grains is dissolved, a shell is formed around the remaining part of a cement grain. This shell bursts open at the end of the early period or the beginning of the middle period, allowing more cement to take part in the hydration process.

During the early period, the cement paste is changed into a colloidal suspension of water and coarse sand saturated with ions and partly dissolved cement particles.

**The middle period (3-6 to 30 hours):** After roughly 6 hours, the middle period starts in which the cement paste begins to hydrate. The main part of this process lasts about 30 hours. During the hydration process, small needles and clusters of needles, but also crystals in the form of thin plates are formed. Fibrils start to grow on the surface of these plates, bridging the distance between them. During the hydration process, energy is released rising the temperature to a maximum after about 12 to 24 hours.

The most important products starting to develop at the end of the middle period are ettringite needles, calcium silicate hydrates (CSH), and calcium hydroxides (CH). As time elapses, a dense structure is formed with a high specific surface area of roughly 200 to 1000 m<sup>2</sup> g<sup>-1</sup>.

After about one hour of hydration the ettringite needles, initially with an average length of up to 0.25 μm and a diameter of 0.05 μm, develop an average length of up to 1 μm and a diameter of 0.1 μm and finally grow to an average length of up to 10 μm and a diameter of 0.25 μm.

CSH particles are formed radiating from active centres into the water-filled pores, building up an increasingly dense network. They appear in fibril form or are plate-shaped and at this stage have characteristic dimensions of 1 μm length and 0.01 μm thick.

CH crystals can develop particles as long as 100 μm, and even lengths of 1000 μm are found. They are in general much larger than CSH and ettringite. About 10 to 20 % of the hydration products are CH crystals.

**The late period (after 30 hours):** During the late period the continuous phase of the cement paste is changed from liquid into a porous solid structure. Meanwhile CSH and CH products are formed during this period. After about 27 days most of the cement has been hydrated, but the cement goes on hydrating for years and continues to develop strength.

#### **Materials and methods to measure the dielectric spectrum of concrete as a function of time**

In the following the chemical and structural development of early-age concrete will be compared to changes in its dielectric properties. The dielectric properties of concrete were measured using a Hewlett Packard HP 8753C network analyser coupled to the S-parameter test set HP 85047A. The frequency range was 10 MHz to 6 GHz. The measuring cell was an open-ended coaxial transmission line buried in the concrete. It was home-made as a look-alike of the HP 85071. The instrumentation was calibrated, and the permittivity was calculated using the accompanying HP software. (See the corresponding factory manuals for instrumentation details.) For this experiment the cement was Portland-A with a water cement fraction  $\omega_{wcc} = 0.53$  on a weight basis. The composition is given in Table 4.6.



Table 4.6. Composition of the concrete used for Figure 4.12.

Constituent	Mass per	Density	Volume fraction
	volume concrete		
	( $\text{kg m}^{-3}$ )	$\rho$ ( $\text{kg m}^{-3}$ )	$v$ ( $\text{m}^3 \text{m}^{-3}$ )
Water	160	1000	0.16
Cement, Portland-A	320	3150	0.10
Sand	750	2650	0.28
Gravel	1130	2650	0.43
Air	-	-	0.02

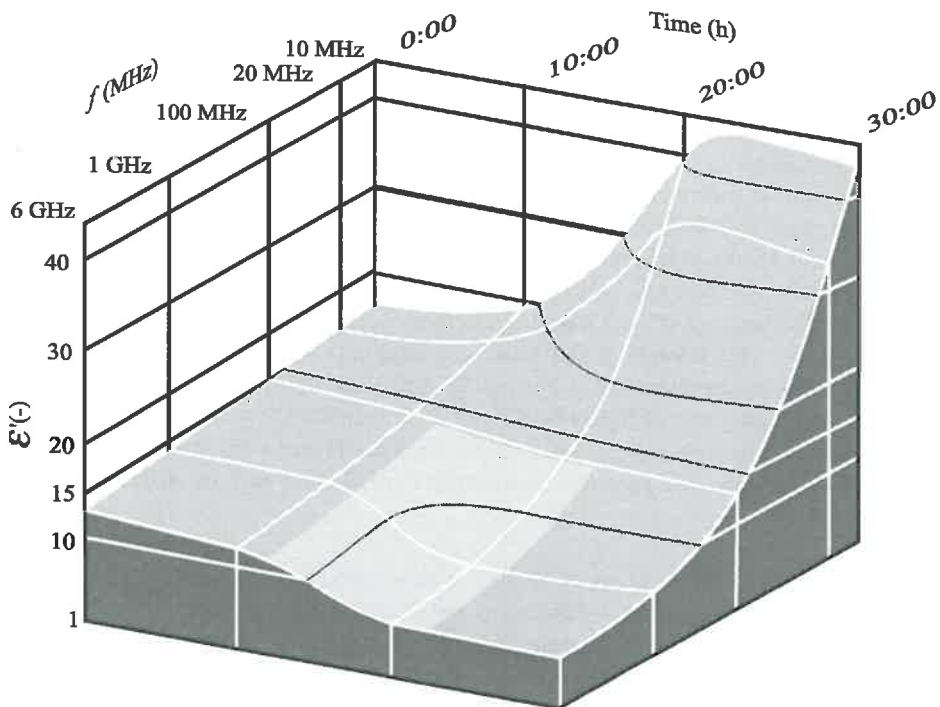


Figure 4.12. Real part of the permittivity,  $\epsilon'$ , measured with a network analyser in Portland-A cement having a water-cement ratio  $\omega_{ce} = 0.53$  versus time,  $t$ , and frequency,  $f$ . The picture is a smoothed version of data measured with an HP 8753C network analyser. An open-ended coaxial transmission line (a look-alike of the HP 85071) was buried in the concrete as sensor. Between 12 hours, 22 hours, 100 MHz and 6 GHz (light grey) was no data available. The data were presented by Breugel *et al.* [1996].



### Permittivity of concrete as a function of frequency

After the concrete was mixed at a commercial mixing plant, it had to be transported to the laboratory. The measurements started about 2 hours after mixing:  $t = 0$ . During the first two days, measurements were taken every half hour, and for the next 5 days twice daily. Unfortunately, some data were lost between  $t \approx 12$  hours, 22 hours, 100 MHz and 6 GHz. The dielectric data are plotted in Figure 4.12 starting at  $t = 0$ . The elapsed time,  $t$ , is plotted on the x-axis, the real part of the measured permittivity,  $\epsilon'$ , on the y-axis and the frequency,  $f$ , on the z-axis.

**Early period:** Considering the dielectric theory, sand and gravel will hardly have any impact on the dielectric spectrum. Dielectric behaviour of concrete as a function of frequency is dominated by the cement paste and is comparable to that of soil mainly containing sand, some silt and-or clay and a high ion content.

During the early period the low-frequency end of the dielectric spectrum of cement paste is mainly affected by counterion polarisation due to colloidal particles formed by cement grains that have not reacted. A Maxwell-Wagner effect is not very likely to occur, as can be seen from Figure 4.12. At the high-frequency end the dielectric spectrum will be affected by osmotic water binding. At  $t = 0$  a curve was observed slightly declining with increasing frequency.

It is reasonable to assume that the depolarisation factors,  $S_i$ , are approximately the same for cement paste as well as for soil. As long as ions do not form macroscopic bodies (clusters or crystals) there will be no  $E$ -field refractions and hence  $S = 1$  for the ions in the fluid. According to (2.42) the permittivity,  $\epsilon'$ , of the pore fluid can be found, from the weighted sum of  $\epsilon'$  of the different ions and that of the water. Therefore,  $\epsilon'$  of the solution in the pores should be lower than that of pure water. The cement grains not reacted yet will adsorb water at their surfaces. This fraction of the water is comparable with the hygroscopically bound water content in soil as discussed in Section 2.6 where the relaxation frequency is low. For the frequency range shown in Figure 4.12  $\epsilon' < 5$ .  $\epsilon'$  of the concrete in this experiment was 17 at 10 MHz, while in later experiments (see for example Figure 4.15)  $\bar{\epsilon}' = 23$  was found. A mixture of coarse sand and pure water can reach  $\epsilon' \approx 27$ . This may be attributed to bound water.

**Middle period:** The process of water binding is most pronounced during the middle period, for which hydration products have dimensions and shapes like that of clay.

During the first part of the middle period the number of particles, with a double layer system rapidly increases. Charged particles exhibit counterion polarisation. As a consequence the real part of the permittivity will increase at the lower end of the dielectric spectrum. Due to the broad particle size distribution a large spread in relaxation frequencies is expected. Relaxation frequencies are inversely proportional to the square of the particle diameters. During the process of hydration, particle dimensions will increase. In addition, ion diffusion will be inhibited as bridges develop between particles and the impact of counterion polarisation decreases. Counterion polarisation is expected to show up in the beginning of the hydration process and fade away when some structure is built up.



Like counterion polarisation the Maxwell-Wagner effect will contribute to the lower end of the dielectric spectrum. As shown before it is a function of the degree of hydration. After some time, as colloidal polarisation fades away, the Maxwell-Wagner effect is expected to be dominant over counterion polarisation. The real part of  $\epsilon'$  reaches a maximum shortly after the peak in temperature. This point is supposed to be the transition point from the fluid phase to the solid one which occurs as a continuum. After this phase transition, the thickness of the solid layers will increase and the Maxwell-Wagner effect will decrease accordingly.

As described in Section 2.2 the relaxation frequency of bound water will be lower than that of free water depending on the binding forces. At the high-frequency end of the dielectric spectrum,  $\epsilon'$  will decrease. As shown in Figure 4.12 a sharp decrease  $\epsilon'$  for  $f > 100$  MHz and  $t > 12$  h takes place. Since bound water relaxation frequencies go down far below 100 MHz, they will be completely overruled by low-frequency effects. No distinction can be made between the amount of "hydrated" water and more loosely bound water that is still available for hydration. *The decrease in  $\epsilon'$  at  $f > 100$  MHz can be a measure of the total amount of bound water but not of the degree of hydration.*

**Late period:** During the late period the permittivity due to the Maxwell-Wagner effect as well as the electrical conductivity of the bulk concrete will decay slowly. This process will probably go on for years as long as the concrete is saturated with water. However, after removing the formwork the concrete will dry and due to lack of water the hydration process will stop and  $\epsilon'$  will be that of the solids-air mixture.

### Maxwell-Wagner effect versus compressive strength of concrete

#### Theory

During hydration concrete will develop compressive strength,  $f_{cs}$  (MPa). The degree of hydration,  $\alpha_h$ , is defined as the ratio of the amount of cement that has reacted and the total amount of cement initially dissolved.  $\alpha_h$  is a function of time,  $t$ , and depends on the water content,  $\omega_{wcc}$ , the mass ratio of water and cement. For a given concrete composition, a unique relationship exist between  $\alpha_h$  and  $f_{cs}$ . In Section 2.4, a texture parameter,  $K$ , was introduced that relates the Maxwell-Wagner effect to textural soil properties. It will be shown that for concrete  $K$  is also related to  $\alpha_h$ , and therefore to  $f_{cs}$ . The Maxwell-Wagner effect takes place in regions of the concrete where a series connection of impedances of water and solids can be found. These are the regions that one passes going from one electrode (plate) to the other. It will affect the lower end of the dielectric spectrum.

Let us consider an average cell of cement paste between two plates analogous to Figure 2.7. It consists of a layer of water with a thickness equal to the average thickness of all water layers between the plates and a layer of solids equal to the average thickness of all solid layers. Initially the average thickness of the water layers,  $\bar{d}_w$ , between the two plates is large and the average thickness of the solid layers,  $\bar{d}_s$ , small:  $\bar{d}_s$  will increase as hydration continues. At the end of the hydration process  $\bar{d}_w \ll \bar{d}_s$ . The average cross section where the Maxwell-Wagner effect takes place is  $\bar{A}$ . This is the area of the capacitor plates of the average cell. In the beginning there are only a few regions to be considered for the Maxwell Wagner effect.  $\bar{A}$  of the average cell starts small and grows to equal the area of the electrode plates. The thickness of the cell is  $d = \bar{d}_w + \bar{d}_s$  and the average volume  $\bar{V} = d\bar{A}$ . As time





passes the volume fraction of water,  $\bar{v}_w$ , available for hydration decreases while the volume fraction of solids

$$\bar{v}_s = \frac{\bar{d}_s}{d} = 1 - \bar{v}_w \quad (4.23)$$

(hydration products) increases. Assume  $\bar{v}_s$  to include both the non hydrated cement and the hydrated cement including the water that was involved in the hydration process. The average volume fraction of the water in the cell,  $\bar{v}_w$ , includes all the water available for hydration in the regions mentioned. Most of the water has been bound to some extent during the first 30 h, but part of this bound water is still available for hydration. The ratio between the average volume of the cell and the average volume of the solid layers is related to the texture parameter  $K$ , as described in Section 2.4 by

$$K = \frac{d}{\bar{d}_s} = \frac{1}{1 - \bar{v}_w} \quad (4.24)$$

According to Reinhardt [1985] the volume fraction of water available for hydration is

$$v_w = \frac{\omega_{wce} - 0.4\alpha_h}{\rho_w/\rho_{ce} + \omega_{wce}} \quad (4.25)$$

where  $\alpha_h$  is the degree of hydration. Let  $v_w = \bar{v}_w$ , the chemical shrink be negligible and total volume of the hydrating cement-water mixture be constant. Then the texture parameter  $K$  can be found from (4.24) and (4.25)

$$K = \frac{\rho_w + \omega_{wce}\rho_{ce}}{\rho_w + 0.4\alpha_h\rho_{ce}} \quad (4.26)$$

$K$  is a function of  $\alpha_h$  and thus of the compressive strength  $f_{cs}$ . Note that  $K > 1$  since  $\alpha_h < 1$ . As explained in Section 2.4 the Maxwell-Wagner effect can be described by a single Debye relaxation function with  $K$  as a parameter.

The foregoing was based on the simplified model of (4.25) which is amenable to discussion. Another complicating factor is the impact of bound water on the dielectric behaviour of concrete. Furthermore, there are some uncertainties in the model of the Maxwell-Wagner effect as discussed in Section 2.4. It is therefore difficult to derive a theoretical expression that relates the measured  $\epsilon'$  to  $f_{cs}$ . *Still, (4.26) shows that the degree of hydration of concrete,  $\alpha_h$ , and therefore its compressive strength,  $f_{cs}$ , is reflected in the Maxwell-Wagner effect and thus in the measured permittivity,  $\epsilon'$ .*

### Experiment

Experimentally, a direct relationship between  $\epsilon'$  and  $f_{cs}$  was derived by Hilhorst *et al.* [1996] and Breugel *et al.* [1996]. For this research nine concrete samples were taken from a commercial concrete mixing plant. These samples varied in water-cement ratios ( $\omega_{wce} = 0.45, 0.50$  and  $0.55$ ) and cement types (CEM III/B 42.5 LH HS, CEM I 32.5 R, CEM I 42.5 R). Betomix 400, a plasticiser, was added to some samples. Pressing of test cubes was used to measure the compressive strength,  $f_{cs}$ , during hardening.





A dielectric sensor as described in Chapter 3, was used to follow  $\epsilon'$  at 20 MHz. Two stainless steel electrodes (3 cm long, 1 cm in diameter and spaced 2 cm), embedded in the concrete were connected to an integrated circuit, containing all high-frequency analogue and digital electronics. The sensor was calibrated using known dielectrics.

With (2.65) and (4.26) in mind, the compressive strength  $f_{cs}$  was derived from  $\epsilon'$  using the empirical expression

$$f_{cs} = \kappa_1 \left( \frac{\epsilon'_{\max}}{\epsilon'(t)} - \kappa_2 \right) \quad (4.27)$$

where  $\epsilon'_{\max}$  is the maximum permittivity developed as a function of elapsed time  $t$ ,  $\kappa_1$  is a scaling constant (MPa),  $\kappa_2$  a dimensionless offset. (4.27) is only valid after  $\epsilon'_{\max}$  has appeared. The best fit was found for  $\kappa_1 = 53$  MPa and  $\kappa_2 = 0.78$ .

Figure 4.13 shows an example of the promising fit between the calculated and measured strength values for one of the concrete samples. Expression (4.27) is a function of the ratio between values measured with the same electronics and therefore relatively insensitive to composition, electrode dimensions and stones in between them. For the nine samples used in this experiment (4.27) was universally applicable, suggesting that it applies to other concrete types as well.  $\epsilon'$  was corrected for temperature by  $-0.5 \text{ \% } ^\circ\text{C}^{-1}$  and  $\sigma_b$  by  $2 \text{ \% } ^\circ\text{C}^{-1}$ . This temperature correction was an approximate estimate, based on that of water. Note that for all nine concrete types according to (4.27)  $f_{cs} = 11.7$  MPa for  $\epsilon'_{\max}$ .

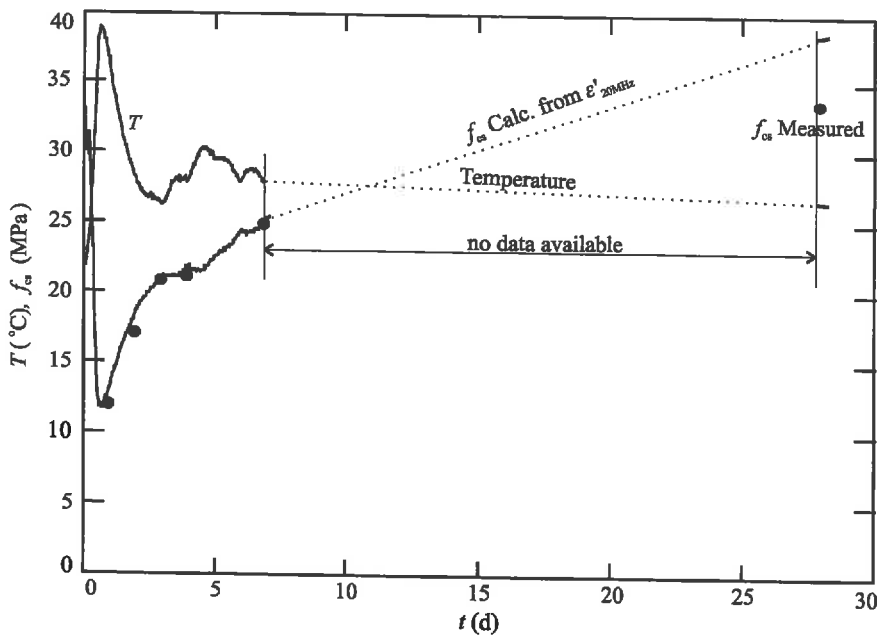


Figure 4.13. An example of the compressive strength,  $f_{cs}$ , as a function of time,  $t$ , for hardening concrete. The dots are the strengths measured using standard techniques. Note how a change in the concrete temperature,  $T$ , is reflected in the development of measured  $f_{cs}$  and how closely this is followed by the strength calculated from  $\epsilon'_{20 \text{ MHz}}$  according to (4.27). The cement is CEM I 42.5 R with  $\omega_{wcc} = 0.5$ .



Errors between measured and calculated  $f_{cs}$  for the nine samples are given in Figure 4.14. The average error was 0.5 MPa and the standard deviation 2.2 MPa. The maximum difference between the measured and the calculated strength values was  $\pm 6$  MPa, which is close to the accuracy of customary methods. According to Van Beek [1996] the accuracy of a compression-testing machine for example is about  $\pm 8$  %. This comes on top of the spread caused by differences in the test samples.

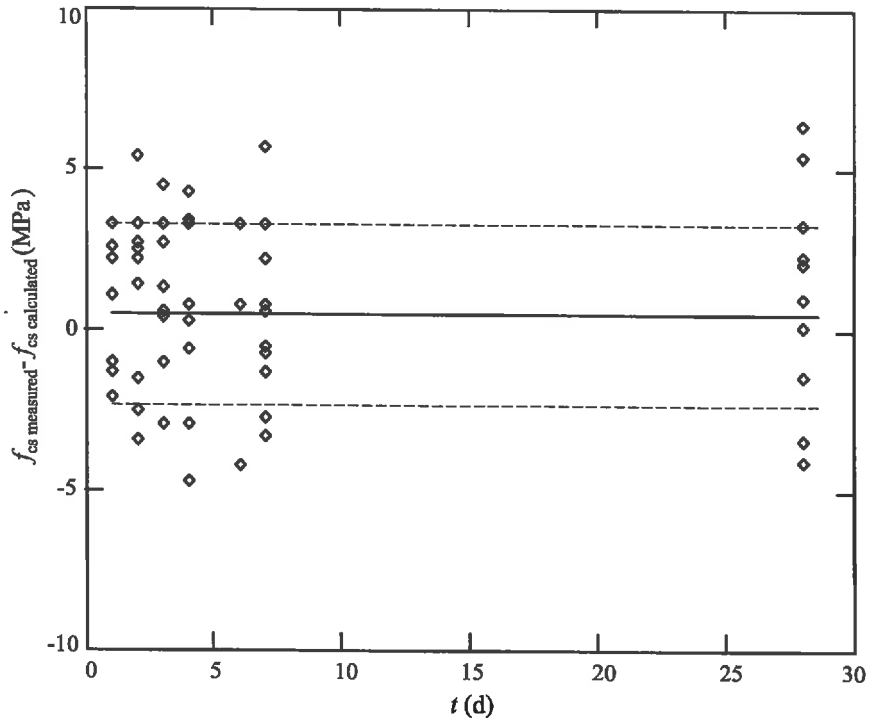
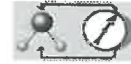


Figure 4.14. The difference between measured compressive strength,  $f_{cs}$ , and the strength calculated from  $\epsilon'$  at 20 MHz according to (4.27) with  $k_1 = 53$  MPa and  $k_2 = 0.78$  ( $\diamond$ ) as a function of time,  $t$ , for nine concrete samples of different compositions. The solid line is the average error and the dashed line the standard deviation. These concrete samples varied in water-cement ratios (0.45, 0.50 and 0.55) and cement types (CEM III/B 42.5 LH HS, CEM I 32.5 R, CEM I 42.5 R). A plasticiser, was added to some samples.

### **An overview of dielectric phenomena observed during the hydration process of concrete**

Apart from the existence of the relationship between the compressive strength of concrete and the Maxwell-Wagner effect, a number of other phenomena can be observed. These phenomena were reproducible for all nine concrete samples and can therefore be regarded as characteristic events during hydration. I will report on these phenomena briefly. The main purpose is to show the existence of a relationship between changes in the dielectric properties of concrete and changes in its microstructural and compositional properties. Although less clear to visualise the same effects may be expected for soils of different textures, bound water contents and ion concentrations.



The phenomena indicated above were derived from measurements using the dielectric sensor as described in Section 3 working at 10 MHz, 20 MHz and 30 MHz. See as an example of one of the nine concrete types the plots shown in Figure 4.15. It shows the real part of the permittivity,  $\epsilon'$ , of cement type CEM III/b 42.5 with  $\omega_{wce} = 0.50$  as a function of time, at the three frequencies involved.  $f_{MW r}$  is calculated using  $\epsilon'_{10 \text{ MHz}}$ ,  $\epsilon'_{20 \text{ MHz}}$  and  $\epsilon'_{30 \text{ MHz}}$  according to the three-frequency method described in Section 2.4. Note that even an error of less than 1 on the permittivity measurements, for instance due to noise, can lead to a substantial error in the calculation of  $f_{MW r}$ , especially if the difference between the readings for the different frequencies is small.

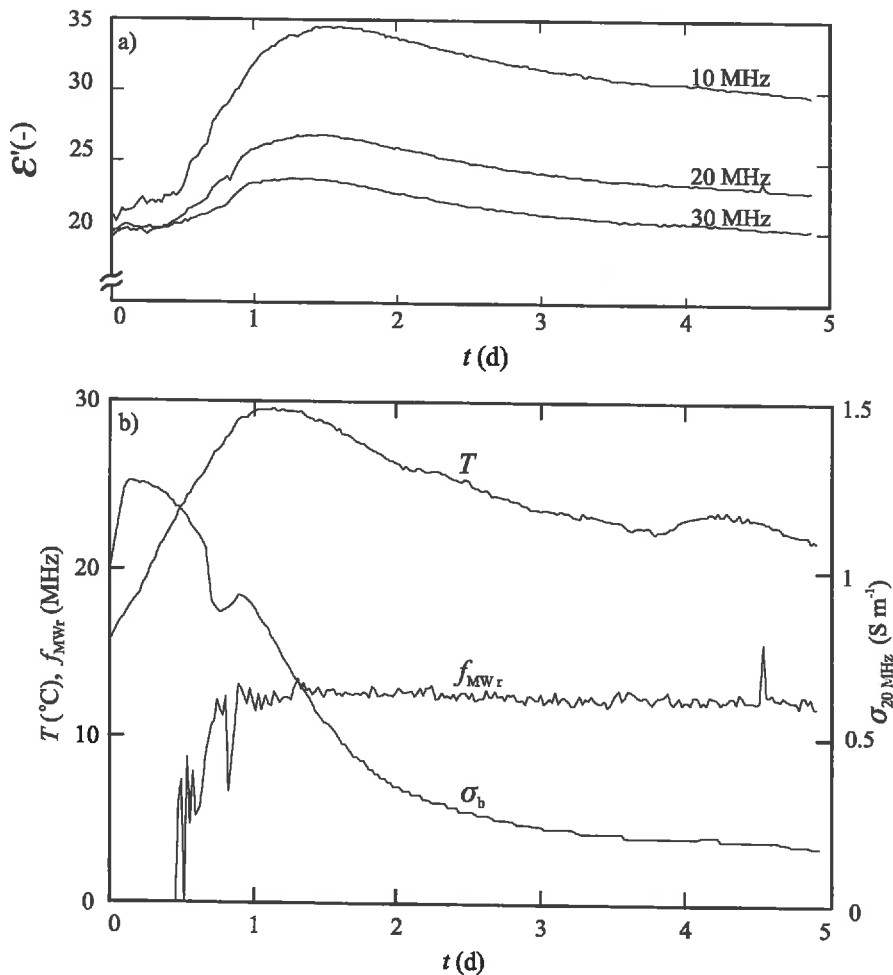


Figure 4.15. Dielectric phenomena observed for hardening cement of type CEM III/b 42.5 with a water-cement fraction  $\omega_{ce} = 0.50$  as a function of time:

- a) the real part of the permittivity,  $\epsilon'_{10 \text{ MHz}}$ ,  $\epsilon'_{20 \text{ MHz}}$  and  $\epsilon'_{30 \text{ MHz}}$ ,
- b) the temperature,  $T$ , the electrical conductivity of the bulk concrete,  $\sigma_b$ , at 20 MHz and the Maxwell-Wagner relaxation frequency  $f_{MW r}$ .



$\epsilon'$  was corrected for temperature by  $-0.5 \% \text{ } ^\circ\text{C}^{-1}$  and  $\sigma_b$  by  $2.5 \% \text{ } ^\circ\text{C}^{-1}$ . The temperature,  $T$ , of the concrete was measured using a sensor located closely to the region where the permittivity was measured.

During the early period the real part of the  $\epsilon'$  does not change much. Counterion polarisation is dominant over the Maxwell-Wagner relaxation. Both are small. Still an increase is observable, which is more pronounced for 10 MHz than for 30 MHz. At this stage, however,  $f_{\text{MW}\tau}$  cannot be calculated since the difference in  $\epsilon'$  at different frequencies is too small.

After the maximum in temperature,  $T_{\text{max}}$ , the Maxwell-Wagner relaxation frequency  $f_{\text{MW}\tau} \approx 12.4$  MHz.  $f_{\text{MW}\tau}$  was calculated according to (2.32) and for all nine concrete samples about constant with time. Since ion conduction is the only variable in (2.27), this implies a constant ionic conductivity and hence a constant ion concentration in the pore water during the late period, which is consistent with Slegers *et al.* [1977]. The maximum in permittivity,  $\epsilon_{\text{max}}$ , appears always after  $T_{\text{max}}$ . The higher the frequency, the closer  $\epsilon_{\text{max}}$  to  $T_{\text{max}}$ .

The measured electrical conductivity of the bulk concrete,  $\sigma_b$ , includes both ion conduction and dielectric losses. At the beginning of the early period, not much difference was measured for  $\sigma_b$  at 10 MHz, 20 MHz and 30 MHz. Because the curves spread only slightly during the late period, only  $\sigma_b$  at 20 MHz will be considered hereafter.  $\sigma_b$  showed some characteristic changes. It increased rapidly at the beginning of the early period. This is due to an increase in the ion concentration since no real change can be observed for  $\epsilon'$ . At the end of the early period  $\sigma_b$  goes down again due to the formation of solids.

At the beginning of the middle period a sharp decrease for  $\sigma_b$  can be observed. Again this is only explainable by a change in the ion concentration. If it was a dielectric phenomenon this effect should be accompanied by a noticeable change in  $\epsilon'$ . Suddenly the drop in  $\sigma_b$  is over and a small increase can be observed, probably due to the rise in temperature of the cement paste. This effect coincides approximately with the point from where  $f_{\text{MW}\tau}$  can be calculated. For some cement types this behaviour was more pronounced than for others. However, they all showed a similar behaviour for the same period of the hydration process. Finally, at the end of the middle period,  $\sigma_b$  decreased in a regular manner.

## Conclusions

The dielectric behaviour of hydrating concrete can be used to illustrate the dielectric behaviour of soil. During hydration concrete shows some characteristic events for the complex permittivity that are related to changes in microstructural and compositional properties of the material. In this way concrete simulates the dielectric behaviour of soil as function of texture, ion concentration and bound water.

*A direct relationship was found between the Maxwell-Wagner effect and the microstructural properties of concrete or porous materials in general.*

*After about 30 hours most water is bound to some extent and consequently shows a low relaxation frequency. It is not possible to distinguish between bound water that is or is not available for hydration. Frequencies higher than 100 MHz cannot be used to monitor compressive strength. The compressive strength is related to the Maxwell-Wagner effect.*







## SUMMARY AND CONCLUSIONS

### *General*

In Chapter 1, it was stated that the dielectric measuring technique is mainly used for water content measurements of soil. Until now, the potentials of the dielectric sensing technology have not been fully explored, which was partly attributed to the complexity and incompleteness of the dielectric theory. Parts of the general theory on dielectrics that apply to soil are collected in Chapter 2. Some parts needed a more detailed study and some lacking parts were developed. Chapter 2 resulted in a theoretical model that can predict the dielectric behaviour of soil. Another problem is the availability of low-cost dielectric sensors suitable for use in agricultural practice. Chapter 3 describes a new dielectric sensor that guarantees the lowest possible cost in mass production and is easy to use.

The developed theory and sensor are applied to a number of applications. A general conclusion from this thesis is that the application of the dielectric sensing technology, apart from soil water content measurements, also facilitates the measurement of the electrical conductivity of the soil solution, the soil water pressure and the soil texture.

### *Influence of water binding on the dielectric properties of soil*

Lacking in the theory was the impact of binding forces on the dielectric properties of water in the soil matrix. Although not in detail, the effect of bound water on the permittivity of soil was already known from the literature. The relationship between (binding) forces acting on a water molecule and the dielectric relaxation frequency was known from the theory on aqueous dielectrics [Hasted, 1973; Grant, 1978]. From this, I related the matric pressure of soil water to its dielectric relaxation frequency. This relationship, given by (2.15), was made plausible using data found in the literature.

A relationship between the water retention properties of the soil and its dielectric properties implies that the hysteresis observed for the soil water retention characteristic should also apply to the dielectric spectrum. It also implies that the soil water retention characteristic can be found from measuring the dielectric spectrum of a saturated soil.

A relative sharp transition for the activation enthalpy as a function of matric pressure appeared around  $-100$  MPa, being the matric pressure under average room conditions. It corresponds with the matric pressure at which a monolayer of water molecules at the surface of the soil particles can exist. The water content at this matric pressure corresponds with the commonly used concept of hygroscopic water content.

### *Polarisable electric double layers around colloids and air bubbles*

The electric double layer around a colloidal particle is polarisable. This effect is often referred to as counterion diffusion polarisation or colloidal polarisation. It contributes to the permittivity of soil, especially for clay. It is difficult to distinguish this type of polarisation from other dielectric phenomena. In Section 2.2, it was hypothesised that for soil this effect will be smeared out over a





wide frequency range. The resulting contribution of colloidal polarisation to the permittivity of soil at a single frequency is negligible.

Soil is a mixture of solids, water and air. Air bubbles in soil, appearing between middle water contents and saturation, will exhibit an electric double layer. It was hypothesised that counterion diffusion polarisation should also apply to these air bubbles. However, no literature was found on the subject. From colloid chemistry, it is known that modelling counterion diffusion polarisation can be quite complicated. Such a treatment is beyond the scope of this thesis. The hypothesis of polarisable air bubbles was treated briefly, but has not been included in the final model.

#### *Maxwell-Wagner effect and soil texture*

Apart from the fact that the Maxwell-Wagner effect "should play a role", little was known of its impact on the dielectric properties of soil. This effect has already been known for a long time from other disciplines in dielectric material research. Some researchers describe this effect as a polarisation phenomenon. After analysing this effect for soil, it should be handled, in my opinion, as a macroscopic phenomenon resulting from the electronic network theory. The introduction of a texture parameter linked the Maxwell-Wagner effect to the dielectric properties of soil. This texture parameter can relate the Maxwell-Wagner effect to the ratio of the average thickness of the water layers and that of both the air and the mineral particles in the matrix. The Maxwell-Wagner effect was described in the form of a normalised Debye function (2.29). Three parameters constitute this special Debye function:

- the relaxation frequency, which is related only to the electrical conductivity and the permittivity of the soil solution;
- the permittivity at very high frequencies as compared with the relaxation frequency, which equals the permittivity of the material without Maxwell-Wagner effect; and
- the increase in permittivity for very low frequencies as compared with the relaxation frequency, which is a function of the solids, the air in the soil and the soil porosity only.

Equations ((2.32), (2.33) and (2.34)) were given to calculate these parameters from permittivity measurements at three frequencies.

#### *New dielectric mixing equation based on depolarisation factors*

The permittivity as measured in the bulk soil comprises the impact of the permittivities of the individual soil constituents. To predict the permittivity of soil, a long list of published dielectric mixture equations is available. However, in my opinion none of these equations is adequately applicable to soil. A new mixture equation (2.42) was developed that includes depolarisation factors to account for electric field refractions at the permittivity transitions between soil constituents. The depolarisation factors are functions of physical soil parameters. Most other mixing equations contain one or more empirical factors, which have no physical meaning. The concept of the depolarisation factor is comparable to that of the "shape factor" of particles described by e.g. De Loor [1956]. A special case of the new mixture equation, for which the depolarisation factors equals 1 (no depolarisations), appeared equal to a mixture equation for fluids derived from using thermodynamics. This equation was already published in 1895 and seems to be forgotten. Published in 1897, and probably also forgotten, are the results of a critical examination of the "refractive index model" for fluids. At the time, this model was found inadequate for deriving the dielectric constants of the different components of a fluid. I



concluded that the refractive index model is confusing. It can lead to erroneous results when used for analysing the microscopic dielectric properties of a soil.

The new mixture equation holds for the static case. Chemical interactions between the soil constituents, however, can affect the electrical permittivity and the dielectric spectrum. For the clarity of this treatment, I assumed that such chemical interactions are not present.

#### *Model to predict the dielectric behaviour of soil as a function of frequency*

The different dielectric phenomena resulted in model (2.61) which can predict permittivity of soil as a function of frequency. The input parameters of the soil are the porosity and the water retention characteristic (water content versus matric pressure). A simplified version, (2.60), uses the soil water content, porosity and the hygroscopic water content. This version was used in a number of applications in Chapter 4. Using De Loor's [1956] theory, I expected that it should be possible to calculate the depolarisation factors from the shape, dimensions and density of the soil constituents. However, for this thesis I used a more experimental-oriented approach. The depolarisation factors could be deduced from some extreme cases of the dielectric behaviour of glass beads. These values were applied to soil, although for soil they may differ due to differing shape and surface conditions of the soil particles. In fact, there is no universal depolarisation factor. The model and its simplified version were tested using data found in literature. The water retention curves were estimated. The results agreed reasonably well with the expectations. Finally, the Maxwell-Wagner effect was included in the model. However, the latter could not be tested since insufficient data were available.

#### *A new sensor for dielectric soil characterisation*

A general model was introduced which is valid for both Frequency-Domain (FD) and Time Domain Reflectometry (TDR) sensors showing their conformity. The introduction of an Application Specific Integrated Circuit (ASIC) enables the lowest possible cost for sensors in mass production and paves the way for many new applications. The design of this ASIC (Section 3.2) was based on the principle of synchronous detection. Possible error sources were investigated and a special developed algorithm appeared to be able to cope with the required high phase accuracy. The algorithm is able to determine and to correct for the main error sources in the measuring system. The circuit, constructed as a four-input vector voltmeter, is not bound to a particular application, and can operate at one or more fixed frequencies. Different applications require different electrode configurations of different electrical length. Whatever shape these electrodes have, the electrical length should be compensated (Section 3.3). The electrical length of the electrodes can be modelled like a transmission line. This involves complex mathematical operations, which can be done on a personal computer, but cannot always be implemented in a simple micro-controller. Therefore, a simple approximation was proposed that proved sufficiently accurate for most applications. With both the electrical length correction and the ASIC, a new FD sensor was developed, operating at a fixed frequency of 20 MHz (Section 3.4). The output of the sensor was calibrated using known dielectrics and showed sufficiently accurate. The sensor can measure the real part of the permittivity for dielectrics with an electrical conductivity of up to about  $0.2 \text{ S m}^{-1}$ .

#### *Applications of dielectric measuring technique*

In Chapter 4, the potentials of the dielectric measuring technique for characterisation of soil were shown. The new FD sensor and TDR were applied to different measuring problems for a



variety of soils. A comparison was made between the values measured with the new FD sensor (at 20 MHz), with TDR (about 150 MHz) and the values predicted using the simplified model (2.60) of Chapter 2. The output of these sensors correlated with soil parameters such as water content, texture and the electrical conductivity of the extracted soil solution. Also the detection of possibly polluted soil layers was demonstrated. Finally, the dielectric properties as a function of soil texture were simulated by means of hardening concrete.

#### *Sensitivity of TDR readings for electrical conductivity*

The TDR readings were shown to be affected by the electrical conductivity for which it should be corrected. The existing relationship between reflection time and permittivity was based on the application of a sine wave, assuming conduction to be negligible. However, this relationship should be based on the application of a step function in the time domain. Such an equation is not available; therefore, an adequate correction is not yet possible. In this thesis, TDR measurements were not corrected.

#### *Dielectric soil water content measurements compared with predicted values*

Comparing the data predicted with the new model and those measured by TDR resulted in a reasonable correlation for all soils at water contents below 0.30. For soils of low specific surface areas, such as sand, the correlation also holds for higher water contents. Since dielectric soil properties are frequency-dependent, the best comparison was found for sand. Water content calibration curves for sand measured with both FD and TDR were almost equal (Figure 4.3). The predictability of the model was high, confirming the theoretical expectation that the dielectric spectrum of sand is flat between 20 MHz and 150 MHz.

For high water contents and a high specific surface area the deviation with predicted values increased. This was attributed to the Maxwell-Wagner effect. The deviations also supported the air bubbles hypothesis posed in Section 2.3. For an average soil the new model was found more accurate as a predictor than Topp's [1980] calibration curve, because this new model can cope with the porosity and the bound water content of the soil. However, in most applications the porosity and hygroscopic water content can only be roughly estimated and the impact of the Maxwell-Wagner effect and the air bubbles will be unknown. It was concluded that for absolute water content measurements both the FD and the TDR methods should be calibrated. No universal calibration curve exists. The calibration curves for the FD sensor indicated that the need for calibration is generally higher for the FD sensor (at 20 MHz) than for TDR (150 MHz). The need for calibration becomes smaller for higher frequencies and comparable with that of TDR at 150 MHz. However, for relative readings the reproducibility of both methods was high. They can be used effectively to maintain e.g. a set point for irrigation control. For such cases, calibration is not required.

The depolarisation factor found for glass spheres might be too high for some soils. This was hypothesised as due to the surface condition and shape of the soil particles. To obtain the highest possible predictability, the depolarisation factor should be determined for the soil under investigation.

#### *In situ measurement of the electrical conductivity of the extracted soil solution*

Prompted by the publication of Malicki *et al.* [1994], a hypothetical relationship was proposed between electrical conductivity of the extracted soil solution and that of the bulk soil. This



relationship is analogous to that between the permittivity of water and that of the bulk soil (Chapter 2). For a variety of soils, the linear relationship between electrical permittivity and conductivity of the bulk soil confirmed the hypothesis. A method was developed to determine the electrical conductivity of the extracted soil solution by simultaneous measurements of the electrical permittivity and conductivity of the bulk soil. This method is accurate for glass beads and appeared to be promising for a variety of soils tested.

#### *Maxwell-Wagner effect versus electrical conductivity and soil texture*

Section 2.2 concentrated on the impact of the Maxwell-Wagner effect on the real part of the permittivity. It was not considered whether and how it applies to electrical conductivity. In Section 4.2, it was shown that a relationship exist between the electrical conductivity of the soil solution and that of the bulk soil, analogous to that for the permittivity. In Section 4.3 it was shown that the Maxwell-Wagner effect is applicable to the electrical conductivity as well. Low-frequency conductivity measurements are affected by the Maxwell-Wagner effect, while high-frequency conductivity measurements are affected by water binding. The situation is opposite to that for the measurement of the permittivity.

Using the three-frequency measuring method described in Section 2.2, the Maxwell-Wagner effect was characterised for three soil types. Results were given (Table 4.5), measured with the new FD sensor at 20 MHz, but also at 10 MHz and 30 MHz. The conductivity for frequencies higher than the Maxwell-Wagner relaxation could be determined. The conductivity increment increased with the specific surface area of the soil. The low-frequency values calculated from the conductivities at the three frequencies were equal to the electrical conductivity measured by TDR. Thus, a TDR electrical conductivity measurement is a low-frequency measurement.

From the foregoing it follows that the Maxwell-Wagner effect can be characterised using electrical conductivity instead of permittivity. At lower frequencies, soil electrical conductivity can be measured more accurately than permittivity. For common soils and at low frequencies, electric currents due to conductance are higher (or can be made higher) than electric currents due to capacitance. Consequently, phase errors have smaller effects on conductivity than on permittivity measurements, enabling a more accurate characterisation of the Maxwell-Wagner effect and consequently of the texture parameter.

#### *Detecting polluted soil layers*

Polluted soil layers can be detected by simultaneously measured electrical permittivity and conductivity of the bulk soil. A pollution indicator was proposed based on the ratio between the derivative of electrical permittivity as a function of soil depth and that of conductivity. The addition of offsets to permittivity and conductivity resulted in a sensitive pollution indicator.

#### *Hardening concrete used to simulate the dielectric properties of differently textured soil*

An analogy was shown between the textural properties of concrete and that of soil. During hydration, the textural properties of concrete are continuously changing from sand-like and clay-like to porous rock-like. This allows to simulate the dielectric behaviour of soils of different textures.

A relationship exists between the Maxwell-Wagner effect and the microstructural properties of concrete or porous materials in general. An overview of the dielectric



phenomena observed during the hydration process of concrete showed a clear relationship between a number of changes in the dielectric properties of concrete and changes in its microstructural and compositional properties. The effect of water binding could partly be illustrated using the change in dielectric properties of hydrating concrete at high frequencies. The concept of a texture parameter showed the possibility of predicting the strength of concrete. There appeared a strong relationship between electrical permittivity and compressive strength at about 20 MHz ((4.26) and (4.27)). The dielectric properties of concrete showed hardly any change around 100 MHz. This also applies to soil, confirming the general knowledge on this point.

### **Recommendations for further research**

#### *A multidisciplinary approach is desirable for dielectric sensor development*

The application of dielectric soil properties to the development of dielectric sensors often involves a number of scientific disciplines such as electronics engineering, thermodynamics, chemistry and of course soil and horticultural sciences. The frequency band involved ranges roughly between 10 kHz and 10 GHz. Testing dielectric soils properties in such a wide frequency range requires specialised instrumentation and skilled operators. There is no general approach in applying the dielectric measuring technique to soil characterisation. Therefore, synergy between disciplines is essential for adequate problem solving.

As an example, TDR can be considered a special case of Time Domain Spectroscopy (TDS). The use of TDR for water content measurements was adopted widely in the eighties, while in other disciplines TDS was already in use in 1951 (Section 1.2).

Another example is the measurement of the electrical conductivity of soil by TDR: this method was reduced to just a series connection of two resistors and a battery (Section 4.3). A specialist in transmission lines would have recognised this reduction immediately, which might have simplified electrical conductivity measurements in soil by TDR considerably.

#### *In situ dielectric measurement of soil water retention characteristics*

The relationship between the water retention characteristic of a soil and its dielectric relaxation frequency was made plausible (Section 2.2). This suggests that the soil water retention characteristic can be derived from the dielectric spectrum of a saturated soil. Routine dielectric spectra determinations can be done in less than 15 minutes, which is significantly faster than e.g. the time consuming pressure plate determinations, which can take month. In addition, this method is suitable for in situ measurements. An experiment is required for full validation of this technique. A rigid proof requires the measurement of dielectric spectra roughly between 1 GHz and 20 GHz for a number of soils with different water retention characteristics and electrical conductivities. An experimental setup should be developed for making routine measurements of these spectra. Instrumentation for this purpose, such as network analysers, are commercially available. The problem is that they require skilled operators and are costly. I expect that a specifically designed dielectric instrument for determining soil water retention characteristics, working at a number of predefined frequencies, is more cost-effective and operationally attractive.





#### *In situ soil texture determination*

The soil texture parameter, introduced in Chapter 2, is related to the dielectric properties of soil. This parameter makes it possible to describe the Maxwell-Wagner effect in terms of the average thickness of water layers and the average thickness of the solids and air layers in the matrix. This parameter could be used for in situ dielectric classification of soil. In this context, it is recommended to study in more detail the relationship between the soil texture parameter and other physical soil properties such as specific surface area, porosity and water content.

#### *Towards a universal calibration equation*

Work on a universal calibration equation is a challenge not only for all dielectric water content sensors; it will be applicable to other materials as well. From this thesis two ways can be deduced for finding a universal calibration equation.

Firstly, the permittivity at low frequencies is affected by the Maxwell-Wagner effect, whereas water binding affects the permittivity at high frequencies. The Maxwell-Wagner effect can be characterised from electrical permittivity or conductivity measurements at three frequencies (Section 4.3). Bound water hardly affects the high-frequency permittivity and conductivity values calculated from the Maxwell-Wagner effect. Thus, it should be possible to deduct permittivity and conductivity values that are affected mainly by water content and porosity, i.e. to obtain a truly universal calibration equation.

Secondly, the permittivity for which the ionic conductivity is zero as used in (4.14) of Section 4.2 constitutes of a part only depending on the air and solids fraction and a part accounting for the Maxwell-Wagner. The latter can be found after registering two or three measurements. Knowing this factor the measured permittivity data can be corrected for the Maxwell-Wagner. This procedure could lead to a standard calibration curve according to (2.61) for all soils.

#### *The new FD sensor at 100 MHz*

The electrical length compensation proposed for the new FD sensor is valid only under certain assumptions (Section 3.3). One of these assumptions is that the frequency should not be too high. At 30 MHz the sensor proved to work reliably. Preliminary tests showed, however, that this electrical length compensation method can not be used at frequencies higher than 50 MHz. At these frequencies, one should use other methods, e.g. measuring standing wave, reflection coefficients or relative phase shifts. Development of such methods would increase the applicability of the new FD sensor considerably.

#### *Temperature dependence of electrical permittivity of bulk soil*

The ambient temperature was assumed to be around 20 °C, in the theoretical part (Chapter 2) as well as in the experiments part (Chapter 4). At first thought, one expects the temperature dependence of the real part of the electrical permittivity mainly due to that of water. Experimentally, positive and negative temperature coefficients were found depending on soil type. The ambient temperature of a greenhouse can range from 10 °C to over 40 °C. The temperature variation of the top soil in an open growth system is even larger. One should be able to correct dielectric measurements for temperature. At present, it is not clear how to correct for temperature. It will be interesting to incorporate temperature dependency in the models developed in this thesis and subsequently compare the outcome with experimental data.







## SAMENVATTING EN CONCLUSIES

### *Algemeen*

In Hoofdstuk 1 is vastgesteld dat de diëlektrische meettechniek tot nu toe voornamelijk is toegepast voor het meten van het watergehalte van de bodem. De potentiële mogelijkheden van deze techniek zijn echter niet volledig benut. Enerzijds kan dit worden toegeschreven aan de onvolledigheid en de complexiteit van de diëlektriciteitstheorie. Delen van de algemene theorie over diëlektriciteit, voorzover van toepassing op de bodem, zijn verzameld in Hoofdstuk 2. Sommige delen vereisten een gedetailleerde studie en ontbrekende delen zijn ontwikkeld. Dit hoofdstuk resulteert in een theoretisch model dat het diëlektrisch gedrag van de bodem kan voorspellen. Anderzijds is er een gebrek aan goedkope diëlektrische sensoren gesignaleerd die geschikt zijn voor de landbouwpraktijk. In Hoofdstuk 3 is een nieuwe sensor beschreven die de laagst mogelijke prijs in massaproductie garandeert en eenvoudig is te gebruiken. De ontwikkelde theorie en de sensortechniek zijn toegepast op een aantal meetproblemen. Een algemene conclusie uit dit proefschrift is, dat de diëlektrische meettechniek ook de meting van de elektrische geleidbaarheid van het poriënwater, de matrixdruk en de textuur van de bodem, kan vergemakkelijken.

### *Invloed van waterbinding op de diëlektrische eigenschappen van bodem*

Onbekend was de impact van bindingskrachten van het water in de bodemmatrix op de diëlektrische eigenschappen van de bodem. Hoewel niet gedetailleerd, was het effect van gebonden water op de permittiviteit van de bodem reeds bekend uit de literatuur. De relatie tussen de (bindings-) krachten op een watermolecuul en de diëlektrische relaxatiefrequentie van dat molecuul was bekend uit de theorie over waterhoudende-dielectrica [Hasted, 1973; Grant, 1978]. Daarmee is de matrixcomponent van de waterdruk van het bodemwater aan de diëlektrische relaxatiefrequentie gerelateerd. Deze relatie, die beschreven is met vergelijking (2.15), is aannemelijk gemaakt met behulp van literatuurgegevens.

Een relatie tussen de waterretentiekarakteristiek en de diëlektrische eigenschappen daarvan houden in dat de hysteresis die kan worden waargenomen voor deze karakteristiek ook voor het diëlektrisch spectrum zou moeten gelden. Voorts houdt die relatie in dat de waterretentiekarakteristiek kan worden gevonden uit een meting van het diëlektrisch spectrum van een verzadigde bodem.

De activeringsenergie als functie van de matrixcomponent van de waterdruk, blijkt een relatief scherpe overgang te vertonen rond een matrixdruk van  $-100$  MPa. Dit is de druk onder gemiddelde kamercondities. Het correspondeert met de matrixcomponent van de waterdruk waarbij nog een monomoleculaire waterlaag op het oppervlak van de bodemdeeltjes kan bestaan. Het bijbehorende watergehalte komt overeen met het algemeen gebruikte concept van het hygroscopisch watergehalte.

### *Polariseerbare elektrische dubbellen rond colloïde deeltjes en luchtbelletjes*

De elektrische dubbellaag rond een colloïde is polariseerbaar. Dit effect wordt veelal aangeduid met "counterion diffusion polarisation" of "colloidal polarisation". Het draagt bij



tot de permittiviteit van de bodem, vooral voor klei. Dit type polarisatie is moeilijk te onderscheiden van andere diëlektrische fenomenen. In Sectie 2.2 is verondersteld dat dit effect voor de bodem verdeeld is over een breed frequentiegebied. De bijdrage van colloïdale-polarisatie tot de permittiviteit van de bodem is dan voor één frequentie verwaarloosbaar.

Bodem is een mengsel van vaste deeltjes, water en lucht. Luchtbelletjes vertonen een elektrische dubbellaag en komen voor tussen een halfnatte en een verzadigde bodem. Verondersteld is dat "counterion diffusion polarisation" ook van toepassing zou moeten zijn op luchtbelletjes, er kon echter geen literatuur over deze hypothese worden gevonden. Uit de colloïdchemie is het bekend dat een model voor "counterion diffusion polarisation" zeer gecompliceerd kan zijn. Een dergelijke behandeling valt buiten het bestek van dit proefschrift. De hypothese over luchtbelletjes is kort behandeld, maar is niet in het model opgenomen.

#### *Het Maxwell-Wagner effect en de textuur van de bodem*

Afgezien van het feit dat het Maxwell-Wagner effect "een rol zou moeten spelen ...", was er weinig bekend over de impact ervan op de diëlektrische eigenschappen van de bodem. Dit effect is echter al langer bekend uit ander disciplines van het diëlektrisch materialenonderzoek. Sommige onderzoekers beschrijven het als een polarisatiefenomeen. Na analyse van dit effect voor de bodem, moet het naar mijn mening behandeld worden als een macroscopisch fenomeen dat het resultaat is van de elektrische netwerktheorie. Het Maxwell-Wagner effect kon gekoppeld worden aan de diëlektrische eigenschappen van de bodem door middel van de introductie van een textuurparameter. Deze textuurparameter relateert het Maxwell-Wagner effect aan de verhouding van de gemiddelde dikte van de waterlaagjes en aan die van de minerale deeltjes en de lucht in de matrix. Het Maxwell-Wagner effect is beschreven in de vorm van een genormaliseerde Debye functie (2.29). Deze speciale Debye functie bestaat uit drie parameters:

- de relaxatiefrequentie, welke alleen gerelateerd is aan de elektrische geleidbaarheid en de permittiviteit van het bodemvocht;
- de permittiviteit voor zeer hoge frequenties ten opzichte van de relaxatiefrequentie, welke gelijk is aan de permittiviteit van het materiaal zonder Maxwell-Wagner effect;
- de toename van de permittiviteit voor zeer lage frequenties ten opzichte van de relaxatiefrequentie, welke alleen een functie is van de vaste deeltjes, de lucht in de bodem en de porositeit.

Vergelijkingen ((2.32), (2.33) and (2.34)) zijn gegeven om deze parameters te kunnen berekenen uit permittiviteitsmetingen bij drie frequenties.

#### *Een nieuwe diëlektrische mengvergelijking gebaseerd op depolarisatie factoren*

De gemeten permittiviteit van het bulkmateriaal van de bodem omvat de invloed van de permittiviteiten van de individuele bestanddelen. Om de permittiviteit van de bodem te kunnen voorspellen is er een lange lijst van mengvergelijkingen beschikbaar. Volgens mij is echter geen van deze vergelijkingen adequaat toepasbaar op de bodem. Een nieuwe mengvergelijking, die gebruik maakt van depolarisatiefactoren om het effect te verantwoorden van de breking van elektrische veldlijnen op de permittiviteitsovergangen tussen bodemdeeltjes is ontwikkeld. Deze depolarisatiefactoren zijn een functie van fysische



bodemparameters. De meeste andere mengvergelijkingen maken gebruik van een of meer empirische factoren, die geen fysische betekenis hebben. Het concept van depolarisatiefactoren is vergelijkbaar met de "vorm-factor" voor deeltjes zoals beschreven is door o.a. De Loor [1956]. Een speciaal geval van de nieuwe mengvergelijking, voor het geval de depolarisatiefactor 1 is (geen polarisatie), blijkt gelijk te zijn aan een in 1895 gepubliceerde mengvergelijking voor vloeistoffen en schijnt te zijn vergeten. Deze vergelijking is afgeleid door gebruik te maken van de thermodynamica. Waarschijnlijk ook vergeten zijn de in 1897 gepubliceerde resultaten van een kritisch beoordeling van het brekings-index-model voor vloeistoffen. In die tijd bleek dit model niet geschikt voor het afleiden van de diëlektrische constanten van de verschillende componenten van de vloeistof. Daarom is geconcludeerd dat het brekings-index-model verwarrend is en kan leiden tot foutieve resultaten indien gebruikt voor het analyseren van microscopisch diëlektrische eigenschappen van de bodem.

De nieuwe mengvergelijking gaat op voor een statische toestand. De chemische interactie tussen bodembestanddelen kan echter de elektrische permittiviteit en het diëlektrisch spectrum beïnvloeden. Om de behandeling zo duidelijk mogelijk te houden is aangenomen dat dit soort chemische interactie niet aanwezig is.

#### *Een model dat het diëlektrisch gedrag van de bodem kan voorspellen als functie van de frequentie*

De verschillende diëlektrische fenomenen resulteerden in model (2.60) waarmee de permittiviteit van de bodem kan worden voorspeld als functie van de frequentie. In dit model is het Maxwell-Wagner effect niet verwerkt. De gebruikte bodemparameters zijn de porositeit en de waterkarakteristiek (watergehalte versus de matrische component van de waterdruk). Een vereenvoudigde versie van model (2.60) maakt gebruik van het watergehalte, de porositeit en het hygroscopisch watergehalte van de bodem. In Hoofdstuk 4 is deze versie gebruikt in een aantal toepassingen. Gebaseerd op de theorie van De Loor [1956] verwacht ik dat het mogelijk moet zijn, de depolarisatiefactoren te berekenen aan de hand van de vorm, de afmetingen en de dichtheid van de bodembestanddelen. In dit proefschrift is echter een meer experimenteel-georiënteerde benadering gebruikt. De depolarisatiefactoren zijn afgeleid van enkele extreme gevallen van het diëlektrisch gedrag van glaskogeltjes. De gevonden waarden zijn toegepast op de bodem, hoewel zij kunnen afwijken door het verschil in vorm en oppervlaktecondities van de bodemdeeltjes. Eigenlijk is geen universele depolarisatiefactor mogelijk. Het model en de vereenvoudigde versie zijn getoetst aan de hand van uit de literatuur bekende gegevens. De resultaten kwamen overeen met de verwachting. Tot slot is het Maxwell-Wagner effect in het model gepast. Helaas kon dit laatste niet worden getest door een gebrek aan geschikte bodemgegevens.

#### *Een nieuwe sensor voor het diëlektrisch karakteriseren van de bodem*

Een algemeen model is geïntroduceerd (Sectie 3.1) dat geldig is voor zowel Frequency-Domain (FD) als Time Domain Reflectometry (TDR) sensoren. Het liet de overeenkomsten zien tussen de twee methoden. De introductie van een Application Specific Integrated Circuit (ASIC) maakt de massaproductie van sensoren mogelijk voor de laagst mogelijke prijs en maakt de weg vrij voor veel nieuwe toepassingen. Het ASIC



ontwerp (Sectie 3.2) is gebaseerd op het principe van synchrone detectie. Mogelijke foutbronnen zijn geïnventariseerd en een speciaal ontwikkeld algoritme bleek overweg te kunnen met de vereiste hoge fasenauwkeurigheid. Het algoritme kan de belangrijkste foutbronnen van het meetsysteem bepalen en corrigeren. Het circuit is geconstrueerd als een vector-voltmeter met vier inputs. Het is niet gebonden aan een bepaalde applicatie en kan werken op een of meerdere vaste frequenties. Iedere applicatie vraagt om een eigen elektrodenconfiguratie met bijbehorende elektrische weglengte. Welke vorm de elektroden ook hebben, voor de elektrische weglengte moet worden gecompenseerd (Sectie 3.3). Daartoe zijn complexe mathematische bewerkingen nodig die op een computer gedaan kunnen worden. Dit kan echter niet altijd worden verwezenlijkt in een simpele microcontroller. Daarom is een eenvoudige benadering voorgesteld, die voldoende nauwkeurig blijkt te zijn voor de meeste toepassingen. Met de correctie van de elektrische weglengte en de ASIC is een nieuwe FD-sensor ontwikkeld. De sensor werkt op 20 MHz (Sectie 3.4). De output van de sensor is gekalibreerd aan de hand van bekende dielectrica en blijkt voldoende nauwkeurig. De sensor kan het reële en imaginaire deel van de permittiviteit meten tot een elektrische geleidbaarheid van ongeveer  $0.2 \text{ S m}^{-1}$ .

#### *Toepassingen van de diëlektrische meettechniek*

De potentie van de diëlektrische meettechniek voor het karakteriseren van de bodem is getoond in Hoofdstuk 4. De nieuwe FD-sensor en TDR zijn toegepast op verschillende meetproblemen voor een verscheidenheid van bodems. De meetwaarden die verkregen zijn met de nieuwe FD-sensor (bij 20 MHz), met TDR (ongeveer 150 MHz) en de waarden die zijn voorspeld met het vereenvoudigd model (2.60) van Hoofdstuk 2 zijn met elkaar vergeleken. De output van deze sensoren correleerde met bodemparameters zoals het watergehalte, de textuur en de elektrische geleidbaarheid van het poriënwater in de bodem. Ook is de detectie van mogelijk vervuilde bodemlagen gedemonstreerd. Tot slot zijn de diëlektrische eigenschappen van de bodem geïllustreerd aan de hand van hardend beton.

#### *Gevoeligheid van TDR-metingen voor de elektrische geleidbaarheid van de bodem*

Aangetoond is dat een TDR-uitlezing wordt beïnvloed door de elektrische geleidbaarheid van de bodem. Eigenlijk zou het daarvoor moeten worden gecorrigeerd. De bestaande relatie tussen de reflectietijd en de permittiviteit is gebaseerd op de toepassing van een sinusgolf, waarbij is aangenomen dat de geleidbaarheid verwaarloosbaar is. Echter, deze relatie zou gebaseerd moeten zijn op de toepassing van een stap-functie in het tijdsdomein. Een dergelijke vergelijking is niet beschikbaar; daarom is geen adequate correctie mogelijk. De TDR-metingen die in dit proefschrift zijn gebruikt zijn daarom niet gecorrigeerd.

#### *Diëlektrische bodemwatergehaltemetingen vergeleken met voorspelde waarden*

TDR-bodemwatergehaltemetingen en de, met het nieuwe model voorspelde waarden, correleerden redelijk voor alle geteste bodems, vooral bij een watergehalte van  $< 0.30$ . Voor bodems met een klein specifiek oppervlak, zoals zand, was de correlatie ook goed voor hogere watergehalten. De diëlektrische eigenschappen van bodem zijn frequentieafhankelijk. Daarom was de vergelijking het best voor zand (Figuur 32). Watergehaltekalibratiecurven voor zand zijn vrijwel gelijk voor FD- en TDR- metingen (respectievelijk



20 MHz en 150 MHz). Deze kalibratiecurven konden nauwkeurig worden voorspeld, waarmee werd bevestigd dat het dielektrisch spectrum van zand vlak is tussen 20 MHz en 150 MHz.

De afwijkingen ten opzichte van de voorspelde waarden nemen toe met het watergehalte en met het specifiek oppervlak. Dit feit is toegeschreven aan het Maxwell-Wagner effect. De waargenomen afwijkingen ondersteunen ook de hypothese van polariseerbare luchtbelletjes zoals beschreven in Sectie 2.3. De voorspellingen met het nieuwe model zijn nauwkeuriger dan die volgens Topp's [1980] kalibratiecurve. Met het nieuwe model kan immers rekening gehouden worden met de porositeit van de bodem en het gebonden water. Helaas kunnen in veel applicaties de porositeit en het hygroscopisch watergehalte alleen ruwweg worden geschat en is de invloed van het Maxwell-Wagner effect en dat van de luchtbelletjes onbekend. Daarom is geconcludeerd dat voor absolute watergehaltemetingen, kalibratie noodzakelijk is voor zowel de FD- als de TDR-methode. Er is geen universele kalibratiecurve beschikbaar. Voor de FD-sensoren, bij 20 MHz, is gebleken dat de behoefte om te kalibreren in het algemeen groter is dan voor TDR, bij ongeveer 150 MHz. De noodzaak tot kalibratie wordt kleiner naarmate de meetfrequentie toeneemt en wordt vergelijkbaar met die voor TDR bij 150 MHz. Voor relatieve metingen is de reproduceerbaarheid van beide methoden hoog. Zij kunnen effectief worden gebruikt voor het handhaven van bijvoorbeeld een setpoint. Kalibratie is dan niet nodig.

De depolarisatiefactoren, gevonden voor glaskogeltjes, zijn mogelijk te hoog voor bodemtoepassingen. Verondersteld is dat dit komt door de oppervlakteconditie van bodemdeeltjes. Voor de hoogst mogelijke voorspelbaarheid van het nieuwe model, moeten de depolarisatiefactoren worden bepaald voor de te onderzoeken bodem.

#### *In situ meting van de elektrische geleidbaarheid van het onttrokken bodemwater*

In een publicatie van Malicki *et al.* [1994] is een hypothetische relatie voorgesteld tussen de elektrische geleidbaarheid van het onttrokken bodemwater en dat van het bulkmateriaal. Deze relatie is vergelijkbaar met die tussen de permittiviteit van het bodemwater en de permittiviteit van het bulkmateriaal (Hoofdstuk 2). Voor een verscheidenheid van bodemsoorten blijkt de lineariteit tussen de elektrische permittiviteit en de geleidbaarheid van het bulkmateriaal te kloppen met de hypothese. Een methode is ontwikkeld waarmee de elektrische geleidbaarheid van het onttrokken bodemwater kan worden bepaald door een simultane meting van de elektrische permittiviteit en de geleidbaarheid van het bulkmateriaal. Deze methode blijkt nauwkeurig voor glaskogeltjes en veelbelovend voor een verscheidenheid aan geteste bodems.

#### *Het Maxwell-Wagner effect versus de elektrische geleidbaarheid en de textuur van de bodem*

In Sectie 2.2 is alleen de impact behandeld van het Maxwell-Wagner effect op het reële deel van de permittiviteit. Of en hoe het van toepassing is op de elektrische geleidbaarheid was niet onderzocht. In Sectie 4.2 is een relatie aangetoond tussen de elektrische geleidbaarheid van het bodemwater en dat van het bulkmateriaal, vergelijkbaar met dat voor de permittiviteit. Aangetoond is dat het Maxwell-Wagner effect ook toepasbaar is op de elektrische geleidbaarheid. Laagfrequente geleidbaarheidsmetingen worden beïnvloed door het Maxwell-Wagner effect, terwijl hoogfrequente geleidbaarheidsmetingen worden





beïnvloed door de waterbinding. De situatie is omgekeerd ten opzichte van permittiviteitsmetingen.

Het Maxwell-Wagner effect kan worden gekarakteriseerd met behulp van de drie-frequentie meetmethode zoals die is beschreven in Sectie 2.2. Dit is gedaan voor drie bodems. De resultaten zijn gegeven (Table 4.5) voor metingen met de nieuwe FD-sensor op 10 MHz, 20 MHz en 30 MHz. De geleidbaarheid voor frequenties hoger dan de Maxwell-Wagner relaxatie kon worden bepaald. De geleidbaarheid neemt toe met het specifiek oppervlak van de bodem. De laagfrequente waarden, berekend met de geleidbaarheden voor de drie frequenties, zijn gelijk aan de geleidbaarheid, die is gemeten met behulp van TDR. Daaruit volgt dat een TDR-geleidbaarheidsmeting een laagfrequente meting is.

Uit het voorgaande volgt dat het Maxwell-Wagner effect kan worden gekarakteriseerd aan de hand van geleidbaarheidsmetingen in plaats van permittiviteitsmetingen. Bij lagere frequenties is de meting van de elektrische geleidbaarheid van de bodem nauwkeuriger dan voor de permittiviteit. Voor normale bodems en bij relatief lage frequenties is de elektrische stroom ten gevolge van elektrische geleiding hoger (of kan hoger worden gemaakt) dan de elektrische stroom ten gevolge van de capaciteit. Derhalve hebben fasefouten minder effect op een geleidbaarheidsmeting dan op een permittiviteitsmeting. Dit maakt een nauwkeuriger karakterisering mogelijk van het Maxwell-Wagner effect en daarmee van de textuurparameter.

#### *Detectie van vervuilde bodemlagen*

Getoond is hoe vervuilde bodemlagen kunnen worden gedetecteerd door een simultane meting van de elektrische permittiviteit en de geleidbaarheid. Een vervuilingsindicator is ontwikkeld, gebaseerd op de verhouding tussen de afgeleide van de elektrische permittiviteit als een functie van de diepte en de afgeleide van de geleidbaarheid als de functie van de diepte. Door de toevoeging van een offset bij de permittiviteit en de geleidbaarheid kan de gevoeligheid van de indicator worden ingesteld.

#### *Bodems van verschillende textuur gesimuleerd met hardend beton*

Een analogie is gedemonstreerd tussen de textuureigenschappen van beton en die van de bodem. Gedurende het hydratatie proces verandert de textuur van beton van zandachtig naar kleiachtig en vervolgens naar poreus rotsachtig. Dit maakt het mogelijk het diëlektrisch gedrag van bodem van verschillende texturen te simuleren.

Er bestaat een relatie tussen het Maxwell-Wagner effect en de microstructurele eigenschappen van beton of poreuze materialen in het algemeen. Een overzicht van de diëlektrische fenomenen, die zijn waargenomen gedurende het hydratatieproces van beton, laat een duidelijke relatie zien tussen een aantal veranderingen in de diëlektrische eigenschappen van beton en de verandering in de microstructurele en compositionele eigenschappen. Het effect van waterbinding kan gedeeltelijk worden geïllustreerd aan de hand van de veranderingen in de diëlektrische eigenschappen van hydraterend beton voor hoge frequenties (>100 MHz). Het concept van een textuurparameter maakt het mogelijk de sterkte van het beton te voorspellen. Er blijkt een sterke relatie tussen de elektrische permittiviteit en de druksterkte bij ongeveer 20 MHz (vergelijkingen (4.26) en (4.27)). De



diëlektrische eigenschappen van beton laten vrijwel geen verandering zien voor frequenties rond 100 MHz. Dit is zoals algemeen bekend ook van toepassing op de bodem.

#### **Aanbevelingen voor verder onderzoek**

*Een multidisciplinaire benadering is gewenst voor de ontwikkeling van diëlektrische sensoren*  
De toepassing van de diëlektrische eigenschappen van de bodem voor de ontwikkeling van diëlektrische sensoren omvat vaak een aantal wetenschappelijke disciplines zoals elektronica, thermodynamica, chemie en natuurlijk tuinbouw en bodemkunde. Voorts gaat het om een breed frequentiegebied dat ligt tussen ruwweg 10 kHz en 10 GHz. Het testen van diëlektrische bodemeigenschappen over zo'n breed frequentiegebied vereist gespecialiseerde apparatuur en deskundig personeel. Er is geen algemeen bruikbare benadering in de toepassing van de diëlektrische meettechniek voor het karakteriseren van bodem. Daarom is synergie tussen de disciplines essentieel voor een adequate aanpak van een meetprobleem.

TDR kan, bijvoorbeeld worden opgevat als een speciaal geval van Time Domain Spectroscopy (TDS). Het gebruik van TDR voor het meten van het watergehalte van de bodem is algemeen geaccepteerd in de jaren tachtig, terwijl TDS in ander disciplines al in gebruik was in 1951 (Sectie 1.2).

Een ander voorbeeld is het meten van de elektrische geleidbaarheid van de bodem met TDR: deze methode kon worden gereduceerd tot een serieschakeling van twee weerstanden en een batterij (Sectie 4.3). Een specialist op het gebied van transmissielijnen zou dit direct hebben opgemerkt, hetgeen de meting van elektrische geleidbaarheid in de bodem met TDR belangrijk zou hebben vereenvoudigd.

#### *In situ meting van de waterretentiekarakteristiek*

De relatie tussen de waterretentiekarakteristiek en de diëlektrische relaxatiefrequentie van de bodem is aannemelijk gemaakt (Sectie 2.2). Dit suggereert dat de waterretentiekarakteristiek kan worden afgeleid uit het diëlektrische spectrum van een verzadigde bodem. Routinematige bepalingen van een diëlektrisch spectrum kunnen in minder dan 15 minuten plaatsvinden, wat belangrijk sneller is dan bijvoorbeeld de tijdrovende "pressure plate" bepalingen, die maanden kunnen duren. Bovendien is deze diëlektrische methode bruikbaar voor in situ metingen. Een experiment is nodig om deze techniek te valideren. Een degelijk bewijs vereist de meting van spectra tussen ruwweg 1 GHz en 20 GHz voor een aantal bodems met verschillende waterretentiekarakteristieken en elektrische geleidbaarheden. Een experimentele set-up zou moeten worden ontwikkeld voor het routinematig bepalen van de spectra. Instrumentatie voor dit doel, zoals netwerkanalysers, is commercieel beschikbaar. Deze instrumentatie is echter kostbaar en vereist deskundig personeel. Verwacht wordt dat een speciaal voor dit doel ontwikkeld diëlektrisch instrument, dat werkt op een aantal vooraf gedefinieerde frequenties, meer kosten-effectief is en gebruikersvriendelijker.

#### *In situ bodemtextuurbepalingen*

De bodemtextuurparameter, geïntroduceerd in Hoofdstuk 2, is gerelateerd aan de diëlektrische eigenschappen van de bodem. Deze parameter maakt het mogelijk het Maxwell-Wagner effect te beschrijven in termen van de gemiddelde dikte van de waterlagen en die van de vaste deeltjes en lucht in de matrix. De textuurparameter kan worden gebruikt voor het classificeren van bodems. In deze context is het daarom aan te bevelen de relatie tussen de





textuurparameter en ander fysische bodemeigenschappen zoals het specifiek oppervlak, de porositeit en het watergehalte, meer gedetailleerd te bestuderen.

#### *Op weg naar een universele kalibratievergelijking*

Het werken aan een universele kalibratievergelijking is niet alleen een uitdaging voor bodemwatergehaltemetingen, maar is ook interessant voor diëlektrische watergehaltemetingen in andere materialen. Uit dit proefschrift kunnen twee wegen worden afgeleid, om te komen tot een universele kalibratievergelijking.

Op de eerste plaats wordt de permittiviteit bij lage frequenties beïnvloed door het Maxwell-Wagner effect, terwijl waterbinding de permittiviteit bij hoge frequenties beïnvloedt. Het Maxwell-Wagner effect kan worden gekarakteriseerd middels de elektrische permittiviteit of middels de geleidbaarheid bij drie frequenties (Sectie 4.3). Gebonden water beïnvloedt vrijwel niet de hoogfrequente permittiviteits- of geleidbaarheidswaarden die berekend kunnen worden volgens het Maxwell-Wagner effect. Het moet mogelijk zijn permittiviteits- en geleidbaarheids-waarden te bepalen die vrijwel alleen door het watergehalte en de porositeit worden bepaald.

Een tweede mogelijkheid is gebruik te maken van de permittiviteit waarvoor de ionische geleidbaarheid nul is zoals beschreven in Sectie 4.2. Deze bestaat uit een deel dat afhangt van de lucht en vaste bodembestanddelen en een deel dat het Maxwell-Wagner effect in rekening brengt. Deze laatste kan worden bepaald aan de hand van twee of drie metingen. Als deze bekend is kan de gemeten permittiviteit worden gecorrigeerd voor het Maxwell-Wagner effect dat kan leiden tot een universele kalibratiecurve.

#### *De nieuwe FD-sensor op 100 MHz*

De elektrische weglengte compensatie, voorgesteld voor de nieuwe FD-sensor, is alleen geldig onder bepaalde aannamen (Sectie 3.3). Een van die aannamen is dat de frequentie niet te hoog mag zijn. Bij 30 MHz blijkt de sensor nog goed te functioneren. Voorlopige tests toonden echter aan dat deze elektrische weglengte compensatiemethode niet kan worden gebruikt voor frequenties van 50 MHz of hoger. Voor die frequenties moeten andere methoden worden gebruikt, zoals bijvoorbeeld staandegolfmetingen, reflectiecoëfficiënten of relatieve faseverschuivingen. De ontwikkeling van dergelijke methoden zal de toepasbaarheid van de nieuwe FD -sensor belangrijk verbeteren.

#### *Temperatuurafhankelijkheid van de elektrische permittiviteit van de bodem*

In de theoretische behandeling (Hoofdstuk 2) maar ook in het experimentele hoofdstuk (Hoofdstuk 4) is uitgegaan van een omgevingstemperatuur ongeveer 20 °C. Op het eerste gezicht, verwacht men voor het reële deel van de permittiviteit een temperatuurafhankelijkheid, die voornamelijk het gevolg is van water. Experimenteel zijn echter zowel positieve zowel als negatieve temperatuurcoëfficiënten gevonden, die ook afhangen van het bodemtype. De temperatuur in tuinbouwkassen kan variëren tussen 10 °C tot boven de 40 °C. De temperatuurvariatie van de toplaag van de bodem in een openteeltsysteem is nog groter. Men moet dus in staat zijn temperatuurseffecten te corrigeren. Op dit moment is het nog onduidelijk hoe een temperatuurscorrectie gerealiseerd moet worden. Het is interessant om de temperatuursafhankelijkheid te verwerken in de modellen die zijn ontwikkeld in dit proefschrift, om vervolgens het resultaat te vergelijken met experimentele data.







## REFERENCES

- AL-QADI, I.L., O.A. HAZIM, W. SU & S.M. RIAD. 1995. Dielectric properties of portland cement concrete at low radio frequencies. *J. of Mat. in Civil Eng.*:192-198
- BABB, A.T.S. 1951. A radio-frequency electronic moisture meter. *Analyst*, v. 76:428-433.
- BALANIS, C.A. 1989. *Advanced Engineering Electromagnetics*. John Wiley & Sons, New York.
- BEEK VAN, A., S.J LOKHORST, K. VAN BREUGEL. 1996. On site determination of degree of hydration and associated properties of hardening concrete. *Proc. 3rd Conf. on Nondestructive Evaluation of Civil Structures and Materials*, Atkinson-Noland & Associates, Boulder Colorado, Sept. 1996:44-51
- BIRCHAK, J.R., C.Z.G. GARDNER, J.E. HIPPE & J.M. VICTOR. 1974. High dielectric constant microwave probes for sensing soil moisture. *Proc. IEEE*, v. 62, No. 1:93-98
- BIRD, G.J.A. 1980. *Design of continuous and digital electronic systems*. McGraw-Hill Book Company (UK) Limited.
- BOER DE, J.H. 1953. *The dynamical character of adsorption*. Oxford at the Clarendon Press.
- BOLT, G.H. & R.D. MILLER. 1958. Calculation of total and component potentials of water in soil. *Trans. American Geophysical Union*, v. 39:917-928
- BORDEWIJK, P. 1973. Comparison between macroscopic and molecular relaxation behaviour for polar dielectrics. *Advances in Molecular Relaxation Processes*, v. 5:285-300
- BÖTTCHER, C.J.F. & P. BORDEWIJK. 1978. *Theory of electric polarisation*. Elsevier, Amsterdam v. 2.
- BÖTTCHER, C.J.F. 1952. *Theory of electric polarisation*. Elsevier, Amsterdam.
- BREUGEL VAN, K. 1991. *Simulation of hydration and formation of structure in hardening cement-based materials*, Ph.D. Thesis, Delft University of Technology, Civil Eng., The Netherlands.
- BREUGEL VAN, K., M.A. HILHORST, A. VAN BEEK, W. STENFERT KROESE. 1996. In situ measurements of dielectric properties of hardening concrete as a basis for strength development. *Proc. 3rd Conf. on Nondestructive Evaluation of Civil Structures and Materials*, Atkinson-Noland & Associates, Boulder Colorado, Sept. 1996:7-20
- CAILON, C. *ET AL*. 1990. A high flexibility BICMOS library for mixed analog/digital applications. *J. Semicustom ICs*, v. 7, no. 3.
- CAMPBELL, J.E. 1990. Dielectric properties and influence of conductivity in soils at one to fifty megahertz. *Soil Sci. Soc. Am. J.*, v. 54:332-341
- CARTER, D.L., M.M. MORTLAND & W.D. KEMPER. 1986. *Methods of soil analysis: Specific surface*. In A. Klute (ed.) part 1. 2nd ed. *Agron. Monogr. 9*, ASA and SSSA, Madison, WI:415-423
- CHEW, W.C. 1982. Dielectric enhancement and electrophoresis due to an electrochemical double layer: a uniform approximation. *J. Chem. Phys.*, v. 77:4683
- COLE, K.S. & R.H. COLE. 1941. Dispersion and absorption in dielectrics I: Alternating current characteristics. *J. of Chem. Phys.*, v. 9:341-351
- DAM VAN, D., G. HEIL, B. HEIJEN & R. BOBBINK. 1990. Atmospheric deposition and sulfur cycling in chalk grassland: a mechanistic model simulating field observations. *Biogeochemistry*, v. 9:19-38.
- DAVIDSON, D.W. & R.H. COLE. 1951. *J. of Chem. Phys.*, v. 19:1484-1493
- DAVIS, J.L. 1975. Relative permittivity measurements of sand and clay soil in situ. In: *Report of Activities, Part C, Geol. Surv. Can., Paper 75-IC:361-365*.



- DEBYE, P. 1929. Polar molecules. Reinhold, New York.
- DELTA-T DEVICES LTD. 1996. Product data sheet of Theta-probe: ML/DS/2/96, Cambridge, England.
- DIRKSEN, C. & M.A. HILHORST. 1994. Calibration of a new frequency domain sensor for soil water content and bulk electrical conductivity. In: Proc., Symposium on TDR in Environmental, Infrastructure and Mining Applications, held at Northwestern University, Evanston, Illinois. Special Publication SP 19-94, US Department of Interior Bureau of Mines, Sept. 1994:143-153
- DIRKSEN, C. & S. MATULA. 1992. Automatic atomised water spray assembly for hydraulic conductivity measurements. In Agronomy abstracts, ASA, Madison, WI:214
- DIRKSEN, C., & S. DASBERG. 1993. Improved calibration of time domain reflectometry for soil water content measurements. Soil Sci. Soc. Am. J., v. 57:660-667
- DOBSON, M.C., F.T. ULABY, M.T. HALLIKAINEN & M.A. EL-RAYES. 1985. Microwave dielectric behavior of wet soil-part II: Dielectric mixing models. IEEE Trans. on Geosci. and Remote Sensing, v. GE-23, No. 1:35-46
- DUKHIN, S.S. & V.N. SHILOV. 1974. Dielectric phenomena and the double-layer in disperse systems and polyelectrolytes. Jhon Wiley & Sons, New York.
- EISENBERG, D. & W. KAUZMANN. 1969. The structure and properties of water. Oxford at the Clarendon Press.
- ENDRES, A.L. & R. KNIGHT. 1992. A theoretical treatment of the effect of microscopic fluid distribution on the dielectric properties of partially saturated rocks. Geophysical Prospecting, 40:307-324
- FELLNER-FELDEGG, J. 1969. The measurement of dielectrics in the Time Domain. J. Phys. Chem., v. 73:616-623
- FERGUSON, J.G. 1953. Classification of bridge methods of measuring impedances. Bell System Tech. J., v. 12:452-459
- FINK, G.D. & D. CHRISTIANSEN. 1982. Electronics Engineers' Handbook. McGraw-Hill, New York, Section 28.
- GILBERT, B. 1974. A new high-performance monolithic multiplier using active feedback. IEEE Journal of Solid Circuits, SC-9:364-373
- GLASSTONE, S., K.J. LAIDLER & H. EYRING. 1941. Theory of rate processes. McGraw-Hill, New York.
- GRANT, E.H., R.J. SHEPPARD & G.P. SOUTH. 1978. Dielectric behaviour of biological molecules in solution. Oxford University Press, Oxford.
- HALBERTSMA, J.M., C. PRZYBYLA & A. JACOBS. 1987. Application and accuracy of a dielectric soil water content meter. Proc. Conference on Measurement of Soil and Plant Water Status, Logan, v. 1:11-15
- HAN D.G. & G.M. CHOI. 1996. Numerical study of D.C. conductivity & A.C. impedance for the close-packed mixture of hard spheres. Mat. Res. Soc. Symp. Proc., v. 411:345-350
- HANAI, T. 1968. Emulsion Science. Ed. by P. Sherman, Academic Press, New York, chap. 5
- HARRISON, L.P. 1963. Fundamental concepts and definitions relating to humidity. In: Humidity and Moisture, ed. by A. Wexler, v. 3, Chapman & Hall, Ltd., London.
- HASTED, J.B. 1973. Aqueous dielectrics, Chapman and Hall, London, 1973.
- HEATHMAN, G.C. 1993. Soil moisture determination using a resonant frequency capacitance probe. International Summer Meeting of the ASAE/CSAE, Nr. 931053.
- HEIMOVAARA, T.J. & W. BOUTEN. 1990. A computer-controlled 36-channel time-domain reflectometry system for monitoring soil water contents. Water Resour. Res. 26:2311-2316
- HeimoVaara, T.J., 1993. Time domain reflectometry in soil science: theoretical backgrounds, measurements and models. Ph.D Thesis University of Amsterdam.



- HEIMOVAARA, T.J., A.G. FOCKE, W. BOUTEN & J.M. VERSTRATEN. 1995. Assessing temporal variation in soil water composition with time domain reflectometry. *Soil Sci. Soc. Amer. J.*, v. 59:689-698
- HILHORST M.A., J. BALENDONCK & F.W.H. KAMPERS. 1993. A broad-band-width mixed analog/digital integrated circuit for the measurement of complex impedances. *IEEE J. of Solid-State Circuits*, v. 28, No. 7:764-769
- HILHORST, M.A. 1984. A sensor for the determination of the complex permittivity of materials as a measure for the moisture content. *Sensors & Actuators*, ed. by P. Bergveld, Kluwer Technical Books, Deventer:79-84
- HILHORST, M.A., J. GROENWOLD & J.F. DE GROOT. 1992. Water content measurements in soil and rockwool substrates: dielectric sensors for automatic in situ measurements. *Sensors in Horticulture, Acta Horti. Cult.*, v. 304:209-218.
- HILHORST, M.A., K. VAN BREUGEL, D.J.M.H. PLUIMGRAAFF, W. STENFERT KROESE. 1996. Dielectric sensors used in environmental and construction engineering. *Mat. Res. Soc. Symp. Proc.*, v. 411:401-406
- HILHORST, M.A., K. VAN BREUGEL, W. STENFERT KROESE. 1996. Dielectric properties versus strength development for hardening concrete. Abstract:A3.P2 of the XXVth General Assembly of the int. union of radio science, Lille, France, Aug. 28 - Sept. 5, 1996:18
- HOEKSTRA P. & W.T. DOYLE. 1971. Dielectric relaxation of surface adsorbed water. *J. of colloid and interface science*, v. 36, No. 4:513-521
- HOEKSTRA P. & A. DELANEY. 1974. Dielectric properties of soils at uhf and microwave frequencies. *J. of Geoph. Research*, v. 79, No. 11:1699-1708
- IMKO-MICROMODULETECHNIK GMBH. 1991. TRIME-System: Materialfeuchtemessung nach dem prinzip der time-domain-reflectometry (Material moisture measurement with principle of time-domain-reflectometry). Product data sheet, Germany.
- ISO 190/SC 5, VERSION 26-2-1996. An update version of ISO/TC 190/SC 5 N77.
- IWATA, S., T. TABUCHI & B.P. WARKENTIN. 1995. *Soil-water interactions: mechanisms and applications*. 2nd ed., Dekker, New York.
- JENKINS, T.E., L. HODGETTS, R.N. CLARKE & A.W. PREECE. 1990. Dielectric measurements on reference liquids using automatic network analysers and calculable geometries. *Meas. Sci. Technol.* 1:691-702
- KAATZE U. & V. UHLENDORF. 1981. The dielectric properties of water at microwave frequencies. *Zeitschrift für Phys. Chem. Neue Folge*, Bd. 126:151-165
- KAATZE U. 1996. Microwave dielectric properties of water. In: *Microwave Aquametry*, ed. by A. Kraszewski. IEEE Press, New York:37-53
- KNIGHT, J.H., I. WHITE & S.J. ZEGELIN. 1994. Sampling volume of TDR probes used for water content monitoring. In: *Proc., Symposium on TDR in Environmental, Infrastructure and Mining Applications*, held at Northwestern University, Evanston, Illinois. Special Publication SP 19-94 US Dep. of Interior Bur. of Mines, Sept. 1994:93-104
- KOBAYASHI, S. 1996. Microwave attenuation in a wet layer of limestone. In: *Microwave Aquametry*, ed. by A. Kraszewski, IEEE press:123-140
- KOOREVAAR, P., G. MENELIK & C. DIRKSEN. 1983. *Elements of soil physics: developments in soil science* 13. Elsevier Science.
- LANDAU, L.D. & E.M. LIFSHITZ. 1960. *Electrodynamics of continuous media*. Pergamon Press, London:20-27
- LAWTON, B.A. & R. PETHING. 1993. Determining the fat content of milk and cream using AC conductivity. *Measurement Science & Technology*, v. 4:38-41
- LIDIARD, A.B. 1957. Ionic conductivity: Electricische leitungsphomene II, in *Handbuch der Physik*, v. 20.



- LOOR DE, G.P. 1956. Dielectric behaviour of heterogeneous mixtures. Ph.D thesis, University of Leiden, The Netherlands. Also. *Sci. Res.*, v. B11, 1964:310-320
- LOOR DE, G.P. 1961. *Appl. Sci. Res.*, B, v. 9:297
- LOOR DE, G.P. 1964. *Appl. Sci. Res.*, B, v. 11:310
- LOOR DE, G.P. 1990. The dielectric properties of wet soils. The Netherlands Remote Sensing Board; bcrs report No. 90-13, TNO Physics and Electronics Laboratory (FEL-TNO).
- LOOYENGA, H. 1965. Dielectric constant of heterogeneous mixtures. *Physica* 31:401-406
- LORRAIN, P., D.P. CORSON & F. LORRAIN. 1988. *Electromagnetic fields and waves*. Third edition, Freeman and Company, New York.
- MALICKI, M.A., R.T. WALCZAK, S. KOCH & H.FLÜHLER. 1994. Determining soil salinity from simultaneous readings of its electrical conductivity and permittivity using TDR. In: *Proc., Symposium on TDR in Environmental, Infrastructure and Mining Applications*, held at Northwestern University, Evanston, Illinois. Special Publication SP 19-94 US Dep. of Interior Bur. of Mines, Sept. 1994:328-336
- MAXWELL, J.C. 1873. *Treatise on electricity and magnetism*. Oxford University Press, London.
- MUALEM, Y. & S.P. FRIEDMAN. 1991. Theoretical prediction of electrical conductivity in saturated and unsaturated soil. *Water Resources Research* 27: 2771-2777
- NYFORS, E. & P. VAINIKAINEN. 1989. *Industrial microwave sensors*. Artech House, Norwood-MA.
- O'BRIEN. 1986. The high-frequency dielectric dispersion of a colloid. *J. of Colloid and Interface Science*, v. 113, No. 1:81-93
- PHILIP, J.C. 1893. Das dielektrische verhalten flüssiger mischungen, besonders verdünnter lösungen. *Zeitschrift fuer Physikalische Chemie*, band 24, C:18-38
- POLK, C & E. POSTOW. 1986. *CRC handbook of biological effects of electromagnetic fields*. CRC Press, Inc. Boca Raton, Florida.
- PRIOU A. 1992. Editor of *PIER 6: Progress In Electromagnetics Research*. Elsevier Science Publishing Co., Inc., v. 6.
- RAYTHATHA, R. & P.N. SEN. 1986. Dielectric properties of clay suspension in MHz to GHz range. *J. of Colloid and Interface Science*, v. 109, No. 2:301-309
- REDMAN, J.D. & A.P. ANNAN. 1992. Dielectric permittivity monitoring in a sandy aquifer following the controlled release of DNAPL. *Proceedings of fourth international conference on ground penetrating radar*, Rovaniemi, Finland. Geological Surveys of Finland, June 8-13.
- REINHARDT, H.W. 1985. *Beton als constructiemateriaal: eigenschappen en duurzaamheid*. Delftse Universitaire Pers.
- REYNOLDS J.A. 1955. The dielectric constant of mixtures. Ph.D Thesis, Faculty of Science of the University of London.
- ROLLAND, M.T. & R. BERNARD. 1951. *C.R. Acad. Sci.*, Paris, 232: 1098
- ROOS, J. & P. WOLLANTS. 1995. *Thermodynamica en kinetica voor materiaalkundigen: Electrochemie en electredekinetica*. Acco Leuven / Amersfoort, v.3
- SCHWAN, H. 1957. *Electrical properties of tissue and cell suspensions*. Adv. in Biol. and Med. Phys., Academic Press, New York, v. 5:147-209
- SCHWARZ, G. 1962. A Theory of the low frequency dielectric dispersion of colloidal particles in electrolyte solution. *J. Phys. Chem.*, 66:2636
- SIHVOLA, A. & L.V. LINDELL. 1988. Polarizability and effective permittivity of layered and continuously inhomogeneous dielectric spheres. *J. Electromagnetic Waves and Applications*, v. 2, No. 8: 741-756





- SIHVOLA, A. 1996. dielectric mixture theories in permittivity prediction: effects of water on macroscopic parameters. In: *Microwave Aquametry* ed. by A. Kraszewski, IEEE Press Piscataway:111-120
- SILBERSTEIN, L. 1895. Untersuchungen über die dielectricitätsconstanten von mischungen und lösungen. *Annalen der Physik und Chemie, Leipzig*:661-679
- SLATYER, R.O. 1967. *Plant-water relationships*. Academic press, London.
- SLEGGERS, P.A., & P.G. ROUXHET. 1977. The hydration of tricalcium silicate: calcium concentration and portlandite formation. *Cement and Concrete Research*, Pergamon Press, v. 7, No. 1:31-38
- SMITH-ROSE, R.L. 1933. The electrical properties of soil for alternating currents at radio frequencies. *Proc. of the Royal Society of London, Series A* 140:359-377
- STEYAERT, M. *ET AL* 1991. A 1 GHz single chip quadrature modulator without external trimming. in *Proc. ESSCIRC Conf., Milan*:261-264
- TINGA, W.R., W.A.G. VOSS & D.F. BLOSSEY. 1973. Generalised approach to multiphase dielectric mixture theory. *J. of Applied Physics*, v. 44, No. 9:3897-3902
- TOBIO, J.M. 1957. A study of the setting process: Dielectric behaviour of several spanish cements. *Silicates Industrials, Communication présentée aux Journées Internationales d'études, Liant hydrauliques 1957, de L'Association belge pour favoriser L'étude des Verres et Composés siliceux*.:30-35 and 81-87.
- TOPP, G.C., J.L. DAVIS & A.P. ANNAN. 1980. Electromagnetic determination of soil water content: measurements in coaxial transmission lines. *Water Resources Research*, v. 16, No. 3:574-582
- TOPP, G.C., J.L. DAVIS & A.P. ANNAN. 1982. Electromagnetic determination of soil water content using TDR: II. Evaluation of installation and configuration of parallel transmission lines. *Soil Science Society of America Journal*, v. 46:678-684
- TOPP, G.C., M. YANUKA, W.D. ZEBCHUK & S. ZEGELIN. 1988. Determination of electrical conductivity using time-domain reflectometry: Soil and water experiments in coaxial lines. *Water Resour. Res.*, v. 24:945-952
- TOPP, G.C. 1996. Time-domain reflectometry techniques for soil water content measurements. Workshop on "Electromagnetic wave interaction with water and moist substances", MTTs International Microwave Symposium, June 17, San Francisco, Edited by A. Kraszewski. (In preparation).
- TURSKI, R., & M. MALICKI. 1974. A precise laboratory meter of a dielectric constant of a different moisture. *Polish J. of Soil Science*, v. 7, No. 1:71-79
- VITEL INC. 1995. Product information.
- WADELL, B.C. 1991. *Transmission Line Design Handbook*. Artech House, Boston MA.
- WAGDY, M.F. *ET AL* 1986. A phase-measurement error compensation technique suitable for automation. *IEEE Trans. Instrum. Meas.*, v. IM-35, no. 1:7-12
- WAGNER, K.W. 1914. The after effect in dielectrics. *Arch. Electrotech Berlin*, 2 and 3.
- WANG, J.R. & T.J. SCHMUGGE. 1980. An empirical model for the complex dielectric permittivity of soils as a function of water content. *IEEE Trans. on Geosci. and Remote Sensing*, v. GE-18, No. 4:288-295
- WENSINK, W.A. 1993. Dielectric Properties of wet soils in the frequency range 1-3000 MHz. *Geophysical Prospecting*, v. 41:671-696
- WHALLEY, W.R. 1993. Considerations on the use of time-domain reflectometry (TDR) for measuring soil water content. *J. of Soil Science*, v. 44, No.1:1-9.
- WHITE, I, S.J. ZEGELIN & G. CLARKE TOPP. 1994. Effect of bulk electrical conductivity on TDR measurement of water content in porous media. In: *Proc., Symposium on TDR in Environmental, Infrastructure and Mining Applications*, held at Northwestern University, Evanston, Illinois. Special Publication SP 19-94 US Dep. of Interior Bur. of Mines, Sept. 1994:294-308



- WHITE, I., J.H. KNIGHT, S.J. ZEGELIN & G.C. TOPP. 1994. Considerations on the use of time-domain reflectometry (TDR) for measuring soil water content-Comment. *European Journal of Soil Science*, v. 45, No. 4:503-508
- WOBSCHELL, D. 1978. A frequency shift dielectric soil moisture sensor. *IEEE Trans. on Geosci. Electron.*, v. GE-16, No. 2:112-118
- WYSEURE, G.C.L., M.A. MOJID & M.A. MALIK. 1997. Measurement of volumetric water content by TDR in saline soils. *European Journal of Soil Science*, 48:347-354







## LIST OF MAIN SYMBOLS

Symbol	Description	Dimension	SI-Units
$A$	Area of a capacitor plate	$L^2$	$m^2$
$A$	Parameter in Arrhenius function	-	-
$B$	Electrical susceptance: $B = \omega C$	$L^{-2}M^{-1}T^3I^2$	S
$C$	Electrical capacitance	$L^{-2}M^{-1}T^4I^2$	F
$C'$	Distributed capacitance of a transmission line	$L^{-3}M^{-1}T^4I^2$	$F m^{-1}$
$E$	Electric field strength	$LMT^{-3}I^{-1}$	$V m^{-1}$
$EC$	Specific electrical conductivity of water extracted from the soil matrix	$L^{-3}M^{-1}T^3I^2$	$S m^{-1}$
$F$	Attraction or repulsion force between two point charges	$LMT^{-2}$	$VC m^{-1}$
$G'$	Distributed electrical conductance of a transmission line	$L^{-3}M^{-1}T^3I^2$	$S m^{-1}$
$G$	Electrical conductance	$L^{-2}M^{-1}T^3I^2$	S
$G$	Gibbs' free energy (Section 2.2)	$L^2MT^{-2}N^{-1}$	$J mol^{-1}$
$\Delta G^*$	Molar Gibbs' free energy of activation	$L^2MT^{-2}N^{-1}$	$J mol^{-1}$
$H$	Enthalpy	$L^2MT^{-2}N^{-1}$	$J mol^{-1}$
$\Delta H^*$	Molar activation enthalpy	$L^2MT^{-2}N^{-1}$	$J mol^{-1}$
$I$	Electrical current (dc)	I	A
$K$	Texture parameter (function of $\phi$ , $\theta$ and $A$ )	-	-
$L$	Electrical inductance	$L^2MT^{-2}I^2$	H
$L'$	Distributed inductance of transmission line	$LMT^{-2}I^2$	$H m^{-1}$
$P$	Electric polarisation	$L^{-2}TI$	$C m^{-2}$
$P$	Intermediate quantity: $P = pq$	$L^{-2}M^{-1}T^3I^4$	-
$Q$	Electrical charge	TI	C
$R'$	Distributed electrical resistance of a transmission line	$L^1MT^{-3}I^{-2}$	$\Omega m^{-1}$
$R$	Electrical resistance	$L^2MT^{-3}I^{-2}$	$\Omega$
$R$	Universal gas constant ( $R = 8.31 J mol^{-1} K^{-1}$ )	$L^2MT^{-2}N^{-1}\Theta^{-1}$	$J mol^{-1} K^{-1}$
$R$	Regression coefficient	-	-
$S$	Dielectric depolarisation factor	-	-
$S$	Entropy (Section 2.2)	$L^2MT^{-2}N^{-1}\Theta^{-1}$	$J mol^{-1} K^{-1}$
$\Delta S^*$	Molar activation entropy	$L^2MT^{-2}N^{-1}\Theta^{-1}$	$J mol^{-1} K^{-1}$
$S_A$	Specific surface area	$L^2M^{-1}$	$m^2 kg^{-1}$
$T$	Absolute temperature in degree Kelvin	$\Theta$	K
$U$	Electrical voltage (dc)	$L^2MT^{-3}I^{-1}$	V
$V$	Partial molar volume of water ( $V = 18 \cdot 10^{-6} m^3 mol^{-1}$ )	$L^3 N^{-1}$	$m^3 mol^{-1}$
$V$	Volume of soil	$L^3$	$m^3$
$Y$	Complex admittance: $Y = 1/Z$	$L^{-2}M^{-1}T^3I^2$	S
$Z$	Complex impedance	$L^2MT^{-3}I^{-2}$	$\Omega$
$Z_0$	Characteristic impedance of a transmission line	$L^2MT^{-3}I^{-2}$	$\Omega$
$a$	Offset constant	$L^4M^{-1}T^3I^2$	$S m^{-2}$
$b$	Offset constant	$L^4M^{-1}T^4I^2$	$F m^{-2}$
$d$	Distance	L	m
$e$	Base of natural system of logarithm ( $e = 2.71828...$ )	-	-



$e/e_s$	Relative humidity	-	-
$f$	Frequency	$T^{-1}$	Hz
$f_{3dB}$	Frequency for which gain reduced 0.5 times	$T^{-1}$	Hz
$f_{cs}$	Compressive strength of concrete	$L^{-1}MT^{-2}$	Pa
$f_T$	Transition frequency (for gain = 1)	$T^{-1}$	Hz
$g$	Transconductance gain	$L^{-2}M^{-1}T^3I^2$	S
$g$	Weighting function	-	-
$g(\theta)$	Function of water content	-	-
$h$	Planck's constant ( $h = 66.3 \cdot 10^{-31} \text{ J s}^{-1}$ )	$L^2MT^{-3}$	$\text{J s}^{-1}$
$i$	Alternating current (ac)	I	A
$j$	Complex number ( $j = \sqrt{-1}$ )	-	-
$k$	Boltzmann's constant ( $k = 13.8 \cdot 10^{-24} \text{ J K}^{-1}$ )	$L^2MT^{-2}\Theta^{-1}$	$\text{J K}^{-1}$
$k_1$	Scaling constant	$L^{-1}MT^{-2}$	MPa
$k_2$	Offset constant	-	-
$l$	Length of transmission line	L	m
$m$	Mass	M	kg
$m_o$	Oven-dried mass of soil	M	kg
$n$	Refractive index for EM-wave propagation	-	-
$p$	Intermediate quantity: $p = g_z 1 g_z 2  \mu_{osc} $	$L^{-2}M^{-1}T^3I^3$	-
$p$	Pollution indicator	$T^{-1}$	$\text{S F}^{-1}$
$p$	Pressure	$L^{-1}MT^{-2}$	Pa
$q$	Intermediate quantity: $q = g_r 1 g_r 2  \mu_{osc}   Z_T $	I	A
$q$	Alternating charge	TI	C
$r$	Radius	L	m
$t$	Time	T	s
$u$	Alternating voltage (ac)	$L^2MT^{-3}I^{-1}$	V
$u$	Surface mobility of counterions	$M^{-1}T^2I$	$\text{m}^2 \text{V}^{-1} \text{s}^{-1}$
$v$	Volume fraction of a soil-concrete constituent ( $\text{m}^3 \text{m}^{-3}$ )	-	-
$w$	Wetness by mass ratio ( $\text{kg kg}^{-1}$ )	-	-
$z$	Depth	L	m
$\Delta\epsilon$	Dielectric increment (Debye function)	-	-
$\Delta\sigma$	Conductivity decrement (Maxwell Wagner effect)	$L^{-3}M^{-1}T^3I^2$	$\text{S m}^{-1}$
$\alpha$	Angle of complex impedance	-	rad
$\alpha$	Empirical constant in Birchak's model	-	-
$\alpha_h$	degree of hydration for concrete	-	-
$\beta$	Phase shifter angle ( $0^\circ$ or $90^\circ$ )	-	rad
$\delta$	Thickness of a monomolecular water layer ( $\delta = 3 \cdot 10^{-10} \text{ m}$ )	-	L
$\delta_0$	Surface charge density	$L^{-2}TI$	$\text{C m}^{-2}$
$\epsilon$	Complex relative permittivity, in this thesis further referred to as permittivity	-	-
$\epsilon''_d$	Dielectric loss (part of $\epsilon''$ )	-	-
$\epsilon_{f \rightarrow \infty}$	Permittivity at frequencies high compared to $f_r$ (Debye)	-	-
$\epsilon_{f \rightarrow 0}$	Permittivity at frequencies high compared to $f_r$ (Debye)	-	-
$\epsilon_0$	Permittivity for free space ( $\epsilon_0 = 8.854 \cdot 10^{-12} \text{ F m}^{-1}$ )	$L^{-2}T^4I^2$	$\text{F m}^{-1}$
$\epsilon_r$	Complex relative permittivity (Section 2.1)	-	-
$\epsilon'$	Real part of permittivity	-	-
$\epsilon''$	Imaginary part of permittivity	-	-



$\varepsilon''_w$	Imaginary part of permittivity for water	-	-
$\phi$	Phase error	-	rad
$\phi$	Volume fraction of pores in soil ( $m^3 m^{-3}$ )	-	-
$\gamma$	Propagation constant of a transmission line	-	-
$\kappa$	Geometry factor of a capacitor or conductor ( $A/d$ )	L	m
$\mu$	Relative permeability (for air $\mu = 1$ )	-	-
$\mu$	Chemical potential	$L^2MT^{-2}N^{-1}$	J mol <sup>-1</sup>
$\mu_0$	Permeability of free space ( $\mu_0 = 4 \pi 10^{-7} H m^{-1}$ )	$L^2MT^{-2}I^{-2}$	H m <sup>-1</sup>
$\pi$	Constant 3.14159	-	-
$\theta$	Volume fraction of water in soil ( $m^3 m^{-3}$ )	-	-
$\rho$	Density	$L^3M$	kg m <sup>-3</sup>
$\sigma$	Specific ionic conductivity of extracted soil water	$L^3M^{-1}T^3I^2$	S m <sup>-1</sup>
$\sigma_b$	Specific electrical conductivity of bulk material	$L^3M^{-1}T^3I^2$	S m <sup>-1</sup>
$\sigma_{ref}$	Specific ionic conductivity of a reference liquid	$L^3M^{-1}T^3I^2$	S m <sup>-1</sup>
$\sigma_w$	Specific electrical conductivity of extracted soil water	$L^3M^{-1}T^3I^2$	S m <sup>-1</sup>
$\tau$	Rise time of electric step to reach 2/3 of its amplitude	T	s
$\omega$	Radian frequency	T <sup>-1</sup>	rad s <sup>-1</sup>
$\omega_{wcc}$	Water cement ratio by weight (kg kg <sup>-1</sup> )	-	-
$\psi$	Potential of soil water	$L^2T^{-2}$	J kg <sup>-1</sup>

Modifiers to symbols	Denotes	Example
a	Air	$\varepsilon_a$
b	For bulk quantities	$\sigma_b$
c	Counterion polarisation	$\varepsilon_{cf \rightarrow 0}$
C	Refers to a capacitor	$i_C$
ce	Cement	$v_{ce}$
cs	Compressive strength	$\sigma_{cs}$
d	Dielectric	$\varepsilon''_d$
$f \rightarrow \infty$	At frequencies high compared to $f_r$	$\varepsilon_{wf \rightarrow \infty}$
$f \rightarrow 0$	At frequencies low compared to $f_r$	$\varepsilon_{wf \rightarrow 0}$
G	Refers to a conductor	$i_G$
h	Hygroscopic	$\theta_h$
i	Variable real number (1,2,3 ... k or 1,2,3 ... n)	$v_i$
ice	Ice	$\varepsilon_{ice f \rightarrow 0}$
k	Number in a data set	$p_{mk}$
m	Matrix	$p_m$
m	Value measured at the output of the ASIC	$I_m$
max	Maximum	$C_{max}$
MW	Maxwell-Wagner effect	$\varepsilon_{MW f \rightarrow \infty}$
n	Number of constituents	$v_n$
offset	Refers to a dc offset current or voltage	$I_{m \text{ offset}}$
osc	Oscillator	$u_{osc}$
p	Due to polarisation phenomena	$\varepsilon_p$
p	Refers to paracitics	$C_p$
r	Refers to a reference	$i_r$
r	Relaxation	$f_{ice r}$
s	Refers to components in series	$L_s$





s	Solids	$\epsilon_s$
t	As a function of time	$v_{cc\ t}$
t	Total	$\psi_t$
t=0	At time zero	$v_{cc\ t=0}$
w	Refers to wiring parasitics	$L_w$
w	Water	$\epsilon_w$
wce	Water cement	$\omega_{wce}$
x	Unknown quantity	$G_x$
z	Refers to the impedance input channel	$Z_z$
0	At reference condition of 0.1 MPa and 20 °C	$p_0$
0°	Refers to 0° phase shift	$Z_{\tau\ 0^\circ}$
90°	Refers to 90° phase shift	$Z_{\tau\ 90^\circ}$
180°	Refers to 180° phase shift	$I_{m\ 180^\circ}$
270°	Refers to 270° phase shift	$I_{m\ 270^\circ}$
$\Delta$	Small change of or difference between	$\Delta C$
$\underline{\quad}$	Vector quantity	$\underline{E}$
$\bar{\quad}$	Average	$\bar{d}$
'	Distributed parameter of transmission line	$C'$
'	Real part of complex quantity	$\epsilon'$
"	Imaginary part of complex quantity	$I''$
	Amplitude of rotational vector	$ \mu_{osc} $
//	Parallel model for MW	$\epsilon_{MW//\ f \rightarrow 0}$
;	Series model for MW	$\epsilon_{MW;\ f \rightarrow \infty}$

### Abbreviations

ac	Alternating current
dc	Direct current
ASIC	Application specific integrated circuit
CH	Calcium hydroxides
CHS	Calcium silicate hydrates
EM	Electromagnetic
EMI	Electromagnetic interference
FD	Frequency domain
IC	Integrated circuit
RF	Radio frequency
RS	Remote Sensing
S	Electronic switch
SPICE	Electrical circuit simulation and analysis software, University of Berkeley, California
TDR	Time domain reflectometry





## CURRICULUM VITAE

Max A. Hilhorst was born in Utrecht, The Netherlands on November 27, 1947. In 1978 he graduated in electrical engineering from the Poly Technical Institute of Arnhem, The Netherlands.

From 1972 to 1983 he was engaged in the research and development of extremely low-noise analogue electronics at the Space Research Organisation in the Netherlands (SRON), Utrecht. In this work he was involved in the design of a proton experiment on board the International Sun-Earth Explorer-C and a Solar-Flare soft X-ray detector on board the International Solar Polar Mission. He then joined the Technical and Physical Research Service of the Dutch Agricultural Research Department (TFDL-DLO), Wageningen, The Netherlands, which in turn is part of the Ministry of Agricultural Nature Management and Fisheries in the Netherlands. There he has been engaged in the research and development of instrumentation for agricultural research. He designed a fast image processing system for animal tracking and an ultrasonic position sensor for a milking robot.

Between 1991 and 1994 he lead the development of a combined high-frequency/analogue/digital integrated circuit for the measurement of the dielectric properties of materials. This circuit is applied to water-content and water-tension sensors.

In 1994 he received the profesional recognition European-Engineer (EUR ING) of the FEANI (Fédération Européenne d'Associations Nationales d'Ingénieurs). Due to a reorganisation of DLO in 1994 he is currently with the DLO Institute of Agricultural and Environmental Engineering (IMAG-DLO), Wageningen, The Netherlands. There he is currently in charge of several research projects on the application of dielectric sensor technology and impedance spectroscopy to specific agricultural research tasks. Part of this research is described in his Doctoral thesis entitled "Dielectric characterisation of soil" published in 1998. He is author of 23 publications or reports and co-author of 10 publication. He holds 8 granted or pending patents.